

DISSERTATION
submitted to the
Combined Faculties for the Natural Sciences and for Mathematics
of the Ruperto-Carola University of Heidelberg, Germany
for the degree of
Doctor of Natural Sciences

Put forward by
Dipl. Phys. Martin Wieser
born in Schwabmünchen

Oral examination: 02.02.2011

**Imprints of climatic and environmental change in a regional
aquifer system in an arid part of India using noble gases and
other environmental tracers**

Referees:

Prof. Dr. Werner Aeschbach-Hertig

Prof. Dr. Augusto Mangini

Abstract

The aim of this multi-tracer study is the investigation of palaeoclimate changes in South Asia over the last 50,000 years based on data from a groundwater aquifer in North-West India. ^{14}C , ^3H , He isotopes, ^{222}Rn and SF_6 were used for dating, while stable water isotopes and excess air allow the reconstruction of palaeohumidity. Temperature records are derived by noble gas thermometry. A mass spectrometer setup was optimised, now allowing to quantify absolute noble gas amounts. Successful cryogenic separation of Ar from Kr reduced the offset of air equilibrated water standards (He, Ne, Ar, Kr and Xe) to 2.6, 0.5, 0.6, -0.2 and 0.4 % with a reproducibility of 0.2, 0.6, 0.3, 0.7 and 1.2 %, respectively. ^{14}C dating agreed with a previous study and is confirmed by He-Rn ages. In deep wells of the sedimentary basin and near fault zones, mantle He was determined to contribute up to 10% of the total terrigenous He. In the crystalline aquifer, high concentrations of Rn (4 Bq/cm^3) and radiogenic ^4He ($3 \cdot 10^{-4} \text{ cm}^3\text{STP/g}$) were found, and SF_6 concentrations showed amounts several orders of magnitude above modern atmospheric equilibrium. Palaeohumidity is consistently reconstructed by excess air and stable water isotope data. Both signals reveal a dry glacial period followed by a humid Holocene, which is interrupted by a dry late Holocene. Monsoonal strength obtained from excess air supports older palaeoclimate studies of the region. Noble gas temperatures show a cold last glacial period compared to a warm Holocene, presuming a warming of $(3.5 \pm 0.5)^\circ\text{C}$. This record provides the first quantitative information on palaeotemperature in South Asia.

Zusammenfassung

Ziel dieser Arbeit ist die Untersuchung paläoklimatischer Schwankungen in Südasien während der letzten 50.000 Jahre. Hierzu wurde eine Multi-Tracer-Studie an einem Grundwasser-Aquifer in Nordwest-Indien durchgeführt. Hierbei werden ^{14}C , ^3H , die Helium-Isotopie, ^{222}Rn und SF_6 zur Altersbestimmung verwendet, während die stabile Wasserisotopie und der Luftüberschuss Aufschluss über Änderungen der Luftfeuchtigkeit geben. Die Temperatur wird mittels Edelgasthermometrie rekonstruiert. Die Edelgasmessungen erfolgen durch Massenspektrometrie, wobei im Rahmen dieser Arbeit eine Messroutine verbessert wurde, die nun auch eine absolute Quantifizierung der Gasmengen erlaubt. Erfolgreiche kryogene Gastrennung von Ar und Kr verringert den nachgewiesenen Offset von mit Luft äquilibrierten Wasser-Standards auf 2.6, 0.5, 0.6, -0.2 und 0.4 % mit einer Reproduzierbarkeit von 0.2, 0.6, 0.3, 0.7 und 1.2 %. Die ^{14}C -Datierung bestätigt die Alter aus einer früheren Studie und wird von He-Rn-Altern gestützt. Tiefe Brunnen in der Ebene und nahe der Störzonen weisen mit 10% des terrigenen Heliums eine Mantel-Signatur auf. Wässer mit kristalliner Herkunft zeigen starke radiogene ^4He - ($3 \cdot 10^{-4} \text{ cm}^3\text{STP/g}$) und Rn-Konzentrationen (4 Bq/cm^3) sowie SF_6 -Konzentrationen, die mehrere Größenordnungen über dem aktuellen atmosphärischen Gleichgewicht liegen. Die Feuchte-Historie weist auf ein trockenes Glazial gefolgt von einem niederschlagsreichen Holozän hin, mit einer vorübergehenden Trockenperiode im Spätholozän. Die Ergebnisse bestätigen damit ältere Studien über das Monsunverhalten der Region. Die Edelgastemperaturen sind die ersten quantitativen Paläotemperatur-Ergebnisse für Südasien und zeigen ein kaltes Glazial verglichen mit einem um $(3.5 \pm 0.5)^\circ\text{C}$ wärmeren Holozän.

Contents

1. Introduction	13
2. Basics	15
2.1. General Hydrogeology	15
2.1.1. Groundwater flow	16
2.1.2. Transport models	17
2.1.3. Ground temperatures	18
2.2. Region of Gujarat	20
2.2.1. Geology	20
2.2.2. Monsoon and Palaeoclimate	23
2.3. Environmental Tracers	26
2.3.1. Stable Isotopes	27
2.3.2. Tritium	33
2.3.3. Carbon	35
2.3.4. Carbonate dating of groundwater	37
2.3.5. Sulphur hexafluoride	45
2.3.6. Noble gases	46
2.3.7. Equilibration	50
2.3.8. Modelling of excess air	52
2.3.9. Non-atmospheric components	55
2.3.10. Fitting	56
3. Sampling campaigns	59
3.1. Sampling Area	59
3.1.1. Hydrogeology of the sampling area	62
3.1.2. Realisation of well-sampling	65
3.2. Measurements	67
3.3. Samples	68
4. Methods	69
4.1. Multiparameter probe	69
4.2. Stable Isotopes	70
4.3. Tritium	71
4.4. Carbon	71
4.4.1. Extraction	71

4.4.2. Measurement via AMS	73
4.5. SF ₆	74
4.5.1. Sample treatment	74
4.5.2. Gas chromatographic measurement	76
4.6. Noble gases	77
4.6.1. MS Method	77
4.6.2. MS measurements	83
4.6.3. Data Evaluation	84
4.7. Radon	88
5. Results	91
5.1. In-situ field data	91
5.2. Dating	93
5.2.1. Tritium	93
5.2.2. Carbon	94
5.2.3. Radon	102
5.2.4. Helium	103
5.2.5. SF ₆	108
5.2.6. Summary for the palaeoclimate group P	111
5.2.7. Summary for group CRY:	111
5.3. Palaeoclimate	112
5.3.1. Stable Isotopes	112
5.3.2. Noble Gases	115
5.3.3. Results of noble gas fitting	123
6. Summary	129
6.1. Discussion of laboratory methods	129
6.2. Discussion of hydrogeology	129
6.3. Discussion of the palaeoclimate	130
6.4. Outlook	131
A. Monsoon	133
B. Methods	135
B.1. Used field chemicals	135
B.2. Noble gas measurement	145
B.2.1. Heidelberg MS	145
B.2.2. Desorption curves	146
B.2.3. “Ghost” krypton	151
B.2.4. Performance tests of the current method	153
B.2.5. Measurement in the mass spectrometer	154
B.2.6. Run54 evaluation	154
B.2.7. Preparing for fitting software	154

C. Fieldbook entries of the sampling sites	157
D. Further results	173
D.1. Figures	173
D.2. Tables	177
D.2.1. Noble 2007	183
References	204

Glossary

Abbreviation	Description
ACT	Activated charcoal trap
AEW	Air equilibrated water, used as a laboratory standard for water samples
ALK	Hydrologic carbon dating model using geochemical parameters under closed system conditions
ALK mod	Hydrologic carbon dating model using geochemical parameters under mixed open and closed system conditions
C13	Hydrologic carbon dating model using carbon isotope ratios under closed system conditions
C13 mod	Hydrologic carbon dating model using carbon isotope ratios under mixed closed and open system conditions
C13 Mün	Hydrologic carbon dating model using carbon isotope ratios under open system conditions
CE	Excess air model considering closed system equilibration
CMB calc	Hydrologic carbon dating model using the chemical mass balance
CMB meas	Hydrologic carbon dating model using the chemical mass balance based on measurements
CRY	Group of wells situated in the recharge area puncturing crystalline rock
DIC	Dissolved inorganic carbon
ECBBF	East Cambay Basin Bounding Fault, extensional fault in Gujarat
F&G Alk	Hydrologic carbon dating model using isotope ratios and geochemical parameters
F&G mod	Hydrologic carbon dating model using isotope ratios and geochemical parameters under mixed open and closed system conditions

Abbreviation	Description
GMWL	Global meteoric water line
LGM	Last Glacial Maximum
LMWL	Local meteoric water line
MAAT	Mean annual air temperature
MAST	Mean annual soil temperature
MORB	Middle ocean ridge basalt
NAAT	North Atlantic air temperature
NAO	North Atlantic oscillation
NGT	Noble gas temperature
OD	Excess air model considering oxygen depletion
P	Group of wells used for the palaeorecord
P GLA	Group of wells used for the palaeorecord, last glacial period
P LHO	Group of wells used for the palaeorecord, late Holocene
P MOD	Group of wells used for the palaeorecord, modern
P OPT	Group of wells used for the palaeorecord, early Holocene and climate optimum
P PLE	Group of wells used for the palaeorecord, late Pleistocene before last glacial maximum
P TRA	Group of wells used for the palaeorecord, transition between Holocene and Glacial
PD	Excess air model considering partial degassing
pmC	Percent modern carbon
PR	Excess air model considering partial re-equilibration
SAT	Surface air temperature
SST	Stainless steel trap (not to be confused with sea surface temperature)
STAT	Hydrologic carbon dating model using statistics
STAT meas	Hydrologic carbon dating model using statistics based on measurements
THC	Thermohaline circulation
TS-CRY	Group of thermal springs situated in the recharge area of crystalline geology

Abbreviation	Description
TS-P PLE	Group of thermal wells (former artesian springs) situated in the discharge area
UA	Excess air model considering unfractionated air
WCBBF	West Cambay Basin Bounding Fault, extensional fault in Gujarat
WTT	Water table temperature

1. Introduction

The best of prophets of the future is the past.

– Lord Byron

Climate change is a major issue of our times. In the past, changes of insolation and albedo on Earth caused cold glacial periods or warm interglacials. In modern times, another aspect affecting climate is the anthropogenic influence due to emission of greenhouse gases. The inter-governmental panel on climate change (IPCC) confirmed a human impact on climate change in the “Fourth Assessment Report” [IPCC, 2007], and predicts global warming. To predict the future of climate change, the complex system of the Earth’s climate, relations, couplings and feedback mechanisms in the environment need to be understood. Understanding the reactions of the system can only be achieved by studying the climate of the past with respect to the factors determining climate, primarily solar forcing. Since human documentation of our climate does not exceed some thousand years (and instrumental documentation only some hundred years), environmental records of climate need to be investigated.

These so-called palaeorecords were found in ice cores from Greenland or Antarctica, in sea or lake sediment cores, coral or tree ring records and stalagmites. The tools to derive climate information from these records are mainly changes in isotope ratios which are affected by climatic changes in particular ways, or inferred e.g. from foraminifer or pollen data in sediments.

As shown in this project, groundwater aquifers are also used as an archive for palaeorecords. Groundwater is a routinely explored continental archive providing a quantitative temperature information with its dissolved noble gas content. For this reason, there is a worldwide search for suitable aquifer systems.

This project is the first attempt to study a groundwater aquifer as a palaeorecord in South Asia. In North-West India, a semi-arid region affected by Indian summer monsoon was studied. The main interest was obtaining information about the recharge temperature behaviour and changes in humidity. Apart from the palaeorecord study, other goals of the project were examining occurrence of natural SF₆, mantle and radiogenic He components, as well as investigating the recharge and flow pattern of the groundwater aquifer in the unconfined and confined zone.

The aquifer contains a palaeotemperature proxy displaying the recharge conditions. The proxy is derived from the archive by measuring dissolved noble gases. Furthermore, monsoon behaviour is studied from combined noble gas concentration and stable isotope data. For this purpose, I increased the performance of the mass spectrometric measurement to meet the high

requirements for determining absolute noble gas concentrations. The aim was creating a complete record of palaeotemperature and precipitation behaviour from the last glacial maximum until today. Data of this kind is of paramount importance for thorough predictions of future climate.

2. Basics

The physical system Earth consists of different subsystems such as the geosphere, the atmosphere, or the hydrosphere. All of the Earth's oceans, the ice caps, rivers, lakes and its groundwater are called hydrosphere. Oceans, rivers and lakes are in contact and therefore exchange with the atmosphere, while moist soil and groundwater infiltrate the geosphere and additionally dissolve and exchange with solids.

To understand the system of groundwater, its interconnection with the geosphere (section 2.1) and the atmosphere (section 2.2), as well as the environmental tracers used in this study (2.3) need to be introduced.

2.1. General Hydrogeology

Groundwater is an eminent part of nature's freshwater resources. However, groundwater is just a trivial small part of the hydrosphere and the Earth's water budget (Table 2.1).

Table 2.1.: The abundance of water in the different components of the hydrosphere [Mook and de Vries, 2001]

Component	Volume 10^3 km^3	% total	% fresh water
Oceans	1350000	97.3	
Freshwater	36000	2.7	100
Ice	27700		77
Groundwater	8000		22
Lakes	225		0.6
Moist soil	70		0.2
Atmosphere	15		0.04
Rivers	2		0.005
Biosphere	2		0.005
Total	1390000	100	

2.1.1. Groundwater flow

Groundwater depends on its geological environment. The soil and rock matrix influences water storage and flow. Sedimentary ground is permeable for water because its pore volume allows constant flow of water masses with some dispersion, while fissures or cavities provide an abrupt and inhomogeneous flow. Dissolution of chemicals or reactions in the water are also influenced by the ground matrix.

An important parameter is the porosity $n_{\text{por}} = \frac{V_{\text{por}}}{V_{\text{tot}}}$ with n_{por} given by the air and water volume in a soil parcel, giving every soil material a characteristic number to describe its water capacity or porosity. Examples are 45-55 % for clay, 40-50 % for silt, 30-40 % for sand, 20-40% for gravel, 1-10 % for limestone [Todd, 1980]. Porosity is mainly influenced by grain shape and size. Pore volume that does not participate in gravitational water movement is excluded from the effective porosity n_{eff} , while n_{tot} includes the whole pore volume.

Groundwater originates from rain or surface drainage. The upper zone of the ground has a mixture of water and air in its pores. This zone is called the vadose or unsaturated zone with a thickness of several meters, in arid regions up to several tens of meters. By gravitation, water is directed deeper to available free space in the soil, and slowed down by capillary and adhesion forces. Between water compounds and ground matrix, empty zones of air occur. These are interconnected with each other up to the atmosphere and often build an open system. The zone where air packages become rare with depth, and the hydrostatic pressure equals atmospheric pressure, is defined as the water table. Below, the saturated zone of groundwater begins. The water table often varies over seasonal or annual timescales, depending on precipitation amounts and evaporation. Due to this fluctuation, an intermediate zone filled with air bubbles develops below the water table.

The unsaturated zone of the soil is mostly a zone of high biologic and chemical activity. Plant roots, microorganisms such as bacteria, fungi and small animals inhabit this reservoir. Gaseous carbonate enters the soil through the plants' root respiration or is transformed through decomposition of biologic material by bacteria. As a result, the atmospheric oxygen fraction in the soil becomes depleted. The degree of oxygen depletion depends on the soil material and its porosity, but also on temperature and humidity. Biologic processes produce fermentation gases such as CO_2 , CO , NO_x , CH_4 or N_2 [Scheffer and Schachtschabel, 1960] as a replacement.

One of the first approaches to determine the flow of groundwater was Darcy's empirical law for the specific discharge called Darcy or filtration velocity $v = \frac{Q}{A} = K \cdot \frac{\partial h}{\partial z}$, applied to laminar flow in small pores and at small gradients. A is the cross section of the aquifer, while $\frac{\partial h}{\partial z}$ denotes the hydraulic gradient. K is called hydraulic conductivity and is a soil material specific value (examples found in Todd [1980]). The actual velocity or tracer velocity

in groundwater $v = z/t$ is connected with the so-called Darcy velocity via the relation $v_{\text{tracer}} = \frac{v_{\text{darcy}}}{n_{\text{eff}}}$. The Darcy velocity can be tested by a strong hydraulic pulse sent through the aquifer. It cannot be observed using the example of normal precipitation peaks as input signals and the corresponding output signals.

An example: With a hydraulic conductivity of about $10^{-2} \frac{\text{m}}{\text{s}}$ for fine sand and a total porosity of about 50%, with a vertical drop of 50 m and a horizontal distance of 10 km travelled, one obtains a Darcy velocity of $v_{\text{darcy}} = 5 \cdot 10^{-5} \frac{\text{m}}{\text{s}} \approx 1.5 \frac{\text{km}}{\text{yr}}$ and therefore a tracer velocity of $v_{\text{tracer}} = 3 \frac{\text{km}}{\text{yr}}$.

2.1.2. Transport models

Darcy's estimation is a very simple approach to describe water flow in groundwater. Three very simple lumped-parameter models describe different ways of tracer transport in aquifers. A lumped parameter model assumes that the flow pattern is constant and the whole system can be described by a mathematical relation. Input and output concentrations of tracers passing the groundwater system are related to the general equation [Mook and de Vries, 2001]

$$C(t) = \int_0^{\infty} C_{\text{in}}(t-t')g(t')\exp(-\lambda t)dt'$$

The function $g(t')$ is called transit-time distribution and has an integral of one over the total timescale of observation. In case of a radioactive tracer, an exponential decay term is included in form of the decay constant λ . The most plain model approach is the **piston-flow** model

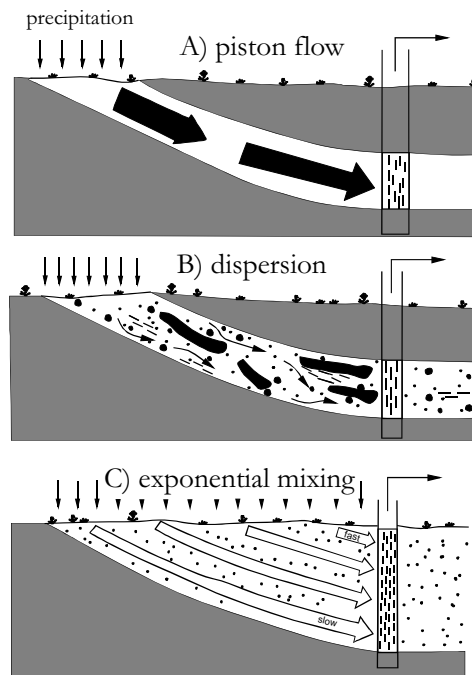


Figure 2.1.: Different flow models: Simple examples of a piston-flow (A), a dispersive flow (B) and an exponential flow model (C) are shown [Mook and de Vries, 2001].

with all flow lines having the same transit time. Between recharge and discharge or the point

of sampling (at a well), the aquifer can be described as a tube behaving just according to the Darcy law (see Fig. 2.1 A). When a new water parcel enters the recharge, all other parcels are shifted “downhill”. Tracer information does not become diluted or changed in any way and always shows just the time stamp of the infiltration time. With conservative flow and very discrete screen depths at wells, groundwater studies may assume piston-flow for their water samples in first approximation. As a mathematical characterisation, the response function (or transit-time distribution) of the system is a delta function.

$$g(t') = \delta(t' - t_t)$$

$$C(t) = C_{\text{in}}(t - t_t)\exp(-\lambda t)$$

In most cases, groundwater undergoes dispersive mixing while flowing through the aquifer matrix due to different flow paths branching and joining again (see Fig. 2.1 B). An instantaneous signal becomes blurred into a Gauss curve which is also the mathematical characterisation. The **dispersion** (parameter is P_D) happening to all groundwater packages limits the resolution of palaeoclimate records derived from groundwater aquifers.

$$g(t') = \sqrt{\frac{t'^2}{4\pi P_D t'/t_t}} \exp\left[-\frac{(1 - t'/t_t)^2}{4P_D t'/t_t}\right]$$

In an open aquifer with groundwater travelling in a certain direction, water on the longest flow line may take a very long time to travel while the shortest flow lines near the surface are covered quickly, mixing excluded. A well with a screen tapping all flow lines of an aquifer produces a mixture of every water parcel in different intensity beginning with the time of first infiltration (see Fig. 2.1 C). Due to the response function, this is called the **exponential** model.

$$g(t') = \frac{1}{t_t} \exp\left(-\frac{t'}{t_t}\right)$$

A combination of different models may be necessary to best describe a realistic aquifer system.

2.1.3. Ground temperatures

Different definitions of temperature play a role in the surface-soil system. Meteorologists measure a place’s surface air temperature (**SAT**) two meters above the ground in a shady place. It is the basis of the mean annual air temperature (**MAAT**). In the ground, temperatures change according to depth. The temperature in the uppermost layer of soil equals roughly the surface air temperature under certain conditions, as long as the soil is not covered with snow, or exposed to sunlight, or does not show abnormal heat flow: Snow-covered soil normally has a higher temperature than air temperature, which is the reason why plant seeds and animals survive winters. Soil exposed to direct sunlight often heats up to much higher temperatures than the region’s air temperature. In regions with abnormal heat flow (volcanic regions as

e.g. Iceland), the ground may be much warmer than the air. In any case, annual oscillations disappear with increasing depth ([Stute and Schlosser, 1993], Fig. 2.2) and balance to a constant mean temperature defined as the ground temperature.

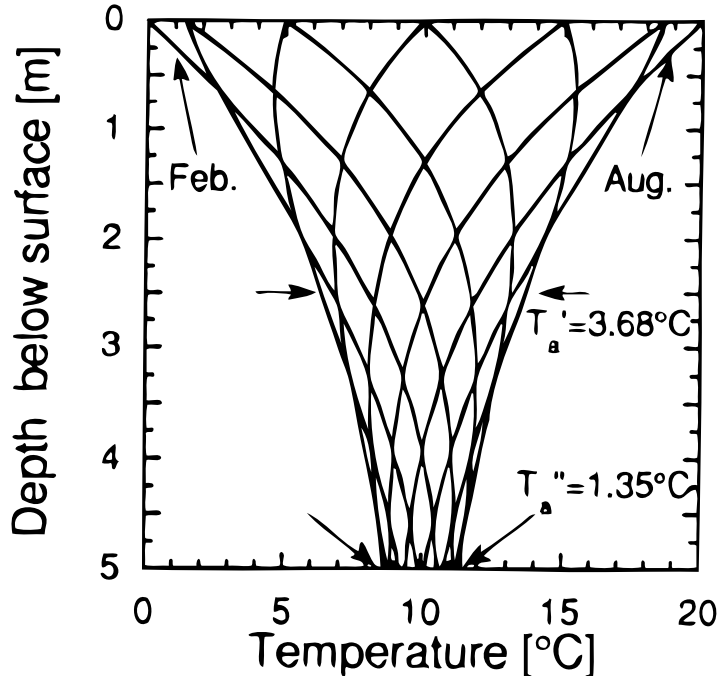


Figure 2.2.: Damping of annual oscillation in air temperature in the ground shown versus increasing depth [Stute and Schlosser, 1993].

With increasing depth, the ground temperature becomes more and more influenced by geothermal heat flow, which is about 30 degrees per kilometre in most parts of the world [Bischof, 1837]. In most cases, the water table in infiltration regions lies at a depth where geothermal heating is still negligible, while the annual seasonal temperature fluctuation is mostly annulated. Water table temperature (WTT) therefore equals ground temperature and the mean annual soil temperature (MAST), but deviates from MAAT. In temperate zones where the length of the snow covered period changed over palaeoclimatic timescales, this deviation between MAAT and WTT changed with different glaciation. In regions with a temperate climate but without snow cover, longterm changes in MAAT show the same changes in WTT [Cey, 2009]. If a region's climate is semi-arid or arid, humidity changes in the soil may influence the MAST. A dry soil heats up in sunny areas to temperatures higher than the MAAT. Vegetation and humidity damp this behaviour and result in a lower MAST [Beyerle *et al.*, 2003]. Therefore, on long timescales, a change in humidity changes the MAST towards cooler (in case of more humidity) or warmer (less humidity) temperatures without an actual MAAT change. For groundwater palaeoclimate studies, it is important to keep these different definitions of temperature in mind.

2.2. Region of Gujarat



(a) Buildings and drainage channels of Lothal



(b) The preserved dock area of Lothal

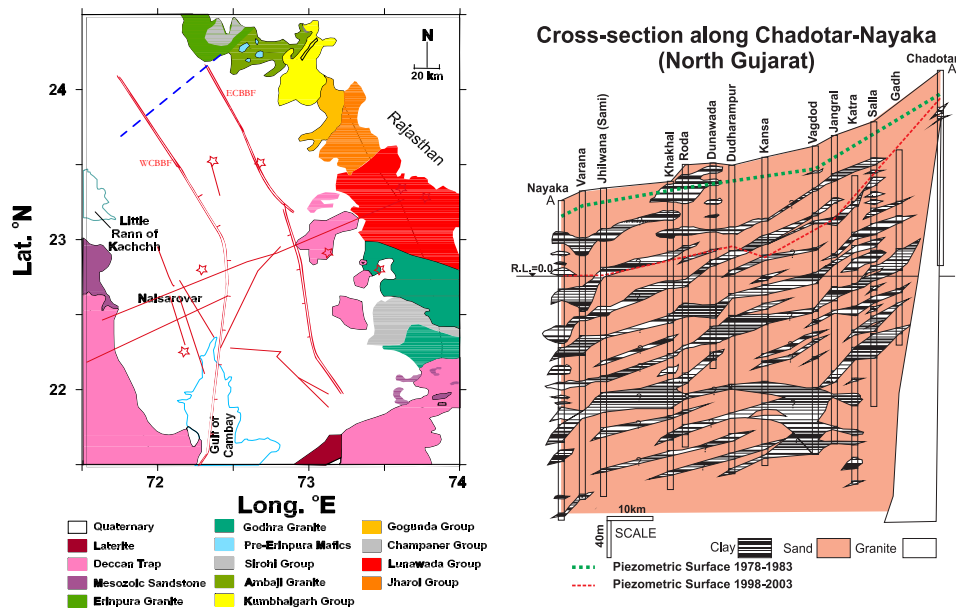
Figure 2.3.: The archeological site Lothal, one of the Indus valley civilisation settlements.

Gujarat is a state of the Republic of India, situated in the North-West of the country. It lies at the coast of the Arabian Sea, near the border of the neighbour country Pakistan. Its population exceeds 50 million people. With roughly six million people, the biggest city of Gujarat is Ahmedabad, the domicile of the Physical Research Laboratory (PRL), the project's cooperation partner. Gandhinagar is its capital. Gujarat is one of India's most prosperous states, and plays a major role in India's economy, energy resources, industrial and agricultural production. Its historic importance includes the first Indus Valley Civilisations (Fig. 2.3), one of the world's first ports with a dockyard (Fig. 2.3(b)) as well as India's "father of the nation", Mohandas Gandhi, whose birth place and legacy is situated in Gujarat.

2.2.1. Geology

Gujarat is situated roughly between 20° and 25° North and 68.5 and 75° East. Its western border is a coastal line drawing the outline of the peninsula Saurashtra, while the eastern border is formed by the rocky foothills of the Aravalli mountains. In the northern area, the Kachchh desert defines the landscape, while the vast alluvial plains shaping the central mainland extend to its southern borders.

The geology of the region is shown in Fig. 2.4(a). The Aravalli foothills in the north-eastern part of the country have an age up to the Precambrium with 2.5 Gyrs and consist of granite and other crystalline plutonites. The Indian continent was part of the Gondwana continent until the Cretaceous. When it broke off and travelled north, it passed the Hot spot of La Reunion, causing huge magmatic eruptions forming the Deccan trap regions [Bhattacharya and Subrahmanyam, 1986] on the peninsula and southern part of Gujarat. The alluvial plains were formed most recently and filled up the Cambay basin formed due to Graben formation (Fig. 2.4(b)). The Indian peninsula is divided from the northern foreland block by the Narmada-Son lineament discovered by Joseph G. Medlicott. Extension faults were formed due to stretching of the Cambay graben as well as the western Continental Shelf (Fig. 2.4), generating the East



(a) Geological map of Gujarat [Deshpande, 2006]. Different deposits are indicated. Fault zones are sketched in as red lines, thermal springs as stars. (b) A cross section from Deshpande [2006] of the blue line shown in Fig. 2.4(a). Clay and sand layers are shown as well as the crystalline rock situated in the recharge. Piezometric surfaces of different times are shown.

Figure 2.4.: Geology of Gujarat.

Cambay Basin Bounding Fault **ECBBF** and the West Cambay Basin Bounding Fault **WCBBF**. The sediments filling the basin descend from both fluvial and aeolian origin, the youngest layers from the Quaternary (referred to as the so-called “Gujarat Alluvium”). These young sediments have a thickness ranging from 300 to 800 m in their deeper places [Deshpande, 2006]. Some deposits originate from marine sedimentation, producing layers of marine calcite, or of fluviomarine (mostly the case on the mainland), fluvial and aeolian deposits. The huge amount of sediment is owed to the large fluvial systems of the major rivers Narmada, Mahi, Sabarmati and Luni [Merh, 1995]. The rivers roughly follow the general slope of the region, descending from the north-eastern highlands to the depression zone between mainland Gujarat and the Saurashtra peninsula in the South-West (Fig. 2.5). Groundwater tapped from the sediments is only consumable from layers of 300 m depth or less, as deeper layers contain too much salt [Merh, 1995]. Due to its history, the depression zone contains high salt concentrations, as it was submerged in prehistoric times by the Arabian Sea. Deeper layers of the basin consist of terrigenous or older sediments such as clay, sand, claystone, sandstone and conglomerate layers. The sediment in the middle of the basin has a depth of several kilometres [Deshpande, 2006] [Gombos Jr. *et al.*, 1995]. Besides the monsoon months in summer, precipitation in Gujarat originates only from thunderstorm events. Most rainfall takes place in the eastern highlands, infiltrating the sedimentary layers and feeding a sedimentary aquifer system which is directed south-west.

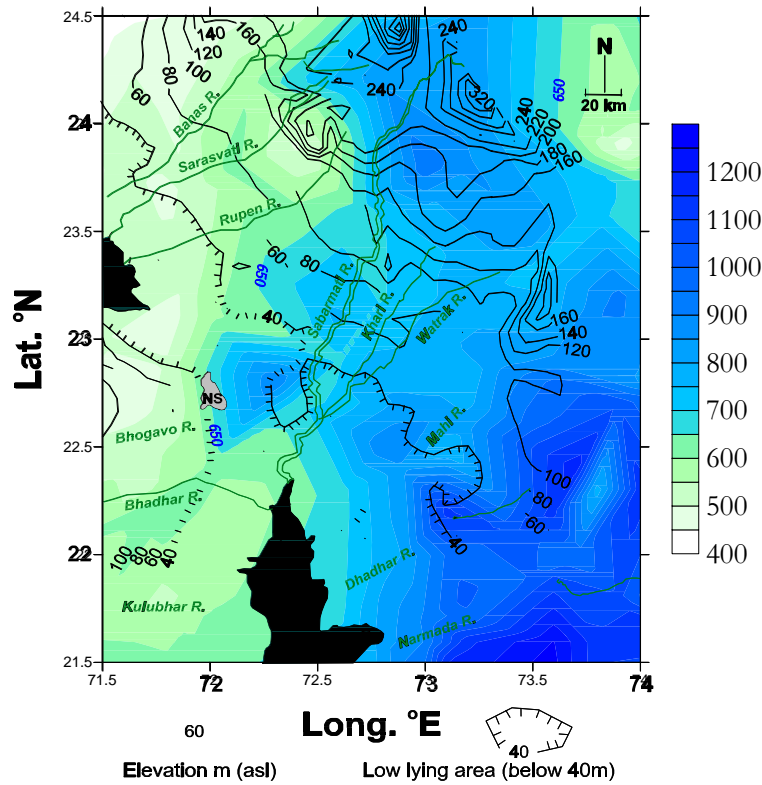


Figure 2.5.: Annual rainfall in mm/yr (see color scale) in Gujarat (data from NOAA [2010a]). Additionally, elevation is indicated by black isolines (meters a.s.l.) [Deshpande, 2006].

Hydrology

Evapotranspiration in Gujarat has a great effect on groundwater due to the high temperature (MAAT of 27.5°C) and strong aridity during most of the year (see Fig. 2.6). Furthermore, intense irrigation in the region since the green revolution has led to a massive piezometric decline of more than 3 m/yr in the course of the last decades (Fig. 2.4, and A.1). Since the aquifer system is confined west of the ECBBF, most of the irrigation water does not reach the aquifer again. This may have a stronger effect in regions of higher vertical permeability such as the recharge area [Rushton, 1986], where most of the region's precipitation feeding the aquifer system occurs (Fig. 2.5).

A distinctive feature of Gujarat's aquifer system is high fluoride concentration (sometimes ten times the drinking water limit) in water of some specific layers [Gupta *et al.*, 2005]. Tapped groundwater from some of these wells is harmful to health. Affected villages show high numbers of skeletal fluorosis, as the poor population cannot afford bottled water or is not aware of the risks. Another characteristic of the aquifer system seems to be a high helium concentration as well as a high geothermal heat flow [Gupta and Deshpande, 2003]. The origin of high helium concentrations will be examined in this project (see section 3.1.1, Fig. 3.7).

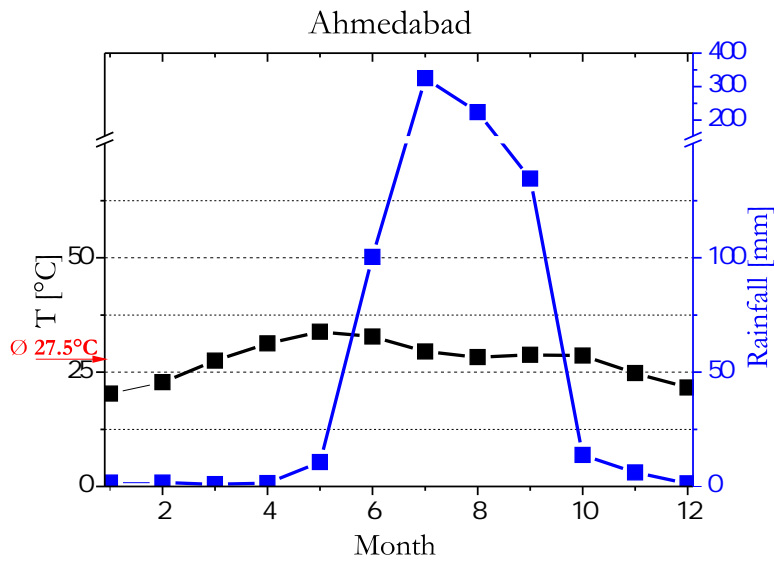


Figure 2.6.: Climate diagram of Ahmedabad. The MAAT of the city is 27.5°C. Data from [www.worldclimate.com, 2010].

2.2.2. Monsoon and Palaeoclimate

Indian Summer Monsoon

The intertropical convergence zone (ITCZ) describes the atmosphere zone near the equator where the passat winds from the northern and southern hemispheres converge. In the zone of maximum solar insolation close to the equator, heated air rises and leaves a low pressure area near the surface embracing the world which is filled up with air flowing towards the equator. Due to the Coriolis force, the air flow is redirected towards the West. The effect of surface heating is much weaker over the oceans than over the continents. Much higher temperatures are reached over land, which again leads to stronger shaped low pressure areas. Therefore, the belt of the ITCZ is situated much more straight-lined over the oceans than over the continents. This continental influence is especially observed in South Asia, resulting in the monsoonal wind.

Due to the strong heating of the airmasses situated over the Asian landmass (Tibetan plateau), the Jun-Aug ITCZ is strongly shifted towards the North in South Asia, with a high pressure area in the South Arabian Sea forcing huge amounts of moist airmasses to travel towards this region. In this region, a change of wind direction due to the Coriolis force occurs as the wind travels away from the equator and is therefore diverted towards the East and not towards the West.

The Dec-Feb ITCZ lies far south of the Indian subcontinent with dry and cool airmasses travelling from the Tibetan plateau over India towards the Horn of Africa where the ITCZ is again shifted further towards the South (compare Fig. 2.7, [Rödel, 1996]).

As a result, the **weather in North-West India** behaves as follows:

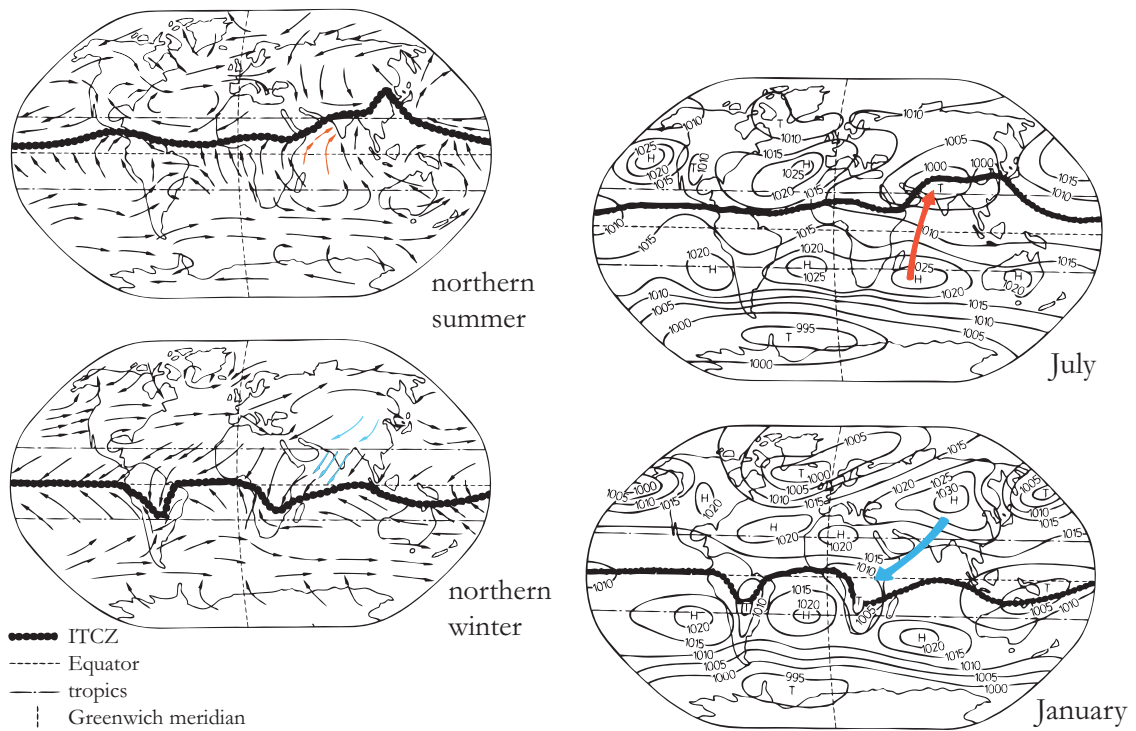


Figure 2.7.: The ITCZ in global perspective. In the summer of the northern hemisphere, the ITCZ is north of the equator, in the winter, it is vice versa. The trade wind on the ITCZ comes from the East and is located in a low pressure zone, while north and south of the ITCZ, air masses travel towards the ITCZ from high pressure zones. Over continents, irregularities of the position occur. Adapted from Rödel [1996].

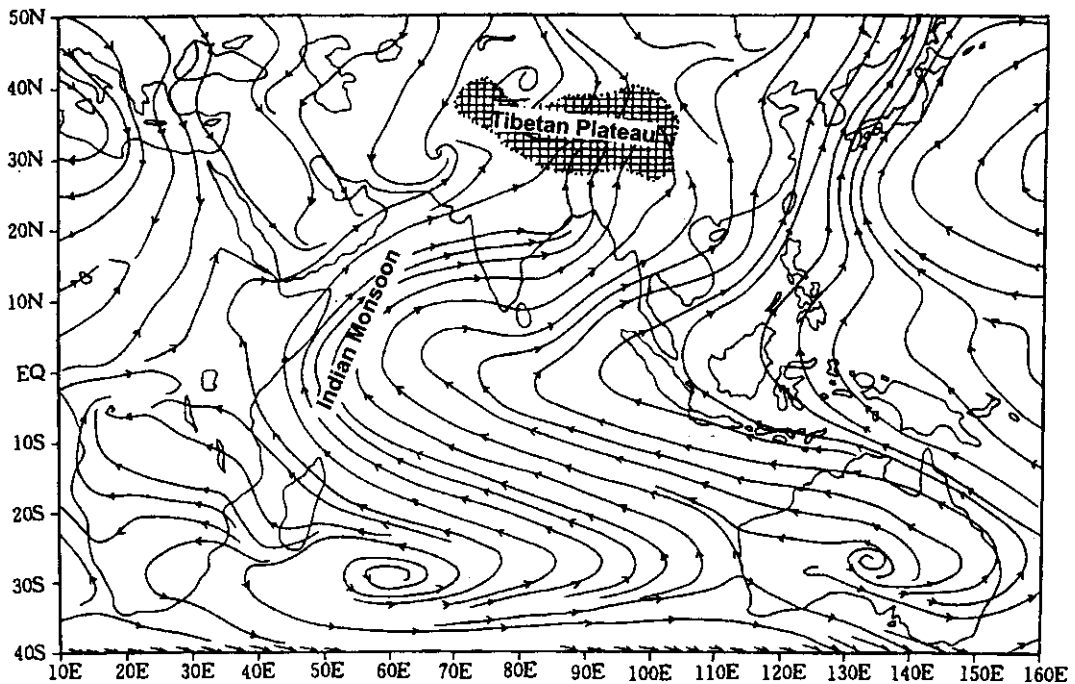


Figure 2.8.: Monsoonal winds of June to August drawn by Shi *et al.* [2001] with data from [Kalnay *et al.*, 1996].

In early summer with increasing heat, moist air masses from the sea bring very strong rainfalls, producing strong precipitation in the summer months which are therefore called the rainy season (red arrows in Fig. 2.7).

In autumn, the rainfall as well as the strong winds from the sea decline, ending in a reversion of the wind direction. Continental wind is established in the winter months with dry and relatively cold air from the Himalayas (blue arrows in Fig. 2.7). In this dry season, rainfall is rare and mostly results from thunderstorms. With oncoming spring and summer, the landmasses begin to heat up again due to insolation. The wind directions of the summer monsoon are shown in Fig. 2.8. Simulations of typical air trajectories over one year are shown in Fig. A.2.

Palaeoclimatic studies have detected an interconnection between warm global climate and intense monsoon occurrence [Kutzbach, 1981], as the ITCZ is forced further towards the North with stronger solar insolation (e.g. [Fleitmann *et al.*, 2007]). Millennial-scale monsoon events are furthermore attributed to changes in North Atlantic Oscillation (NAO) ([Gupta *et al.*, 2003] among others). Higher solar variation [Neff *et al.*, 2001] and north atlantic air temperature (NAAT) [Fleitmann *et al.*, 2003a] coincide with enhanced monsoon precipitation. Monsoon behaviour is correlated to the Greenland GISP ice cores with certain phase shifts [Schulz *et al.*, 1998]. This is explained by a weaker thermohaline circulation (THC) which induces a lower NAAT and an increase of snow cover in Eurasia [Barnett *et al.*, 1988]. As a consequence, the Tibetan plateau experiences a reduced spring heating due to a higher albedo. Therefore, the summer temperature is lower, leading to a weaker land-sea pressure gradient and therefore weaker monsoon winds. A direct linear link between solar insolation and monsoon behaviour without time lags was not established until the global decline of glaciers in the early Holocene [Overpeck *et al.*, 1996].

Implications for the future may be a monsoonal strengthening due to global warming [IPCC, 2007].

Prospects of palaeoclimate studies

The palaeoclimate of India is described by numerous studies. While many of these studies were situated in the region that is the topic of this project such as the Tharr desert, Lake Nal Sarovar, sea sediment cores from the Arabian Sea, river sediment cores or dune sediment cores from Sabarmati or Mahi river, others target a wider area. Nonetheless, their information is important, as palaeomonsoon behaviour was very similar all over India [Ramesh, 2001].

Pleistocene: In late Pleistocene times from 30 to 50 kyrs BP, moderate wet conditions occurred in Central Asia [Herzschuh, 2006]. Dune and alluvial deposits [Juyal *et al.*, 2003] [Juyal *et al.*, 2006] near the project location indicate an enhanced monsoon that declined around peak glacial times from 28 kyr to 11 kyr BP. Few precipitation is indicated and arid conditions

found, as the alluvial deposits from flood plain aggradation make room for aeolian deposits. Furthermore, pollen studies in salt lakes show arid conditions [Singh *et al.*, 1990]. Stalagmite data supports these discoveries [Fleitmann *et al.*, 2003b] [Wang *et al.*, 2008].

Early Holocene: With the end of the last glacial maximum (LGM), a strong monsoon phase occurred and left marks in lake [Enzel *et al.*, 1999] [Prasad *et al.*, 1997] and river sediments [Juyal *et al.*, 2003] and their isotopic condition. Due to the drainage, climate information is also obtained from sea sediment cores analysing the growth-rate of pollen or the stable isotope ratio of foraminifera [Gupta *et al.*, 2003] [Overpeck *et al.*, 1996] [Staubwasser *et al.*, 2002]. Stalagmites in Oman [Fleitmann *et al.*, 2003a] [Fleitmann *et al.*, 2007], China [Wang *et al.*, 2001] [Wang *et al.*, 2005] [Wang *et al.*, 2008] and India [Ramesh, 2001] with stable isotope data also show enhanced precipitation due to the amount effect (introduced later in 2.3.1), which is also predicted by model simulations [Lee and Swann, 2010]. Temperature information is not provided by isotopic data in this subtropic region [Fleitmann *et al.*, 2007] [Neff *et al.*, 2001] [Yadava and Ramesh, 2005]. Noble gas palaeotemperatures give a quantitative WTT record, as used in this project. The most adjacent studies of this type were done in Oman indicating a present-LGM temperature change of 6.5 °C [Weyhenmeyer *et al.*, 2000], and in China with a result of 4.5 °C [Kreuzer *et al.*, 2009], also indicating an enhanced monsoon in early Holocene. The wet period laid the foundations for the blooming of Indus valley civilisations, a further method to identify this “climate optimum” period with strong humidity and vegetation by archaeological studies [Enzel *et al.*, 1999] [Gupta *et al.*, 2006]. In all these different studies, the climate optimum ranges between 10 to 12 and 5 to 8 kyr BP.

Mid to late Holocene: The wet phase is superseded by a weak monsoon phase with less precipitation which set in gradually [Fleitmann *et al.*, 2003a] [Wang *et al.*, 2005]. Desiccated lakes [Enzel *et al.*, 1999] [Prasad *et al.*, 1997] and piston core data from the Arabian Sea [Gupta *et al.*, 2003] [Staubwasser *et al.*, 2003] [von Rad *et al.*, 1999] as well as a change in vegetation and civilisation [Gupta *et al.*, 2006] indicate this dry period with events of drought. The noble gas study of Niger [Beyerle *et al.*, 2003] also mentions this dry phase in the late Holocene. Several records place this time period from around 5 to 8 until 1 to 2 kyr BP. According to some records, recent time shows more fluctuation [Prasad *et al.*, 1997] [Yadava and Ramesh, 2005] with dry phases around 1 to 2 kyr BP and a wet phase which started about 600 yr BP. The most recent increasing monsoon precipitation may among other reasons result from global warming [Anderson *et al.*, 2002] [IPCC, 2007].

2.3. Environmental Tracers

Tracers are used to “trace” a certain information in the environment. They are properties of a medium or particles enclosed in it traveling freely within the system in small concentra-

tions. They should not have sinks or sources. Tracers in the environment have natural or anthropogenic input uninfluenced by the investigator, or are released as an artificial tracer by scientists (tracer release experiments TRE). TREs cannot be used in palaeoclimate studies ranging over very long timescales. In this study, the research system is a groundwater aquifer, and tracers used are deuterium (isotope ^2H , written as D), oxygen-18 (^{18}O) and carbon-13 (^{13}C) often summarised as the stable isotopes. Furthermore, tritium (^3H , written as T), radiocarbon (^{14}C), sulphur hexafluoride (SF_6) and the noble gases dissolved in water, He, Ne, Ar, Kr, Xe, as well as the radioactive noble gas radon (^{222}Rn) are analysed.

2.3.1. Stable Isotopes

^2H and ^{18}O are rare isotopes of hydrogen and oxygen and are among others found in water molecules. A mathematical way to describe variations in isotope ratios is introduced.

An isotope abundance ratio R is defined by $R = \frac{\text{abundance of rare isotope}}{\text{abundance of abundant isotope}}$ (see [Mook and de Vries, 2001]). In case of isotope fractionation in the reaction $A \rightleftharpoons B$, the *isotope fractionation factor* $\alpha = \frac{R_B}{R_A}$ is the ratio of both isotope ratios. As this ratio is a value close to 1 in most cases, the *fractionation* is defined as

$$\epsilon = \alpha - 1 \quad (2.3.1)$$

for a better resolution (generally given in permil). In a reaction, the rare isotope becomes enriched when $\epsilon > 0$ and depleted when $\epsilon < 0$. When isotope ratios are observed, international comparison becomes important. To report isotope abundances, the delta-notation is used. The observed isotope ratio of a sample A is compared to a reference sample or standard std by

$$\delta = \frac{R_A}{R_{\text{std}}} - 1.$$

For the investigated isotopes, the equations are

$$^2\delta = \frac{^2\text{H}/^1\text{H}_A}{^2\text{H}/^1\text{H}_{\text{std}}} - 1 \text{ for deuterium,}$$

$$^{13}\delta = \frac{^{13}\text{C}/^{12}\text{C}_A}{^{13}\text{C}/^{12}\text{C}_{\text{std}}} - 1 \text{ for carbon - 13 and}$$

$$^{18}\delta = \frac{^{18}\text{O}/^{16}\text{O}_A}{^{18}\text{O}/^{16}\text{O}_{\text{std}}} - 1 \text{ for oxygen - 18.}$$

In these cases, std refers to the Vienna Standard Mean Ocean Water (VSMOW) for $\delta^{18}\text{O}$ and $\delta^2\text{H}$, and Vienna Pee Dee Belimnite (VPDB) for $\delta^{13}\text{C}$. Values are shown in Mook and de Vries

[2001].

Isotopes have the same chemical but different physical attributes. The different mass of the atom may have an influence on reactions and phase transitions, as the mass is connected to the speed of a particle via the Boltzmann distribution:

$$E_{\text{kin}} = \frac{3}{2}kT = \frac{1}{2}mv^2, \Rightarrow m \propto 1/v^2$$

Heavier particles react slower, which is called normal isotope fractionation. It is shown that normal fractionation becomes less apparent with warmer temperatures, which is not astonishing as fractionation is a thermodynamic process dependent on temperature.

The thermodynamic partition function of a system contains information about its statistical properties, and can be used to describe fractionation ratios [Urey, 1947]. It can be expressed by the product of the individual partition functions for the three modes of motion translation, rotation and vibration, $Q = Q_{\text{trans}} \cdot Q_{\text{rot}} \cdot Q_{\text{vibr}}$. While translation and rotation are nearly identical for isotopes of an element, vibration can differ (as e.g. mentioned in Hoefs [2009]). For a chemical reaction, the reaction constant K is defined as

$$K_i = 10^{-pK_i} = \frac{\prod[\text{product}_j]}{\prod[\text{educt}_j]} \quad (2.3.2)$$

The squared brackets indicate molar concentrations of the ion or molecule products and educts. For the isotope exchange reaction $X + Y^* \rightarrow X^* + Y$, the formula is

$$K = \frac{[X^*] \cdot [Y]}{[Y^*] \cdot [X]} = \frac{[X^*]/[X]}{[Y^*]/[Y]},$$

and, as the partition function ratio behaves like the isotope concentrations, can be converted to

$$K = \frac{[Q_X^*]/[Q_X]}{[Q_Y^*]/[Q_Y]} = \frac{R_X}{R_Y} = \alpha_{X \rightarrow Y}$$

The partition function's logarithm is approximately $\ln \frac{Q_2}{Q_1} = \ln \alpha \approx \epsilon$ and is a function of temperature [Criss, 1991] [Hoefs, 2009] [Urey, 1947] linear in $1/T$ for low and $1/T^2$ for high temperatures, ultimately approaching zero fractionation at a temperature infinitely high. The effect is not trivial and dependent on the molecule form. The fractionation can even change sign (called crossover) depending on the thermal effect on vibration and the effect of vibration on isotope fractionation [Stern *et al.*, 1968]. For tracers of the hydrological cycle, a temperature increase normally means a weaker fractionation effect (as studied by [Bottinga, 1969], shown in Fig. 2.9).

Other types of fractionation exist, inverse isotope fractionation favours the heavy isotopes in reactions, and mass independent fractionation is not dependent on the isotope mass at all. In that case, characteristics of the atom's core are varying for different isotopes.

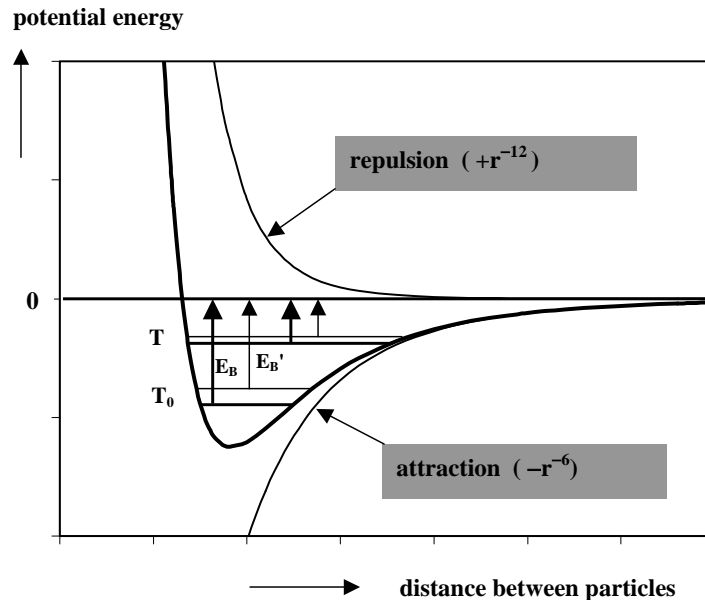


Figure 2.9.: Normal isotope fractionation occurs e.g. as heavier particles can emerge less easily from a bound state in an energetic potential well. The effect becomes less apparent for higher temperature [Mook and de Vries, 2001].

Generally, fractionation can be separated into equilibrium fractionation (reactions in either direction are equally pronounced) and kinetic fractionation happening under non-equilibrium conditions (one direction of reaction is favoured).

Isotopes in Hydrology

In the hydrologic cycle, fractionation occurs in every step of evaporation or precipitation caused by condensation in clouds.

In **evaporation**, it is eminent to discuss the nature of fractionation. The fractionation in isotopic equilibrium can only be reached in a well mixed system and at slow reaction rates with chemical reaction rates in equilibrium forward and backward. Equilibrium fractionation in evaporation is based on different molecular binding energies of the water molecule. Heavier isotopes are enriched in the liquid phase and depleted in vapour, while water molecules with light isotopes change into the gaseous phase more easily.

If a process does not take place under equilibrium conditions, the molecular binding energy is not as important for fractionation processes as diffusion coefficients or particle velocities.

Therefore, this kinetic fractionation results in different isotope fractionation ratios. This is the case with evaporation over the oceans. Under ideal conditions, equilibrium fractionation would take place, but in reality kinetic fractionation prevails. An indicator for the degree of kinetic fractionation is the surface water vapour, as vapour saturated air indicates a quasi stable milieu for equilibrium.

Condensation of water in clouds happens in vapour saturated air and is an equilibrium reaction. Heavy isotopes are enriched in the liquid phase and depleted in the remaining gaseous phase.

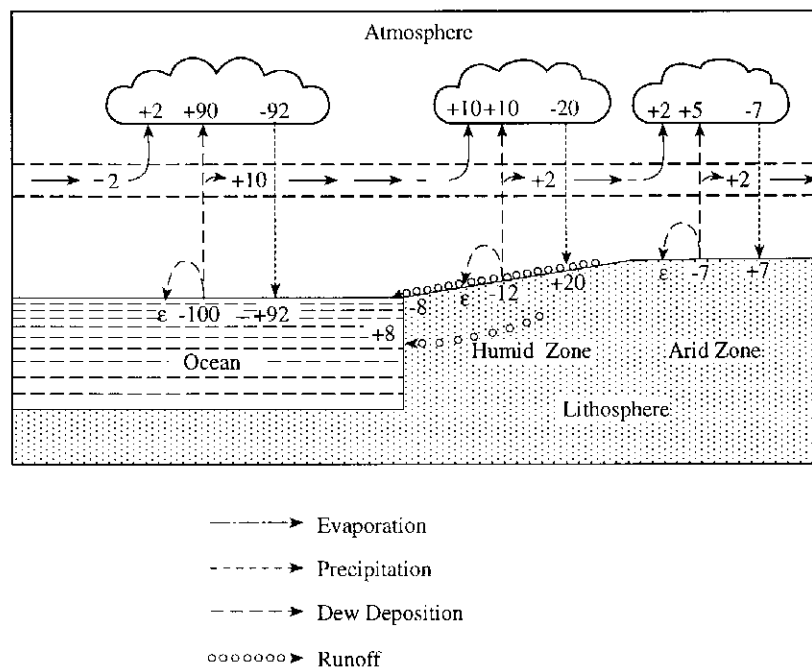


Figure 2.10.: Evaporation and vapour production in different regions [Gat, 1996]. The numbers are relative flux units with 100 units as the marine evaporation flux. It is evident that the greatest source of evaporation is the ocean.

Most water is assumed to evaporate over the ocean (see Fig. 2.10), and mostly in the tropics where the solar radiation is highest. Due to the reservoir size, evaporation hardly changes the isotopic composition of the oceans.

As a result of the two different sorts of fractionation taking place in the cycle, the isotope ratio of precipitation is behaving differently for δD than for $\delta^{18}O$. Gonfiantini [1986] approximates kinetic fractionation of oxygen and hydrogen with humidity and empirically shows a greater fractionation for oxygen than hydrogen, leading to a deuterium excess in the vapour reservoir. For an average humidity of 85%, the global meteoric water line (GMWL),

$$\delta D = 8 \cdot \delta^{18}O + 10[\text{‰}],$$

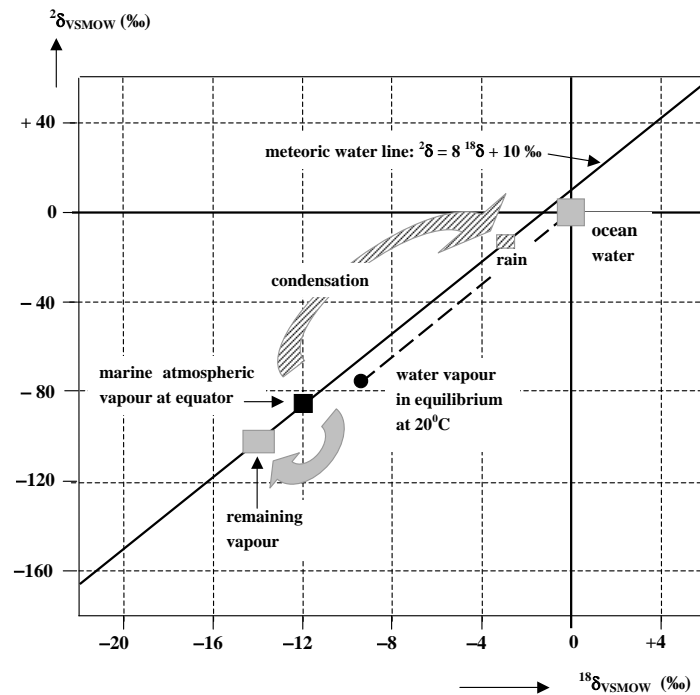


Figure 2.11.: δD is plotted versus $\delta^{18}O$ for precipitation, generating the meteoric water line. Due to continuous evaporation and condensation steps, a line is generated [Mook and de Vries, 2001].

is the global average of precipitation, as observed by Craig [1961] (shown in Fig. 2.11) and extensively studied in the GNIP database [Rozanski *et al.*, 1993]. Local meteoric water lines (LMWL) of different locations differ from this line in slope and deuterium excess. According to Merlivat and Jouzel [1979], deuterium excess is mainly dependent on the humidity in the source region. A change of deuterium excess in a region may therefore indicate a change of the precipitation source. This may result from a change in overall meteoric wind directions, or a change in humidity of the source itself [Sonntag *et al.*, 1979].

Environmental effects of isotope fractionation

Certain environmental parameters change isotope ratios (demonstrated in Fig. 2.12) and are therefore introduced shortly.

Progressive rainout of water vapour masses travelling to regions with lower temperatures (higher latitudes, higher altitudes) leaves the precipitation depleted in $\delta^{18}O$ and δD values. These effects are called **latitude effect** and **altitude effect**.

Local changes and temporal changes in temperature have to be distinguished. Fricke and O'Neil [1999] observed that according to Gat [1996] it is exchange between condensate and water vapour at the warmer temperatures of the cloud base that provides the most reasonable physical basis for the relation between surface temperature and $\delta^{18}O_{\text{precip}}$ values, while the

temperature of the air mass itself controls occurring condensation.

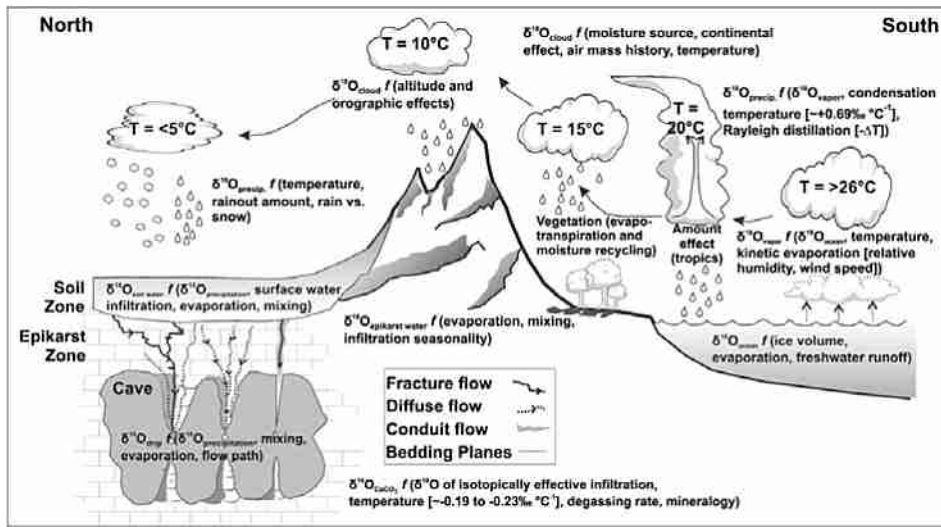


Figure 2.12.: Overview of possible effects on clouds causing isotopic fractionation in the hydrologic cycle [Lachniet, 2009].

The temperature effect was first observed by Dansgaard [1964] in polar regions,

$$\delta^{18}\text{O} = 0.69 \cdot t_{\text{air}} - 13.6\text{‰} \quad (2.3.3)$$

Yurtsever [1975] found a similar correlation derived from four stations Thule, Groenmedal, Nord and Vienna,

$$\delta^{18}\text{O} = 0.52 \cdot t_{\text{air}} - 15\text{‰} \quad (2.3.4)$$

but later [Yurtsever and Gat, 1981] observed in a study of 91 worldwide stations including tropical stations the relationship

$$\delta^{18}\text{O} = 0.34 \cdot t_{\text{air}} - 12\text{‰} \quad (2.3.5)$$

Rozanski *et al.* [1993] observed strong local variability of the slope in the GNIP data. These gradients describe a local temperature effect. The temporal temperature effect is less pronounced [Fricke and O'Neil, 1999]. In the tropics, no noteworthy temperature correlation can be found [Dansgaard, 1964] [Fricke and O'Neil, 1999] [Rozanski *et al.*, 1993] [Yurtsever and Gat, 1981].

Furthermore, as soon as clouds travel over a landmass and no evaporation from an ocean surface occurs, much less water vapour feeds the clouds, and precipitation becomes depleted with increasing distance to the coast, called the **continental effect**.

The amount of rainfall also has an influence on the isotopic ratio of precipitation. Several reasons sum up to the **amount effect** [Lee and Fung, 2008]: Dansgaard [1964] indicates that clouds with heavy rainfall arrive significantly depleted at the region of interest [Lachniet, 2009].

Furthermore, he suggests that little drop sizes equilibrate more completely with the enriched water vapour under clouds, as equilibrium is achieved much faster. Moreover, while there is low humidity in an arid precipitation area, light isotopes are lost much faster from precipitation and transfer into vapour. [Rozanski *et al.* \[1993\]](#) adds to Dansgaard's three reasons a fourth, arguing that in a cloud the isotopic enrichment of raindrops and depletion of vapour declines over precipitation time due to the continuous isotopic exchange between drops and vapour, depleting the rain even further. This effect plays a major role in monsoon rainfall. [Lee and Fung \[2008\]](#) calculated the amount effect with a quantitative model to bring the effect into use for global circulation models. The model showed more detailed information on the amount effect. The vapour under a storm cloud is modelled as well as the rain drop itself, and vapour and drop are gradually depleted for heavier rain rates. The more depleted the original water, the stronger the effect. Heavy isotope depletion correlates with bigger drop sizes. It also correlates with higher relative humidity under the cloud. To sum it up, fractionations of several permil depletion can be achieved in heavy rainfall precipitation. [Lee and Swann \[2010\]](#) modelled a difference in $\delta^{18}\text{O}$ ratio between LGM and the present due to the amount effect. The results for the region of Gujarat are about 1‰.

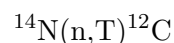
The most depleted precipitation is stored as snowfall and ice at the poles or alpine glaciers. In times of global cooling and great accumulation of ice sheets, the mean oceanic isotope ratio and therefore the source of precipitation becomes enriched. This is called the **global ice-volume effect**. Since the global ocean level was lowered by around 120 m in the last Glacial [[IPCC, 2007](#)] [[Shackleton, 2000](#)], with an average depth around 3800 m and isotope ratios of ice ranging around 40 – 50‰ in $\delta^{18}\text{O}$ [[Lorius and Oeschger, 1994](#)], the resulting enrichment of the sea water is estimated:

$$\delta^{18}\text{O}_{\text{sea}} = -\frac{V_{\text{ice}}}{V_{\text{sea}}} \cdot \delta^{18}\text{O}_{\text{ice}} = 1.2\text{‰} \quad (2.3.6)$$

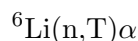
Since all these effects change the isotope ratios in the identical or opposite directions, a palaeoclimatic study of stable isotope measurements can never be trivial. It should be coupled with other climatic tracers, and viewed in respect to other published information about the region.

2.3.2. Tritium

Tritium is the radioactive hydrogen isotope with two neutrons. It is produced naturally by cosmogenic radiation in the stratosphere [[Libby, 1946](#)]



and natural radiation in the lithosphere



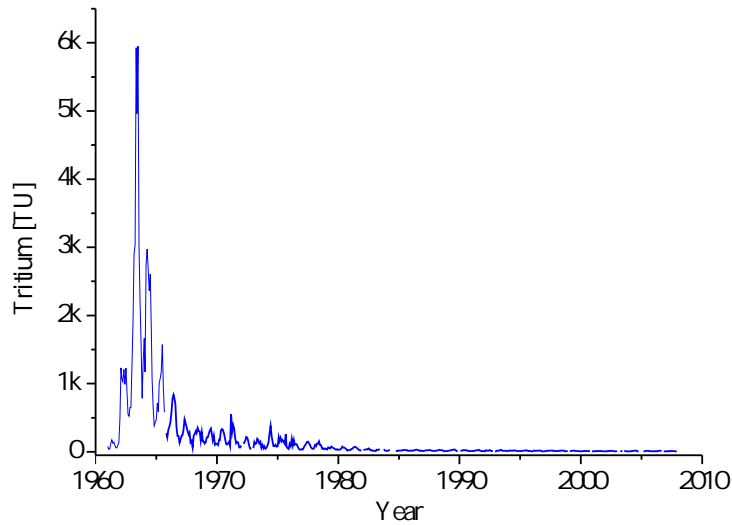


Figure 2.13.: Atmospheric concentration of tritium in TU over the last century in Vienna. The bomb peak around the year 1963 is clearly visible. Tritium concentration has by now nearly reached natural background again. ([Weiss *et al.*, 1979], data derived from IAEA [2007] database for Vienna)

as well as by atmospheric thermonuclear bombtests mainly in the 1960s [IAEA, 2007] [Weiss *et al.*, 1979]. It is part of the hydrological cycle, and decays to ${}^3\text{He}$ via beta decay $\text{T} \rightarrow {}^3\text{He} + \beta^-$ with a half life of 12.32 years [Lucas and Unterweger, 2000]. The chosen unit is called a tritium unit (TU) and is a defined ratio of hydrogen atoms:

$$1\text{TU} = \frac{{}^3\text{H}}{{}^1\text{H}} \cdot 10^{18}$$

While the cosmogenic production rate lies around $2500 \text{ atoms m}^{-2} \text{ s}^{-1}$ varying with geomagnetic latitude [Rozanski *et al.*, 1991], the geogenic production should be at least one order of magnitude smaller and leads to groundwater concentrations of around 0.1 TU [Clark and Fritz, 1997]. However, regional exceptions with high geogenic tritium amounts may occur ([Clark and Fritz, 1997] cite a value of 250 TU in Cigar Lake observed by Fabryka-Martin *et al.* [1994]). Bomb tritium superposed all natural signals since the 1950s with a peak of several thousand TU at 1963, when atmospheric nuclear bomb tests of the US and the USSR were banned. Since that time, the peak has been declining to the natural background of 5 – 10 TU on the northern hemisphere ([Roether, 1967], study of vintage wine), while the southern hemisphere had a lower initial bomb signal of up to 80 TU.

Tritium can be used as a dating tool for young hydrologic records (e.g. for mixing profiles in the ocean [Roether *et al.*, 1970] or groundwater [Münnich, 1968]). The radioactive decay

equation is

$$C(t) = C_0 \exp\left(-\frac{t}{\tau_{1/2}} \ln 2\right) \quad (2.3.7)$$

Since the input curve is highly variable, an unambiguous value of C_0 cannot be found. Therefore, knowing the amount of the daughter isotope ${}^3\text{He}$ can provide much less ambiguous results [Schlosser *et al.*, 1988] [Tolstikhin and Kamenskiy, 1969]. The radioactive decay equation provides the T- ${}^3\text{He}$ age:

$$t = \frac{\tau_{1/2}}{\ln 2} \cdot \ln\left(1 + \frac{C({}^3\text{He}_{\text{trit}})}{C(t)}\right) \quad (2.3.8)$$

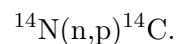
Tritium is widely used e.g. in gaciological dating experiments, since the bomb peak is a very good time marker (e.g. [Schuster *et al.*, 2002]). Recently, a thoroughly done study on dripwater in caves used the pure tritium as well as the T- ${}^3\text{He}$ dating method [Kluge *et al.*, 2010a] [Kluge *et al.*, 2010b]. In groundwater studies observing water older than a hundred years, tritium can be used as knock-out criterion for wells polluted with recent water.

2.3.3. Carbon

For this study, the carbon isotope ${}^{13}\text{C}$ is used as a tracer, and ${}^{14}\text{C}$ as a radioactive dating tracer. In 1950, the average abundance of ${}^{14}\text{C}$ in the atmosphere was about 10^{-12} relative to ${}^{12}\text{C}$. ${}^{13}\text{C}$ has a natural atmospheric abundance of 1.1%.

Production

${}^{14}\text{C}$ is naturally produced by secondary neutrons from cosmogenic radiation entering the atmosphere,



This production rate is dependent on the solar activity visible in sunspot activity [Crowe, 1958] and the variability of the Earth's magnetic field [Beiser, 1957].

Another source is anthropogenic production including bomb testing ([Münnich, 1958] [Rafter and Fergusson, 1957], modern studies with trends by [Levin *et al.*, 2010b]), which is also responsible for anthropogenic tritium production. The bomb tests resulted in a peak in 1963 approximately two times the height of the natural ratio in 1950. By now, it has nearly declined to the natural atmospheric background (Fig. 2.14, [Levin *et al.*, 2010b]).

Carbon cycle

Produced ${}^{14}\text{C}$ is successively oxidised to gaseous CO_2 and mixed into the atmosphere, thereby entering the carbon cycle. Input of CO_2 in surface waters are a hydrosphere carbon reservoir, input in plants are a biosphere carbon reservoir. In hydrology, dissolved carbon can transform

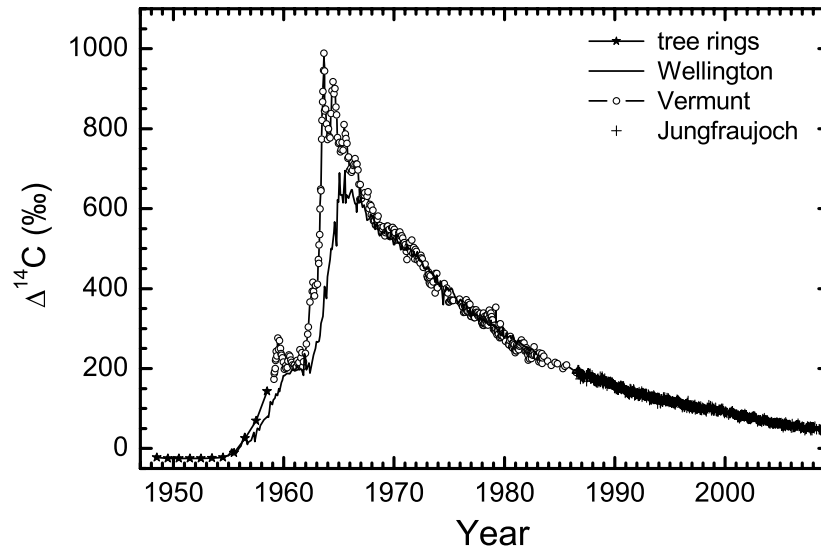


Figure 2.14.: Atmospheric concentration of radiocarbon over the last century [Levin *et al.*, 2010b]. The bomb peak around 1963 is clearly visible (as examined by Münnich [1958], Rafter and Fergusson [1957], modern observations by Levin *et al.* [2010b]). Modern concentrations lie around 105 pmC (converted from $\Delta^{14}\text{C}$ by $\text{pmC} = \left(\frac{\Delta^{14}\text{C}[\text{‰}]}{1000} + 1\right) \cdot 100 [\text{‰}]$). A depletion of the signal is visible before the 1950s, indicating the Suess effect [Lerman *et al.*, 1970] [Tans *et al.*, 1979] of fossil fuel burning.

to calcite and form biogenic or chemical deposits, summarised as “inorganic carbon”. “Organic carbon” is found in the biosphere and can partly reenter the atmosphere by decomposition in the soil.

Radioactive decay

^{14}C is a radioactive carbon isotope with a half life of 5730 years [Godwin, 1962]. Besides archaeological studies, ^{14}C is widely used as an age tracer for palaeontologic and palaeoclimatic dating of reservoirs containing organic carbon of ages up to 50 kyr [Kromer, 2007]. Ages can be derived from the activity ratio $\frac{A(T)}{A_0}$ by

$$T = -\frac{\tau_{1/2}}{\ln 2} \cdot \ln \frac{A(T)}{A_0} \quad (2.3.9)$$

Activity is expressed as “percent modern carbon” (pmC) relative to an oxalic acid international standard. Activity of the year 1950 is declared 100 pmC.

As the initial activity A_0 is dependent on solar radiation and therefore variable in time, tree ring [Becker and Kromer, 1993] [Muscheler *et al.*, 2008], foraminiferal [Hughen *et al.*, 2004] [Hughen *et al.*, 2006] or coral [Fairbanks *et al.*, 2005] records can provide a calibration curve, summarised by Reimer *et al.* [2009]. This calibration curve is used to receive actual sample ages.

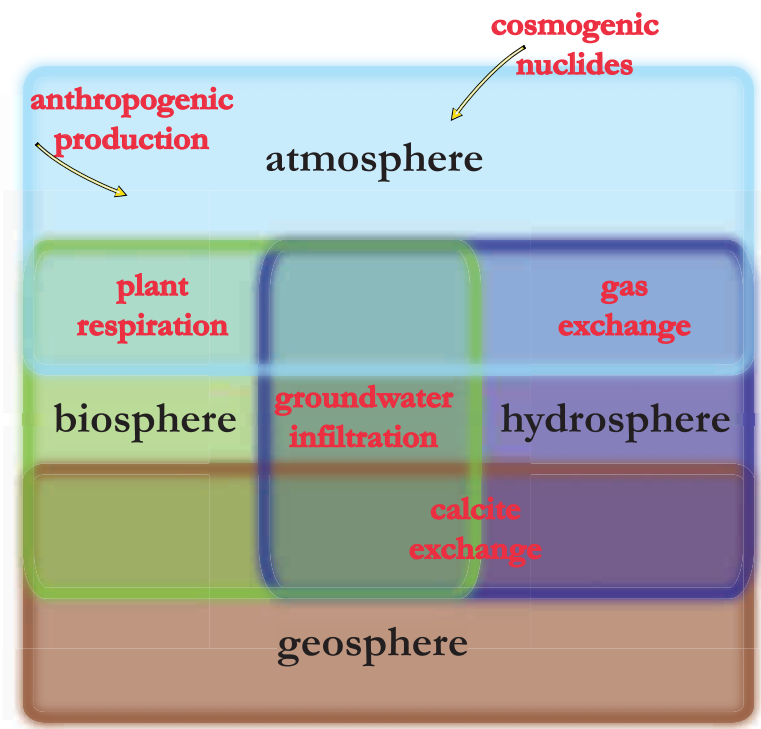


Figure 2.15.: Connection of different carbon reservoirs in the environment. Input of ^{14}C is indicated with yellow arrows.

When different carbon reservoirs are mixed, isotope dilution can occur. This effect is called reservoir effect. Reservoir ages differ in several orders of magnitude. Marine calcite or fossil fuel reservoirs are orders of magnitude older than the radiocarbon half life and are therefore free of ^{14}C , called old or dead carbon. An observed phenomenon is the “Suess” effect which was observable in the early 20th century [Lerman *et al.*, 1970] [Tans *et al.*, 1979]. Massive input of fossil fuel into the atmosphere dilutes atmospheric ^{14}C isotope ratios.

An example for a reservoir effect is the hard water effect in groundwater. In this case, dissolution of old calcite is responsible for the dilution (discussed in the next section).

2.3.4. Carbonate dating of groundwater

Regarding the cycle of dissolved inorganic carbon (DIC) in groundwater, information on low-temperature aqueous geochemistry may be derived from standard reference books such as Stumm and Morgan [1996] or Drever [1997], which are summarised in Clark and Fritz [1997].

CO_2 enters the soil through plant respiration and bacterial decomposition of plants (see Fig. 2.17). The photosynthesis cycle of plants will therefore affect the stable $\delta^{13}\text{C}$ isotope composition of CO_2 . CO_2 concentrations in the soil can range between a few ppm and over 10% atmospheric partial pressure (10^5 ppm) [Baver *et al.*, 1972] [Scheffer and Schachtschabel, 1960] [Schneider, 2009] (while Brook *et al.* [1983] proclaims an upper boundary of 4%). Due to the

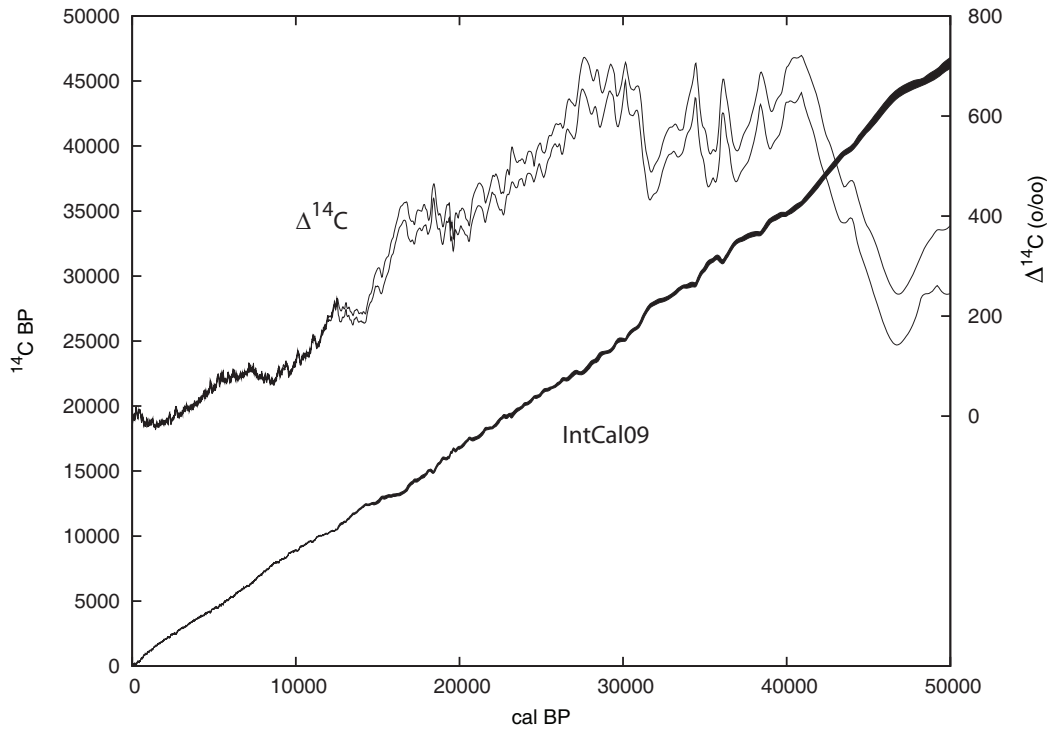


Figure 2.16.: Calibration curve of radiocarbon. The ^{14}C age (left axis) and $\Delta^{14}\text{C}$ (right axis, see Fig. 2.14) is plotted versus the calibrated date (published by [Reimer *et al.*, 2009])

high concentration in soil, an eminent fraction of soil CO_2 outgasses back into the atmosphere [Cerling, 1984]. When rain enters the hydrogeological cycle through infiltration into the soil, the water takes up the strongly soluble soil CO_2 .

In most groundwater aquifers (depending on their composition), sedimentary layers of CaCO_3 , e.g. from marine sediments [Merh, 1995], are deposited. A lower pH in the water causes partial dissolving of this sediment and adds ^{14}C -free carbon to the DIC. The higher the CO_2 concentration in the water, the lower the pH, and the more calcite is dissolved. All dissolved inorganic carbon species are connected by an equilibrium reaction system (shown in Fig. 2.18)



with the reaction constants K_i (2.3.2) determining the reactants' concentrations dependent on pH and temperature.

Empirical derivations of numerous existing data for pK_i were done by Plummer and Busenberg [1982] for different temperatures. Simple regression lines of this data for the different K_i were suggested by Clark and Fritz [1997]. Therefore, the chemical mass balance for water with weak saline concentrations can be determined from the CO_2 concentration, the pH and the water temperature. If concentrations of other ions are significant, the mixing enthalpy is no longer zero. Reactions are constrained and effective concentrations are derived by an

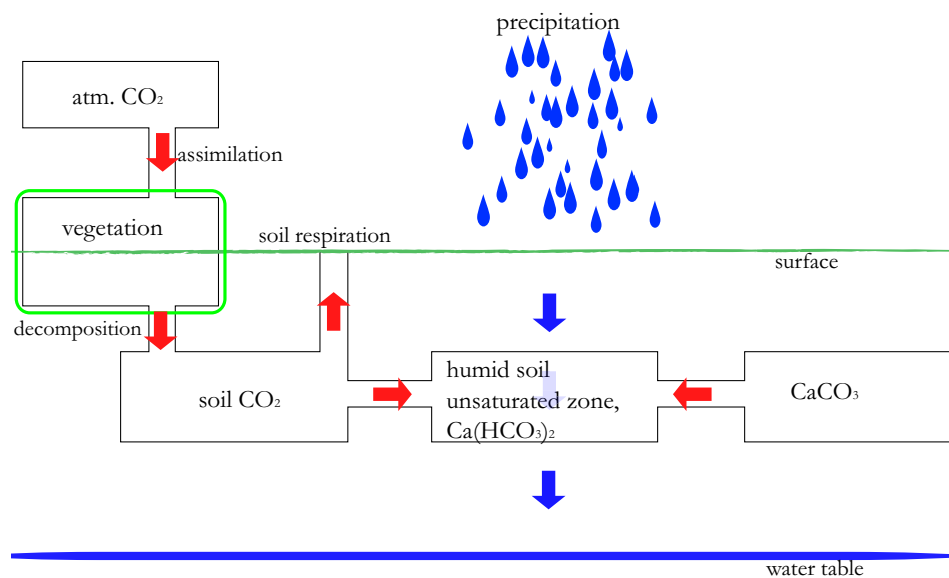


Figure 2.17.: Diagram of the carbon uptake into rain water which infiltrates the soil (adapted from Münnich [1968]).

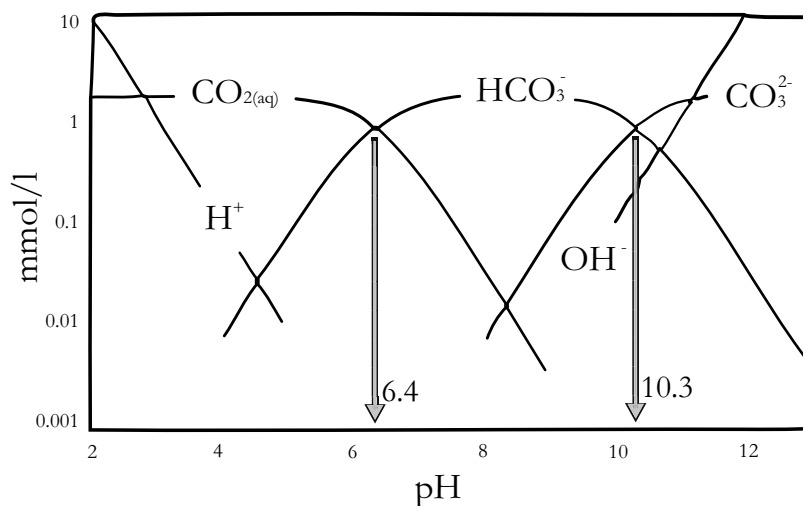


Figure 2.18.: Concentrations of all dissolved inorganic carbon components dependent on pH [Clark and Fritz, 1997] for 25°C (see 2.3.10).

activity coefficient as a factor. Activity can be expressed by ionic strength using the Debye Hückel equation. Especially calcium ions may accumulate, as solution of soil CO_2 dissolves calcite. With the Ca^{2+} concentration known and assuming it is the most abundant ion, the ionic strength can be estimated as $I = 1/2 \sum_i c_i z_i^2 = 1/2 (c_{\text{Ca}^{2+}} (+2)^2 + c_{\text{HCO}_3^-} (-1)^2)$. If no chemical concentrations are known, the equation of Dreybrodt [1988] can be used to estimate calcium concentration by $2 [Ca^+] = [HCO_3^-]$. It is derived by the equation of electro-neutrality and neglecting minor ions such as H^+ , OH^- , CO_3^{2-} , which is a good approximation for typical groundwater pH values.

Another important quantity for a better understanding of the carbon cycle in water is the $^{13}\text{C}/^{12}\text{C}$ isotope ratio. Clark and Fritz [1997] summarise temperature dependent numeric regression curves of fractionations (2.3.1) $^{13}\epsilon_{\text{CO}_2(\text{aq})-\text{CO}_2(\text{g})}$ [Vogel *et al.*, 1970], $^{13}\epsilon_{\text{HCO}_3-\text{CO}_2(\text{g})}$ [Mook *et al.*, 1974], $^{13}\epsilon_{\text{CO}_3-\text{CO}_2(\text{g})}$ [Deines *et al.*, 1974] and $^{13}\epsilon_{\text{CaCO}_3-\text{CO}_2(\text{g})}$ [Bottinga, 1968]. Examples for 25°C are -1.1‰ , 7.9‰ , 7.6‰ and 10.4‰ , respectively (shown in Fig. 2.19). A summary of all mentioned formula is shown by Clark and Fritz [1997].

It is necessary to understand the importance of the plant photosynthesis cycles [Peisker, 1984]: **C3** plants are allocated in temperate climate regions or tropical forests with moderate temperature and sunlight intensity, high concentration of carbon dioxide, and groundwater supply. According to their photosynthesis pathways, they lose most of their water due to respiration [Raven and Edwards, 2001]. Most of the Earth's plant biomass consists of C3 plants which predate the more specialised C4 plants.

C4 plants use another reaction step in their photosynthesis cycle to avoid transpirational loss of water. The isotope discrimination is inversely related to the water-use efficiency of the plant [Ehleringer *et al.*, 1991]. This explains the abundance of C4 plants in arid regions as a result of filling an ecological niche. They are therefore more homely in dry and warm regions with high aridity. Even salty deserts shelter C4 plants. These regions of at least seasonal strong aridity can sometimes be inhabited exclusively by C4 species [Ziegler *et al.*, 1981]. Ziegler's special study in Rajasthan confirmed great abundances of C4 plants in a desert region near the project area.

The $\delta^{13}\text{C}$ ratio in atmospheric CO_2 lies around -7‰ . When plants respire CO_2 , they cause fractionation of the emitted gas at very characteristic ratios depending on their photosynthesis cycles: C3 plants deplete $\delta^{13}\text{C}$ to about -25‰ , while C4 plants cause a smaller depletion of about -13‰ [O'Leary, 1981] [Troughton, 1979] [Ziegler *et al.*, 1981]. Decomposed plant material and CO_2 from bacteria have about the same isotope composition. Furthermore, diffusive outgassing of soil CO_2 into the atmosphere can produce an enrichment of $\delta^{13}\text{C}$ by about 4‰ [Cerling, 1984]. All these fractionation steps need to be considered when treating $\delta^{13}\text{C}$ in groundwater. Finally, marine calcite sediments have a $\delta^{13}\text{C}$ of $0 - 1.5\text{‰}$ [Mook and Vogel, 1968]. Dissolution of this old carbon characteristically enriches the resulting dissolved inorganic carbon. The amount of dissolved calcite depends on the pH. Therefore, more acidic solutions and higher soil CO_2 cause more dissolution of calcite.

If the system is always in contact with soil CO_2 during the dissolution, it is called an "open system". If dissolution of carbonates takes place isolated from a soil gas phase, it is a "closed

system” [Hendy, 1970]. In an open system, saturated solutions with respect to calcite reach higher DIC concentrations than closed systems. Furthermore, the resulting $\delta^{13}\text{C}$ and ^{14}C ratio is more depleted in closed systems. After calcite saturation is achieved, $\delta^{13}\text{C}$ or ^{14}C may still evolve by exchange of carbon ions between the aquifer’s rock matrix and the DIC.

Carbon dating models in Hydrology

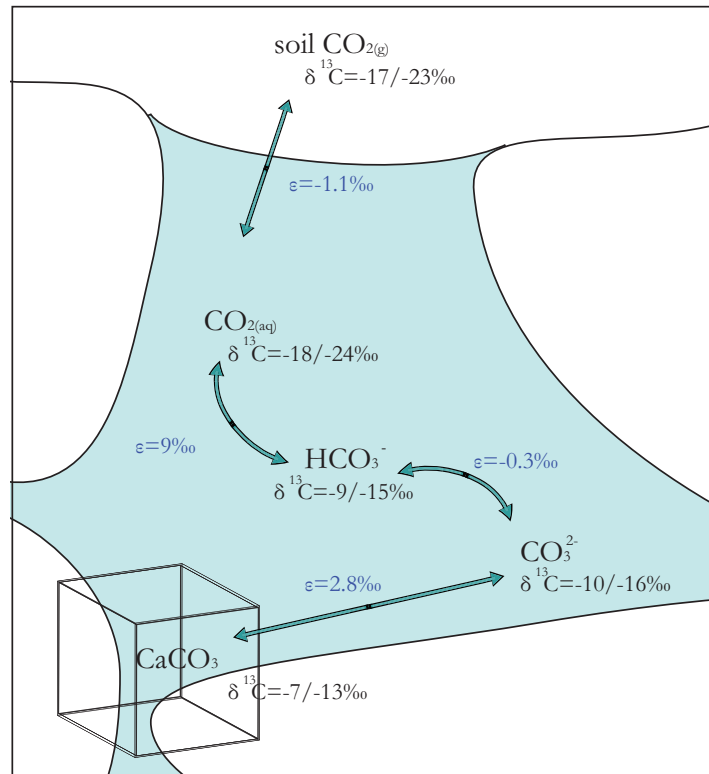


Figure 2.19.: Diagram of carbonate fractionation in the different reaction steps (examples for 25°C) (adapted from Clark and Fritz [1997]).

Different models to calculate groundwater ages try to estimate the reservoir effect. A reservoir factor q is named, which is the fraction of active carbon to total carbon. The reservoir effect results in an age reduction of $\frac{\tau_{1/2}}{\ln 2} \cdot \ln q$, changing the formula of conventional ^{14}C dating:

$$T = -\frac{\tau_{1/2}}{\ln 2} \cdot \ln \frac{A(T)}{q \cdot A_0} = -\frac{\tau_{1/2}}{\ln 2} \cdot \ln \frac{A(T)}{A_0} + \frac{\tau_{1/2}}{\ln 2} \cdot \ln q \quad (2.3.11)$$

The models are introduced as follows.

The **Vogel** model [Vogel, 1967] [Vogel, 1970] is an empiric approach based on typical European areas. It assumes a constant contribution by calcite in the aquifer and therefore reduction of the available initial activity. Therefore, all ages are reduced by a constant offset, as q is assumed to be the same for all samples. Mostly, a factor of $q = 0.85$ is used, but depending on

the aquifer environment, q is applied as 0.65 – 0.75 for karst systems, 0.75 – 0.90 for sediments containing loess and 0.9 – 1.0 for crystalline rocks.

The Vogel model does not take into account dissolution of ^{14}C -free carbon individually by measuring any chemical differences in the samples of one aquifer. Therefore, it is not very sensitive to special characteristics of the system. However, it can be used as a **statistical** approach to date groundwater in an aquifer, since it cannot be influenced by local measurements of a well's characteristics. In chapter 5.2.2, these model calculations will be labelled **STAT** for a q derived from geological data and **STAT meas** for a q derived from other data such as tritium and coinciding ^{14}C measurements of young samples.

The **Pearson** model [Ingerson and Pearson Jr., 1964] [Pearson Jr., 1965] is defined by **isotopic** relations and estimates the modification of the initial activity using $\delta^{13}\text{C}$ values in the soil. The $\delta^{13}\text{C}$ of calcite on one hand is 0‰ (or in some rare cases, around 1 – 2‰), while the soil CO_2 $\delta^{13}\text{C}$ value depends mainly on the regional growth of plants and their transpiration on the other hand. By measuring $\delta^{13}\text{C}$, one may estimate the amount of dissolved calcite, and thereby estimate the amount of old carbon diluting the initial activity of ^{14}C while infiltrating. Pearson uses a simple isotope mixing formula based on the assumption that closed system conditions predominate. As CO_2 is brought into solution and the water parcel closed off afterwards, it will react to bicarbonate without significant fractionation. Since the parameter q is already in use, dilution can be described as follows:

$$q = \frac{\delta^{13}\text{C}_{\text{tot.DIC}} - \delta^{13}\text{C}_{\text{calcite}}}{\delta^{13}\text{C}_{\text{soilCO}_2} - \delta^{13}\text{C}_{\text{calcite}}} \quad (2.3.12)$$

This model will be labelled **C13**.

The **Tamers** model [Tamers, 1975] studies the **geochemistry** of groundwater and assumes closed system conditions. Every dissolved CO_2 molecule reacting to bicarbonate releases one carbonate ion from the soil to keep the stoichiometry intact. In this case, the dilution factor ranges between 0.5 and 1 is

$$q = \frac{[\text{H}_2\text{CO}_3] + 1/2[\text{HCO}_3^-]}{[\text{H}_2\text{CO}_3] + [\text{HCO}_3^-]} \quad (2.3.13)$$

It can be calculated by the measured alkalinity. The model will be labelled **ALK**.

Clark and Fritz describe the **chemical mass balance** model [Clark and Fritz, 1997] in which the infiltration DIC for the system can be calculated by the initial parameters pH, pCO_2 and formula (2.3.2) to model the carbonate equilibration reactions.

$$[\text{HCO}_3^-] = K_1 \frac{[\text{H}_2\text{CO}_3]}{[\text{H}^+]}; \quad [\text{DIC}_{\text{recharge}}] = [\text{HCO}_3^-] + [\text{H}_2\text{CO}_3]$$

The initial activity of radiocarbon is then corrected by the factor of recharge DIC relative to the total measured dissolved inorganic carbon:

$$q = \frac{[\text{DIC}_{\text{recharge}}]}{[\text{DIC}_{\text{meas}}]} \quad (2.3.14)$$

The model will be labelled **CMB calc**, or **CMB meas** if a DIC measurement of a modern sample is used as $\text{DIC}_{\text{recharge}}$.

Using both the amount of DIC and its $\delta^{13}\text{C}$ isotope ratio, **Fontes and Garnier** established a more complex model [Fontes and Garnier, 1979] to include both geochemical and isotopical ideas, and to take into account **matrix exchange** with the aquifer. All DIC is apportioned into two fractions, one resulting from exchange with soil CO_2 , another resulting from exchange with the ground matrix of the aquifer (DIC_{carb}). The DIC_{carb} is either estimated by chemical measurement of all ions taking part in the carbon dilution or by measuring the alkalinity in the field. Half of the alkalinity is conventionally used as an estimate for the relevant DIC_{carb} [Dreybrodt, 1988]. DIC_{carb} is divided into an active component which has exchanged with the soil CO_2 under open system conditions, and an inactive one resulting from exchange with the aquifer matrix under closed conditions. The active DIC is estimated as follows:

$$[\text{DIC}_{\text{CO}_2\text{-exch}}] = \frac{\delta^{13}\text{C}_{\text{meas}}[\text{DIC}_{\text{meas}}] - \delta^{13}\text{C}_{\text{carb}}[\text{DIC}_{\text{carb}}] - \delta^{13}\text{C}_{\text{soil}}([\text{DIC}_{\text{meas}}] - [\text{DIC}_{\text{carb}}])}{\delta^{13}\text{C}_{\text{soil}} - \epsilon_{\text{CO}_2\text{-CaCO}_3} - \delta^{13}\text{C}_{\text{carb}}}$$

q results as follows:

$$q = \frac{[\text{DIC}_{\text{meas}}] - [\text{DIC}_{\text{carb}}] + [\text{DIC}_{\text{CO}_2\text{-exch}}]}{[\text{DIC}_{\text{meas}}]} \quad (2.3.15)$$

The model is labelled **F&G Alk**.

Additionally, another model is introduced, which works as the only one with **open system** conditions [Münnich, 1968]. **Münnich** used a very simple approach of soil CO_2 outgassing back into the atmosphere and leaving an enriched component infiltrating into groundwater under completely open conditions. Therefore, an active carbon fraction of

$$q = \frac{\delta^{13}\text{C}_{\text{meas}}}{\delta^{13}\text{C}_{\text{soil}} - \epsilon} \quad (2.3.16)$$

is expected. The model was already used in a precedent study of ^{14}C ages in groundwater in Gujarat [Agarwal *et al.*, 2006] [Deshpande, 2006] as its model assumptions of open system saturation may fit best for the regional conditions. As it is an isotope model, it will be labelled **C13 Mün**.

For all alkalinity related models, an approach can be made to modify closed system models into semi-open system models. By using an initial pCO_2 value, the sample's pH and the recharge's temperature, Fohlmeister [2008] shows how to estimate the ratio of open system and closed system equilibration. A model calculation provided by Jens Fohlmeister can lead to a unique solution by simulating soil carbon dissolution from initial pCO_2 under open (straight line) and subsequently under closed system conditions (curve, see Fig. 2.20) to reach the saturation point

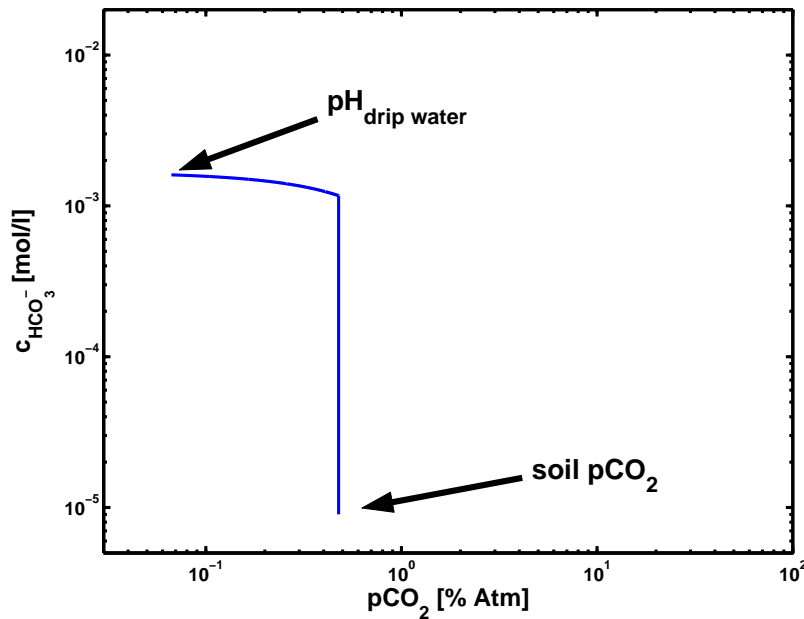


Figure 2.20.: The diagram shows a carbon infiltration simulation done by Fohlmeister [2008] to determine the ratio of active to old carbon for speleothem drip water. According to initial soil CO_2 partial pressure (x-axis) and temperature, and the sample's pH value, the diagram shows open system infiltration by the vertical line and closed system infiltration shown by the curve. The final bicarbonate concentration in water is shown on the y-axis.

of dissolved bicarbonate determined by the pH of the water. This is a more realistic estimation of active carbon and therefore alkalinity than the Tamers model. The active alkalinity can also be used in other models such as Fontes & Garnier. This alkalinity model is labelled **ALK mod**, while modifying the alkalinity introduced in the Fontes & Garnier model will be labelled **F&G mod**.

For isotope related models, a modelled ratio of the considered “recharge water” (suggested in Clark and Fritz [1997]) can be used instead of the assumed soil gas isotope ratio. Therefore, the modified Pearson model will be labelled **C13 mod**.

More complex models exist, as the aim changes from one analytic formula to complex box-model calculations and geochemical evolution models. Programs such as NETPATH [Plummer *et al.*, 1994] try to use every possible information about the aquifer system to model the appropriate reactive transport system.

A reasonable approach for dating groundwater is comparing different models and take the mean \bar{q} which is the most likely age, as well as the standard deviation as error, since the choice of model produces the biggest uncertainty.

Conventionally, the ^{14}C age is calculated with the radioactive decay equation (2.3.11), using Libby's half life of 5568 years:

$$T = -\frac{\tau_{1/2}^{\text{Libby}}}{\ln 2} \ln \frac{A(T)}{A_0} \quad (2.3.17)$$

For the conventional model, the initial atmospheric activity of the year 1950 is set to $A_0 = 100\%$. These conventions were used before the estimation of the corrected half life of ^{14}C and the discovery of a variable input. For this reason, this age is by definition called “(conventional) ^{14}C age”.

The real age is derived by programs such as OXCAL [Bronk Ramsey, 2009] using the calibration curve INTCAL09. These programs are able to convert activities, activity ratios or conventional ages to calibrated ages.

As a novelty for hydrogeological dating, this study uses the modified activity ratio $\frac{A(T)}{\bar{q} \cdot A_0}$ to derive calibrated ages.

2.3.5. Sulphur hexafluoride

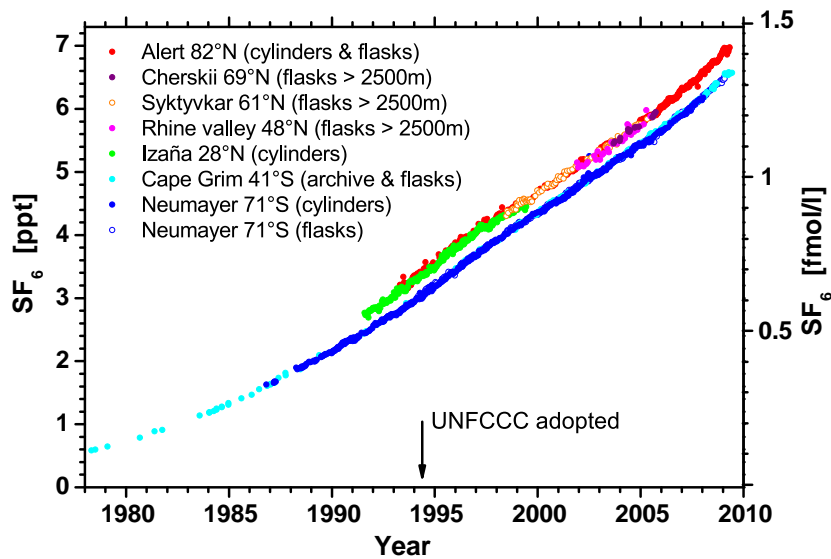


Figure 2.21.: Atmospheric concentration of SF_6 (adapted from [Levin *et al.*, 2010a]). The anthropogenic input is clearly observable. The right axis refers to the SF_6 equilibrium concentration in surface waters at 29°C .

SF_6 is a chemically inert gas with extremely low solubility in water. In hydrology, it is mainly used to date young groundwaters due to its anthropogenic production and monotonously rising input curve since the 1950s [Wanninkhof and Ledwell, 1996]. The reason for its industrial production is amongst others its great applicability as isolation gas in high voltage switchgear. With a global warming potential of 23900 IPCC [2007] [Maiß and Brenninkmeijer, 1998] identified SF_6 as the strongest of the observed greenhouse gases, with an atmospheric life span of 1937 [Patra *et al.*, 1997] to 3200 years [IPCC, 2007].

By measuring dissolved SF_6 in young water samples and comparing it to the atmospheric input

curve (shown in Fig. 2.21), the date of infiltration can be estimated, assuming a piston flow. Condition is the knowledge of the infiltration temperature.

Apart from its anthropogenic component, it is already known that a natural source of SF₆ can be found in regions with crystalline geology or regions with volcanic activity [Busenberg and Plummer, 2000] [Harnisch *et al.*, 2000]. Harnisch and Eisenhauer [1998] expect a general relation between high SF₆ production and high natural radioactivity of rocks. Plutonic rocks and minerals rich in fluoride (another requirement) are known for their high concentration of uranium ore. Radioactive processes are supposed to provide the necessary activation energy for the synthesis of SF₆. These relations were also observed in other studies [Friedrich, 2007]. As a previous IUP study indicated [von Rohden *et al.*, 2010], natural SF₆ can also be found in sedimentary aquifers, which was not expected and questions the further use of SF₆ as anthropogenic age tracer in such cases.

Excess air always has to be considered when investigating SF₆ in water: Bubbles of young air containing anthropogenic SF₆ may add a component to the total amount of gas. The phenomenon of excess air will be discussed in detail in the next section 2.3.8.

2.3.6. Noble gases

Due to the completely filled shells in their electron configuration, noble gases are chemically inert and therefore good tracers. Except for some rare fluoride compounds, noble gases are in their elemental gaseous state. Individual sources and sinks in the atmosphere or lithosphere are discussed in this subsection.

Helium with the highest ionisation energy is the universe's most inert element, yet still has sources and sinks: As gas particle velocities are characterised by the Maxwell-Boltzmann distribution, the helium atoms in the distribution's tail have a higher velocity than the Earth's escape velocity. As a result, the exosphere is a sink for all ³He and ⁴He in the atmosphere [Torgersen, 2010]. Helium is produced by natural radioactive decay in the lithosphere (the radiogenic component), or exists stored in reservoirs in the crust or mantle (terrigenic component, [Kipfer *et al.*, 2002]). Due to its high mobility, this stored helium diffuses out of the Earth's solid reservoirs into the atmosphere. Over time, these processes led to an equilibrium of helium concentration in the atmosphere. The isotope ratio of helium is very characteristic and differs in the Earth's atmosphere ($R_A = 1.38 \cdot 10^{-6}$, [Clarke *et al.*, 1976]), crust ($1 - 3 \cdot 10^{-8}$, [Mamyrin and Tolstikhin, 1984]), and mantle (10^{-5} in middle ocean ridge basalt (MORB), varying up to $35R_A$, [Breddam and Kurz, 2001], and $50R_A$, [Class and Goldstein, 2005] in hot spots, with an estimated primordial mantle component of $230R_A$). For this reason, isotope measurements of helium can be quite revealing. The concentration of ⁴He in the atmosphere is 5.24 ppm [Porcelli *et al.*, 2002]. In old groundwater, a prevailing radiogenic component of ⁴He and ³He is expected and can be used for qualitative dating, depending on the sample's age (as shown in Fig. 2.22, [Kipfer *et al.*, 2002]). If the helium accumulation rate J_{He} is known,

Table 2.2.: Noble gas partial pressures and isotope abundances (summarised by [Porcelli *et al.* \[2002\]](#)):

Elements	Volume mixing ratio	err	Isotopes	Relative abundance	err	molar abundance [%]
He	$5.24 \cdot 10^{-6}$	$5 \cdot 10^{-8}$	^3He	$1.384 \cdot 10^{-6}$	$1.3 \cdot 10^{-8}$	0.000138
			^4He	1		100
Ne	$1.818 \cdot 10^{-5}$	$4 \cdot 10^{-8}$	^{20}Ne	9.8	0.08	90.5
			^{21}Ne	0.029	0.0003	0.268
			^{22}Ne	1		9.23
Ar	$9.34 \cdot 10^{-3}$	$1 \cdot 10^{-5}$	^{36}Ar	1		0.3364
			^{38}Ar	0.188	0.0004	0.0632
			^{40}Ar	295.5	0.5	99.6
Kr	$1.14 \cdot 10^{-6}$	$1 \cdot 10^{-8}$	^{78}Kr	0.6087	0.002	0.3469
			^{80}Kr	3.9599	0.002	2.2571
			^{82}Kr	20.217	0.004	11.523
			^{83}Kr	20.136	0.21	11.477
			^{84}Kr	100		57
			^{86}Kr	30.524	0.025	17.398
Xe	$8.7 \cdot 10^{-8}$	$1 \cdot 10^{-9}$	^{124}Xe	2.337	0.008	0.0951
			^{126}Xe	2.18	0.011	0.0887
			^{128}Xe	47.15	0.07	1.919
			^{129}Xe	649.6	0.9	26.44
			^{130}Xe	100		4.07
			^{131}Xe	521.3	0.8	21.22
			^{132}Xe	660.7	0.5	26.89
			^{134}Xe	256.3	0.4	10.43
^{136}Xe	217.6	0.3	8.857			

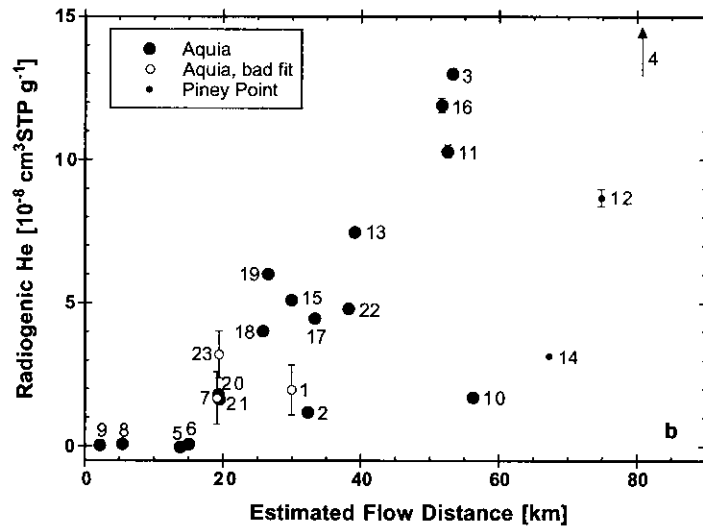


Figure 2.22.: Aeschbach-Hertig *et al.* [2002] show the use of radiogenic ^4He as an qualitative age tracer in this plot.

it is possible to quantitatively estimate the residence time $\tau = \frac{\text{He}}{J_{\text{He}}}$. This method can be improved in combination with ^{222}Rn measurements [Torgersen, 1980]. In young groundwater, the tritiogenic component of ^3He is necessary for a thorough tritium dating.

Deviations from a radiogenic character can give insight to an interesting geological history. Production mechanisms of ^3He on Earth carry no weight compared to ^4He (contrary to cosmogenic or anthropogenic neutron reactions in the atmosphere producing exclusively T). Aging of the lithosphere by continuous melting and solidification deletes all stored He information in the moment of melting. After solidification, the radiogenic component is accumulating again. The radiogenic ^4He production rate is $4 \cdot 10^{-15}$ (mantle) and $4 \cdot 10^{-13}$ (crust) $\frac{\text{ccSTP}}{\text{g yr}}$ [Ballentine and Burnard, 2002]. The only source for high $\frac{^3\text{He}}{^4\text{He}}$ ratios therefore has to come from relatively “juvenile” geologic sources with the original imprint of the solar system’s formation age. Findings of Clarke *et al.* [1969] in deep ocean water, of Craig *et al.* [1978], Lupton *et al.* [1989] or Poreda and Craig [1989] in MORB or Kaneoka and Takaoka [1980] and Rison and Craig [1983] in hot spots [Class and Goldstein, 2005] indicate such a reservoir. Classical interpretation of these findings indicate a so-called “primordial” mantle theory dividing the Earth’s mantle in a depleted upper section feeding MORB and a “primordial” lower section feeding hot spots. Another theory arguing against a primordial component explains different isotope ratios in helium by a mixture with subducted lithosphere and a “quasi” primordial ratio at the D” layer feeding hot spots [Class and Goldstein, 2005].

Neon consists of three stable isotopes ^{20}Ne , ^{21}Ne and ^{22}Ne . ^{20}Ne is the main isotope without sources and sinks. All isotopes have a rather low production rate in the Earth’s crust from secondary spallation reactions. A good summary is provided by Ballentine and Burnard [2002] citing studies of Kyser and Rison [1982], Leya and Wieler [1999] and Yatsevich and Honda [1997] that shows production rates around 10^{-23} (mantle) and 10^{-21} (crust) ccSTP/g yr for

^{20}Ne , similar for ^{22}Ne and ten times stronger for ^{21}Ne . These production rates are strongly suppressed compared to primary alpha production. The relative $^{21}\text{Ne}/^4\text{He}$ production rate is around 10^{-7} . Results are summarised in [Ballentine and Burnard, 2002]. Atmospheric ratios and concentrations are shown in Table 2.2.

Argon is the world's most abundant noble gas with an atmospheric mixing ratio of about 1%. It originates mainly from EC- and β^+ -decay of ^{40}K (main reaction (89%) to ^{40}Ca) in the Earth's crust and subsequently degassing into the atmosphere. The half life of this decay is $1.25 \cdot 10^9$ yrs. As the natural background is that high, only very old groundwaters and waters in a strongly radiogenic environment may have a non-atmospheric ^{40}Ar component (production rate in the crust from Ballentine and Burnard [2002] roughly estimated as $3 \cdot 10^{-14} \frac{\text{ccSTP}}{\text{g}\cdot\text{yr}}$). Heaton and Vogel [1981] give the ratio of radiogenic He/Ar production as in the range of 8 to 1 for a typical sandstone, but numbers may vary around 1:1 and 6:1. Residence times for significant argon amounts deviating from atmospheric ratios have to be in the range of millions of years. Other stable isotopes of argon are ^{36}Ar and ^{38}Ar . Ratios and concentrations are shown in Table 2.2. A very rare radioisotope of argon is ^{39}Ar with a half life of 269 yrs. Argon's perfect applicability as a dating tool is only constrained by its rare isotope abundance of 10^{-16} in air. Apart from the old method of using huge sample sizes, in-the-field degassing and low level counting [Loosli *et al.*, 2000], the new technology ATTA may be used for groundwater dating in the future [Welte *et al.*, 2010].

Krypton and xenon are the rarest heavy stable noble gases with six and nine stable isotopes (shown in Table 2.2). When phenomenons such as natural fission reactors [Meshik *et al.*, 2004] or reservoirs with high radiogenic activity [Lippmann *et al.*, 2003] are studied, isotope ratios of xenon and krypton can give evidence of certain fissiogenic imprints in the isotope ratios. These accumulation rates need residence times around 10^8 to 10^{10} years in normal aquifers. For conventional groundwater studies, the main isotopes are analysed (compare Table 2.2). The radioactive isotopes ^{81}Kr and ^{85}Kr can be, if measurable, used as dating tools (half life of ^{81}Kr is 229000 yr, of ^{85}Kr is 10.76 yr), like ^{39}Ar .

Radon is a radioactive noble gas participating in the uranium and thorium decay chains with the mother radium and the daughter polonium with several isotopes. ^{222}Rn is the most long-living isotope with a half life of 3.82 days (^{219}Rn , ^{220}Rn). As its mothers uranium and radium are part of the Earth's lithosphere, radon originates from crustal material and soil, and emerges into groundwater and the atmosphere. Radon can be used to analyse the air exchange rate in soil [Lehmann *et al.*, 2000], as well as to estimate groundwater influx in lakes [Kluge *et al.*, 2007]. Radon measurements of groundwater are crucial for the He-Rn dating method [Torgersen, 1980].

He-Rn-dating is described by [Torgersen \[1980\]](#) as follows: As radiogenic ^4He and ^{222}Rn originate from the same decay chains of alpha-decaying uranium or thorium, a correlation may be used for dating. While estimation of a ^4He age needs approximations of ground density or porosity, this method is independent from these factors, as both tracers have equal dependencies which can be reduced [[Craig and Lupton, 1976](#)] [[Torgersen, 1980](#)]. [Torgersen \[1980\]](#) introduces He-Rn age as follows:

^{222}Rn activity is equal to uranium activity, its mother ^{238}U is the most common uranium isotope with 99.27 %:

$$^{222}A'_{\text{Rn}} = 0.734[\text{U}],$$

with $^{222}A'_{\text{Rn}}$ radon's activity in $\frac{\text{dpm}}{\text{g}_{\text{rock}}}$ and $[\text{U}]$ the uranium concentration in ppm. Activity in the pore fluid therefore is:

$$^{222}A_{\text{Rn}} = ^{222}A'_{\text{Rn}} (\rho\Lambda_{\text{Rn}}/P),$$

with ρ and P density and porosity of the rock matrix. Λ_{Rn} is the fraction of radon released into the fluid.

Helium production is calculated similarly:

$$J'_{\text{He}} = 0.2355 \cdot 10^{-12}[\text{U}] \{1 + 0.123([\text{Th}]/[\text{U}] - 4)\},$$

with J'_{He} production of He in $\frac{\text{ccSTP}}{\text{g}_{\text{rock}} \cdot \text{yr}}$. In water, the rate is

$$J_{\text{He}} = J'_{\text{He}}(\rho\Lambda_{\text{He}}/P).$$

With these two tracers combined and porosity and density disappearing, [Torgersen \[1980\]](#) calculates a $^4\text{He}/^{222}\text{Rn}$ age ($[\text{Th}]/[\text{U}]$ is approximated to be about 4, while $C_{4\text{He}_{\text{rad}}}$ is the concentration of radiogenic ^4He) to

$$\tau = \frac{\Lambda_{\text{Rn}} C_{4\text{He}_{\text{rad}}}}{\Lambda_{\text{He}} \cdot ^{222}A_{\text{Rn}}} 3.12 \cdot 10^{12} \quad (2.3.18)$$

The unknown variables are the different release factors for He and Rn, which can be conceptually estimated by different mechanisms all mainly depending on grain size of the rock matrix. These resulting ages vary depending on used mechanisms. Another aspect of the method is more problematic: As radon is far more “short ranged” than He due to its half life, and as [Torgersen \[1980\]](#) showed that the prevailing fraction of He does not come from radiogenic but from weathering release, Rn-He ages overestimate groundwater ages by far (sometimes by two orders of magnitude [[Deshpande, 2006](#)] [[Solomon *et al.*, 1996](#)]).

2.3.7. Equilibration

Gas solubility in water depends on the equilibration temperature. For inert gases, this can be used to identify the infiltration temperature of water masses from past times, as no temporal alteration takes place. Noble gas concentrations extracted from water samples in a confined aquifer therefore produce the WTT that prevailed in the recharge area in the time of infiltration. The noble gas temperature ([NGT](#)) is therefore the key parameter to investigate.

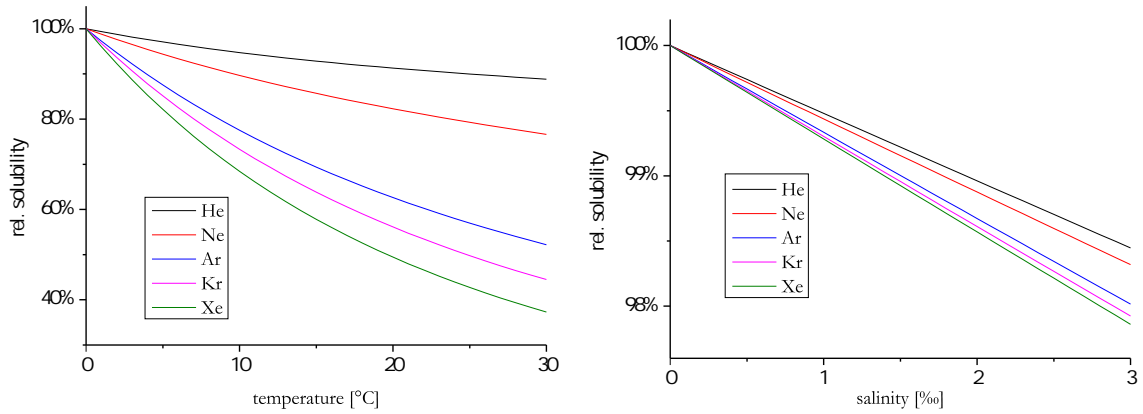


Figure 2.23.: Solubilities of the observed noble gases dependent on temperature in freshwater (and salinity at constant temperature of 20°C).

This relationship can be described by Henry's law of solubility with $C_{ig}(P_a, T)$ as the concentration of gas i in the gas phase, $C_{iw}(P_a, S, T)$ in the water phase, and the Ostwald solubility $L_i(S, T)$:

$$L_i(S, T) = \frac{C_{iw}(P_a, S, T)}{C_{ig}(P_a, T)} \quad (2.3.19)$$

The solubility is dependent on the salinity S and temperature T of the water. Permeability is disregarded in this case. The Ostwald solubility can be given as a dimensionless number when C_{ig} and C_{iw} have the same units (for example when $L_i(S, T)$ is given by the ratio of V_w , the gas volume in the water phase in litres, and V_g , the gas volume in the gas phase in litres). Other sizes to describe solubility are the Bunsen coefficient or the Henry coefficient, depending on the units used in the ratios [Battino, 1979] [Benson and Krause, 1980] [Smith and Kennedy, 1983] [Weiss, 1970] [Weiss, 1971] [Weiss and Kyser, 1978]. For analysis, the equilibrium concentration of the noble gas i in air equilibrated water (AEW) for a certain temperature and salinity is given in mol/l:

$$C_{iw}^{eq}(P_a, S, T) = C_{ig}(P_a, T) \cdot L_i(T, S)$$

The conventional notation is ccSTP/g and can be converted by

$$C_{\frac{ccSTP}{g}} = C_{\frac{mol}{l}} \frac{V}{\rho_{groundwater}(P_a, S, T)}$$

Atmospheric pressure P_a can be described with the barometric formula (with its isothermal simplification) and the altitude of the selected area:

$$p = p_0 e^{-\frac{h}{h_0}}, \quad h_0 = 8300\text{m}, \quad \text{and}$$

$$p_i = RT \cdot n_i/V = RT \cdot C_i^g$$

When pressure during infiltration is unknown, this estimation can be helpful.

2.3.8. Modelling of excess air

In most natural groundwater, the concentration of dissolved noble gases is higher than just the equilibrium component. The roughly observed excess of air has atmospheric isotope composition and originates from bubbles in the saturated zone of the infiltrated soil. Different models try to explain this “excess air” component (found first by [Andrews and Lee \[1979\]](#) and [Heaton and Vogel \[1981\]](#)) and are presented here. Fig. 2.24 demonstrates the process of excess air generation.

UA model

The first approach is to subtract atmospheric air from the noble gas concentrations until best agreement is obtained [[Andrews and Lee, 1979](#)]. This approach is the most simple excess air model (Unfractionated Air, UA):

$$C_{i\text{UA}} = C_i^{\text{eq}} + A \cdot C_{i\text{atm}} = C_i^{\text{eq}} (1 + A/L_i), \quad (2.3.20)$$

with A the fraction of trapped air in the water volume. This model is based on the idea of gas bubbles in infiltrated water totally dissolving due to pressure increase from water level fluctuations. For many groundwater samples, an enrichment of heavier noble gases compared to atmospheric composition can be observed.

PR model

[Stute et al. \[1995\]](#) therefore modified the UA model for a second step of partial re-equilibration (PR) of the enriched groundwater, which has, due to higher diffusion constants for He and Ne, a stronger depleting effect for lighter noble gases, fitting the observed pattern:

$$C_{i\text{PR}} = C_i^{\text{eq}} + A \cdot C_{i\text{atm}} \cdot \exp\left(-R \frac{D_i}{D_{\text{Ne}}}\right) = C_i^{\text{eq}} \cdot \left(1 + A/L_i \exp\left(-R \frac{D_i}{D_{\text{Ne}}}\right)\right), \quad (2.3.21)$$

with R the degree of re-equilibration. The diffusivities D_i result from the kinetic gas theory and Fickian laws as dependent on the square root of the mass. As a consequence, isotope fractionation may be strongly observable in this model [[Peeters et al., 2003](#)] [[von Oehsen, 2008](#)]. According to [Bourg and Sposito \[2008\]](#), this is not the right assumption in liquid water. Their modelled isotope diffusivities lead to much smaller fractionations. The physical motivation of the PR model is that after first dissolving all air bubbles in the infiltration zone due to large water level fluctuations, a situation of re-equilibration occurs with part of the water degassing again in a non-equilibrium reaction.

The same model can be slightly modified to work as a partial degassing model (PD) with groundwater that initially had an UA component.

$$C_{i\text{PD}} = C_i^{\text{eq}} \cdot (1 + A/L_i) \exp\left(-R \frac{D_i}{D_{\text{Ne}}}\right)$$

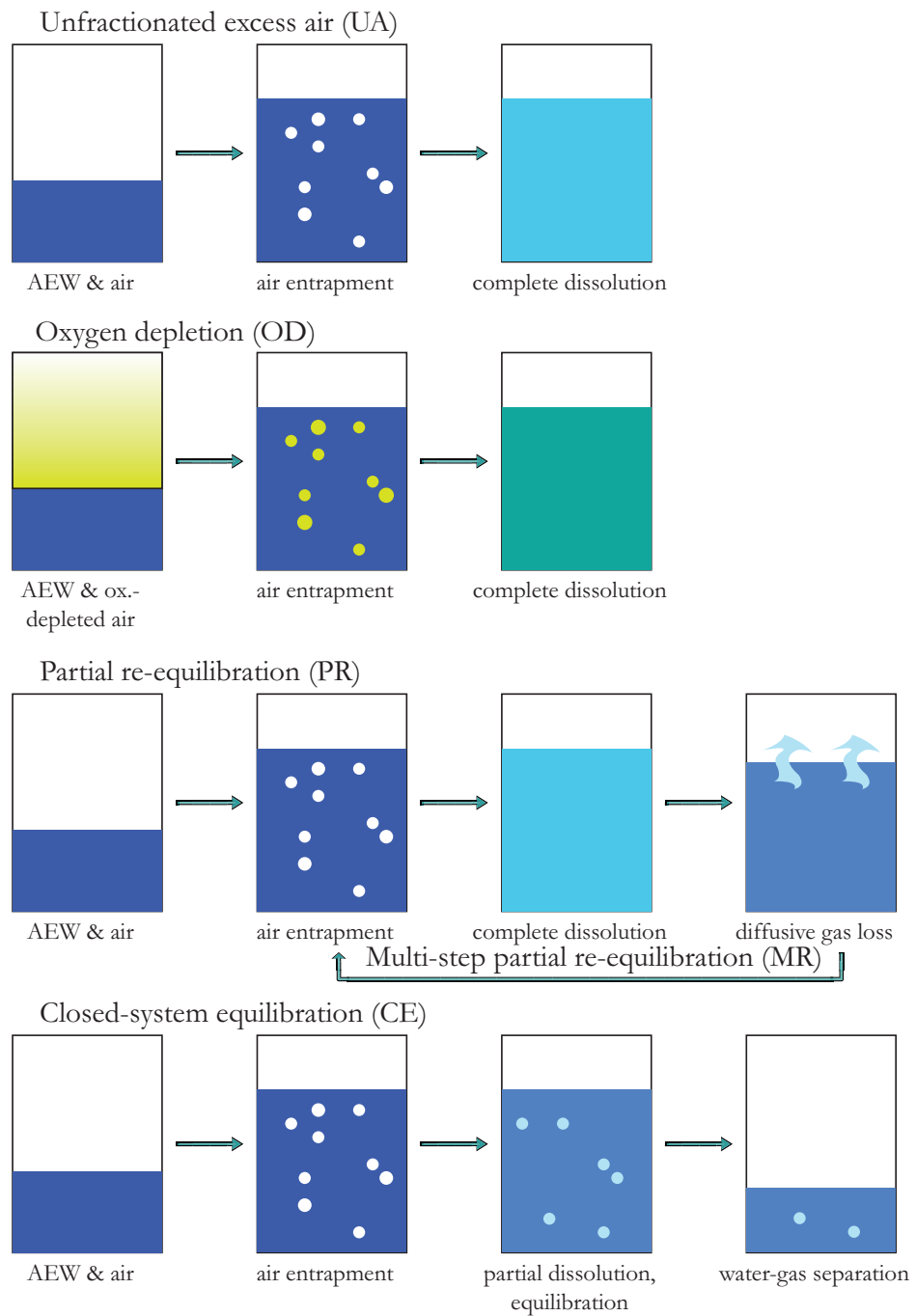


Figure 2.24.: Common excess air models with their physical explanation (adapted from Kipfer *et al.* [2002])

This model can be used to describe groundwater which suffered degassing and has a noble gas content less than the initial combined equilibrium and unfractionated excess air concentration.

For some observed groundwater samples, the modelled excess air fraction A reaches large numbers that can only be reached by strong water level fluctuations with pressure changes of several atmospheres. Therefore, in a further development of the PR model, the so-called MR model, many small dissolution steps of small amounts of gas and re-equilibration happen. The resulting effect can be described as a one step PR model, which provides an actually more realistic physical background for the PR model. However, noble gas concentrations from some datasets cannot be reproduced with the PR model [Ballentine and Hall, 1999].

CE model

A different mechanism to explain excess air in water is the model of Aeschbach-Hertig *et al.* [2000] of closed system equilibration (CE), which is dependent on solubilities and not diffusivities. In this situation, the air bubbles experience a weaker pressure increase that results not in total dissolution but partial dissolution of the gases of bubbles according to the solubility. The initial fraction of bubbles A in the system becomes reduced to the fraction B . In the original model description, the parameter $F = B/A$ called fractionation was used instead of B :

$$C_{i\text{CE}} = C_i^{\text{eq}} \cdot \left(1 + \frac{(1-F)A/L_i}{1+FA/L_i} \right) = C_i^{\text{eq}} \cdot \frac{1+A/L_i}{1+B/L_i} \quad (2.3.22)$$

By setting $F > 1$, degassed water can be investigated. The new notation is capable to observe potential degassing without explicit changes in the initial parameters. Other differences of the notations are discussed in chapter 2.3.10 and 5.3.2.

The parameters resulting from this model show much more realistic hydrostatic pressure changes than other models.

OD model

As was mentioned by Stute and Schlosser [1993], oxygen is depleted in the soil due to biogenic processes. All so far discussed models assume the replacement of oxygen by a product gas such as CO_2 or, depending on the biochemical process, nitrogen or methane. The possibility exists that the partial pressure of oxygen is not replaced by a generated gas. In this case, the partial pressures of nitrogen and the noble gases are increased depending on the permeability of the soil. While Stute and Schlosser [1993] rate this effect as a minor issue, Hall *et al.* [2005] and Castro *et al.* [2007] believe the effect to influence most groundwater infiltration by increasing the noble gas concentration. Their model (oxygen depletion OD), which is in essence an UA model with a flexible pressure parameter, can be described [Aeschbach-Hertig *et al.*, 2008] as:

$$C_{i\text{OD}} = C_i^{\text{eq}} \cdot G + Az_i \quad (2.3.23)$$

$G := \frac{1-0.21\alpha}{0.79}$ shows the partial pressure increase, and $\alpha = 0 - 1$ the degree of oxygen consumption. Depending on the degree of oxygen depletion, G can range between 1 and 1.27. To leave G as an open parameter is not sensible, as the physical meaning would be to have arbitrary changing oxygen consumption in the soil of the recharge area. Temperature and excess air influence the noble gas concentrations nearly opposite to pressure, and trying to fit a higher resulting partial pressure due to more depletion automatically shifts the temperature to higher values, without any control mechanisms at all. [Castro *et al.* \[2007\]](#) fixed the parameter to a certain value derived from an ensemble fit for all samples of a record, leaving the parameter G free but identical for all samples. This assumes that the depletion of oxygen was the same over the observed time. Alternatively, leaving the parameter free may show whether converging fits at least keep the parameter in its allowed constrains.

The choice of excess air model should be done from a physical relevance point of view. If no excluding information exists, the accuracy of the fit and its χ^2 value can show the best fitting model (see chapter 5.3.2).

Excess air as a climate proxy

No matter what model, the amount of excess air stands in direct relation to the pressure increase on the water table or its fluctuation. In arid regions, a fluctuating water table may imply strong rain events between periods of aridity, as several publications imply [Aeschbach-Hertig *et al.* \[2002\]](#) [Beyerle *et al.*, 2003](#) [Heaton *et al.*, 1983](#) [Kulongoski *et al.*, 2004](#). The effect is more pronounced in regions with temporal aridity such as monsoon-affected regions, but can also be observed in temperate zones [Ingram *et al.*, 2007](#). Therefore, excess air promises to be an interesting climate proxy for changes in the degree of precipitation [Zhu and Kipfer, 2010](#). Excess air is expressed by ΔNe , which is the neon excess in relation to the equilibrium concentration of neon, given in percent:

$$\Delta\text{Ne} = \frac{C_{\text{Ne}}^{\text{exc.air}}}{C_{\text{Ne}}^{\text{eq}}} [\%] \quad (2.3.24)$$

2.3.9. Non-atmospheric components

To sum it up, there exist several components for each noble gas i :

$$C_i^{\text{sum}} = C_i^{\text{eq}} + C_i^{\text{exc.air}} + C_i^{\text{non-atm.}} \quad (2.3.25)$$

An equilibrium fraction, an excess air fraction described by a chosen excess air model, and in some cases a non-atmospheric component of radiogenic or terrigenous origin. This non-atmospheric component can be ignored for all noble gases but ^3He and ^4He when studying conventional groundwater (see Fig. 2.25). The different possible non-atmospheric components of noble gases were discussed at length in the last section.

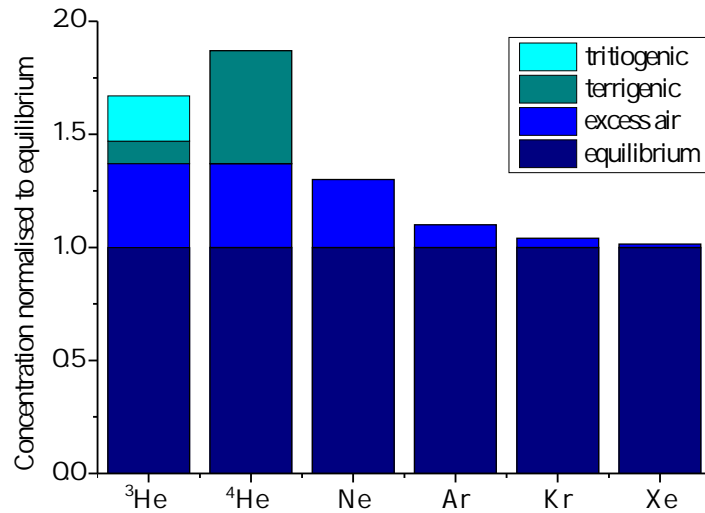


Figure 2.25.: Components of the measured noble gas isotopes. For all elements but helium there exist in essence two components. For the heavier noble gases the excess air component loses importance.

2.3.10. Fitting

These concentrations for all noble gases can be considered as a system of equations. The variables C_i^{meas} are measured by mass spectrometric analysis. The equilibrium concentrations depend on temperature, air pressure and salinity $C_i^{\text{eq}}(P_a, S, T)$. Depending on the model, the excess air concentrations depend on temperature, excess air volume and fractionation (or another model parameter) $C_i^{\text{exc.air}}(A, B/F/G, T)$. As a result, the measured concentrations need to be compared with the modelled concentrations:

$$C_i^{\text{meas}} - C_i^{\text{non-atm.}} \stackrel{?}{=} C_i^{\text{mod}} = C_i^{\text{eq}}(P_a, S, T) + C_i^{\text{exc.air}}(A, B/F/G, T)$$

With helium ignored, no non-atmospheric component needs to be considered. Five parameters A , F , P_a , S and T need to be found to solve the equations. Since only four noble gas concentrations are left for measurement, the system of equations is under-determined and therefore cannot be solved. It is necessary to use some assumptions, as e.g. to assume the precipitation's salinity being zero, or to approximate the air pressure at the time and location of infiltration with the barometric formula only depending on the altitude of the recharge area. The result is an over-determined system of equations that can be solved elegantly by inverse modeling [Aeschbach-Hertig *et al.*, 1999]. The χ^2 method fits the best set of modelled concentrations by trying to minimise the residuals of each noble gas.

Under the assumption of Gaussian distribution, the error weighted deviation of the modelled concentration to the measured one, $f_i = \frac{|C_i^{\text{mod}} - C_i^{\text{meas}}|}{\sigma_i}$, is called residual. The sensitivity j_k of a model to one of the free parameters x_k is defined as

$$j_k := \begin{pmatrix} \frac{\partial f_1}{\partial x_k} \\ \vdots \\ \frac{\partial f_n}{\partial x_k} \end{pmatrix}$$

All free parameters form the vector x . The sum of the residuals is defined as chi-square χ^2 .

$$\chi^2 = \sum_i \left(\frac{C_i^{\text{mod}} - C_i^{\text{meas}}}{\sigma_i} \right)^2 \quad (2.3.26)$$

An error weighted least square fit now tries to minimise this quantity. Depending on the degrees of freedom the differential of χ^2 needs to be zero for a minimum:

$$\nabla_x \chi^2(x) = 0$$

For this problem with several free parameters [von Oehsen \[2008\]](#) calculates

$$d\chi^2 = 2 \begin{pmatrix} f_1 \\ \vdots \\ f_n \end{pmatrix} \cdot \sum_l j_l dx_l$$

This equation leads to a local minimum for χ^2 when the sum becomes zero. For a physically meaningful result, that should only be the case with a trivial solution for all $dx_l = 0$. The sensitivity vectors for parameters where a non-trivial solution can be found are linearly dependent or collinear. Then a minimum in χ^2 is not unique and no solution can be found. While this may be a quite implausible situation for practical problems, a near collinearity can be just as harmful: In this case, the change of two parameters leaves the outcome of the fit nearly unchanged. As a result, a great change in parameter values $x_k + \Delta x_k$ only produces a very small increase in $\chi^2 + \epsilon$ which may still be accepted as a minimum by a fitting routine. Therefore, [Brun *et al.* \[2001\]](#) estimate a collinearity index $\gamma_{m,n,\dots}$ for the parameters m, n etc.:

$$\gamma_{m,n,\dots} := \frac{1}{\min_{x, \|x\|=1} \|S_{m,n,\dots} x\|} = \frac{1}{\sqrt{\min(\lambda_m)}} \quad (2.3.27)$$

with $S_{m,n,\dots} = \left(\frac{j_m}{\|j_m\|}, \frac{j_n}{\|j_n\|}, \dots \right)$, and λ_m the eigenvalues of the matrix $S_{m,n,\dots}^t \cdot S_{m,n,\dots}$. The collinearity index measures how collinear different parameters are. An index of 1 means orthogonality, while indices of 5 – 20 or higher are problematic [[Brun *et al.*, 2001](#)] and prove that the collinear parameters cannot be estimated exactly at the same time. This results in higher standard deviations for the wanted parameters.

Different collinearities of parameters for noble gas fitting with the CE model were estimated by [von Oehsen \[2008\]](#) for artificial data:

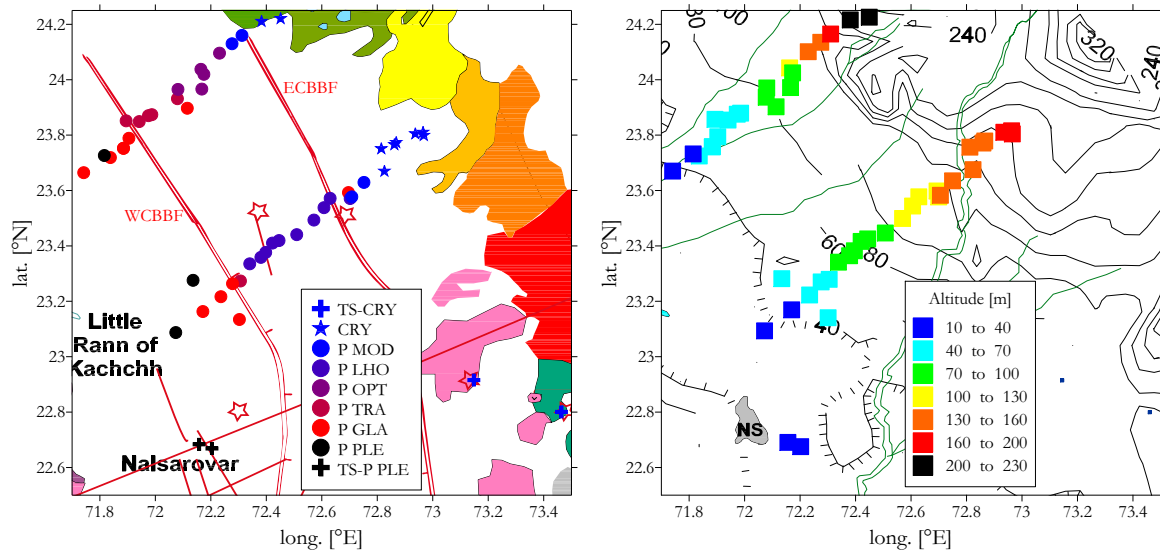
The use of the classic model with parameters A, F and T made a difference compared to the new model with A_B, B and T . The uncertainty to estimate A_B and B is much higher than the uncertainty for A and F , meaning that A and B are much more collinear than A and F . Collinearity indices for the simultaneous fit of A and T were around $\gamma_{AT} \approx 8 - 12$ for high A and T values of synthetic data, while $\gamma_{A_B T}$ remained always smaller than 2. To have a use of this, B however needs to be known. Collinearity indices between F and T are about similar to B and T .

No matter whether the new or the old method were used for fitting, collinearity indices are

calculated by the model program and should be controlled for the evaluation of fitting results to check if actual sample data behaves the same way as the above discussed artificial data.

The fitting technique with different excess air models is implemented in the MATLAB programs NOBLE90 and NOBLE2007 and will be discussed in the results section.

3. Sampling campaigns



(a) Geology of the sampling area and groups of wells. (b) Elevation of the wells and the sampling area above sea level.

Figure 3.1.: Map of the sampling area with added sampling site positions. The wells are grouped into: Thermal springs in the crystalline region in the recharge (TS-CRY, cross), wells puncturing crystalline rock (CRY, star), normal wells for the palaeoclimate study (P with subgroups introduced in chapter 5.2.2, circles) and thermal springs in the discharge (TS-P PLE, cross)

A joint research campaign was initiated between the Indian Physical Research Laboratory (PRL), Ahmedabad, and the German Institute of Environmental Physics (IUP), Heidelberg, to study groundwater in the Indian State of Gujarat.

3.1. Sampling Area

In the North Cambay Basin, a groundwater aquifer was analysed as a palaeoclimate archive. From 2008 to 2010, three sampling campaigns on two different transects took place. After every campaign, laboratory measurements were done to gather information and optimise further campaigns. Sampling expeditions were done by scientists of PRL and IUP, basically by Dr. R. D. Deshpande, Tim Schneider and the author, with the help of Dr. A. S. Maurya, Prof. S. K. Gupta and Prof. Werner Aeschbach-Hertig. The sampling area is shown in Fig. 3.1.

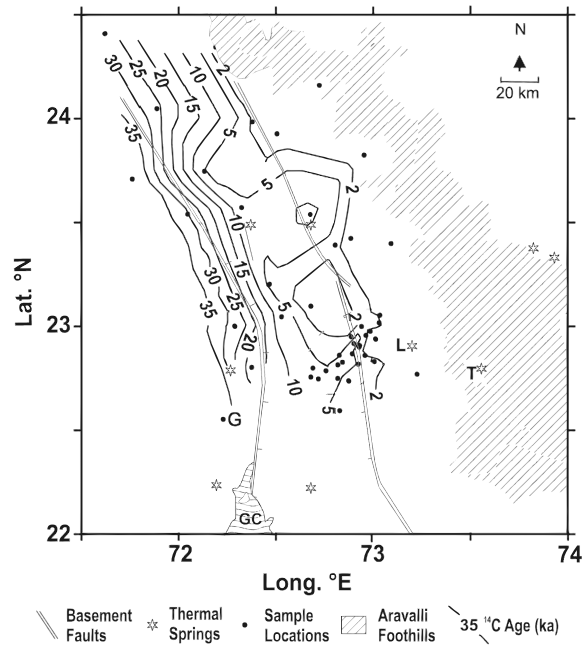


Figure 3.2.: Age of groundwater in kyr indicated by isolines as found by [Deshpande, 2006]. A clear trend from North-East to South-West in age can be seen. Confinement of the aquifer system begins west of the ECBBF. The northern transect has a linear age increase over distance, while the southern transect does not increase in age very much east of WCBBF.

As discussed in chapter 2.2.1, the sampled wells tapped the aquifer system of the North Cambay Basin. The aquifer had already been the target of a hydrogeological study performed by Dr. Deshpande, among other things to determine age behaviour of the aquifer (shown in Fig. 3.2). A typical well is assembled as follows (see Fig. 3.3, other typical well constructions are shown in Todd [1980]): The well shaft with a diameter of approximately 40 cm has a casing of metal pipes, and is driven into the ground. The depth where hydraulic exploitation takes place has a casing with gaps to enable surrounding water to enter, the so-called screen of the well (see Fig. 3.4). In this well shaft, the water level rises up to the piezometric head of the connected aquifers. A submersible pump is lowered to a certain depth, connected to a metal or PVC water pipe. The top of the well is sealed off with a concrete cap from which the pumping pipe emerges. At a high position of the pipe close to the well shaft, air valves are attached which suck air into the well shaft as soon as the motor of the pump switches off and the water column in the pipe collapses down into the ground (see Fig. 3.3). Without this air valve, a connected water reservoir would be pumped empty again with the water seeping into the ground, and the weight of the falling water column can break the water pipe in the well resulting in the loss of the pump.

Most of the sampled wells were agricultural wells (see Fig. 3.5(b)) of private owners who use the wells for irrigation of their fields and to sell surplus water to other farmers. Some wells belonged to non-agricultural owners such as schools. The rest of the wells were the property of village administrations and used to supply drinking water, mostly combined with a water tower that was filled on a daily basis. While community wells often provided better sampling

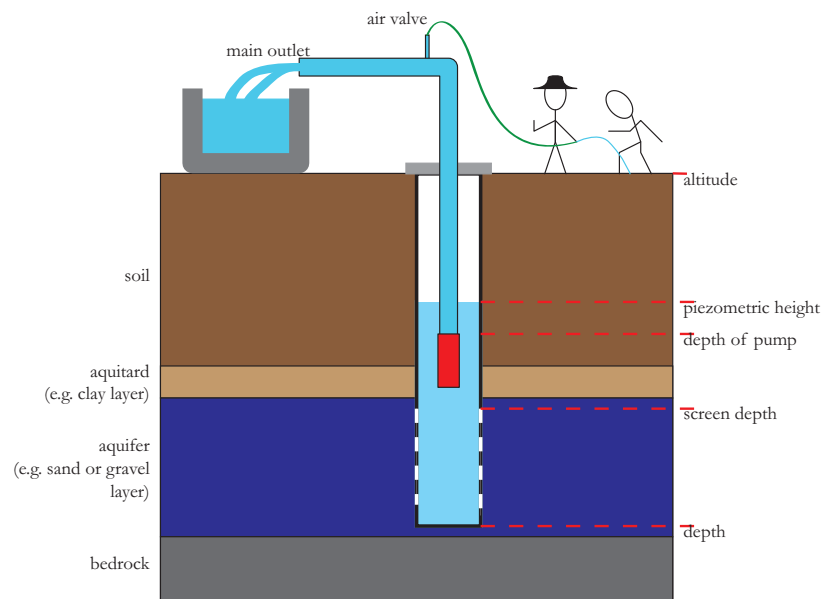


Figure 3.3.: Schematic drawing of a typical Gujaratian well. Noted are depth positions of the water level, the screen which enables groundwater to enter the shaft, the pump and the actual well shaft.



Figure 3.4.: Picture of the used pipes for the well's screen.



(a) A groundwater well drilling site. (b) A typical agricultural well of Gujarat.

Figure 3.5.: Pictures of Indian wells.

conditions and power supply than agricultural wells, they were not as common, since villages begin to change water supply sources from groundwater to irrigation channels from river water. Moreover, the villages did not often fit to the desired sampling positions along the transects. A list of the sampled wells is provided in Fig. 3.6 and table D.1.

3.1.1. Hydrogeology of the sampling area

The transects running from north-eastern to south-western direction follow the flow direction and slope of the basin, beginning with very shallow wells in the recharge area of the aquifer. In this region, it is still unconfined and infiltration still takes place in an open system. The prevailing terrain consists of layered quaternary sediments such as sand, gravel and clay. The clay layers do not form a continuous aquitard but appear scattered along the sedimentary orientation. With increasing distance to the recharge area, the sedimentary layers are found deeper below the surface (see cross section in Fig. 2.4). For the northern transect, well 18 defines the recharge, while on the southern transect, well 26 is declared as the recharge. Deshpande [2006] showed that confinement of the aquifer occurs only west of the East Cambay Basin Bounding Fault (ECBBF, see Fig. 3.1). Along the transects, tapped water layers become deeper with increasing distance from the recharge. To achieve continuous aging of the sampled water, the screens of the wells should not change in depth but should be approximately parallel to the piezometric head of the aquifer system, as was shown in theoretical considerations in chapter 2.1.2. All the wells taking part in the palaeorecord study are summarised in group P. Some wells did not fulfill this criterion but were sampled for additional scientific information: Especially some deep wells in the recharge area that penetrated the bedrock of the terrain were sampled. The casing of the well ends when it touches solid bed rock, while the well shaft goes

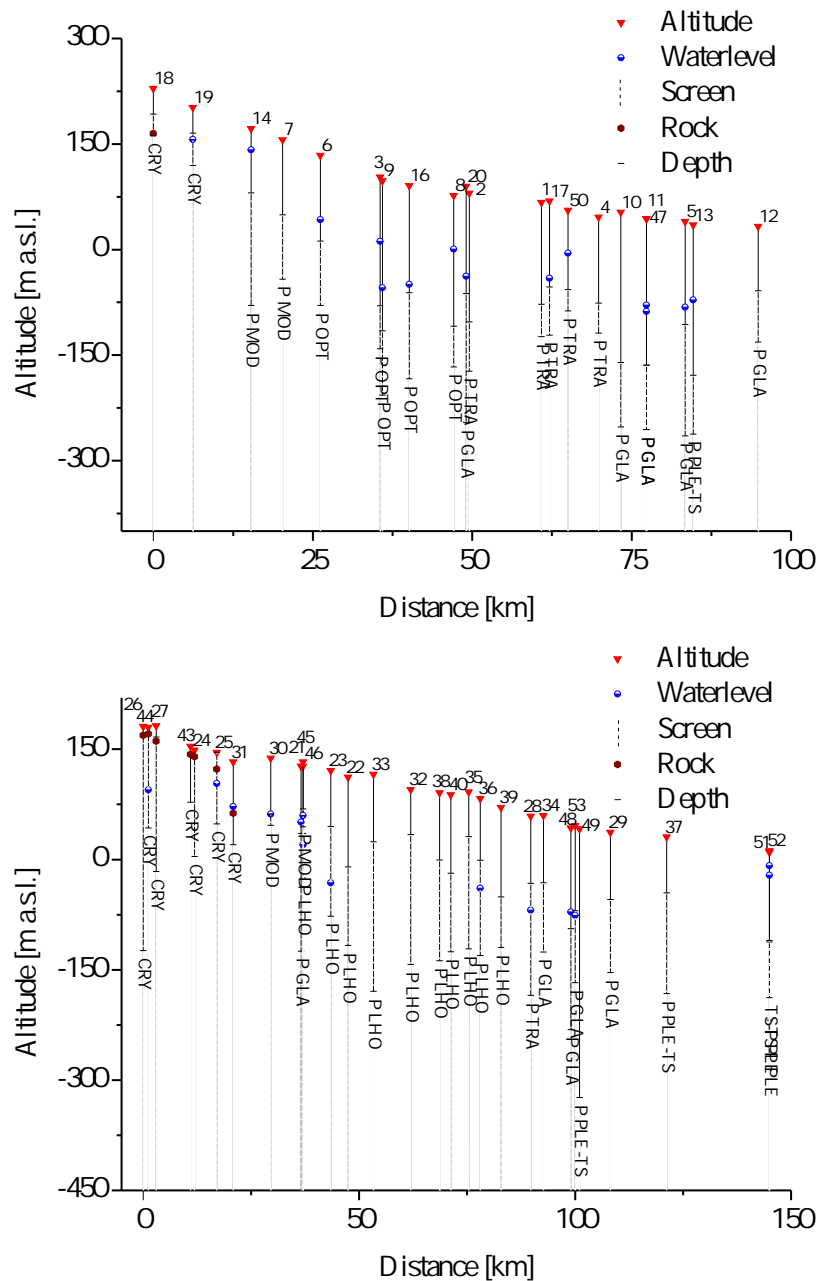


Figure 3.6.: Cross sections of the two sampled transects. For the northern transect, distance to well 18 is declared as distance to the recharge, while on the southern transect, it is well 26. The descending altitude from the recharge to the discharge can be observed as well as the increasing well and screen depths. Where CRY wells were sampled, the position of bedrock is marked if known.

much deeper into the solid rock. These wells are not representative for the sedimentary aquifer system and do not provide freshly infiltrated water. However, they can provide significant information about the geology of the hilly recharge area. They are summarised as group **CRY** and will not take part in the palaeoclimate discussion.

The area of the northern transect was less populated and had a poorer agriculture than the area of the southern transect, resulting in a more difficult search for suitable wells. Moreover, the salinity of groundwater was worse in the North, with increasing salinity towards the discharge area. As the convergence zone in the discharge in prehistoric times was submerged by the Arabian Sea, this is not astonishing. The southern transect is on one hand more populated, closer to big cities and has a more established agriculture, which facilitates the search for suitable wells. On the other hand, the age increase along the transect as observed by [Deshpande, 2006] is much more even in the North (see Fig. 5.17), which is one of the major reasons for the analysis of two transects.

Furthermore, for the study of hydrogeological information in the area, a special aim was put on thermal springs. These were found in two varieties. In the discharge area, some deep wells are known to be artesian. While the artesian character of the well sometimes is not existent anymore, as the piezometric head has dropped below the surface, the wells are now operated by submersible pumps. They are organised as group **TS-P PLE**. The water of these pseudo “artesian” wells show similarities to the very old aquifer water, yet may have been strongly influenced by exchange with very deep aquifer water. This deep water partly originates from crustal faults such as the mayor fault zone in the discharge area, the West Cambay Basin Bounding Fault (WCBBF), or one of the plenty minor fault zones (Fig. 3.7, [Deshpande, 2006]). Another variety of thermal springs could be found far off the observed region situated

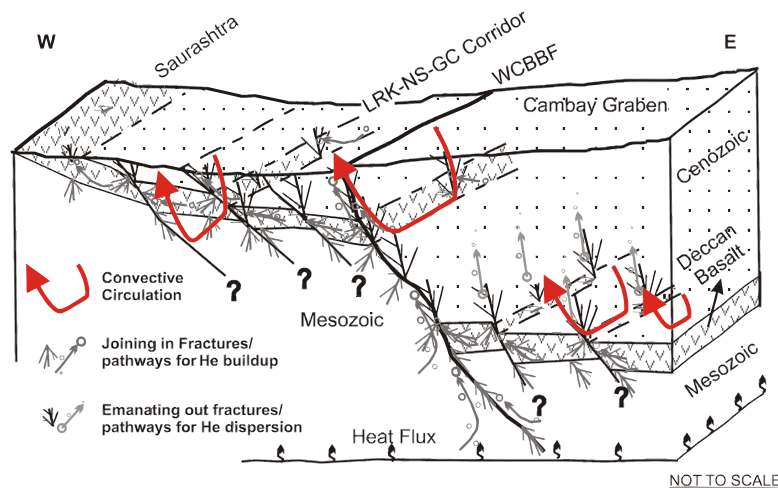


Figure 3.7.: Model of helium and groundwater behaviour in connection with the fault zones of the Cambay graben region. The idea is that groundwater (flow shown as red arrows) interchanges with formation water and gets impregnated with a non-atmospheric helium load [Deshpande, 2006].

south-east of the recharge area, where two religious places Lasundra and Tuaa have developed due to thermal springs, now used for ritual bathing or as a sanctuary. In Lasundra, a traditional dug well exists, while in Tuaa, water just emerges from the sandy ground in a temple

area. One of the findings of this project (discussed later in chapter 5.2.4) is that the origin of this thermal spring is a different one than the origin of the thermal springs in the discharge and may be more comparable to the crystalline recharge wells. They are therefore organised as group **TS-CRY**. Sampling of these samples was different from the usual sampling (described in section 3.2).

In addition to all these types of wells, a few dugwells with handpumps were analysed for the water's parameters, to have a better understanding of the recharge region's very shallow groundwater.

The well positions are shown in Fig. 3.1.

3.1.2. Realisation of well-sampling

Wells with submersible pumps

When a suitable well with working power supply¹ is found, air tight connectors are attached to the pipes, mostly using the air outlet (as can be seen in picture 3.8). The outlet is flushed



Figure 3.8.: Picture of a sampling at an Indian irrigation well. Tubes are connected to the air outlet of the pipe.

for a considerable time to provide fresh groundwater.

Pressure: Holding the hose in vertical position and measuring the height of the jet is a first indication of the connected well's pressure. As groundwater originating from deep layers in the aquifer may have a dissolved gas pressure significantly higher than atmospheric air pressure, keeping the samples under pressure is crucial to keep the dissolved gases in solution. Pressure

¹Power supply is everything but self-evident in India. In the countryside, power is provided on certain schedules which change weekly and in arbitrary looking sequence. Power blackouts during sampling did happen sometimes and resulted in restarting parts of the procedure.

can be increased by closing outlets of the well other than the sample outlet. Higher pressure implies higher strain on the well's pipes which, in India, are mostly in very bad shape in form of very rusty metal pipes or even the use of much weaker PVC pipes. Therefore, the risk to break the pipe and loose the pump in the well shaft exists. As these events would cause high additional costs and political stress, sampling sometimes had to take place under suboptimal pressure conditions.

Therefore, recording of sampling conditions is extremely crucial for a thorough evaluation. Besides, well information such as the depth of the tubewell, position of screen depth, position of the pump and, if known, piezometric head information needs to be checked. The coordinates of the well and the altitude are taken via GPS device. Collected well information is shown in table D.1 in the appendix.

The sampling begins with observation of the water's parameters (see Fig. 4.1). When the well is reasonably flushed and all stagnant water rinsed at least twice, sampling of non-gaseous tracers begins. The sampling concludes with the collection of samples with gaseous tracers and another reading of the water's parameters. Detailed discussion follows.

Other wells

Additionally, wells without submersible pumps were sampled. Some handpumps in the recharge area were used to analyse the water temperature and other parameters of the water. No standard sampling was done here and the wells did not receive a sequential well number.

Next, two thermal springs were also sampled without the help of submersible pumps. In the case of TS1 (Lasundra), which is a dugwell used for ritual washing and bathing, samples were collected from a big bucket filled in the well with a hose connection at the bottom of the bucket. Sampling was completed as fast as possible to alter the gaseous tracers in the water as little as possible. For this reason, the results have to be considered as a lower limit mixed with atmospheric signature instead of values with absolute accuracy.

The other thermal spring TS2 (Tuaa) was basically a hot, bubbling puddle in a small hollow with sandy soil. Here, samples were collected by submerging the sampling containers under water for a time of several minutes in a position suitable to flush them. Additionally to the imminent problem of atmospheric contamination, great amounts of sand contaminated the samples. The results may therefore also be a mixture with an unknown atmospheric component.

Wells 15, 41 and 42 were rejected during the sampling process due to air contamination.

Protocols of all wells are shown in the Appendix (Fig. C.1 and following).

3.2. Measurements

The pumping of a well changes the system. The piezometric head is lowered and forms a cone around the well, and if the screening of the well is too wide, different layers may be influenced and pumped at different times. If the well is situated in the unconfined zone, and the piezometric head is equal to the actual water table, refilling of the cone may produce artificial excess air from air bubbles forming in the dry cone body, or delete excess air information due to pressure loss. Therefore, information about screen depth, water level and pump depth is crucial.

A typical sampling situation is shown in Fig. 3.8.

Parameters analysed on a running well were water temperature, specific conductivity, alkalinity, dissolved oxygen and pH. Dissolved oxygen can change in the course of the first few minutes of flushing, as stagnant water gets removed from the pipes and the well shaft. When the readings are constant, pure aquifer water is pumped.

- The water temperature resembles the temperature of the soil from which the groundwater originates. As the geothermal heat gradient shows at which rate ground temperatures rise with increasing depth [Bischof, 1837] [Gupta and Deshpande, 2003], high water temperatures indicate either a deep well or a mixture with geothermal water from deeper regions of the crust. In addition to this, the soil (and therefore water) temperature in the recharge area is a first estimate for the expected recent infiltration temperature of the palaeorecord.
- Conductivity of groundwater is an estimation of total dissolved solids and salinity of the water. Since conductivity is temperature dependent, the specific conductivity for a fixed temperature is used (conversion shown by Bühner and Ambühl [1975]).
- Alkalinity consists of the dissolved bicarbonate and carbonate ion concentration and is a measure for the ability to neutralise acids via the carbonate-bicarbonate equilibrium. (To understand the geochemistry in the recharge area and in the aquifer, it is crucial to know the amount of dissolved carbonates and bicarbonates.) It is necessary for ^{14}C dating.
- The pH of the water is also essential for evaluating geochemistry of the water and all calculations related to carbonate dating.
- When water infiltrates into the soil, biogenic processes may absorb the dissolved oxygen in the water. High dissolved oxygen concentrations therefore indicate water which has infiltrated the aquifer very recently, or leaks from higher unsaturated layers into the aquifer or the well shaft. High oxygen concentrations in an expectedly old well are suspicious and may indicate contamination, while comparatively low oxygen concentrations in a well in the recharge area may point to a deeper well and undesired mixture with

older. The oxygen concentration is dependent on the water's temperature and salinity, described by the Henry law (2.3.19 and Fig. 2.23, oxygen is similar to argon).

3.3. Samples

When the parameters do not change anymore, the samples for tracer measurement are collected.

- Stable isotopes and tritium are sampled in small water bottles with headspace.
- The bottles for radon samples are equipped with a flexible diaphragm in the cap, as the water in the bottle has to be free of bubbles to avoid atmospheric contamination.
- ^{14}C samples are protected against biogenic activity with 0.1 g silver nitrate to avoid biological alteration of the sample (details are found in the appendix B.1), and stored in a dark place.
- SF_6 is collected in stainless steel cylinders which are closed after considerable times of flushing and knocking off air bubbles attached to the sampler's inner walls. The time it takes to fill a cylinder is a good indication to measure the water flow and pressure of the connected well.
- Finally, the noble gas samples are taken. A copper tube fit into an aluminium rack and fixed with steel clamps is flushed for a considerable time. During this process, the rack can be shaken by knocking a wrench against it, to make sure that bubbles stuck in the pipe are flushed through the pipe. Clamps are tightened first on the outlet side, then on the inlet.

After a last record of the probe's readings, the sampling is finished. All critical information needs to be logged in the field notebook. The time of collection for all samples and parameter readings should be noted. A general sequence in the procedure should be kept up for the whole campaign.

Radon concentrations were measured between field days and evaluated immediately.

4. Methods

4.1. Multiparameter probe



Figure 4.1.: Picture of the WTW water probe in use. Sensors measure groundwater collected in a flushed bucket. The brass connectors used to attach tubes to the air outlet are shown on the right.

Water parameters were recorded with a WTW water probe (see Fig. 4.1). Temperature and conductivity were measured with the sensor TetraCon©325. It has an accuracy of 0.2 K for temperature and an accuracy of 1 $\mu\text{S}/\text{cm}$ for conductivity below a signal of 2 mS/cm and 10 $\mu\text{S}/\text{cm}$ above. The pH sensor SenTix©41 has an accuracy of 0.01 as long as it is properly calibrated. Dissolved oxygen was measured with a CellOx©325 Clark cell sensor. Its accuracy is 0.01 mg/l for the observed oxygen concentration range. However, the probe and sensor accuracy was influenced by numerous factors, as there were no laboratory conditions. Firstly, the high air temperatures were not suitable for a good calibration and stability of the sensors' readings. Secondly, despite the fact that it is a condition for sampling, the water pumped from the well may experience minor changes in parameters. Parameter's errors therefore may be worse.

As problems with sensor calibration on site due to high temperatures occurred on the first trip, thorough calibration logs were recorded for the trips 2009 and 2010. Instead of cali-

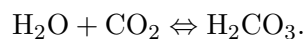
bration before measurement, a morning calibration was done under cool indoor conditions. The temperature sensor does not need calibration as it is calibrated by factory settings. The conductivity sensor was stable and reproduced the value of the calibration solution for several days without the necessity of setting a new calibration. Calibration was done with a one point calibration. The pH sensor caused some problems in 2008, but was also mostly stable and did not change much in 2009 and 2010. In these years, the calibration solutions for the two point calibration were kept at cool conditions and were not corrupted. The sensitivity of the dissolved oxygen sensor may have deteriorated on the 2008 trip, but was working fine in 2009 and 2010. The sensor was calibrated with respect to the atmospheric oxygen content before each sampling procedure. Therefore, accuracies should be determined by calibration logs (2009 and 2010) in detail which can be found in the appendix (Fig. C.15). Accuracy for 2008 should be determined from the field protocol, the measurement scattering and the parameter records of Dr. Deshpande (shown in field protocols, Fig. C.1 and following).

A detailed display of the sensors' characteristics can be found in the instruction manual of WTW.

The sum of HCO_3^- and CO_3^{2-} can be measured as the alkalinity in water with simple field testing kits using titration. The alkalinity measurement was done by Dr. Deshpande with the Merck quicktest titration kit Aquamerck 111109 (manual shown in Fig. B.8 in the appendix).

4.2. Stable Isotopes

For the analysis of stable water isotopes, a MAT 252 Finnigan mass spectrometer of IUP's carbon cycle group is used. As water vapour should be avoided inside mass spectrometers due to its adsorption capability in the machine, all samples have to be brought into gaseous form, and all water vapour has to be removed from the gas. For oxygen analysis, 5 ml of the water equilibrates with a CO_2 headspace for 6 hours. This is enough to get the oxygen isotopes of CO_2 into equilibrium ([Friedman and O'Neil, 1977] cited in Clark and Fritz [1997]) with the oxygen isotopes of the water molecule described by the reaction (2.3.10)



Occurring fractionation (described in chapter 2.3.1) is taken into account. The CO_2 gas is then measured in the mass spec [Neubert, 1992].

For analysis of hydrogen, 2 μl of water are brought to reaction with chromium at 850°C to produce H_2 which is analysed in the mass spec. As there is total reduction, no fractionation between D and H is involved [Coleman *et al.*, 1982] [Florkowski, 1985]. The absolute accuracy of the analysis is 0.05‰ for oxygen and 0.1‰ for deuterium [Keck, 2001]. The analysis accuracy derived from repetitive measurements for all measured isotopes is approximately 0.05 ‰.

4.3. Tritium

Tritium measurement was done in a low level proportional counting chamber situated in the basement of the IUP [Grothe, 1992] [Mahrla, 1978]. For one measurement, 9 ml of sample water were reduced with magnesium at 600°C to produce H₂ gas, which is observed in the counting chamber for a minimum of 24 hours. The detection limit of the Heidelberg counting chamber is only 2 TU¹, making it difficult to use these results in a quantitative way. (As the interest of this study is on water older than a few hundred years and a measurable tritium concentration would only be expected in very young water in the recharge area, the tritium results are used mainly as a knock-out criterion for contaminated old wells).

Another method to analyse low tritium concentrations is the so-called helium ingrowth method. In this case, water is degassed and stored in an evacuated glass bulb for several months. The tritium decays to ³He which can be measured at a mass spectrometer capable to analyse helium isotopes [Bayer *et al.*, 1989]. The method was not used in this study.

4.4. Carbon

4.4.1. Extraction

The extraction method: DIC has to be removed from water samples and collected. Isotopes in carbonate minerals are usually brought into the gaseous phase via acidification (see McCrea [1950]). By adding hydrochloric acid and by removing the produced gaseous CO₂ from the system, a complete conversion of the DIC can be achieved due to the reaction inequilibrium. Therefore, no fractionation of ¹³C or ¹⁴C should be expected.

It should be mentioned that another method to obtain carbonate samples exists. This method uses huge water samples mixed with barium chloride and sodium hydroxide solution (as described in Clark and Fritz [1997]). In alkaline milieu, hardly soluble barium carbonate precipitates and is collected for analysis. The method was not used for this project, as greater amounts of poisonous chemicals have to be used. Furthermore, huge amounts of water have to be collected for sampling, and the risk of contamination from atmospheric CO₂ may exist.

An extraction line was built by Kreuzer [2007] and Unkel [2006] to extract carbon from water samples and archaeological samples. The diagram 4.2 shows the procedure with water samples:

- The initial situation of the experiment is the following: 150 ml of the sample water are put into the Erlenmeyer flask together with a separated amount (12 ml) of 3-molar hydrochloric acid. The amount of water may vary depending on the alkalinity: For $\delta^{13}\text{C}$

¹The detection limit is derived from three times the standard deviation of the background.

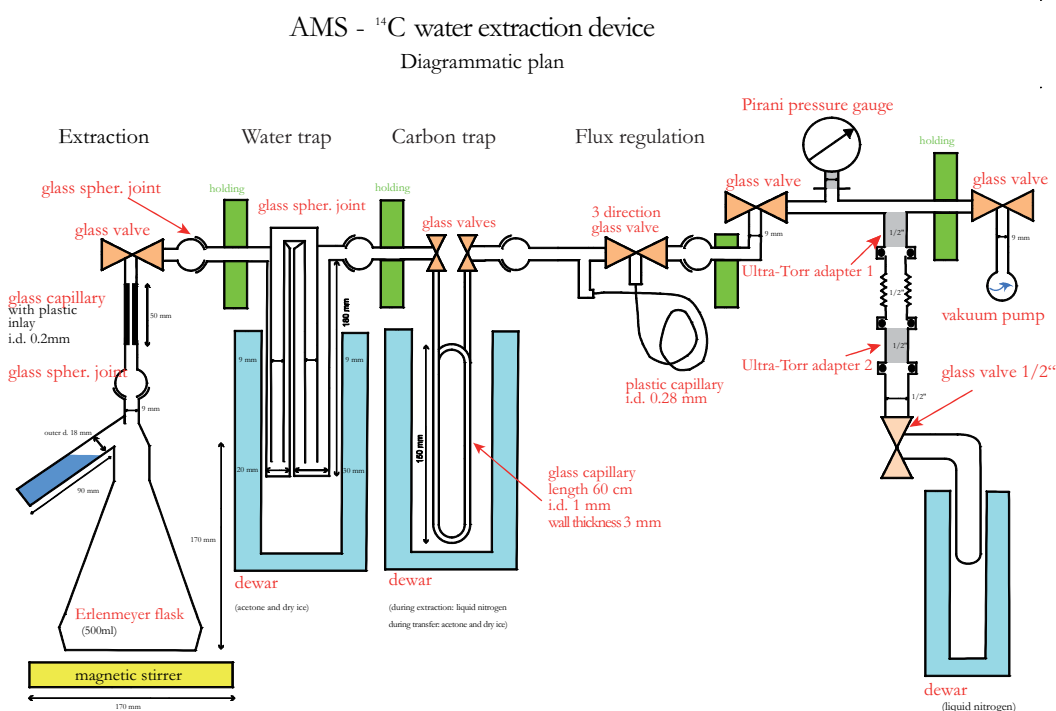


Figure 4.2.: Diagram of the extraction line used for the CO_2 extraction from purified water samples, adapted from Kreuzer [2007]. From the left to the right are shown: an Erlenmeyer flask containing the sample, the water trap, the CO_2 trap, a flux reduction, a glass vial for gas collection and the pumping line.

measurements, a total amount of $15 \mu\text{mol}$ is necessary for analysis (Michael Sabasch, personal communication), while targets for a ^{14}C AMS analysis should strongly exceed a lower limit of $40 \mu\text{mol}$ (or 0.5 mg carbon) [Wölfli, 1987]. Water samples with alkalinities around 5 mmol/l provide more than enough DIC in a water sample of 150 ml for both purposes. The danger of contamination or high background is minimised this way due to their small relative contribution.

The flask is attached to the extraction line and evacuated for ten minutes to remove all atmospheric air. A water trap cooled by an acetone and dry ice mixture (195 K) is used to keep as much water vapour from the pump as possible. The carbon trap is still inactive and at room temperature.

- After ten minutes, the pressure in the system should be around 0.05 mbar or less, which is sufficient to remove all atmospheric gas from the line. Evacuation is stopped, the Erlenmeyer flask is closed, and the hydrochloric acid is poured into the water sample. As a result from the change in pH, the carbon species transform to dissolved CO_2 which degasses due to the attached vacuum and the use of a magnetic stirrer.
- Now the carbon trap is brought to 77 K (temperature of liquid nitrogen) and the flask is opened again. A flow reduction behind the carbon trap is established to enable constant pumping of the system without removing gaseous CO_2 before its freezing in the carbon trap. For 45 minutes, the degassing CO_2 is now continuously frozen on the carbon trap.

As the reaction is in a non-equilibrium due to the removal of the product, all dissolved CO_2 is collected.

- After 45 minutes, the carbon trap is closed and heated; the Erlenmeyer flask is closed. The carbon trap is brought to the temperature of acetone and dry ice mixture to bind the rest of the water vapour. The water trap is defrosted and dried. Analysis of $\delta^{13}\text{C}$ has to take place under completely dry conditions, while carbon target generation for AMS measurements of ^{14}C is not sensible to water vapour. The CO_2 is frozen to a previously evacuated glass vial which is brought to the temperature of liquid nitrogen. This way, the total DIC of the water sample is stored in a glass vial in gaseous form.
- The glass vial can now be analysed by a stable isotope mass spectrometer for $\delta^{13}\text{C}$ ratios, and part of the gas can be used to produce carbon targets for AMS analysis [Wölffi *et al.*, 1983].

The extraction setup was tested and used by Kreuzer [2007] for just the same purpose, except the chosen water poison. As a result, iodide was used for the extraction which produced huge amounts of nitrogen in the extraction step. This is not a problem in this project due to the use of silver nitrate as poison.

The disposal of the sample needs to be considered. Metallic ions must not be washed back into the water cycle (the limit in drinking water is according to the German “Trinkwasserverordnung” [Bundesministerium für Justiz, 2001] $10 \mu\text{g}/\text{l}$). Used sample water has a pH value around 0 – 1 due to addition of hydrochloric acid. The remaining free silver ions bind to chloride ions and create silver chloride which is hardly soluble. The water is filtered and the filtrate is collected and dried. It is possible to dispose of the acid water by adding tap water.

4.4.2. Measurement via AMS

As the ^{14}C signal in mass spectrometric measurements overlaps with signals of ^{14}N or $^{12}\text{CH}_2$, it cannot be measured in a normal mass spectrometer. The separation can be done with the help of accelerator mass spectrometry (AMS). After the first acceleration, all isobars and molecules of the same mass pass through a thin layer of foil or gas called stripper where molecules are sorted out and the isobars are “stripped” of their electrons, hence accelerating away from the stripper. After that, magnetic fields separate the appearing isobars sufficiently. To measure a sample, gaseous CO_2 has to be brought into solid state on a copper plate which can be used as source in the AMS [Wölffi *et al.*, 1983]. According to Wölffi [1987], the measurement accuracy is determined by counting statistics above the level of 0.3 %. The detection limit for samples as small as 0.5 mg is determined by the blank value of about 0.5 pmC which represents an age limit of 42 kyr ^{14}C age.

It is necessary to emphasise that laboratories give a standardised activity ratio corrected according to observed ^{13}C fractionation [Stuiver and Polach, 1977]. Due to sample treatment, fractionation in the measurement process is corrected by comparing a standard ^{13}C ratio

(for organic samples assumed $\delta^{13}\text{C}_\text{N} = -25\text{‰}$ as value for C3 plants) to the observed one. Therefore, normalised activity $^{14}\text{A}_\text{N}$ and uncorrected laboratory activity ^{14}A are connected by the formula [Craig, 1954] [Mook and van der Plicht, 1999]

$$\frac{^{14}\text{A}_\text{N}}{^{14}\text{A}} = \left(\frac{1 + \delta^{13}\text{C}_\text{N}}{1 + \delta^{13}\text{C}} \right)^2 \quad (4.4.1)$$

Hydrologic studies of dissolved inorganic carbon show different $\delta^{13}\text{C}$ amounts. Mook and van der Plicht [1999] suggested therefore another correction in hydrologic studies with an actual ^{13}C fraction differing from -25‰ . Therefore, the right activity for hydrologic samples can be retrieved by reversing 4.4.1 and replacing $\delta^{13}\text{C}_\text{N}$ with the actual measured ^{13}C ratio of the sample [Mook and van der Plicht, 1999] [Stuiver and Polach, 1977]. As a result, the calculation is

$$^{14}\text{A}^\text{S} = ^{14}\text{A}_\text{N} \left(\frac{1 + \delta^{13}\text{C}}{0.975} \right)^2 \cdot e^{(t_{\text{sampling}} - 1950)/8267} \quad (4.4.2)$$

The last term corrects the activity to the sample's exact amount of ^{14}C at the time of sampling.

4.5. SF₆

4.5.1. Sample treatment

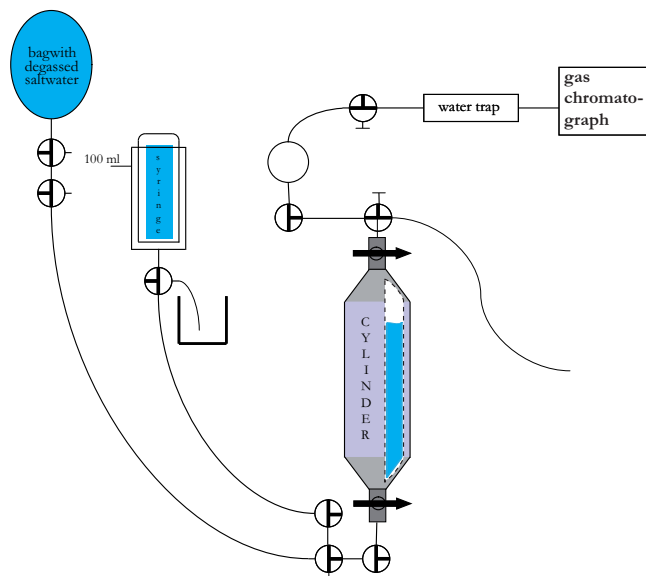


Figure 4.3.: Diagram for SF₆ sample treatment, adapted from Sorger [2010]. The lower valve of the cylinder is prefilled with degassed salt water, the upper valve with nitrogen. Before every injection, the syringe is filled with degassed salt water and used to push the headspace (see cut-out) from the cylinder into the sample loop of the GC system.

Due to the low solubility of SF₆, sample contamination with atmospheric air must be avoided. Based on a method by Wanninkhof and Ledwell [1996], the conventional sampling method of SF₆ samples developed in Heidelberg is described in von Rohden and Ilmberger [2001]:

Evacuated glass bottles are used to collect sample water together with a nitrogen headspace which is measured in the laboratory. By recording the temperature controlled equilibrium, the SF₆ concentration of the original water sample can then be calculated from the measured headspace concentration.

For reasons of robustness and manageability, I used 0.5 l stainless steel cylinders instead of glass bottles for the sampling.

Sampling with steel cylinders is described in chapter 3.3.

In order to measure the SF₆ in the samples, a headspace has to be created which can be injected into the GC. Two procedures were attempted to create this headspace. For the first samples of the 2008 campaign, a “decanting” procedure was done. Samples were decanted to glass bottles and subsequently measured. The water was transported from the steel cylinder to the evacuated glass bottle by pure nitrogen. The nitrogen then was used to create an overpressured headspace.

This method was used for both of the the first campaign’s twin sample sets. The sample containers were filled with water of temperatures of 30°C or higher in the field and were stored in the temperature controlled laboratory at about 24°C. As a result of the thermal contraction of water in the steel cylinder, small air bubbles containing degassed SF₆ occurred, altering the water’s concentration of SF₆. For the samples of the second campaign, both the glass bottle and the steel cylinder were pressurised with nitrogen. Both containers were measured and the final SF₆ concentrations from both measurements evaluated.

A new method was established by Sorger [2010] which takes into account air bubbles in the cylinders by heating them for analysis to temperatures above the water temperature they had at the time of sampling. Furthermore, the method avoids the use of different containers for the processing of each sample. In this “headspace” method, a headspace of nitrogen was produced in the steel cylinders. Due to the absence of air bubbles, the SF₆ concentration is not altered. The headspace in the steel cylinders is then measured in the GC (as shown in Fig. 4.3). The procedure was used for the remaining set of twin samples of campaign 2009 as well as both sets of samples of the campaign 2010. Some special treatment was necessary as the original steel cylinders had normal valves, while the glass bottles have much more adequate three-way valves which can be flushed with water or nitrogen to avoid contamination in the tubes. Thorough flushing of the connection parts with nitrogen or in other cases degassed salt water was used to avoid further contamination with SF₆. For future use, three-way valves are employed.

The results (which are in detail discussed later in chapter 5.2.5) showed that the “headspace” method achieves to measure all SF₆ in the sample without alteration due to bubble forming. Additionally, the method implies less risks of contamination due to extraction steps, as the

“decanting” method may have done. Nonetheless, the results from the “decanting” method can at least be interpreted qualitatively, as comparison with twin samples of the 2009 campaign indicates. For future use, the “headspace” method is recommended.

A thorough study of different SF₆ sample containers, extraction methods and measurement techniques is shown in [Sorger \[2010\]](#).

4.5.2. Gas chromatographic measurement

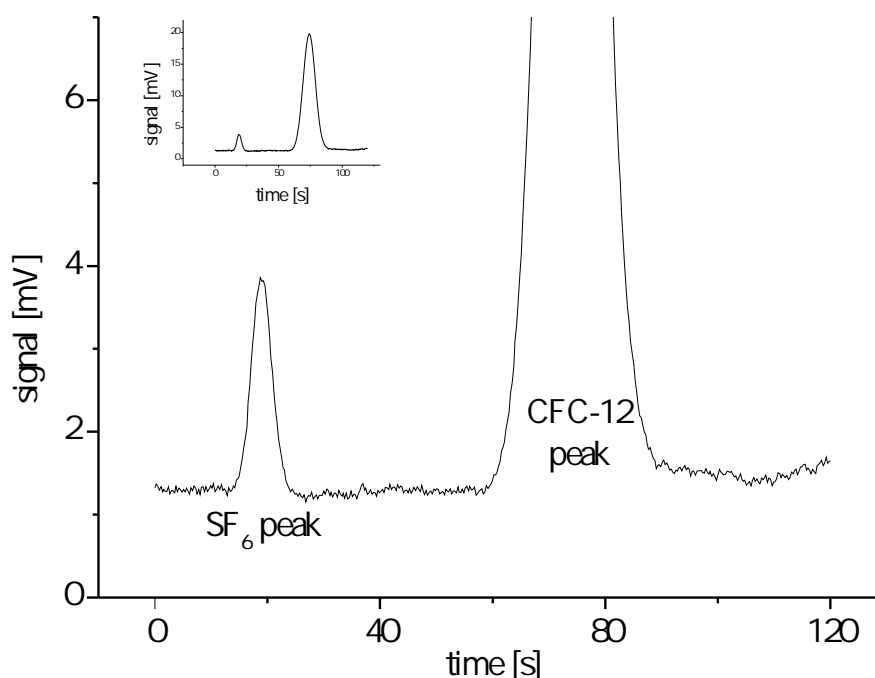


Figure 4.4.: Typical GC peakscan of an Indian sample. Peaks of SF₆ and CFC-12 were recorded for each sample.

Measurement of the gaseous SF₆ is done with a GC-ECD system (Shimadzu GC-8AIE) of IUP’s limnophysics group specifically optimised for SF₆ measurements, described by [von Rohden \[2002\]](#).

To check SF₆ results of old samples for atmospheric contamination, the CFC-12 peak adjacent to the SF₆ peak was also recorded. A typical peak scan is shown in Fig. 4.4. Lately, results for CFC-12 could be evaluated by Christoph v. Rohden, but will only shortly be discussed in the results chapter 5.2.5.

Gas chromatographic measurement of the samples is done together with blank measurements and measurements of an SF₆ standard. A non-linearity correction of the machine is used which is working best for concentrations lower than the standard. The obtained peak areas are evaluated and an absolute SF₆ concentration is calculated. Detailed information about the use of the Heidelberg SF₆ GC is shown in [von Rohden and Ilmberger \[2001\]](#).

4.6. Noble gases

4.6.1. MS Method

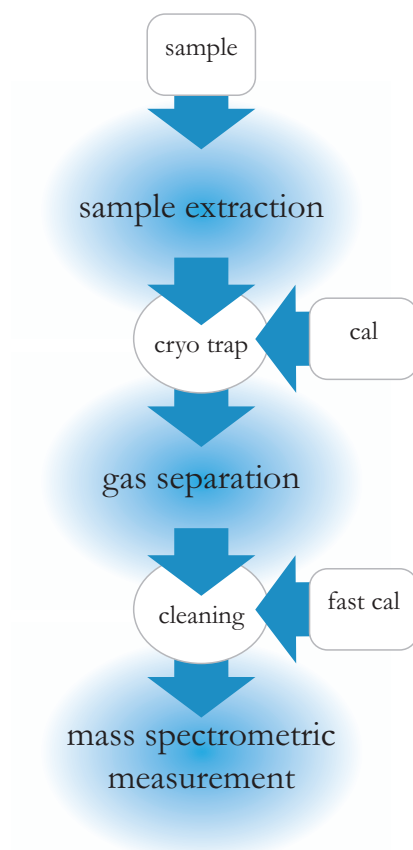


Figure 4.5.: Schematic diagram of the MM5400. Extracted samples as well as calibrations are collected in the cryo. By using different freezing temperatures, gases are separated, cleaned, and measured in the mass spec. A detailed diagram of the line is part of the appendix (Fig. B.10).

The principle of a mass spectrometer is measuring the mass-to-charge ratio of charged particles. Basically, the Lorentz force and the electrical force are used in varying ways to separate particles in most mass spectrometric devices.

The Heidelberg NG MS 5400

The Heidelberg noble gas mass spectrometer is a common system for the purpose of noble gas analysis. As shown in Fig. 4.5, noble gases are extracted from a sample, collected, cleaned and finally measured successively in the mass spectrometer. A calibration standard² which is

²In Heidelberg at the Institut für Umweltphysik, in Zürich at the Eidgenössische Technische Hochschule [Beyerle *et al.*, 2000] and in New York at Lamont-Doherty Earth Observatory, Columbia University, the standard consists of normal atmospheric air. Laboratories such as the Woods Hole Oceanographic Institution

processed analogously provides absolute amounts for measurements. A detailed discussion of the noble gas measurement procedure at the Heidelberg MS is presented in the following section.

Noble gas measurement in Heidelberg

The MM5400 is a sector field mass spectrometer. Mass separation is achieved by sending the ionised sample gas through an adjustable magnetic field. The ions are diverted by the Lorentz force according to their charge-to-mass ratio. The signal is detected in either a faraday cup detector or a multiplier detector. The height of the peak depends on the strength of the beam. To correct signals for sensitivity fluctuations of the detectors, a fast calibration measurement (short “fastcal”) of a pure He, Ne or Kr/Xe³ gas pipette is performed prior to every measurement.

A diagram of the sampling procedure is shown in Fig. 4.6. Due to necessary improvements, different procedures for Ar, Kr and Xe analysis were used in this thesis. The initial procedure is shown in Friedrich [2007] and is repeated here for direct comparison (shown in the first half of Fig. 4.6). An interim procedure and the current procedure (which is shown in the second half of Fig. 4.6) are also described in this section.

Extraction and collection: An online in vacuo extraction procedure is done for samples. Water of a sample is degassed and the extracted gases are dried in a zeolithe trap. The gas is collected on a stainless steel trap (SST) at 25 K for 20 min to adsorb all gases other than H₂, He and Ne, which are adsorbed afterwards for another 20 min in an activated charcoal trap (ACT) below 10 K.

For calibration, pipettes with an air standard of atmospheric composition are taken (gas amounts of 0.2 to 4 cm³ can be managed) and collected the same way.

He and Ne measurement: He is measured separately from other gases, as for an effective resolution of the ³He peak and optimum He ionisation, the source of the mass spectrometer has to be run with a higher electron energy. Another necessary step is the separation of Ne and Ar. Double charged ⁴⁰Ar has nearly the same mass-to-charge ratio as ²⁰Ne and is the

[Stanley *et al.*, 2009] can compare their samples to a gas composition different from air composition by using two different standards, an air standard and a pure Ar/Kr/Xe standard which can be mixed to simulate warm or cold water compositions.

³Until spring 2010, a fastcal of Ar/Kr/Xe was used. Production of the original Ar/Kr/Xe fastcal is described in Friedrich [2007]. The Kr/Xe fastcal was generated by extracting a 40 ml water sample. By many adsorbing and desorbing steps and numerous pumping steps in the cryo, an argon-free gas composition was produced (considering the desorption curve Fig. B.11).

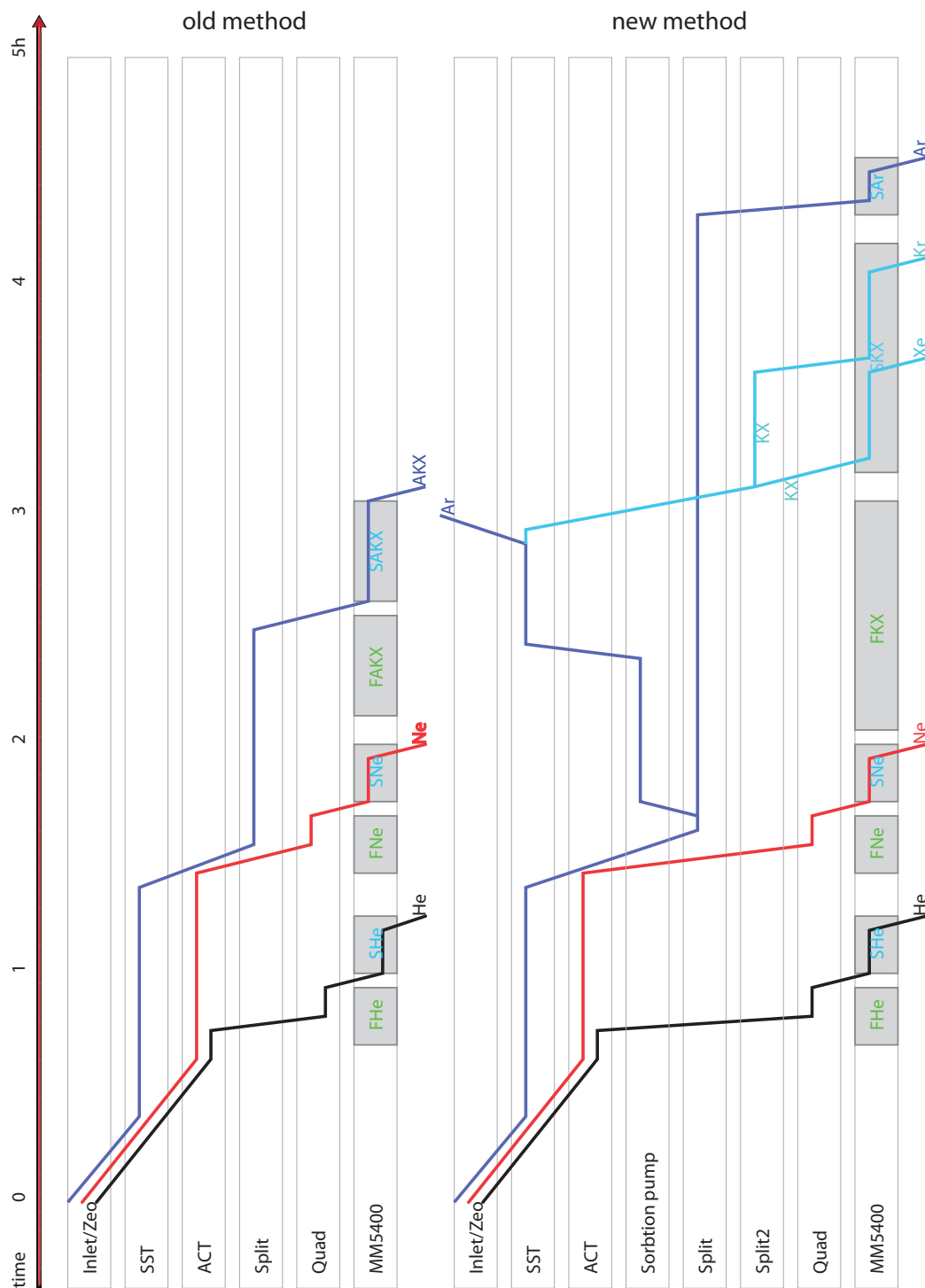


Figure 4.6.: Event diagrams for the old (derived from Friedrich [2007]) and the new sampling method of noble gas samples at the MM5400. The MS is divided into the inlet part with a zeolite water trap, a stainless steel trap (SST), an activated charcoal trap (ACT), splitting volumes, a quadrupol residual gas analyser, a heated sorption pump to absorb reactive gases, and the actual mass spectrometer MM5400. Measurements are indicated as grey boxes.

most abundant noble gas isotope. Necessity to separate Argon from the heavier noble gases will be discussed subsequently.

After the collection of the gases, the charcoal trap is heated to 42 K, releasing helium which is expanded into the line for pre-analysis in a quadrupole residual gas analyser. This is done to find the right range for analysis in the MM5400, and to split the sample if required, as He concentrations can range over several orders of magnitude. The gas is then measured in the MS.

After pumping away all He from the line and the charcoal trap, the trap is heated to 90 K to desorb Ne. Now the procedure is similar to He.

Old procedure for Ar, Kr and Xe: The old procedure is shown in Fig. 4.6. The SST is heated to 130 K and the permanent gases are expanded to a splitting volume. A single pipette with a volume splitting factor of 1/4000 is taken. The pipette's contents are expanded to a getter pump to absorb the reactive gases. The resulting noble gas mixture of Ar, Kr and Xe is sent to the MS and measured.

The total sampling routine per measurement took about 200 minutes, resulting in a measurement reproducibility of better than 1 % for all main isotopes except ^{132}Xe (1.4%). It was not possible to achieve correct concentrations of air equilibrated water and lake standards with this method. Different offsets for the different noble gases were found. In 2006, observed offset values were (Dr. Palcsu, personal communication):

$$\text{He} : 4\%, \text{Ne} : 2\%, \text{Ar} : 2.7\%, \text{Kr} : 4.7\%, \text{Xe} : 3.8\%$$

In 2008, Friedrich described the offset as follows:

$$\text{He} : 3.4\%, \text{Ne} : 3.7\%, \text{Ar} : 3.1\%, \text{Kr} : 5.9\%, \text{Xe} : 1.3\%$$

Tests showed an offset dependence on the gas composition, as measurements of laboratory air samples showed a relatively similar offset of approx 3 % for all noble gases [Wieser, 2006].

Comparison to a known volume showed volume overestimation of the automatic pipettes with an offset of 1.5 %. Only an offset for krypton remained and was corrected in measurement results. First results of Indian samples (Run42) were produced and corrected by a 4.4 % Kr offset. Besides, Xe and ^{36}Ar signals showed high measurement errors due to low count rates.

Higher Xe gas amounts revealed a negative offset for Xe. Ar in the gas mixture was suspected to be responsible for Kr and Xe deviations. Therefore (interpretations are shown in the appendix B.2.3), separation of Ar and Kr was requested.

Cryogenic desorption: With the old method, a complete separation of Ar from Kr was not possible (see Fig. B.11), due to the majority of the reactive gases blocking the SST for the noble gases. Furthermore, desorption curves are pressure dependent, meaning less steep and

shifted towards higher temperatures for higher gas pressures [Langmuir, 1916] [Wonneberger, 2008] [Wutz, 2010] (discussion in appendix B.2.2; Fig. B.13 shows theoretical and observed data).

Interim procedure: It was possible to achieve reduction of sample gas by expanding about 99.9% of the gas from the SST at room temperature and by successfully trying perfect gas separation with the rest (0.01%). The tested desorption was complete for different gas amounts and temperatures. Additionally, filament currents in the mass spectrometer for He measurement was reduced from 800 to 600 mA to reduce noise and the life span of the filament without loss of sensitivity.

Due to the used volume splittings, the measured gas amount of Kr and Xe was huge, which should be avoided in favour of a low background in the MS. Fast calibrations were still mixed Ar/Kr/Xe gas, producing unreliable fast calcs which deteriorated measurement results. Nonetheless, a part of the Indian samples was measured with this method (Run49).

The current method

For the current setting, the fastcal gas was renewed and a pure Kr/Xe gas produced to guarantee argon-free Kr and Xe fastcals. There does not exist a fastcal for argon at the moment. However, faraday measurement of argon is the most stable recording. When calibrations of ^{40}Ar for temporal trends were monitored over time (see 4.6.3), no negative consequences occurred.

A more sophisticated method to process the gases was found. The SST is heated to room temperature and the gases expanded into a splitting volume. A single pipette (1/4000) is taken. This gas is expanded to a sorption pump to absorb the reactive gases and to reduce pressure by a factor 100. The resulting noble gas mixture of Ar, Kr and Xe is again transmitted into the SST where Kr and Xe are trapped at a temperature of 56 K. The remaining gaseous Ar is pumped from the line and the SST. To get rid of Ar unintentionally trapped in the adsorbed Kr matrix, the closed SST is cycled to 75 K, refrozen to 57 K, and pumped again [Stanley *et al.*, 2009]. Resulting residual Ar content lies in the range of background measurements for all customary gas amounts without any loss of Kr due to pumping. Desorption curves for different calibration sizes as well as for different temperatures were made. The result shows (Fig. B.14 and B.15 in the appendix) that, due to the low pressure achieved, separation at a constant temperature can be guaranteed for all expected sample sizes. The resulting Kr/Xe gas mixture is transmitted to the MS for analysis. To reach similar signal intensities for the multiplier, the bigger part of the Kr/Xe gas is injected for xenon measurement, and the smaller part for Kr measurement. This is achieved by using a sorption pump as another splitting volume.

During the Kr/Xe measurement, another pipette is taken from the splitting volume and cleaned from reactive gases in the sorption pump. After the Kr/Xe measurement, Ar is measured in this gas amount.

The current method was used to measure most of the noble gas samples in Run53 and Run54

discussed in this project. Differences in measurement results will be discussed in 5.3.2.

Performance of the current method

To check whether offset problems are avoided, eighteen samples of air equilibrated water were measured in the same run as the majority of this project's samples (single sample results are shown in table B.1). Results showed a measurement uncertainty for water samples of

$$\text{He} : 0.4\%, \text{Ne} : 0.5\%, \text{Ar} : 0.5\%, \text{Kr} : 1.9\%, \text{Xe} : 1.4\%$$

The standard deviation of the results and therefore the reproducibility was

$$\text{He} : 0.2\%, \text{Ne} : 0.6\%, \text{Ar} : 0.3\%, \text{Kr} : 0.7\%, \text{Xe} : 1.2\%$$

The deviation of the results from theoretical values was

$$\text{He} : 2.7\%, \text{Ne} : 0.5\%, \text{Ar} : 0.6\%, \text{Kr} : -0.2\%, \text{Xe} : 0.4\%$$

The deviation of He is not astonishing, as the laboratory water standard is produced in an environment of enhanced use of He gas. Usage of a standard made of lake water may avoid this problem. The big measurement error of Kr may result from the fact that, for testing reasons, after the Xe and the Kr scans a measurement of residual Ar in the MS was done prior to pumping. This measurement disturbs the Kr measurement, but was until now necessary to ensure a thorough evaluation of the measurement. As a result, all calibrations and therefore the calculation of absolute gas amounts has an increased measurement error. Since the reproducibility of Kr shows a much smaller value, it can be assumed that the measurement uncertainty of Kr highly overestimates the machine's error. This does not occur for other elements. For future improvements of gas analysis and evaluation, improvement of the Kr measurement error is considered.

The current method still has a great potential for improvements. In addition to preserving and mentioned improving of the measurement error and reproducibility, to achieve a reduction of measurement time is crucial. Nonetheless, the total measurement error lies in the same range as the ETH noble gas mass spectrometer of

$$\text{He} : 0.6\%, \text{Ne} : 0.9\%, \text{Ar} : 0.8\%, \text{Kr} : 1.0\%, {}^{136}\text{Xe} : 1.3\%,$$

as shown in [Beyerle *et al.* \[2000\]](#), which was the guideline for the Heidelberg MS. While the MS setup shown by [Stanley *et al.* \[2009\]](#) can achieve better measurement errors, two mass spectrometers are needed. Sample sizes of 90 ml water are necessary for the result, while Heidelberg standard sample sizes do not exceed 20 ml. In addition to this, the sorption pump used in our system only has to adsorb less than a thousandth of the total dissolved reactive gases resulting in less frequent reconditioning.

4.6.2. MS measurements

After gas inlet into the mass spectrometer, peak scans (shown in Fig. B.18) determine the mass position for measurement. Noble gas isotopes are depleted over time by consumption in the source. To determine the initial amount, peak heights are repeatedly integrated for extrapolation to the moment of inlet (what is shown e.g. in Fig. 4.7).

Magnet and detector problems

In general the setup is suitable for measuring many isotopes in the same turn of gas inlet. Continuous jumps between the masses are suggested as this reduces the time between the inlet and the first signal information for each isotope and therefore produces low extrapolation errors. This practice creates however two difficulties:

Firstly, the magnetic field is not stable enough for changes between masses. The risk exists that repeated measurements miss the middle position of the peak and with it the signal⁴. A method to avoid these problems is precycling the magnet and erasing its hysteresis.

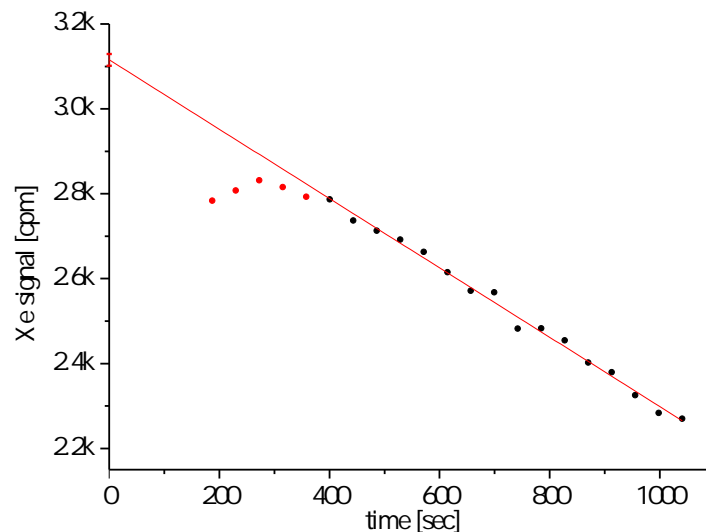


Figure 4.7.: Peak integrations of ^{132}Xe over time are shown. To determine exact amounts of a noble gas, peak integrations need to be extrapolated to the moment of inlet. In this plot, increasing sensitivity and therefore signal strength of a multiplier measurement is observed during the first readings.

Secondly, the multiplier detector has a variable efficiency, depending on the primary energy of the beam [Burroughs, 1969]. Sudden exposure to strong beam intensities and changes in the counting efficiency lead to imperfect integrations. Resulting data points cannot be used for signal determination (as is shown in Fig. 4.7 and 4.8). A feature called multiplier protection exists in principle [Friedrich, 2007] which could be used to shield the multiplier during magnet

⁴Optimal peakshapes are aspired. Calculation of peak resolution is shown in Fig. B.19.

scans. However, this function is not working properly with the current software.

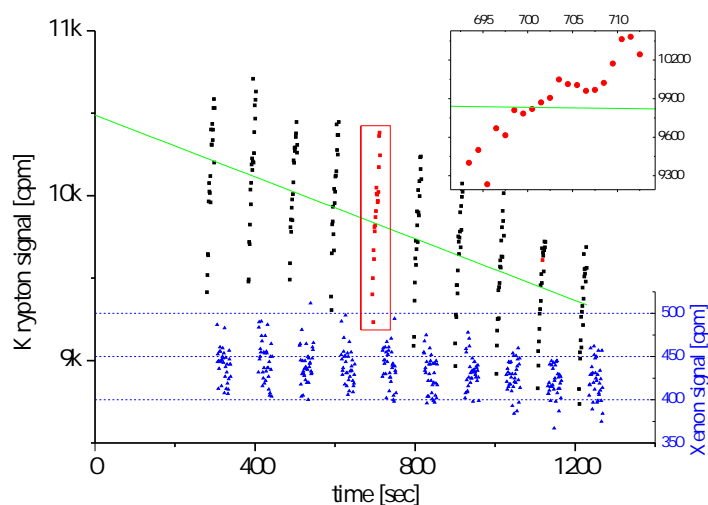


Figure 4.8.: Increasing sensitivity and therefore signal strength of a multiplier measurement of krypton. Between each group of krypton measurements, the krypton beam is moved away from the detector and a much lower signal of xenon (blue triangles) strikes the detector. As a result, the signals climb in every group of krypton (see red dots in subfigure) but drop in general due to gas consumption.

Therefore, to avoid magnet and detector problems, single isotope measurement with individual gas inlets were performed. Thus, by longer measurement times, proper peak trends and reduction of outliers were achieved.

These measurements were done for every analysed isotope, sample, calibration, blank and fast calibration.

4.6.3. Data Evaluation

After the measurement, these results are evaluated. Different evaluation steps are performed with the software WUCEM⁵.

The accurate operation of the mass spectrometer needs to be monitored. A daily check of the measured peak scans is necessary. An evaluation with WUCEM needs to be done for every measurement run, which may comprise several weeks of sample analysis, consisting of sample, calibration, fastcal and blank measurements.

⁵acronym for german “Wincalc- und Calc5400-Ersatz von Michael”, produced by Michael Jung, former diploma student of the group

Wucem

For each measurement, several files are generated, e.g. a fast calibration, a calibration, a blank or a sample. The files contain the peak measurements of the chosen isotopes with their corresponding time signature as well as further information such as pipette counters or, in the case of calibrations, the isotopic gas amounts. Firstly, peak trends of every single measure-

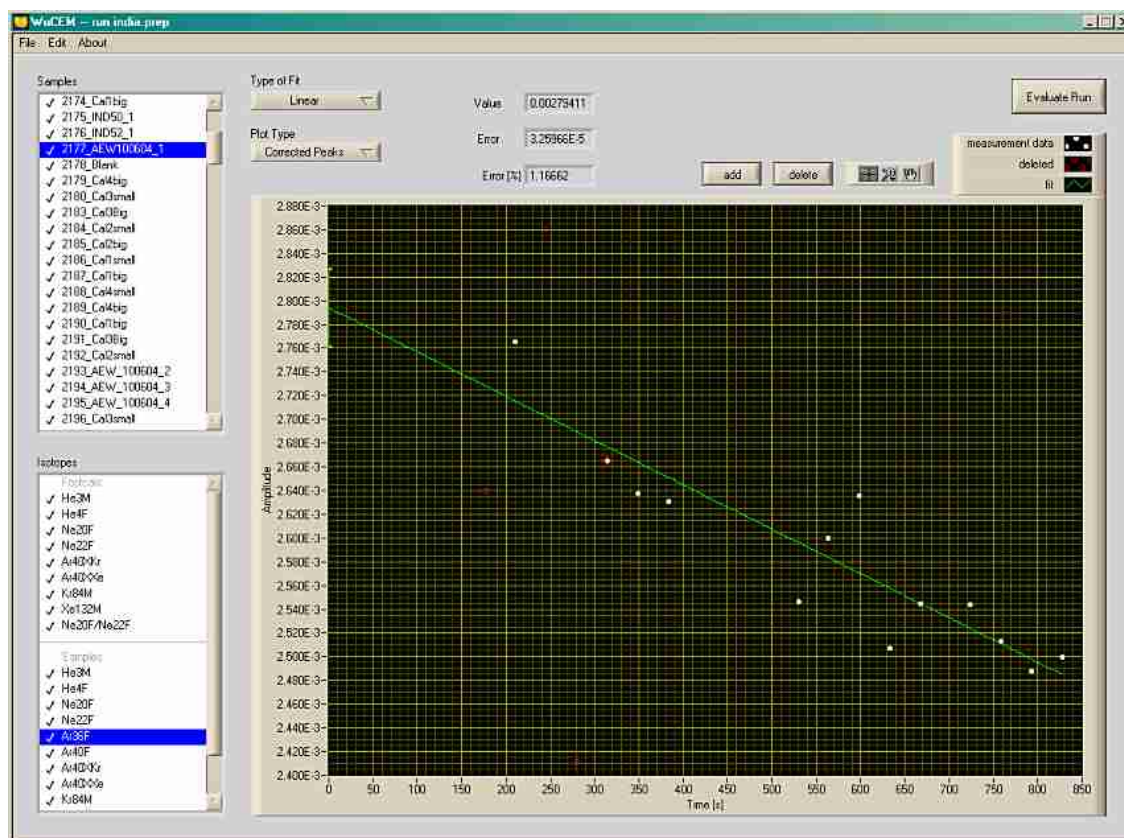


Figure 4.9.: Screenshot of the WUCEM peak trend evaluation. The user’s task is deleting outliers (red dot) or defining a fit (green line) to receive the initial signal via extrapolation. This has to be done for each measurement. Lists on the left show these measurements of samples and calibrations (top), and the individual isotope measurements (bottom). Fit parameters and the error are also displayed.

ment are checked to remove outliers, set fitting curves to derive the extrapolated initial signal, define isotope ratios or disable specific isotopes irrelevant for the evaluation. Isotope ratios at this stage of the evaluation only make sense for “same-detector” ratios, as the non-linearity correction for different detectors would exclude “mixed-detector” ratios. A typical peak trend can be seen in Fig. 4.9. In the next step, the fast calibrations (which were done prior to each sample or calibration measurement) are examined and if necessary edited by removing outliers. They are assigned with a substitution value from trends, constant values or nearest neighbours (see Fig. 4.10). Afterwards, all calibration, blank and sample data is corrected with the fast calibrations or their trend to eliminate e.g. sensitivity fluctuation or diurnal trends from the data.

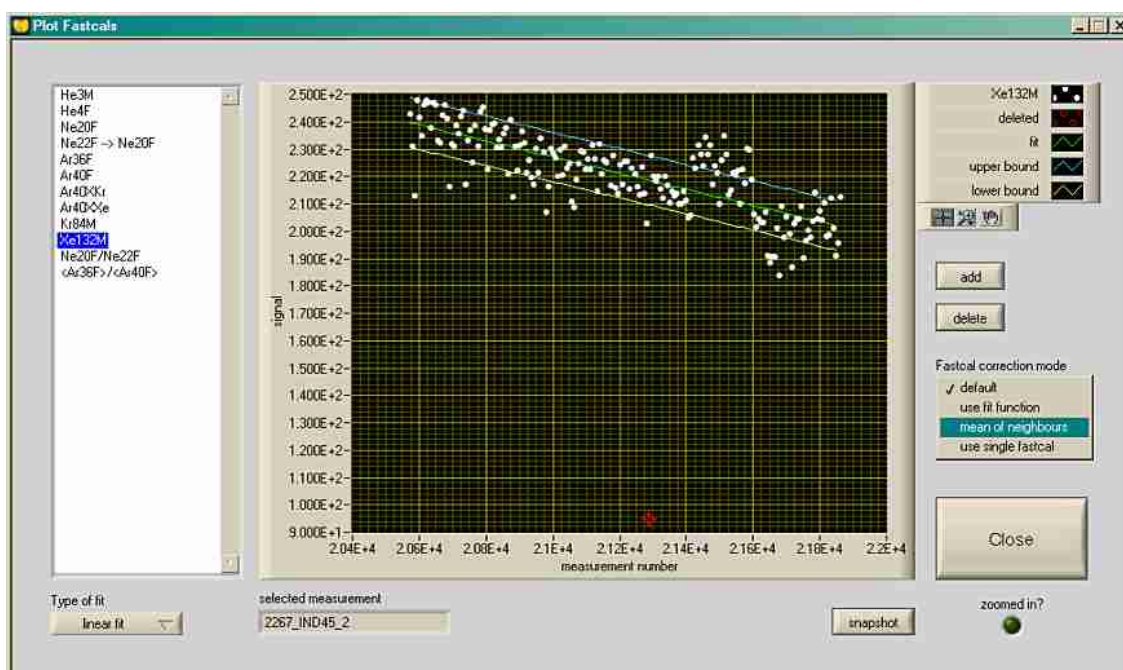


Figure 4.10.: Screenshot of the WUCEM fast cal evaluation. The user’s task is to check the fastcals done prior to every measurement. Single outliers can be deleted (red dot), and replaced by the mean of nearest neighbours’ values, trends (green line), or constants. This has to be done for each isotope (left columns). Trends or leaps in the fastcals indicate a change in the machine sensitivity. Strong declining trends may predict a filament burn-out.

After that, it is possible to view calibrations versus time of measurement. Temporal trends of the fastcal corrected calibrations can be observed if existent. If no fastcal measurement was done for an isotope (as e.g. for ^{36}Ar and ^{40}Ar), observing the calibrations versus time is the only way to ensure that no fastcal correction was necessary.

The next step is the evaluation of blank measurements of the processing line, which are then used to correct all calibration and sample measurements of the isotopes for blank offsets. Ratios are not corrected. A “same-detector” ratio cannot be used for evaluation if a significant blank background exists for one of the affected isotopes. Increasing trends in the blank information may indicate the possibility of leakage, decreasing trends indicate cleaning of the MS after a contamination. Up to this evaluation step, all sample data is based on voltage or cps readings. To extract actual gas amounts, these values have to be compared to some air standard with a known noble gas composition. Neither detectors nor the source do always have linear sensitivity. The sensitivity of e.g. the electron multiplier detector is dependent on the number of particles hitting it [Burroughs, 1969]. As already mentioned, the gas amount may have a repressive effect on ionisation. Furthermore, one of the big problems of sensitivity was found to be the amount of gas in the ion source, influencing the efficiency of ionisation. Because of all these phenomena, no one-point calibration can be used to estimate the actual gas amount in a sample. Therefore, air calibrations of different sizes (0.2, 0.4, 0.6, 0.8, 1.0, 2.0, 3.0, 4.0 and for big sample sizes also 5.0 and 6.0 cc) are used. In the next evaluation step, the non-linearity trends for each isotope are observed and fitting curves are used to evaluate

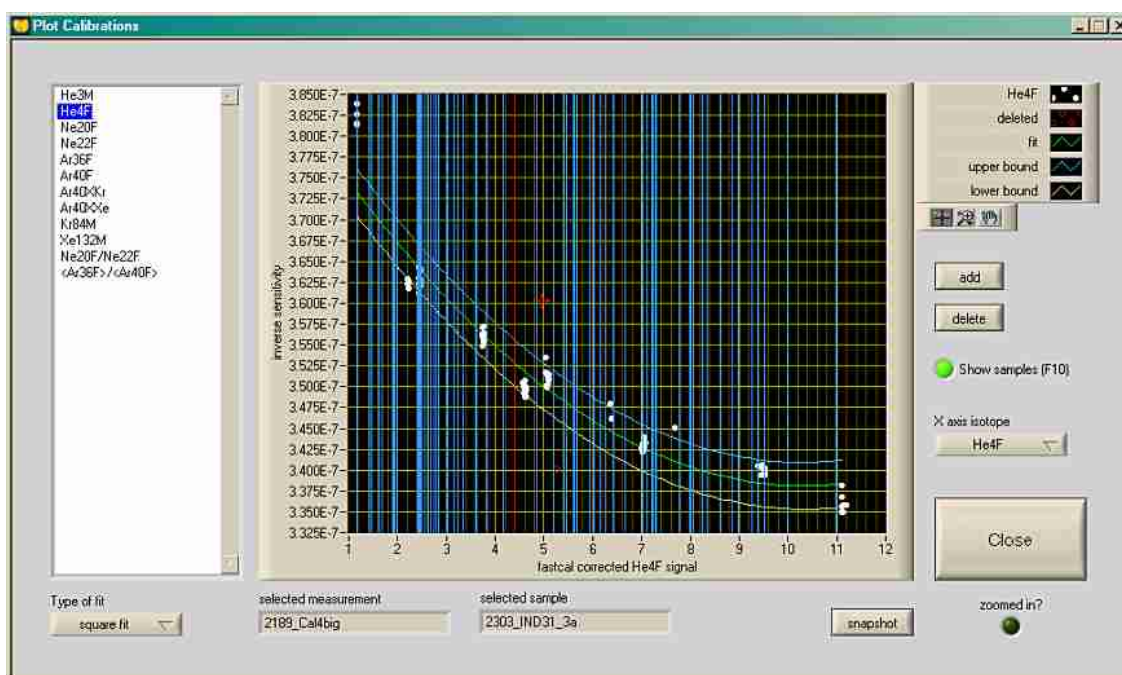


Figure 4.11.: Screenshot of the sample calibration. The calibrations' inverse sensitivity (more information shown in Friedrich [2007]) is plotted against their real signal. An analytical trend needs to be found (green line) to convert all samples' signals (blue lines) to actual gas amounts. Outliers can be deleted (red dot). The conversion error is derived from spline curves running parallel to the fit curve.

an actual gas amount for each sample signal (a typical example can be seen in Fig. 4.11). Extrapolation should be avoided in this case as it messes up the error evaluation. The order of the polynomial fit function with the best data emphasis should be chosen as low as possible to avoid large conversion errors.

In the end, the total amounts of every isotope and selected ratio of all samples in the run are displayed and can be saved to file or copied to the clipboard. It is recommended to save the evaluation of the run as well as log files.⁶

Every run contains some water standards such as air equilibrated water, which have to be compared to their expected theoretical concentrations. If deviations occur, errors in the evaluation process have to be considered.

Preparing for Fitter

The isotopic amounts of each sample have to be converted to total gas concentrations, by dividing them by the amount of sample water and the abundance of the element's measured isotope. In this case, the weight of the water is obtained by weighing the sample before and after each measurement. If the sample contained sand or other residuals, the concentration may be inaccurate. This rare case has to be considered for further evaluation. For further processing, the data is treated to fulfill the requirements for the fitter routine MATLAB software.

⁶A short summary of the run 54 evaluation is shown in the appendix B.2.6.

Requirements for input files used by the NOBLE90 and NOBLE2007 software are listed in the appendix B.2.7.

Fitting

The fitting procedure is done with a Levenberg-Marquard algorithm of the mentioned (chap. 2.3.10) non-linear χ^2 fitting routine described in von Oehsen [2008] or Peeters *et al.* [2003]. Results for every wanted fitting model are stored in an output file. Additional information is provided such as χ^2 and the probability of the fit, as described in 2.3.10, as well as collinearity of the parameters or deviations of the particular noble gas concentrations. The modelled concentrations and the equilibrium concentrations can also be displayed.

Inverse fitting methods bear the risk of ending up with unreasonable convergence results. The initial parameters are crucial information. Sometimes, certain measured concentrations cannot be brought into desired convergence with model data. All problems related to the fitting program will be discussed in the results chapter 5.3.2 on the basis of the actual results.

4.7. Radon

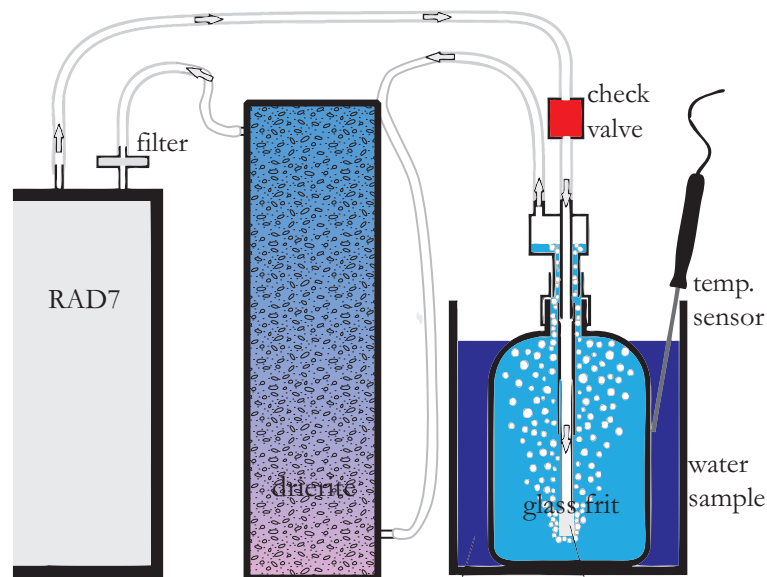


Figure 4.12.: Diagram of the RAD-H₂O measurement (adapted from Reichel [2009]). The water sample is connected with the RAD7 via a gas loop containing a water trap.

Radon samples were collected on the second field campaign in 2009. The airtight and bubble-free water samples were measured over night on a RAD-7 radon alpha detector. The radon detector only analyses gaseous samples. Therefore, the sample water has to be equilibrated with a gas phase. The gas needs to be dried before entering the RAD7 as the detector is more

inefficient and may even suffer from water vapour. The drying is done by a drierit (anhydrit) cartridge in the circuit and the water sample is kept in a water bath for temperature controlled gas equilibration. A special glass frit guarantees fast equilibration. The alpha detector detects the decay of radon's daughter isotope polonium-218 which is collected at the anode of the detector chamber. The semiconductor detector can resolve the exact decay energy of the polonium-218 decay. Before every sample, a background measurement is done. Water samples were measured between field days. The setup for the RAD-H₂O measurement (Fig. 4.12) and machine technical data can be found in [Durrige Co \[2000\]](#), [Durrige Co \[2001\]](#), [Kluge *et al.* \[2007\]](#) and [Reichel \[2009\]](#).

5. Results

For results of a sound groundwater palaeoclimate record, the tapped water of the wells first has to be identified to be part of the same waterbody. Moreover, a proper dating of the samples is necessary. Under these conditions, a continuous climate record is observable.

As a consequence, project results are classified as in-situ field data, information used for dating of the studied water, and palaeoclimate information.

Table 5.1.: Measured tracers of the project:

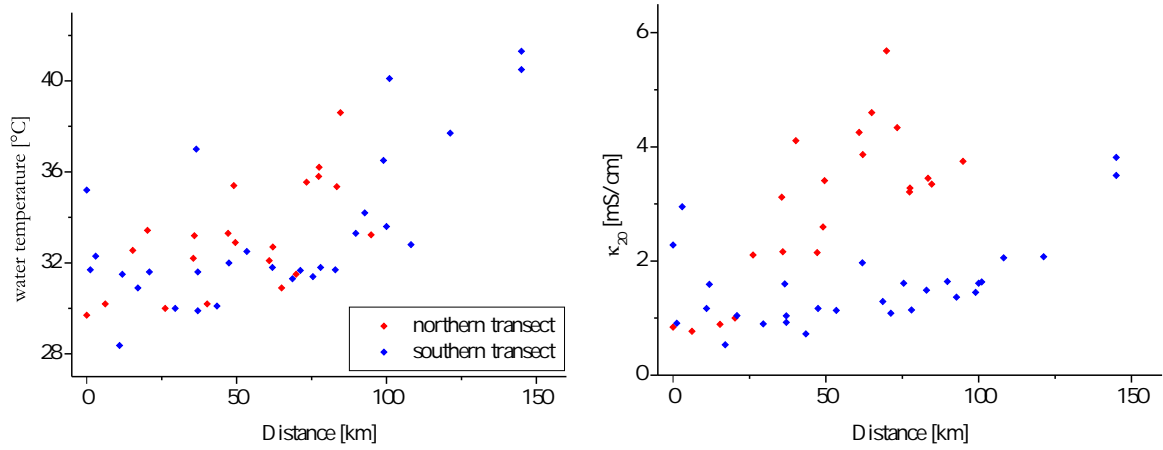
In-situ field data	Dating	Palaeoclimate information
water temperature	tritium	stable isotopes
specific conductivity	carbon isotopes	noble gas concentrations
pH	radon	
dissolved oxygen	helium isotopes	
alkalinity	sulphur hexafluoride	
anions		

5.1. In-situ field data

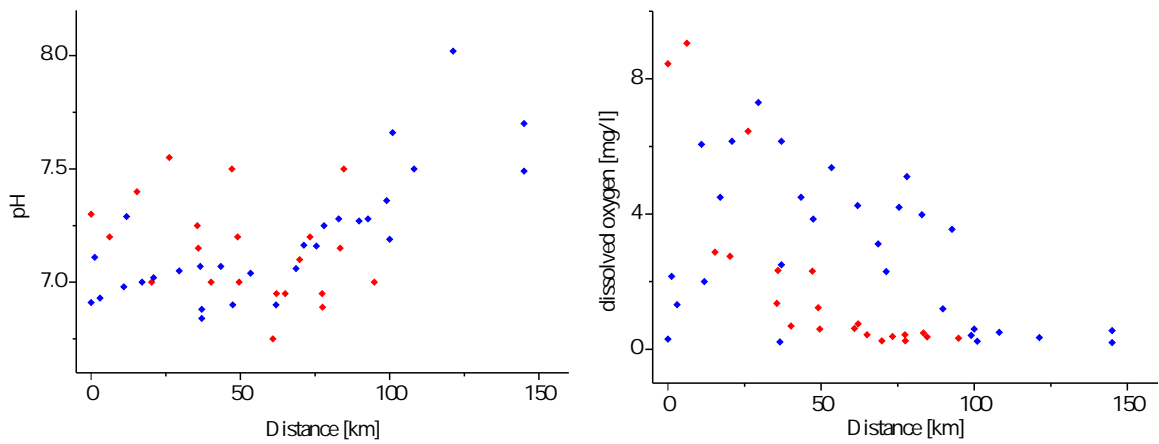
During sampling of a well, the parameters temperature T , specific conductivity κ_{20} , pH and dissolved oxygen did not change significantly. Logged readings (two to four readings during an hour of sampling) are averaged and used for evaluation. An exception is the well 27, where parameter changes occurred during the sampling procedure due to changing mixture of two tapped aquifers. Conductivity changed from 4.63 mS/cm to 3.2 mS/cm, and the pH from 7.18 to 6.81 in one hour. The parameters are shown in table D.1, Fig. 5.1, Fig. D.1, and discussed here.

Fig. 5.1(a): For group P, temperatures showed cool water (29°C) in shallow wells and hand-pumps in the recharge area, and warm water (about 35°C) in deep wells and in the discharge area. Wells of group CRY showed higher temperatures than other wells in the recharge area. Groups TS-CRY, and TS-P PLE showed highest water temperatures up to 60°C.

Fig. 5.1(b): Specific conductivity shows lowest values (about 500 $\mu\text{S}/\text{cm}$) in the recharge and growth towards the discharge. The northern transect shows higher signals than the southern transect. Discharge and groups TS-CRY and TS-P PLE showed highest conductivities (5 – 10 mS/cm).



(a) Water temperature increases with distance to the recharge area. (b) Values of specific conductivity on the northern transect are comparatively higher than on the southern transect. Both transects show growing signals with distance to the recharge area.



(c) pH of observed wells on the southern transect change from acid to basic milieu over distance to the recharge. The northern transect shows scattered values. (d) Dissolved oxygen becomes depleted with distance to the recharge area.

Figure 5.1.: The most important measured parameters of the wells plotted versus distance. Plots versus age are shown in Fig. D.1. Group TS-P PLE is attached to the southern transect at 145 km. Results of group TS-CRY do not fit to any transect and are shown in table D.1.

Fig. 5.1(c): pH values of samples taken in 2009 and 2010 show an increasing pH with growing distance to the recharge area ($\text{pH}_{\text{recharge}} \approx 6.8-7$). Samples of 2008 from the northern transect are scattering, which prevents clear observation of a trend. While the TS-CRY group shows more acid conditions ($\text{pH} = 6.6 - 6.7$), the TS-P PLE group shows a more basic character ($\text{pH} = 7.5 - 8$) similar to other discharge wells.

Fig. 5.1(d): Dissolved oxygen decreases from recharge to discharge, the recharge wells showed atmospheric equilibrium or even higher values (7-9 mg/l). Wells of group CRY showed comparatively low dissolved oxygen concentrations.

Fig. 5.5: Alkalinity showed high and relatively constant values of about 8 mmol/l for most wells of the P group. Wells in the discharge have low alkalinity concentrations of about 5 mmol/l. In 2010, no alkalinity measurements were done.

Furthermore, anion data of the northern transect was measured after the campaign 2008 by PRL (shown in table D.1), and shows no significant trend or separation of groups.

Observed trends are a typical sign for increasing age of a water body. Temperature increases due to the geothermal heat gradient, conductivity growth is caused by dissolution of solids, pH turns basic due to calcite dissolution, and oxygen becomes depleted by anaerobic biogenesis. This behaviour together with anion data support the hypothesis that group P tap similar water bodies of the Gujarat aquifer system. Scattering of some pH values of wells on the northern transect may indicate measurement problems at particular wells during the 2008 campaign. Parameter measurements of the group CRY wells do not fit into the general pattern of the region. This implies the existence of a different aquifer which is tapped by the CRY and the TS-CRY group. The behaviour of parameter readings for well 27 support this assumption and are interpreted as a gradual increasing fraction of young groundwater tapped by the well. Furthermore, the northern transect shows a stronger evolving behaviour westwards of the ECBBF, while the southern transect shows no great development between the fault zones.

5.2. Dating

The absolute age of the water samples is determined by radiocarbon dating. However, information from other parameters is used to qualitatively verify the relation between samples and observed trends of increasing age.

5.2.1. Tritium

To detect young wells or contamination of old wells due to shallow aquifer water, tritium in the water samples was analysed.

Tritium contents in precipitation of New Delhi from 1995 as well as Karachi and Mumbai from

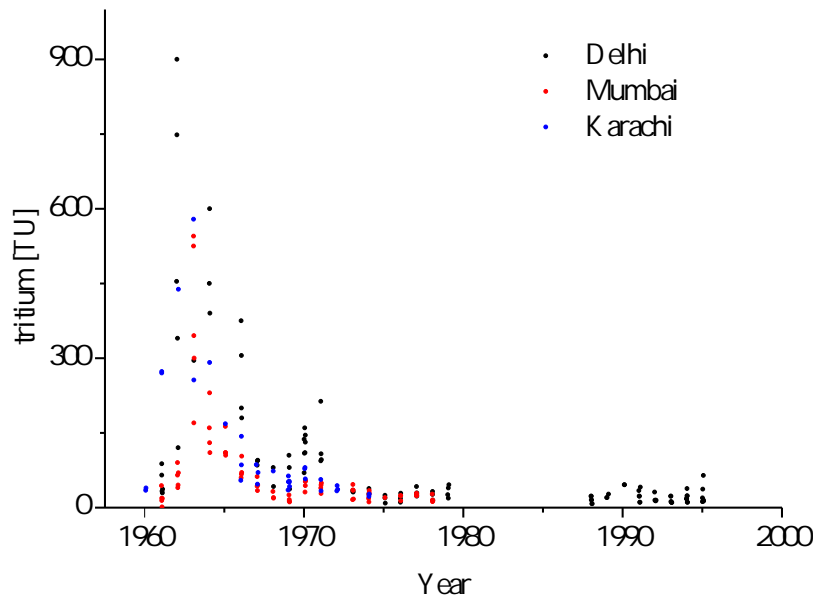


Figure 5.2.: The tritium concentration in TU recorded at the IAEA [2007] stations of Mumbai, Karachi and New Delhi, in the vicinity of the study area. About 300 km north of the study area and about 550 km west of New Delhi, the Indian nuclear test site Pokaran is situated, maybe explaining relatively high values in the New Delhi tritium record around 1998.

1978 range between 10 to 30 TU [IAEA, 2007], while the averaged bomb peak in 1963 had a maximum of about 1000 TU at these stations (data is shown in Fig. 5.2). Eight wells show a significant tritium signal above 2 TU (see table D.2). All other samples had tritium results below the detection limit.

Significant tritium signals range from 2 to 5 TU. A general trend is observed showing decreasing tritium concentrations with increasing distance to the recharge area (shown in Fig. 5.3). A bomb signal of 1000 TU should still show a peak of 70 TU in water nowadays (see 2.3.7). Since no such peak can be observed, mixing with a groundwater reservoir is assumed. Other options are slow infiltration times or deprivation due to evaporation, or, in modern times, irrigation. Initial pre-bomb tritium is expected to be about 10 TU [Roether, 1967] in Europe and less than 10 TU in the intertropical belt [Rozanski *et al.*, 1991]. Therefore pre-bomb signals are not detectable in the data (0.6 TU of modern signal remain after four half lives). As a consequence, detectable tritium amounts have to originate from bomb or post bomb times, indicating modern influx of times younger than 50 yr in affected wells. Bomb-affected wells are situated in the recharge area, and partly belong to group CRY. With use of tritiogenic ^3He concentrations, more information will be derived from tritium concentrations in section 5.2.4.

5.2.2. Carbon

^{14}C was used as main dating tool for the palaeoclimate record. A preceding groundwater study of Agarwal *et al.* [2006] and Deshpande [2006] in the Cambay basin already dated groundwater

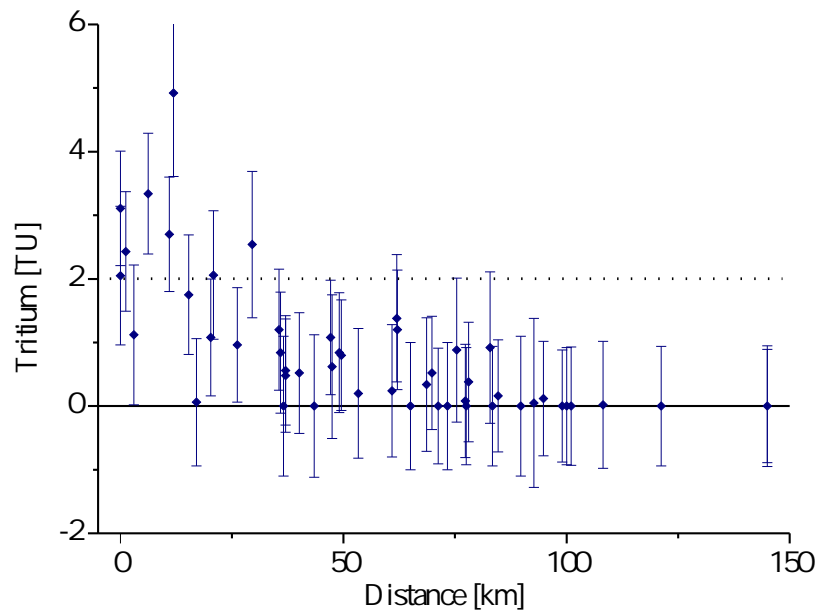


Figure 5.3.: The results of tritium analysis. Significant values are above the detection limit of 2 TU. A decline in tritium with increasing distance to the recharge area is observed.

in the region (see Fig. 3.2). The existing results could be used for best site selection and for dating comparison. Radiocarbon results were corrected by 4.4.2 and show a decreasing activity with growing distance to the recharge area (shown in Fig. 5.4). It is directly observable that the northern transect shows a more constant age increase than the southern transect which ages slowly over more than half of the total distance. In both cases, the last samples in the discharge show nearly zero activity.

Due to contemporary publications about palaeoclimate (P) of the observed region (see 2.2.2), group P (as introduced in section 3) will be divided according to the age of the water. Subgroups are made for modern samples (P MOD), for late Holocene samples (P LHO), for early Holocene samples with suspected climate optimum (P OPT), for samples in the transition to glacial times (P TRA), for last Glacial samples (P GLA), and for late pleistocenic water at the boundary of ^{14}C dating range (P PLE). Table 5.3 at the end of this section provides age information for the groups.

Relatively high alkalinities in groundwater (shown in Fig. 5.5) indicate a high openness of the groundwater-soil atmosphere system. Alkalinity measurements show a young group with alkalinities of 8 mmol/l, and a small group of older samples with 5 mmol/l.

Data of $\delta^{13}\text{C}$ is used for the C13 and F&G dating models. $\delta^{13}\text{C}$ shows (see Fig. 5.6) no great fluctuation, but a small increasing trend over time, starting at -10‰ for young samples and ending at -8‰ for old samples (comparable to [Deshpande, 2006]). Outliers which all belong to group P PLE have very low values.

Interpretation of these outliers suggests influence of a different water component. A possible source is old thermal water originating from deep ground layers which experienced different

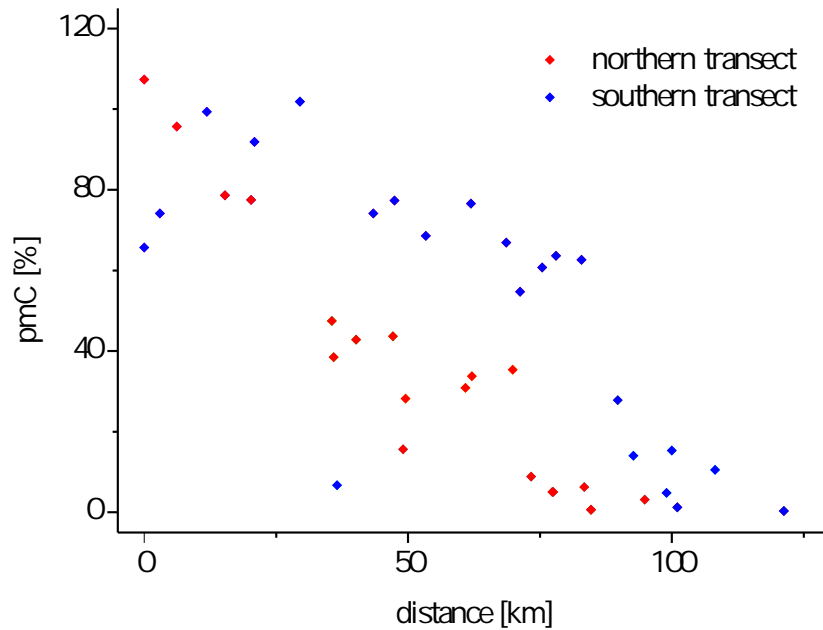


Figure 5.4.: ^{14}C activities versus distance to the recharge show that the water has a relatively monotonous increase in age along the flow path. The northern transect shows a much more homogeneous decrease in radiocarbon activity, while the southern transect has a slow decrease in the first place but much faster decline of activity in the discharge.

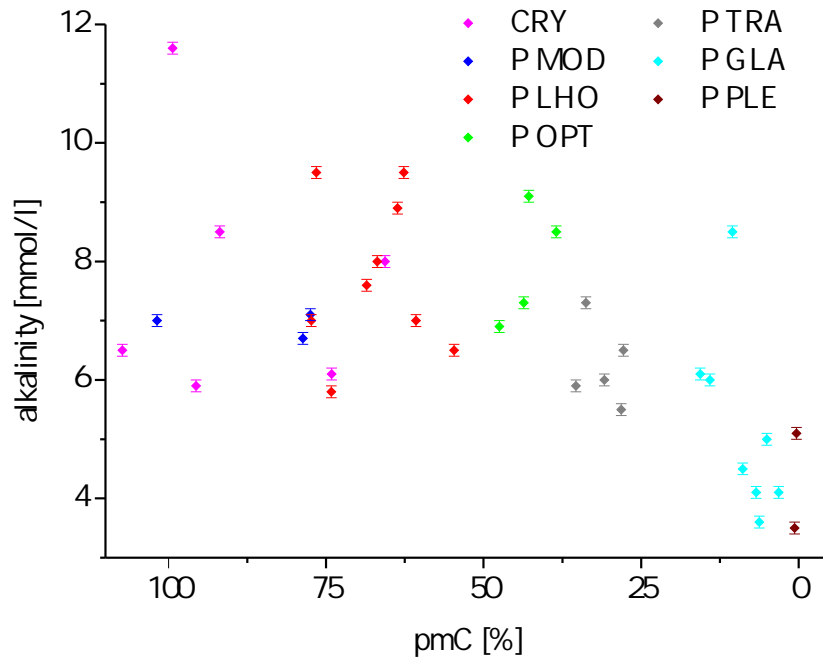


Figure 5.5.: Alkalinity versus ^{14}C activity shows a scattering for all of the younger samples between 6 and 10 mmol/l, and a small group of old samples with much lower alkalinity around 5 mmol/l. No longterm trend as in $\delta^{13}\text{C}$ is visible but a rapid decline from 30 to 10 pmC. The different average alkalinities in the young and the old group are used e.g. in the CMB model.

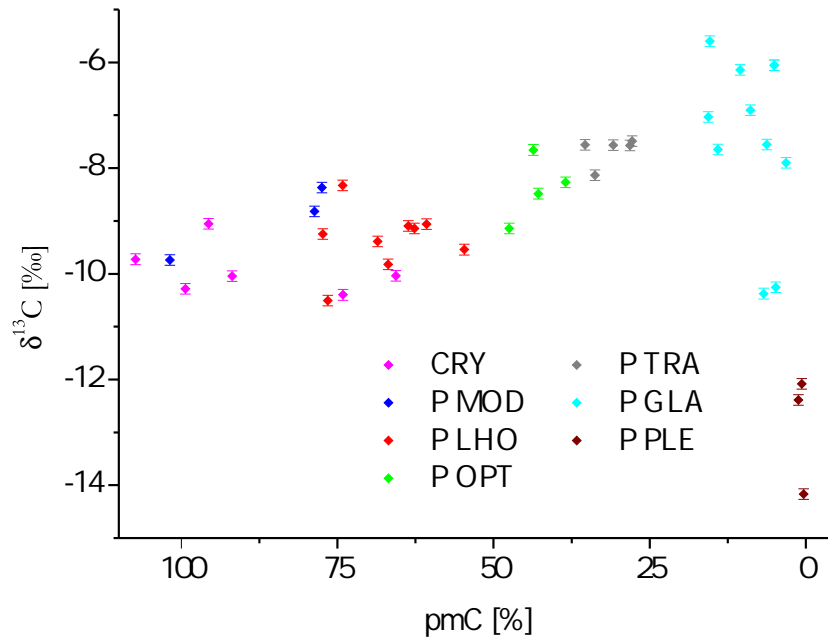


Figure 5.6.: $\delta^{13}\text{C}$ shows a trend of $\delta^{13}\text{C}$ from -10 to -8‰ over ^{14}C activity. Values of young samples range from -9 to -11‰. Oldest samples are outliers of this trend with a significantly more depleted isotope ratio.

infiltration conditions and geothermic alteration [Agarwal *et al.*, 2006].

There are two possible sources for the observed trend in $\delta^{13}\text{C}$. Firstly, matrix exchange can occur, enriching $\delta^{13}\text{C}$ values with a calcite endmember ($\delta^{13}\text{C} = 0\text{‰}$) [Gonfiantini and Zuppi, 2003]. Secondly, if $\delta^{13}\text{C}$ is not affected by matrix exchange over time, a direct infiltration signal may be reflected, giving insight to biologic and therefore climatic conditions in the recharge area. If the openness of the system did not change over time, enriched $\delta^{13}\text{C}$ amounts would indicate lower soil CO_2 concentrations and therefore decreased biologic activity.

The slope of the curve (see Fig. 5.7),

$$\ln A = - (1 + \lambda/K_D) \ln(\delta^{13}\text{C}_{\text{matrix}} - \delta^{13}\text{C}_{\text{meas}} -^{13}\epsilon_{\text{HCO}_3-\text{CaCO}_3}), \quad (5.2.1)$$

is observed. $\lambda = 1/\tau_{1/2}$ is the ^{14}C decay constant and K_D is the kinetic constant of dissolution (see Gonfiantini and Zuppi [2003]). A matrix exchange half life $1/K_D$ of $\tau_{\text{m.e.}} = (17 \pm 4)$ kyr can be obtained. This value shows a reasonable order of magnitude (examples in the paper range from 10 to 40 kyr). Therefore, the change in the $\delta^{13}\text{C}$ value can be sufficiently described by matrix exchange. Carbon dating models using isotope results take this phenomenon into account.

As the pH does not change easily in the same region, a change in alkalinity may result from different soil CO_2 concentrations. Changes in alkalinity may therefore be an indicator of a different climate in the past, indicating different recharge conditions. The tracer is however too ambiguous to provide a reliable climate signal.

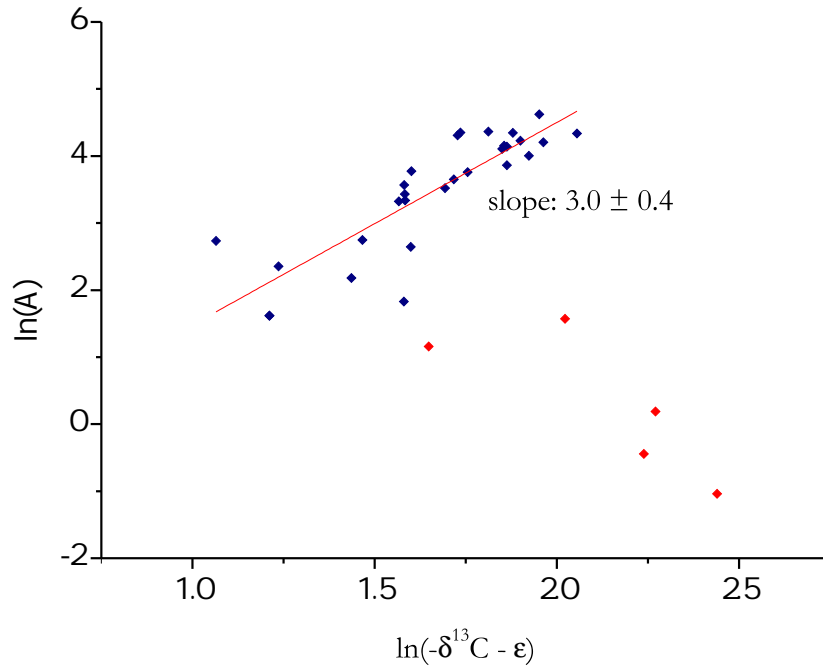


Figure 5.7.: Activity and $\delta^{13}\text{C}$ isotopy show a linear trend in a logarithmic plot. As shown by [Gonfiantini and Zuppi \[2003\]](#), a matrix exchange half life can be derived from the slope (shown in [\(5.2.1\)](#)).

Carbon dating models

Dating of the samples is done with the help of a multi-model approach. As all available data from the samples was alkalinity, pH, $\delta^{13}\text{C}$ and ^{14}C activity, the used models were STAT, STAT meas, C13, C13 mod, C13 Mün, ALK, ALK mod, CMB calc, CMB meas, F&G alk and F&G mod, precisely as introduced in chapter 2.3.4. The aim is deriving the reservoir factor q from the models and using it for further age estimation. Models are overestimating the reservoir effect when samples without any bomb radiocarbon receive a negative age, and they are underestimating it when very recent samples have ages significantly higher than zero. Therefore, an age information is much more transparent than the estimated q factor. As a consequence, ^{14}C ages from every model are calculated to evaluate the estimation by [\(2.3.17\)](#), using the Libby half life $\tau_{\text{Libby}} = 5568$ yr and an initial activity of $A_0 = 100$ PMC. Sample parameters and ^{14}C model ages can be found in table D.3.

STAT, STAT meas The factor q for the Vogel model is either defined as 80% for sandy aquifers (STAT), or estimated by the tritium plot Fig. 5.8, in which tritium signals disappear with carbon activity of 80% and lower (STAT meas). The ages of the STAT models show a reasonable distribution with the youngest bomb-affected samples having negative ages and the oldest ranging around the detection limit of 40-50 kyr. This is not astonishing as the ages are among others tuned by the bomb-affected samples. The results of the statistical approach will be used as a reference for the other model results.

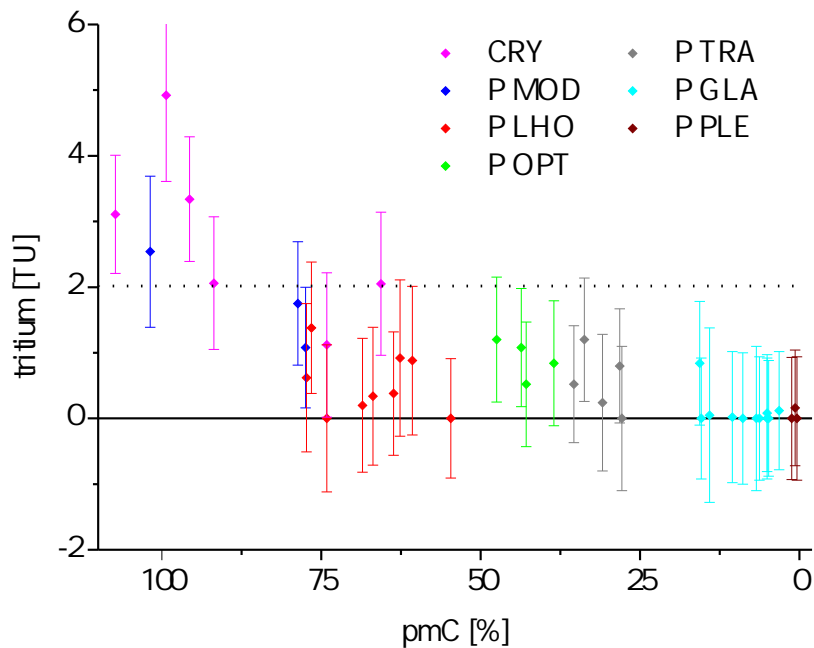


Figure 5.8.: Tritium is plotted versus ^{14}C activity of the water. All samples with significant tritium concentration have a pmC above 80%.

ALK, ALK mod In geochemical models, q describes the ratio of active dissolved inorganic carbon to total inorganic carbon (2.3.13). The samples have a very high alkalinity indicating open system equilibration causing the Tamers model to overestimate the fraction of old carbon. As a result, pre-bomb water is estimated with highly negative ages of several thousand years. Therefore, the original Tamers model ALK will not be used for the multi-model approach. Fohlmeister's approach for the estimation of a ratio of active to total alkalinity is used to take into account an open system. The DIC concentration has to reproduce values of younger recharge wells. For this reason, an initial soil CO_2 concentration of 4%, a pH of 7 and a recharge temperature of 29°C is assumed. Founded on the observed alkalinity change (Fig. 5.5), a separate simulation for old wells with 2.8% and 26°C is done. A change in pH in recharge water in the past does not seem likely. The estimated ratio is used as q (ALK mod) and describes the situation of the samples better than Tamers. This is shown by the resulting ages, as the only samples with negative ages have bomb signature in the form of tritium.

CMB calc, CMB meas In the CMB model, another estimated recharge DIC is compared to the measured DIC, with the ratio q describing depletion of the initial activity (2.3.14). The initial parameters for the chemical mass balance are set to a temperature of 29°C , a pH of 7 and a soil CO_2 partial pressure of 4% (CMB calc) for young samples, and 26°C and 2.8 % CO_2 for old samples. If DIC in freshly recharged wells is known, the value can be used instead of the calculated recharge DIC to receive a model age (CMB meas). For old samples

the change in alkalinity is taken into account. The results obtained from the CMB models are working fine for younger samples, as the only negative ages are identified as samples containing bomb tritium. The CMB meas model may underestimate the fraction of old carbon for older samples, as their ages are older than the STAT ages.

C13, C13 mod Soil air is assumed to range between $\delta^{13}\text{C} = -17$ and -22‰ resulting from C3 and C4 plant respiration and outgassing, while calcite is known to have $\delta^{13}\text{C}$ amounts of $0 - 1.5\text{‰}$. As the parameter $\delta^{13}\text{C}$ is crucial, both endmembers are tried out for calculation. Since the most depleted $\delta^{13}\text{C}$ amounts of all samples do not range near -17 or -22‰ , the Pearson model (2.3.12) overestimates the fraction of old carbon for all samples, resulting in negative ages for pre-bomb samples, independent of the photosynthesis cycle. Therefore the C13 model will not be used for the multi-model approach.

A method to tune this model (C13 mod) is using the simulated $\delta^{13}\text{C}$ amount of the open system “recharge water” as one mixing partner (see Clark and Fritz [1997]). The simulated ^{13}C ratio is much more in the range of the youngest samples with a value of about -11‰ for an initial value of -17‰ . For an initial value of -22‰ , the resulting recharge water isotope ratio is again too depleted (about -16‰). The resulting ages for a -17‰ soil CO_2 endmember are in reasonable range. Young bomb-affected samples result in negative ages while the other samples tend to ages which are younger than most other observed models. Since models using carbon isotopes take into account the matrix exchange as estimated by 5.2.1, this is not astonishing. Therefore, this result is taken into account for the multi-model approach.

For a 22‰ soil CO_2 endmember, the old carbon fraction is overestimated resulting in too negative ages. For the multi-model approach, this choice of endmember will not be used.

F&G alk, F&G mod For the F&G alk model (2.3.15), measured alkalinity is used, and comparable to Tamers half of the measured alkalinity is assumed to result from old carbon. This assumption is, as in Tamers, a closed system postulate. As initial isotope ratio, both endmembers -17‰ and -22‰ are discussed. Independent of isotope ratios, the model overestimates the old carbon fraction by far and produces unrealistic negative ages. The use of half the alkalinity as active carbon is not a correct description of the situation. For this reason, a tuning possibility is using the active alkalinity estimated by Fohlmeister in the modified Fontes & Garnier model (F&G mod). The use of alkalinity is not necessary when chemical parameters of the water are known (F&G chem). Due to the lack of some chemical parameters, it was not possible to use this model. For an initial isotope ratio of -17‰ , the ages of the tuned model show reasonable ages comparable to the tuned Pearson ages. Since the matrix exchange is taken into account by the F&G mod model as well, the comparatively young ages of the F&G mod model are used for the multi-model approach. In case of depleted soil ^{13}C , the model is overestimating the old carbon fraction.

C13 Mün For the Münnich model (2.3.16), ages were retrieved for a fractionation factor (2.3.1) of $\epsilon_{\text{HCO}_3 \rightarrow \text{CO}_2(\text{g})} = -9\text{‰}$ and both initial soil isotope ratios. Conventional ages for enriched soil carbon underestimate the old carbon fraction as even young wells are dated to considerable ages. Use of depleted soil carbon does not seem reasonable as more complicated models have indicated the existence of enriched soil air. Therefore, the model is not used for the multi-model approach.

As mentioned, the chosen models are STAT meas, ALK mod, CMB calc, CMB meas, C13 mod and F&G mod, with an initial soil CO_2 composition of -17‰ . The estimated q_i values are used to produce a mean \bar{q} . The error of \bar{q} is primarily dominated by the standard deviation of all these single models. Exceptions are samples at the detection limit of ^{14}C dating, as most models correlate for very low ^{14}C activities resulting in a small error for \bar{q} . In this case, the error of the ^{14}C activity dominates.

The real age of the sample can be retrieved with the help of the modified initial activity

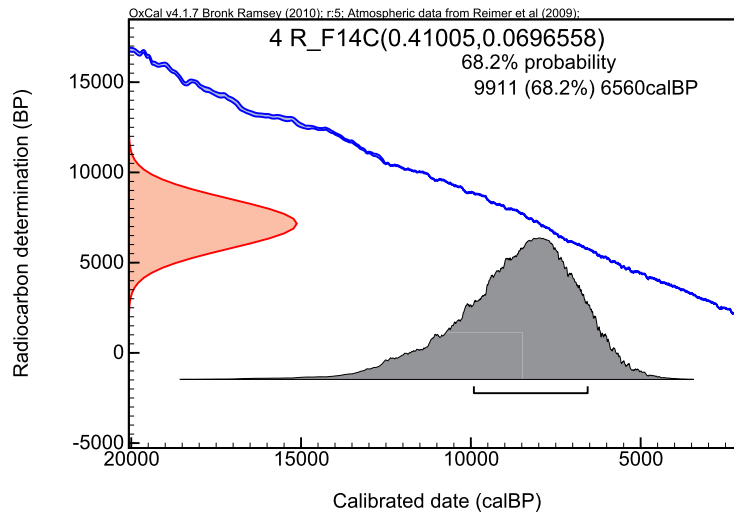


Figure 5.9.: Oxcal input and output probability distributions for the sample India_04. As upper and lower boundaries for the calibrated age, 68% (1σ) of the curves area is considered.

ratio $\frac{A(T)}{\bar{q} \cdot A_0}$. By using the calibration software OXCAL [Bronk Ramsey, 2009], the results are converted to real calendar ages. These take into account the ^{14}C half life $\tau_{1/2} = 5370$ yr and a variable initial activity ratio, as described in 2.3.4.

As input, OXCAL needs either a conventional ^{14}C age or a $\frac{A(T)}{A_0}$ ratio. For this hydrologic study, the diluted ratio of $\frac{A(T)}{\bar{q} \cdot A_0}$ and its error are used as input. As mentioned, the standard deviation of \bar{q} provides the major error and will be used for this purpose. The calibration software creates the input information as a probability distribution shaped like a Gauss curve and produces an output probability distribution resulting from the calibration curve (shown in Fig. 5.9). Other parameters can be chosen, such as different calibration curves, or additional reservoir ages for marine records.

For the calibration age results, the arithmetic mean instead of the median is taken. The wells

13, 37 and 49 range at the detection limit of ^{14}C dating and will therefore be supplied with greater age uncertainties of 5 kyr.

Table D.2 shows the calibrated ages.

As some wells were not dated with the ^{14}C method¹, a raw age estimation is done. The position on the transect cross section and the depth of the wells is examined. If they are surrounded by wells that are well dated and of a similar screen depth, a mean value is calculated. This approach works quite well for samples 6 (mean of the wells 3, 7, 9 and 14), 25 (mean of wells 24 and 31), 43 (mean of the wells 25 and 31), 44 (mean of the wells 24 and 26), 45 (mean of the wells 23 and 30), 46 (mean of the wells 30 and 45) and 50 (mean of the wells 1, 4 and 17). Errors are postulated to be 3000 yr. Due to their resemblance to the oldest palaeoclimate wells, the two wells of group TS-P PLE received an assumed raw age of 50-55k yr with an error of 10k yr. Results are shown in table D.2. The raw ages can be recognised by their red color and characteristic errors.

Alkalinity results imply a possible lower CO_2 partial pressure in the past, resulting from less biologic activity in older ages.

An interpretation of $\delta^{13}\text{C}$ dating models is that C4 plants seem to play a major role in the vegetation of Gujarat, which is primarily the case in semi-arid regions. Furthermore, outgassing of soil CO_2 as mentioned in Cerling [1984] and Münnich [1968] occurs, which is a realistic assumption due to a high prevailing partial pressure of soil CO_2 .

Before discussing the age pattern (Fig. 5.17), other dating techniques are introduced in the next sections.

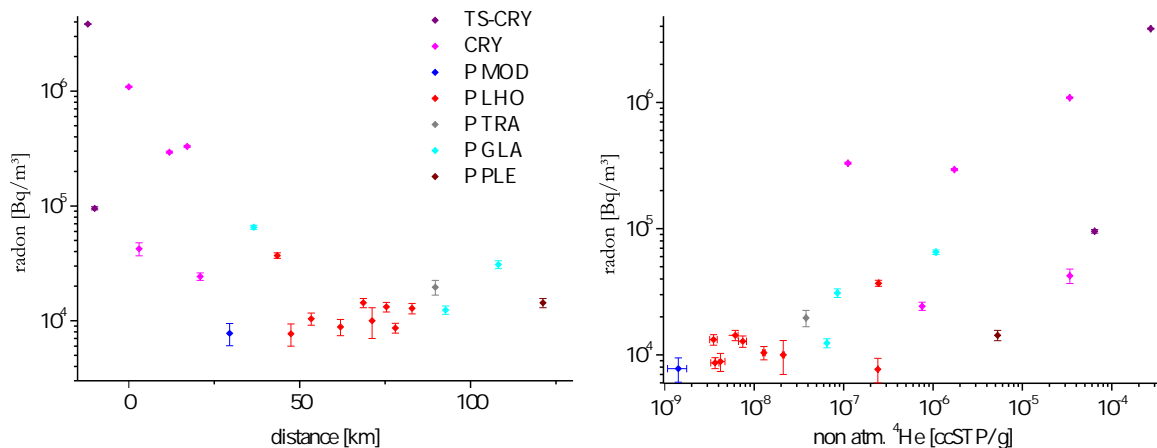
5.2.3. Radon

Rn activities of the 2009 campaign are shown to provide information about geogenic activity in the study area.

Results show relatively constant values between 5 and 20 Bq/l for most wells of group P in the sedimentary area (see Fig. 5.10). Some outliers with higher values occur. Furthermore, samples of group CRY and TS-CRY all show higher values of up to 4 Bq/cm³.

It is not astonishing that Rn concentration and non-atmospheric ^4He show qualitative correlation (Fig. 5.10(b)), as both tracers have the same production mechanism of natural radioactive decay. The occurrence of non-atmospheric ^4He is a conservative size, as He does not decay or react. Rn with its half life of four days however does decay over time. Therefore, while radiogenic ^4He concentration grows with increasing age of the aquifer and can be transported away from its source, Rn will only be found in the immediate vicinity of radiogenic sources. Under these circumstances, Rn concentrations can be interpreted. Rn in groundwater indicates water originating from aquifers with very high uranium and thorium concentrations in the matrix. In wells of the group CRY where water originates from crystalline rock, very high Rn concen-

¹Project budget did not allow radiocarbon dating of all wells.



(a) Radon concentrations show highest concentrations in the recharge area. (b) Radon concentrations correlate with non-atmospheric ^4He concentrations.

Figure 5.10.: Radon concentrations measured in the year 2009. Signals are significantly higher for the CRY group. Highest values were found in thermal spring TS2 (group TS-CRY). A correlation to non-atmospheric ^4He was expected and observed, since both tracers have the same production mechanism.

trations appear simultaneously with high non-atmospheric ^4He , supporting this theory. With growing distance to the recharge, Rn concentrations decline and stagnate to values around 10 Bq/l which is a normal radon concentration for sedimentary aquifers (Fig. 5.10(a)). Three outliers occur which also have high ^4He surplus. These wells are situated in the neighbourhood of the fault zones WCBBF and ECBBF. The fault zones therefore seem to provide an admixture with old water from deep layers with geogenic origin.

5.2.4. Helium

Helium is the only common noble gas (others see in 5.3.2) with a significant non-atmospheric component. The modelled He concentration consisting of equilibrium and excess air component of helium can be subtracted from the measured concentration (see chapter 2.3.9). Actual modelled noble gas concentrations will be discussed in section 5.3.2. Thereby, non-atmospheric ^3He and ^4He concentrations are derived (which will be shown in one of the following sections) and shown in table D.4. Non-atmospheric He isotopes give evidence of geogenic processes in the mantle or crust, which improves the understanding of the geologic situation of the region. Furthermore, helium can be used as a qualitative age tracer, supporting the results derived from radiocarbon dating in an independent way.

Results of non-atmospheric ^4He are shown in Fig. 5.11. Accumulation of ^4He over age is observed. Exceptions from this rule are wells of group CRY and TS-CRY, which show young ages but very high He excess. The concentrations of both He isotopes are presented in an isotope plot (see Fig. 5.12). The $^3\text{He}/^4\text{He}$ isotope ratio is plotted versus the fraction of measured Ne to He to take into account the excess air component. In this plot, samples show a mixing

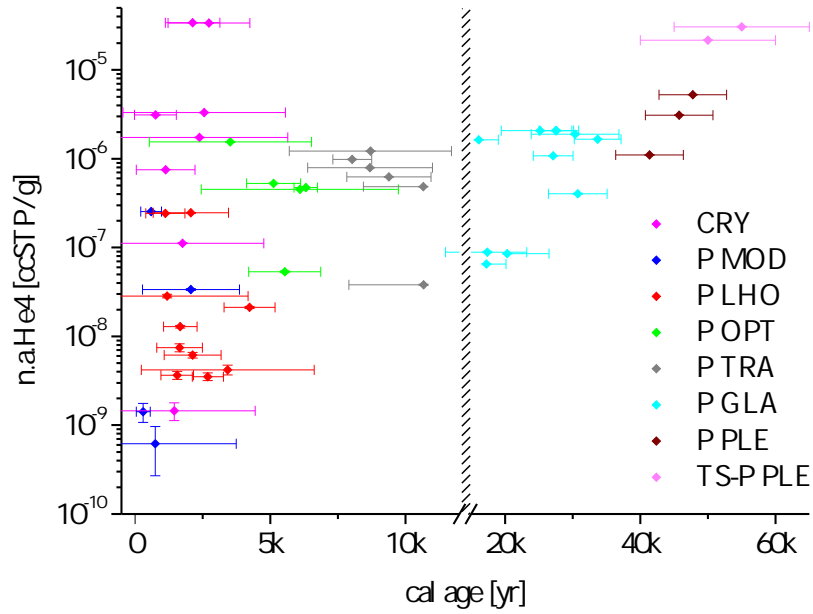


Figure 5.11.: Non-atmospheric ^4He plotted against calibrated ages. A general trend of accumulating helium over time can be observed. However, outliers exist, mostly belonging to group CRY. A reasonable quantitative trend cannot be estimated from the data.

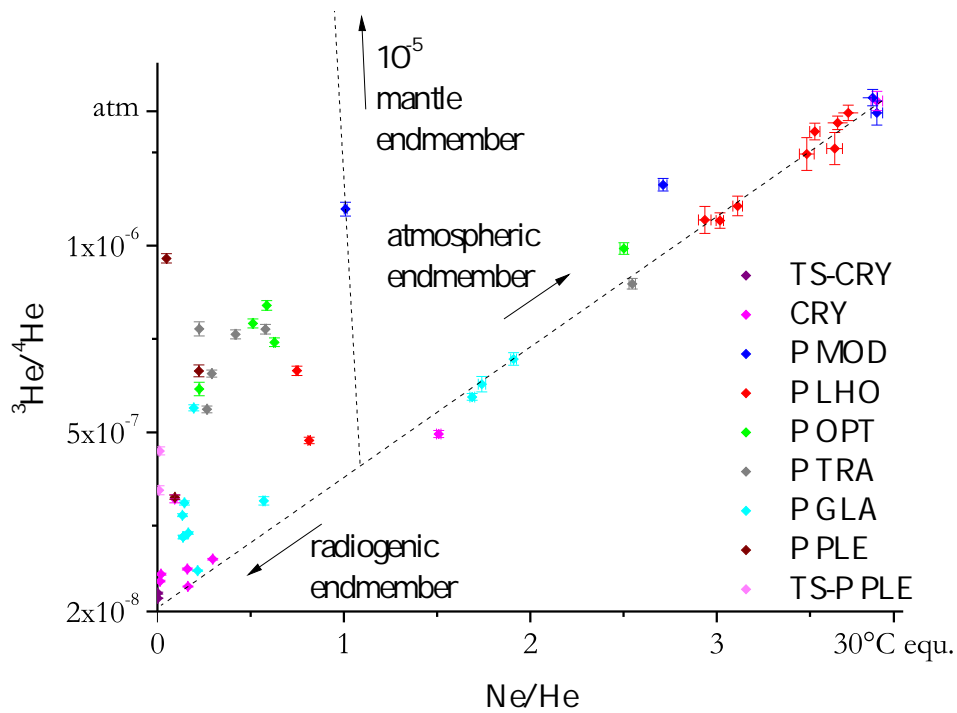


Figure 5.12.: Isotope plot indicating mixing of atmospheric helium with a non-atmospheric component. A possible endmember is radiogenic helium with a ratio of $2 \cdot 10^{-8}$, but outliers indicating a mantle component are also observed. Mixing lines for the different endmembers are shown for well 7. The interception of mixing lines shows the pure radiogenic helium component.

line between their mixing endmembers. One of the endmembers is water with an atmospheric ${}^3\text{He}/{}^4\text{He}$ ratio of $1.36 \cdot 10^{-6}$, while another expected endmember has a pure radiogenic He isotope ratio of about $2 \cdot 10^{-8}$. Deviations in the plot occur. For the young samples, these are caused by tritiogenic ${}^3\text{He}$ shifting the sample vertically; for samples with high non-atmospheric helium concentrations, mantle He is an additional mixing component with an expected ratio of $1 \cdot 10^{-5}$. Mixing of three components can be shown by drawing a line through the mantle endmember and the concerned well. The intersection of this line and the before mentioned mixing line presents the radiogenic component of non-atmospheric He. An example is shown in the isotope plot for well 14.

Different sources of ${}^3\text{He}$ have to be investigated.

Tritiogenic ${}^3\text{He}$: Natural tritium concentrations (5-10 TU) produce a tritiogenic ${}^3\text{He}$ concentration of $1 - 2 \cdot 10^{-14}$ ccSTP/g. In the tropics, numbers are smaller. These concentrations cannot be seen in the isotope plot as they are part of the atmospheric ratio. If wells are affected by tritium generated by nuclear bomb tests, ${}^3\text{He}/{}^4\text{He}$ ratios deviate from the mixing line.

To distinguish wells which can be explained with a pure tritiogenic addition of ${}^3\text{He}$ and wells for which another source of ${}^3\text{He}$ must be considered, a simple calculation is done. Results of tritium measurements (shown in section 5.2.1) are used to calculate an imaginary maximum tritium concentration of the year 1963 by 2.3.7. The tritium lost via decay, $C_{\text{trit.}}(1963) - C_{\text{trit.}}(2010)$, is converted into a ${}^3\text{He}$ concentration $C_{3\text{He}}^{\text{trit}}$, as an imaginary upper boundary of the tritiogenic ${}^3\text{He}$ concentration of the sample.

By comparing this imaginary tritiogenic ${}^3\text{He}$ concentration $C_{3\text{He}}^{\text{trit}}$ with the measured non-

Table 5.2.: Summary of T- ${}^3\text{He}$ characteristics in wells:

${}^3\text{He}$ characteristics	Well no.
${}^3\text{He}$ can be solely described by tritium decay	14, 19, 24, 25, 30, 31, 32, 33, 35, 36, 38, 39, 43, 45, 46
Detectable tritium	18, 19, 24, 26, 30, 31, 43, 44
Sample containing tritium which can be solely described by tritium decay	19, 24, 30, 31, 43
Dateable tritium sample (no group CRY)	30

atmospheric ${}^3\text{He}$ component for young wells $C_{3\text{He}}^{\text{non-atm.2}}$, sites are separated in a group which can solely be described by tritiogenic ${}^3\text{He}$, and a group which additionally has a mantle source of ${}^3\text{He}$. This is particularly interesting for sites close to the WCBBF and ECBBF. Results of this comparison are shown in table 5.2 and are identifying wells whose ${}^3\text{He}$ concentration can

²The non-atmospheric component was corrected for radiogenic ${}^3\text{He}$.

solely be described by tritiogenic ^3He . Some of these wells do not show a significant tritium concentration and are therefore neglected.

Only well 30 remains of the palaeoclimate group P. T- ^3He ages (equ. 2.3.8) are shown in table D.4. Well 30 is confirmed to be the youngest well of the record with (9 ± 4) yr.

For wells of group CRY, mixing is suspected. In this group, some samples show impact of terrigenous ^3He combined with a significant tritium concentration, which overestimate the T- ^3He ages of these wells (compare table 5.2 and table D.4).

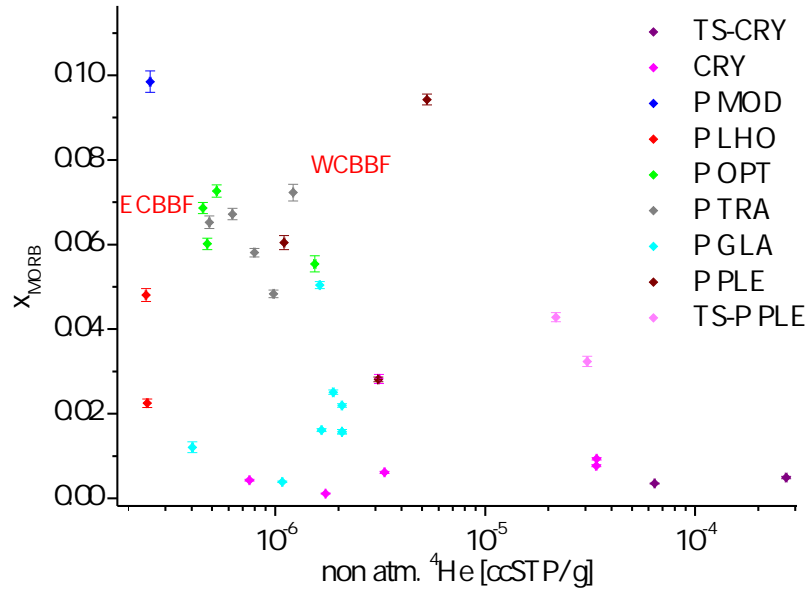


Figure 5.13.: In this figure, the calculated fraction of mantle ^4He (5.2.2) is shown versus non-atmospheric ^4He . With some scattering, a group of samples can be isolated which is influenced by MORB He (wells close to the fault zones, especially wells of the northern transect between ECBBF and WCBBF, the group P PLE and group TS-P PLE), and another group of samples (CRY and TS-CRY, among others) that contains purely radiogenic ^4He . Only samples too old to be influenced by bomb tritium are shown. Young wells with tritiogenic ^3He are below the range of the plot due to their amount of low non-atmospheric ^4He .

Mantle ^3He : Another source of ^3He is a mantle reservoir. An equation to determine the fraction of mantle He is shown in Aeschbach-Hertig [2005]. It calculates the fraction x of the MORB ^4He fraction by a simple two-component mixing equation

$$x = \frac{R_{\text{sample}} - R_{\text{rad}}}{R_{\text{MORB}} - R_{\text{rad}}} \quad (5.2.2)$$

where R_i represents the assumed He isotope ratios of different components. For a radiogenic He isotope ratio of $2 \cdot 10^{-8}$ and a mantle He isotope ratio of $1 \cdot 10^{-5}$, the MORB fraction is shown in Fig. 5.13. Again, groups can be recognised. While CRY and TS-CRY show a purely radiogenic $^3\text{He}/^4\text{He}$ ratio, P PLE and TS-P PLE show influence by MORB He. Especially wells close to the ECBBF and WCBBF show high mantle He signature. Influence of mantle He is stronger on the northern than the southern transect. Between and especially close to ECBBF and WCBBF, most northern wells have a considerable MORB He fraction.

Particularly interesting is the fact that the northern transect west of the WCBBF does not show any mantle signature.

The source for mantle He seems to be correlated to the fault zones. Furthermore, the northern transect seems to be influenced more by MORB He, but also by non-atmospheric ^4He in general. This implies a stronger influence of the ECBBF on the aquifer water in the North. The fault zones may provide mixing with very old waters from deep layers. These conclusions are supported by Rn data.

The argon isotope ratio did not show any results deviating from atmospheric ratios.

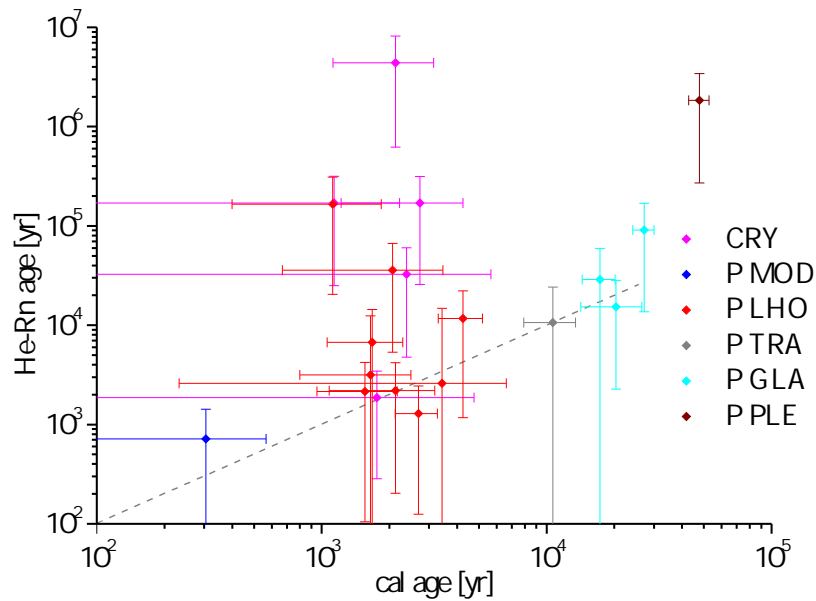


Figure 5.14.: He-Rn ages are plotted versus calculated ages. For wells of group P, increasing age trends of He-Rn ages match the age trend of calibrated ages. Group CRY shows far too high He-Rn ages compared to the calibrated age.

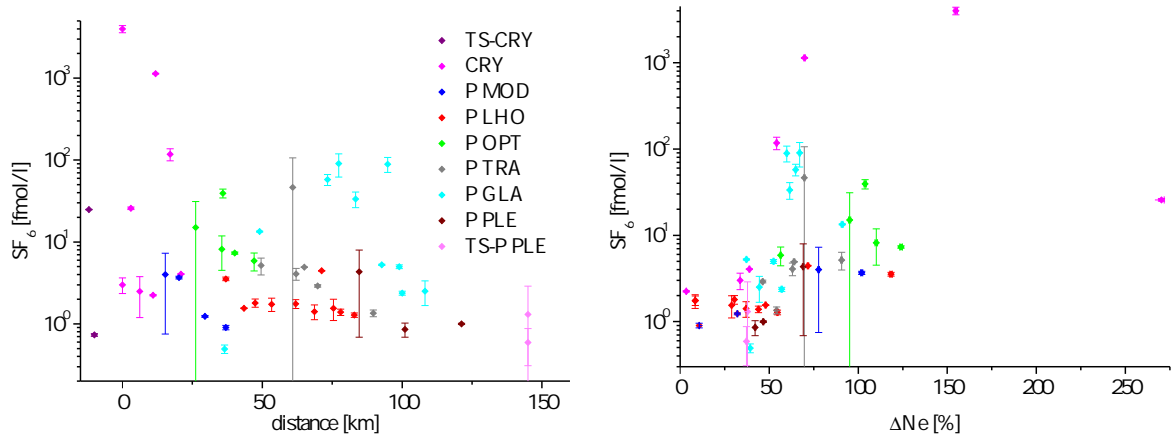
He-Rn ages are calculated for all wells with radon data by (2.3.18). A typical factor $\frac{\Lambda_{\text{Rn}}}{\Lambda_{\text{He}}}$ is quoted by Agarwal *et al.* [2006] as 0.15 ± 0.07 , whereas the authors proclaim a regional factor of 0.4 ± 0.3 caused by a lower He release factor Λ_{He} . When minimum relative deviation of He-Rn ages and calibrated ages is determined by fitting the factor $\frac{\Lambda_{\text{Rn}}}{\Lambda_{\text{He}}}$, the result is a value of $\frac{\Lambda_{\text{Rn}}}{\Lambda_{\text{He}}} = 0.11$, offering a moderate confirmation for the typical choice of release factor. The proclaimed He release factor of 0.4 cannot be reproduced.

Results are shown in Fig. 5.14 and table D.4. Many wells show a distinct qualitative agreement of He-Rn ages and calibrated ages. For wells of group CRY, overestimations of one to three orders of magnitude occur. It is significant that wells with high He concentrations (CRY group, 37) deviate from calibrated ages. Due to the two water components, the two age tracers show differing results. The error of He-Rn ages is too big to use it as quantitative information.

As a result, He isotopes show a small influx (5 – 10%) of water with a mantle helium character near the fault zones of the graben formation, the discharge, and on the northern transect, while

wells of group CRY have high He concentrations with a radiogenic character. He-Rn ages offer an independent age information of the samples and can be used to support radiocarbon dating for the P group in a qualitative way.

5.2.5. SF₆



(a) SF₆ versus distance from recharge shows no trend. (b) SF₆ versus excess air shows no trend for wells of group P, and no quantitative relation for wells of group CRY.

Figure 5.15.: SF₆ concentration of all wells in the sampling area. Group CRY shows high values orders of magnitude above recent atmospheric equilibrium. Plots of SF₆ vs tritium and age are found in Fig. D.3 in the appendix.

Most SF₆ results exceed concentrations of water equilibrated with recent atmospheric air. Some samples show results several orders of magnitude above modern equilibrium concentrations. Data is shown in Fig. 5.15 and in table D.5.

The reproducibility of the twin measurements is mediocre, the error exceeds the machine reproducibility (conservative estimate of 1% for water samples) by far. The greatest errors are therefore expected in field sampling or extraction in the laboratory. Samples processed with the “headspace” method showed better reproducibility than the alternative “decanting” method. The standard deviation of twin samples is used as error for the concentration. The wells with highest SF₆ concentrations were found in the group CRY, and in some wells on the northern transect.

For interpretation of the results, atmospheric contamination needs to be considered.

SF₆ concentrations are independent of the water’s fluoride concentration (which in some cases ten times exceeds medical limitations in the region [Gupta *et al.*, 2005]), shown in tables D.2 and D.2.

There is no relation between SF₆ and tritium values (see Fig. 5.15(a)). Furthermore, no

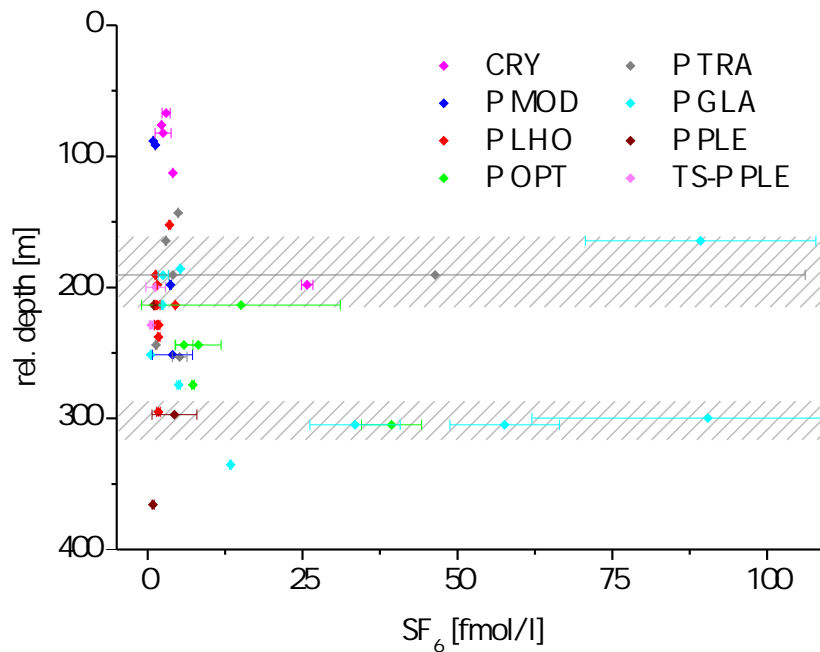


Figure 5.16.: SF₆ concentrations of all group P wells, plotted vs. relative depth of the well. High SF₆ concentrations are found in layers at 300 m and 160-200 m.

trend between SF₆ and excess air can be observed (see Fig. 5.15(b)), altogether making the influence of atmospheric SF₆ unlikely. As additional information, CFC-12 peak evaluation by von Rohden for the samples was not able to find correlations, which would have suggested air contamination.

While no tracer or physical variable could show a quantitative relation to SF₆ values, some connections are found. According to Harnisch *et al.* [2000], natural SF₆ originates from sources with high natural radioactivity, which can be investigated by ⁴He or ²²²Rn. SF₆ concentrations of the CRY group support these arguments, as this groundwater originates from crystalline rocks (shown in Fig. 5.29). Natural production of SF₆ in hard rock is strongly suggested.

In the sedimentary area, high concentrations of SF₆ are found as well, even though concentrations are one or two orders of magnitude lower. As shown in Fig. 5.16, especially the aquifer layers in depths of 300 m and 200-160 m below the surface of the sedimentary basin show high SF₆ results. Interpretation of these results is difficult, especially as final CFC evaluation and measurements of crystalline rocks by the laboratory of the Institute of Earth Sciences in Heidelberg are still pending. As the main attention of the project is the palaeoclimate record, further interpretations are postponed. As a side information, it is noted that Deshpande [2006] and Gupta *et al.* [2005] found certain aquifer layers responsible for harmful fluoride concentrations in groundwater of Gujarat, which include the two mentioned depths.

Table 5.3.: Summary of obtained ages for different palaeoclimate groups:

group	minimum age	error	maximum age	error
P MOD	300	260	2100	1800
P LHO	1100	700	4200	900
P OPT	3500	3000	6300	400
P TRA	8000	700	10600	2800
P GLA	16100	2900	33700	3500
P PLE	42000	5000	48000	5000

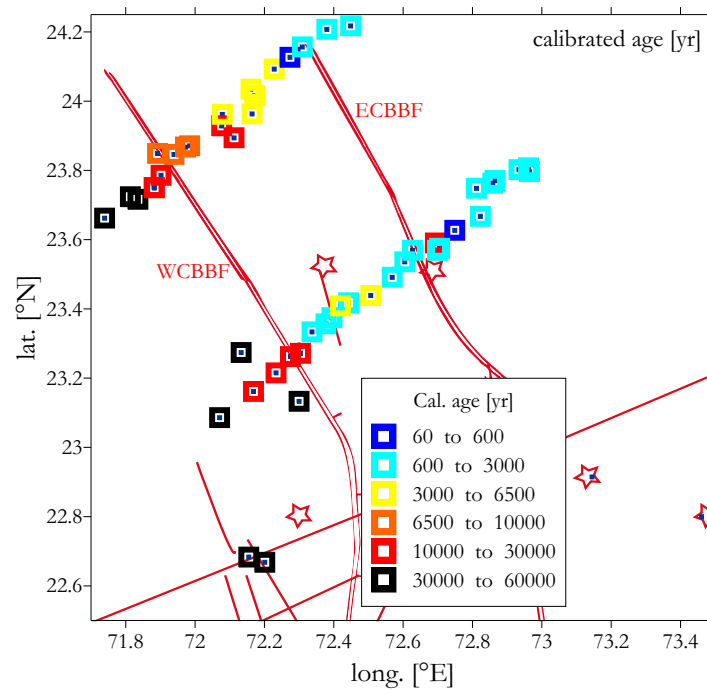


Figure 5.17.: Calibrated ages of the wells shown on the map of the sampling area. A clear trend in age from North-East to South-West is observed. Fault zones are drawn as red lines. East of the ECBBF, all bomb-affected wells are found. Confinement of the aquifer system begins west of the ECBBF. The northern transect has a linear age increase over distance, while the southern transect does not increase in age very much east of the WCBBF. The age pattern agrees with the study of [Deshpande \[2006\]](#) (shown in Fig. 3.2).

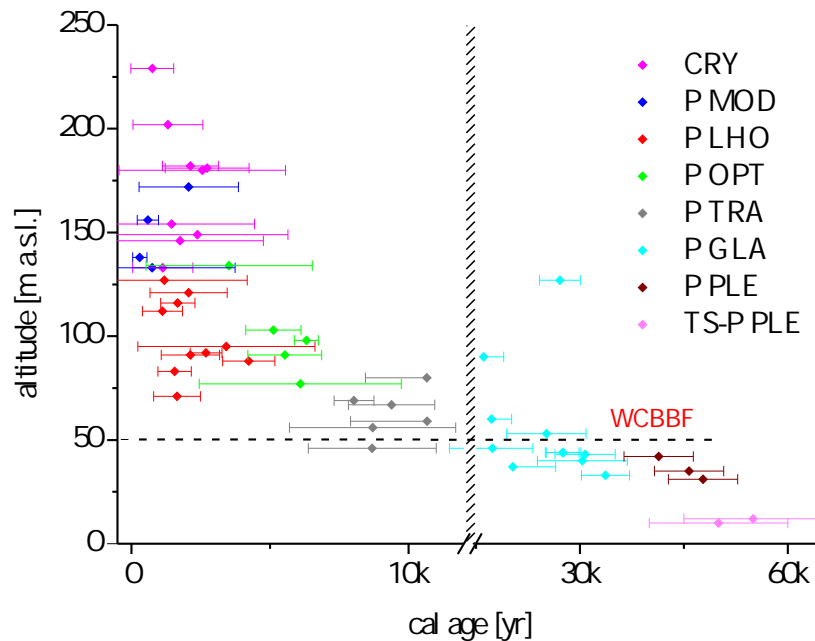


Figure 5.18.: Calibrated age is plotted against the altitude of the well. The great difference between the northern and southern transect cannot be observed here.

5.2.6. Summary for the palaeoclimate group P

The resulting ages of the groups are summarised in table 5.3. Due to the high errors, overlaps exist. Affected wells are associated to their groups by other parameters of the results. When discussing the results of ^{14}C dating together with qualitative results from other dating methods, a few characteristics are pointed out and displayed in Fig. 5.17. Firstly and as expected, it is shown that the ages of the wells increase with growing distance to the recharge area in the North-East. Secondly, ages increase gradually on the northern transect, while on the southern transect the ages increase slowly east of the WCBBF, but increase strongly west of it. As is shown in Fig. D.2, age does not increase with depth of the tubewell. Since the northern transect is situated in higher altitudes than the southern transect, age versus altitude (Fig. 5.18) shows more coincidence. The topography is different for the northern and the southern transect, which may have an influence on the different flow velocities of the two transects. Ages of all wells in the P group east of the ECBBF are very young. Tritium measurements support this result, all bomb-affected wells can be found here, with an age of 50 yr or younger. This supports the statement of Deshpande [2006] that confinement of the aquifer system does begin west of the ECBBF.

5.2.7. Summary for group CRY:

Wells of the group CRY are strongly influenced by geothermal water originating from deep crystalline rock. They carry characteristic gas compositions such as high ^4He and SF_6 on the

one hand, but on the other hand show rather young carbon ages and in some cases tritium signals. Therefore, it is suggested that these wells tap two aquifer reservoirs. The first is a shallow aquifer containing young water with tritium and radiocarbon, with a relatively cool water temperature. The second originates from fragmented-rock aquifers deep in the crystalline rock of the Aravalli foothills. It carries great amounts of radiogenic ^4He , ^{222}Rn and SF_6 and has a much warmer water temperature.

A sign of mixture of two aquifers in group CRY can be seen in the field protocol of well no. 27 where, after a considerable time (about one hour) of pumping, conductivity dropped from 4.6 mS/cm to 3.4 mS/cm and pH from 7.2 to 6.8, while at the same time oxygen rised from 0.8 mg/l to 2.4 mg/l (details are shown in the appendix). Therefore, wells of the CRY group will not be used for palaeoclimatic studies but will be interpreted separately. Mixture will be discussed in section 5.3.3.

5.3. Palaeoclimate

The precedent section provided a thorough age determination for the studied water. Observing results such as alkalinity, first indices of possible palaeoclimatic changes and trends are observed. More tracers are observed to detect changes in palaeoclimate in the region.

5.3.1. Stable Isotopes

Results of stable isotope measurements are shown in table D.5. $\delta^{18}\text{O}$ signals are plotted

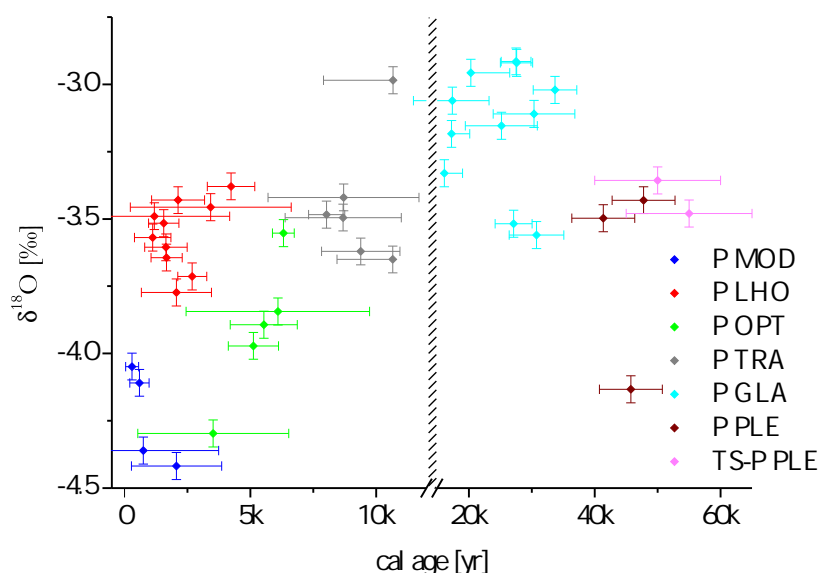


Figure 5.19.: Stable isotope $\delta^{18}\text{O}$ is plotted versus calibrated age. The group P GLA shows enriched ratios due to the ice-volume effect among others. Groups P MOD and P OPT show depleted values, indicating an amount effect. Modern precipitation in the region shows weighted annual means of $-3.9 \pm 3.2\text{‰}$ [Deshpande *et al.*, 2010].

against age and spread over a narrow interval (Fig. 5.19). Samples show moderate values around -3.7‰ in preglacial times (P PLE), while during peak glacial times, the P GLA group shows enriched stable isotope ratios of about -3.1‰ . With the end of the last Glacial, the enrichment disappears (P TRA) and evolves to moderate ratios of -3.6‰ in the Holocene (P LHO). Modern samples (P MOD) and a small group P OPT show depleted ratios, of about -4.2‰ during early Holocene and of about -3.9‰ in modern times. Modern precipitation values of Ahmedabad around $-3.9 \pm 2.3\text{‰}$ (weighted annual mean) [Deshpande *et al.*, 2010] are comparable to the P MOD group results. CRY wells show scattering over the whole range of -4.2‰ to -2.8‰ . Mean values of the palaeoclimate groups are summarised in table 5.4.

Deuterium shows in essence a similar behaviour as oxygen. In Fig. 5.20, δD is plotted against

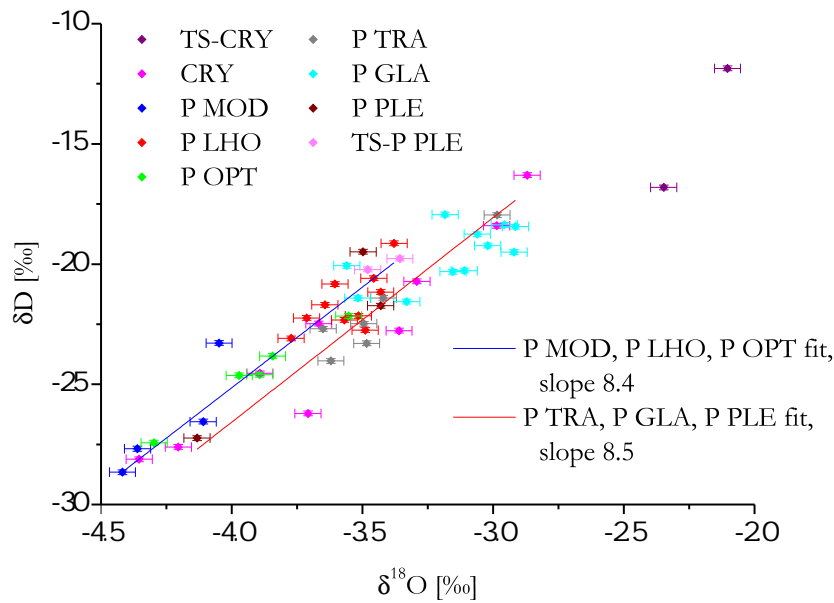


Figure 5.20.: $\delta^2\text{H}$ is plotted versus $\delta^{18}\text{O}$. The samples are allocated on a local meteoric water line. Glacial samples group in the enriched zone, while modern samples are situated in the most depleted zone. Groups P MOD, P LHO and P OPT form a MWL of their own, as do the groups P GLA, P TRA and P PLE.

$\delta^{18}\text{O}$ for all samples. A local meteoric water line is shown. While group P GLA is at the upper right end of the plot, P OPT and some samples of P MOD are situated at the lower left end. The slope of the total curve is insignificantly lower than the slope of the GMWL. The groups P GLA and P TRA show a lower deuterium excess than groups P OPT, P LHO and P MOD. When groups P PLE, P GLA and P TRA are treated separately from P OPT, P LHO and P MOD, both slopes are about 8. Therefore, no evidence for evaporation effects are found. However, deviations of the fits are very high due to scattering. Observance of the deuterium excess (in Fig. 5.21) shows a change between the P GLA group and the P OPT group, with a transition phase in P TRA. P OPT, P LHO and P MOD show a deuterium excess of about $7.3 \pm 0.6\text{‰}$ which roughly fits to modern recordings such as Mumbai (8.8‰) or Karachi (9.0‰) [Rozanski *et al.*, 1993] as well as modern rainfall in Ahmedabad ($8 \pm 6\text{‰}$ weighted annual mean, [Deshpande *et al.*, 2010]). Last Glacial values have a mean of 5.5‰ (see table 5.4).

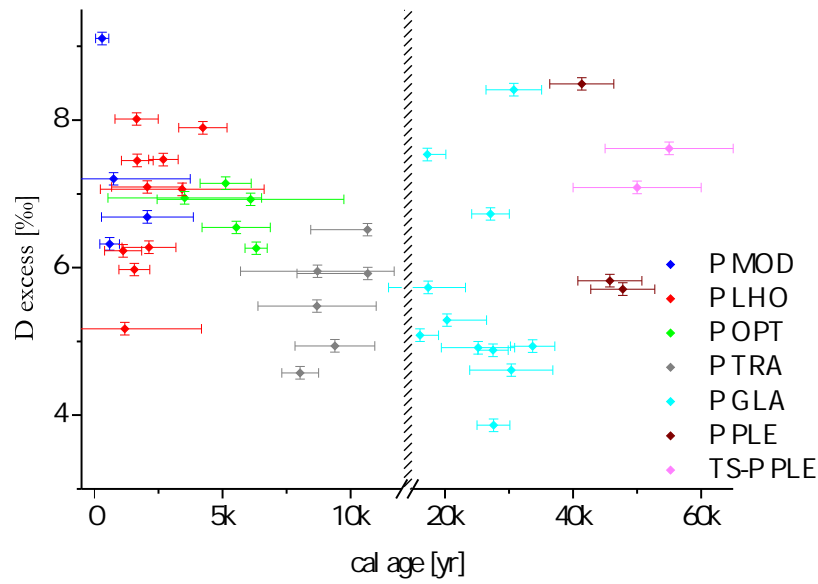


Figure 5.21.: Deuterium excess is plotted versus age. High amounts (7‰) in recent times change to low amounts during the last Glacial (5‰). Modern precipitation in the region shows values of $-8 \pm 6‰$ (weighted annual mean) [Deshpande *et al.*, 2010].

For interpretation of the stable isotope information, influence by the rock matrix needs to be investigated. As observed in chapter 5.2.2, exchange of groundwater DIC with the aquifer matrix changes the isotopy of ^{13}C . The effect on ^{18}O is however negligible due to the high abundance of oxygen atoms in water and will therefore be ignored.

As discussed in 2.3.1, stable isotope ratios are affected by several relationships. Therefore, signal interpretation always has to take into account all isotope effects. Since the dimension of particular effects in this region is not completely understood, ratios are shown unmodified in the plots (e.g. no global ice-volume effect was corrected). Palaeoclimate information of other tracers will be taken into account later to support interpretation of stable isotope data.

A temperature effect would imply depletion of stable isotopes in the past compared to modern times, cooler temperatures in the last glacial period provided. If anything, contrary signals are the case. Furthermore, no correlation between stable isotope ratios and the MAST record of the region can be observed (see Fig. D.4). This confirms the presumption that temperature effects play a minor role in the region. Therefore, other effects need to be taken into account to explain the enrichment.

Isotope enrichment of group P GLA is anticipated by the global ice-volume effect. However, an enrichment of $1.2‰$ as estimated in (2.3.6) cannot be observed, indicating other effects. Large glacial and polar ice formations result in a lowering of the sea level. As the Gujaratian coast shows a considerable continental shelf, the distance of the recharge area to the coast increases with lower sea level up to hundreds of kilometres (20 to 40 % of the total distance).

As a result, different continental effects influence precipitation in glacial and in modern times. The continental effect works contrary to the ice-volume effect and may mask the resulting isotope fractionation.

Surface waters of the oceans do not have the same isotopic composition everywhere. The Arabian Sea as an example is enriched in $\delta^{18}\text{O}$ compared to the Bay of Bengal [LeGrande and Schmidt, 2006] which can, to some extent [Deshpande *et al.*, 2010] [Sengupta and Sarkar, 2006], be source of Indian monsoon precipitation. In addition to differing isotope ratios of the sources, the traversed continental landmass causes an additional continental effect. If, due to major shifts in meteorologic behaviour, a change in source occurred, it would leave its footprint in isotope records. Therefore, relative enrichment of the P GLA group is considered a global ice volume effect, masked by continental effects or a change in the source.

As basis for relative depletion of the P OPT and the P MOD group, the amount effect may be responsible. An effect of 1‰ as modelled by Lee and Swann [2010] may be in the range of the observed data. To support this theory, signs of strong precipitation events have to be searched in other tracers.

Interpretation of the change in deuterium excess may indicate changes in the source of precipitation.

Possible sources for the Indian summer monsoon are the Bay of Bengal and the Arabian Sea. Evidence that both sources influence northern Indian summer precipitation are given by Deshpande *et al.* [2010] and Sengupta and Sarkar [2006]. Depending on the isotopy of the sources, overall change of the source region may therefore effect the groundwater's observed deuterium excess signal.

The moisture source can also change its isotopic character over time. Deuterium excess proxies in Antarctic ice cores [Jouzel *et al.*, 1982] show a similar trend to Fig. 5.21. Moisture sources for Antarctic precipitation are mainly situated in the tropics [Vimeux *et al.*, 2001]. Other groundwater studies situated in the Sahara [Sonntag *et al.*, 1979] show the same change in deuterium excess. The reason for this change in deuterium excess is associated with higher relative humidity at the oceanic surface during the last Glacial [Jouzel *et al.*, 1982], as cooler global temperatures cause a less pronounced deuterium excess in the source water vapour [Merlivat and Jouzel, 1979].

As described in Deshpande *et al.* [2010], precipitation and evaporation in the target region may also have an effect on deuterium excess. Therefore, interpretation of the exact origin of the effect is difficult. Whichever effect is responsible, the situation changed after the last Glacial, as was also observed in other mentioned records.

5.3.2. Noble Gases

Noble gas concentrations represent the major palaeoclimate tool used in this study. Geologic and chronologic information based on observation of He isotopes was anticipated in the last chapter. Information about soil temperature and relative precipitation amount will be gained

with the help of other noble gases. To achieve best extraction of information, a thorough evaluation is discussed here.

Sample statistics:

From field sampling, 146 samples of 52 wells were transported to the mass spectrometer laboratory for sampling. Out of these 146 samples, two (45_2 and 48_2) could not be measured due to computer problems, while three samples (21_3, 22_3 and 23_3) broke in the process of measuring. Three samples (24*_1, TS2_2 and 52_2) were not measured.

Seventeen (2_1, 3_1, 4.2b, 5_1, 7_1, 8_1, 9_1, 10_1, 11_1, 12_1, 13_1, 14_1, 16_1, 17_1, 18_2, 19_1 and 20_1) of the measured samples were rejected as they showed outliers deviating more than 10σ after direct comparison of particular concentrations. These samples were all done in the first interval (run no. 42) of measurements using the old processing method (described in section 4.6). Other samples show outliers in certain noble gas concentrations e.g. due to failed fastcals or peak scans, but were kept for the moment. The samples were preliminarily fitted (Table D.6 & D.7).

Noble gas evaluation and fitting

The concentrations of 121 samples were fed into the fitting programs NOBLE90 and NOBLE2007 (described in B.2.7). When fitting the excess air models PR and CE in the programs, both fitting tools produce equal results. As NOBLE2007 allows to fit more excess air models, its results will be presented here. As described in chapter 2.3.10, the searched parameters such as A , B , F , G , T (depending on the used model) can be inversely derived from the concentrations. The PR (2.3.21), CE (2.3.22) and OD (2.3.23) model were fitted preliminarily. While other models will be presented in detail later, the following discussion about different strategies describes only the CE model results, showing in detail the functionality of the fitting tool.

Collinearity

Collinearities are calculated for each pair of parameters as well as the multicollinearity of the regression model for parameters A , F and T by (2.3.27). If collinearity of the fitted parameters exceeds a certain range (5-20 according to Brun *et al.* [2001]), distinct solutions for χ^2 may become difficult to find.

Most samples show the same behaviour of collinearities as artificial data from von Oehsen [2008] discussed in 2.3.10. The highest collinearity arises between A and F (ranging around 4 to 9), or A , F and T (about 11 to 21). When fitted with the CE model, these samples in the main produce reasonable parameters with adequate errors.

A certain group of samples (samples 6_3, 19_2, 19_3, 25_1, 25_2, 25_3, 29_2, 32_1, 32_2, 33_2, 43_1, 43_2, 43_3 and 53_2) however shows high collinearities above 50 and up to several hun-

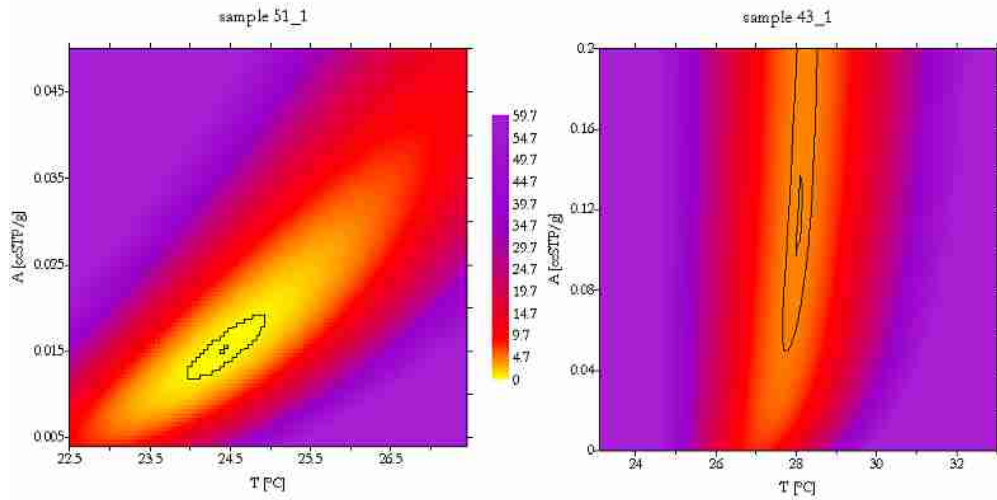


Figure 5.22.: Observed χ^2 valleys for samples 51.1 and 43.3. The parameters A and T are shown on the axis, the parameter F is fitted for best results. Chi square is shown as colour contour plot. Most samples such as the left figure show a good convergence with small errors. The right figure and some other samples with high collinearity between A and T cannot achieve a solution with a narrow convergence and small errors. Collinearities for the shown samples are $\gamma_{AF}^{51.1} = 6.96$, $\gamma_{AT}^{51.1} = 1.78$, $\gamma_{FT}^{51.1} = 1.49$, $\gamma_{AF}^{43.1} = 13.48$, $\gamma_{AT}^{43.1} = 2.52$, $\gamma_{FT}^{43.1} = 14.73$, $\gamma_{FT}^{43.1} = 2.18$ and $\gamma_{AFT}^{43.1} = 64.29$. Note that the dimension of collinearity alone does not suffice as a characteristic of poor fits, but the referred parameters.

dreds for the multicollinearity (see table D.8 – D.11, marked in red). Moreover, high collinearity of just the excess air parameter A and the temperature T (10 to 60) persist, and therefore a great uncertainty in the estimated temperatures. By using the new notation of the CE model, collinearity of A and T can be avoided, but at the expense of enormous collinearities for A and B and the multicollinearity, which is not helpful (shown in table D.8 – D.11). These samples will play a major role in the following methods of evaluation. By plotting χ^2 in a contour plot with axes A and T , the consequence of this collinearity behaviour is made observable (Fig. 5.22). The lowest χ^2 values form a valley at the position where the fitted parameters A and T are situated. The shown figures correspond to the collinearities calculated for the respective sample: the higher the observed collinearities, the longer the resulting χ^2 valley. In case of a sample with “normal” collinearity behaviour, a well-defined minimum can be found, while in case of “abnormal” collinearity behaviour between A and T , these parameters cannot be determined simultaneously when it comes to single sample fitting. When the CE model with parameters A , B and T is used, collinearities are even worse (similar to the example shown in section 2.3.10). The model with B as parameter will therefore not be used for the evaluation. Collinearity results in high errors and values for A and T . For the indicated example, the values are $A = 0.1 \pm 2.2$ ccSTP/g and $T = 29 \pm 13$ °C. As a rule of thumb, from the physical point of view, excess air results above $A = 0.1$ ccSTP/g are not reasonable. In order to obtain reasonable results for these wells, or at least find an unambiguous mathematical identifier, a few methods are introduced in this chapter. As the methods are discussed with the help of the measurement data, it was not part of chapter 4.6.

Physical explanation

The actual physical reason for this mathematical fitting problem of the CE model is not understood at present. However, several facts can be summarised to identify these troublemakers. Identifying samples by their collinearity has already been shown.

Another information comes from observing the concentrations of the samples: Assuming an

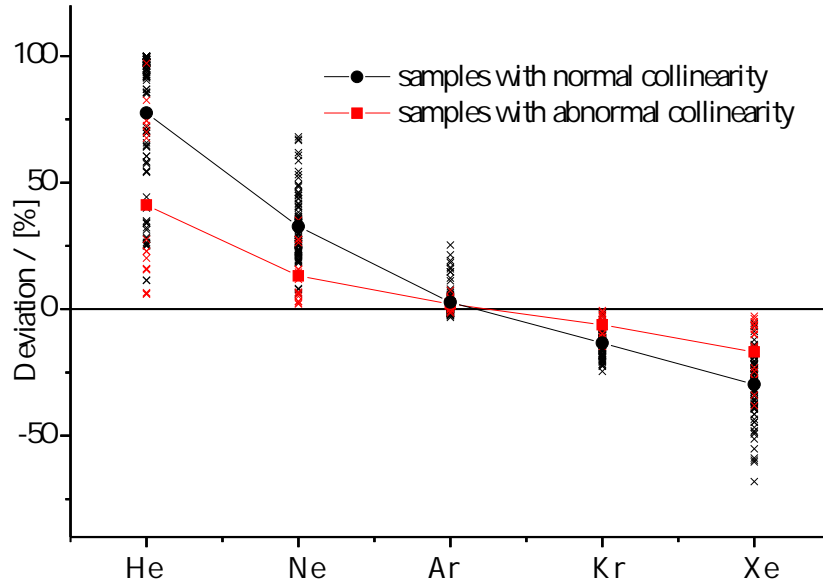


Figure 5.23.: Deviation of sample gas concentrations from assumed equilibrium concentration. Most samples show normal excess air pattern. The problematic samples show a pattern slightly shifted towards dissolved equilibrium concentration. In order to fit a typical fractionated excess air pattern (e.g. a CE model, shown in 2.24) into this signal, the fitting routine reduces the equilibrium concentration and inflates the excess air component to allow a reasonable result. This result however has huge deviations for the particular noble gas concentrations and produces a huge error for excess air, a big excess air component, and due to the lower equilibrium concentrations too high noble gas temperatures with also huge errors (see table D.6 & D.7).

equilibrium model with all noble gases in a water sample resulting from equilibration with the atmosphere at one temperature, every groundwater sample shows strong deviations. This resulted in the postulation of excess air (see chapter 2.3.8). Observing the problematic samples, less deviation is observed, reducing the deviation of all noble gas concentrations (especially He and Xe which usually have a strong deviation) to the equilibrium concentration (see Fig. 5.23). A second information will be observed later when actual solutions for the samples are found: Apparently, the physical minimum can be found at very low values for A , implying a low amount of excess air, which is supported by the concentration observations. Thus, the samples have a very small excess air component which however has a signature more similar to concentrations in a water sample than to air composition. It does not astonish that in this case the excess air parameter is collinear to the equilibrium temperature. While the reason for this strange concentration pattern may in some cases result from sampling or measurement

errors, repeated samples as for well no. 19, 25, 32 or 43 show consistently that this is also a problem of groundwater concentrations. By different approaches, I try to retrieve as much information as possible.

Observing χ^2 : Studying the χ^2 valley in detail may help to understand the problem. In

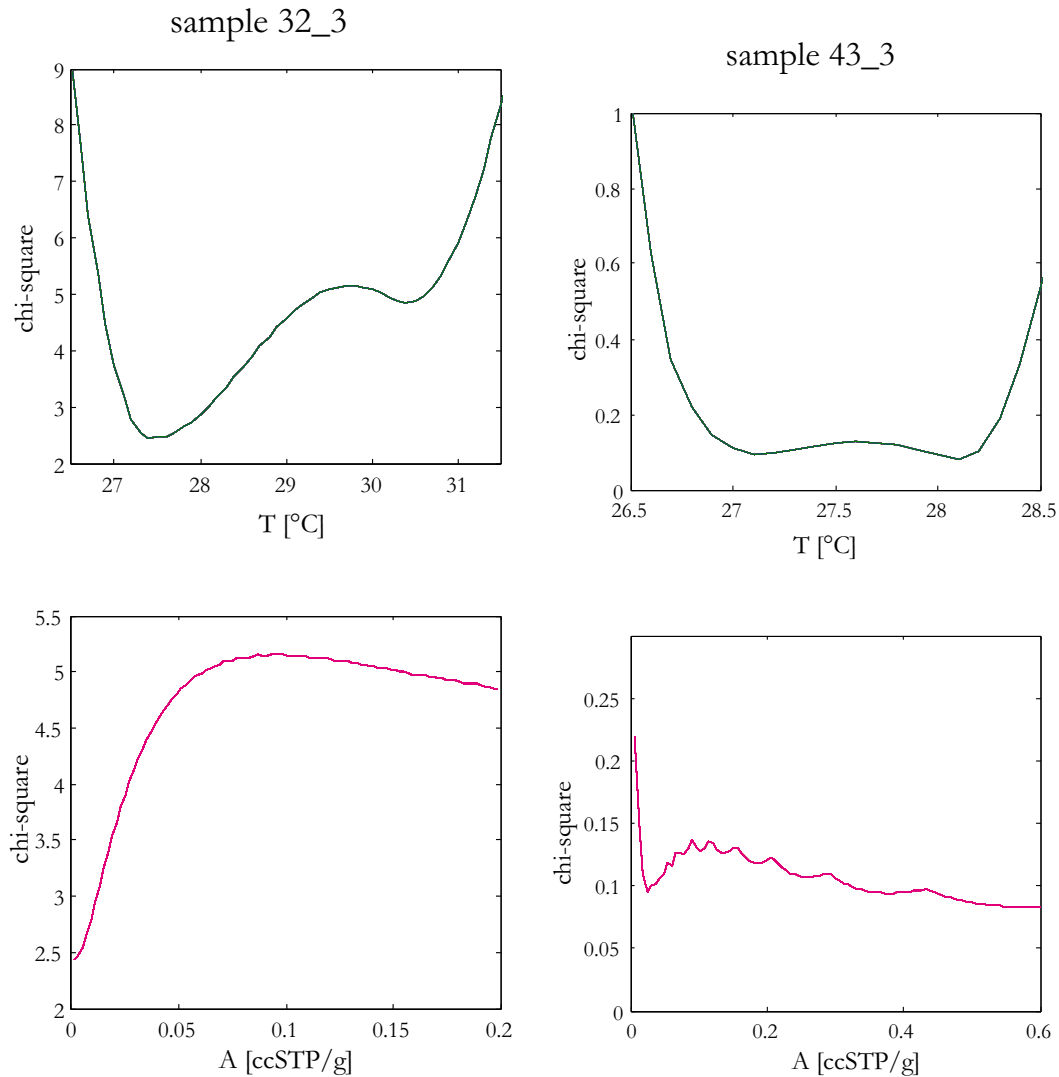


Figure 5.24.: A one-dimensional projection of a two-dimensional colour plot as shown in Fig. 5.22 is made by concentrating on the curve running along the “valley” of minimal χ^2 . The χ^2 in this “valley” is plotted versus either A or T . This way, the minima in the χ^2 “valley” along A and T are shown for the samples 32.3 and 43.3. Two minima are observed for T as well as for A . Convergence with physical relevance typically shows $A < 0.1$ ccSTP/g and thus a colder T . While for 43.3, the physical minimum is more shallow, the physical minimum for 32.3 is the deeper one and can be found by the single fit method without any problems.

Fig. 5.24 and 5.25, the contour plot of sample 43.3 in the area of low A values is examined. By zooming into a χ^2 plot, or by viewing a χ^2 vs. A or T plot, a second minimum can be

found. This minimum is the actual physical solution for the fit, while the other (in case of 43_3 deeper, in case of another sample 32_3 more shallow) minimum is resulting from mathematical collinearity. For samples of the “normal” group, only the physical minimum exists. While this information is quite interesting for a better understanding of the problem, it is due to its complexity of no actual use for the physical evaluation, especially as for most samples the physical minimum is superimposed by the collinearity minimum.

Ensemble fit: The ensemble fit does not try to fit the free parameters for every single sample (which makes i free parameters and j given parameters for every sample). An ensemble fit made on a group of samples assumes one free parameter being equal for all samples which should be fitted all together (making for n samples $n(i - 1) + 1$ free parameters and $n \cdot j$ given parameters). By increasing degrees of freedom, the opportunity exists to achieve parameters of less collinearity. The ensemble fit is commonly used to solve model parameters of the OD model where a general parameter G is assumed to be equal for all wells in a study area. These results are discussed in subsection 5.3.2.

Ensemble CE model: In this actual case of e.g. three samples taken from the same well, the concentrations should in principle all be equal for the triplicate samples. However, small differences exist due to measurement deviations. These deviations are sometimes enough to avoid collinearity and receive a physical solution. Therefore, instead of fitting the parameters A_i , F_i and T_i for every single sample i (each with four concentrations of Ne, Ar, Kr and Xe) of a well, one parameter such as T_{fix} may be assumed equal for all samples, and only the other parameters A_i , F_i and the fixed parameter T_{fix} need to be estimated, leaving more degrees of freedom compared to single sample fitting. As was mentioned earlier, for most results using the CE model in this case, the three parameters A , F and T are estimated with low errors. For the majority of the samples, the parameter T can be set as fixed parameter for all samples of a well. This is convenient as the noble gas temperature is the most interesting parameter. Using T as fixed parameter improves the estimation error of T and produces the statistically most meaningful mean. For some samples however, problems occur.

The samples which already caused problems in single fitting (table D.6 & D.7) now have problems to converge to a narrow minimum using T as ensemble parameter. Possibly, the different samples of the same well may be too equal to be of help to reduce collinearity. If the ensemble fit is tried with one of the other parameters, in some cases improvements can be achieved, especially for samples 25_1, 25_3, 43_1 and 43_3. In these cases, F as a fixed parameter can find a solution that could not be found else with single or ensemble fitting (see table D.12, table D.13 and Fig. 5.25). Furthermore, due to unreasonable parameter fits (e.g. of $A > 0.1$), other outliers were identified (27_3, 33_2, 39_2 and 53_1) and will be ignored for the end evaluation. Still, some samples were not able to converge in a satisfying way.

Monte Carlo simulations: Monte Carlo simulations are a mighty tool to gain improved information about fitting results. Monte Carlo simulations are numerous runs of one sample.

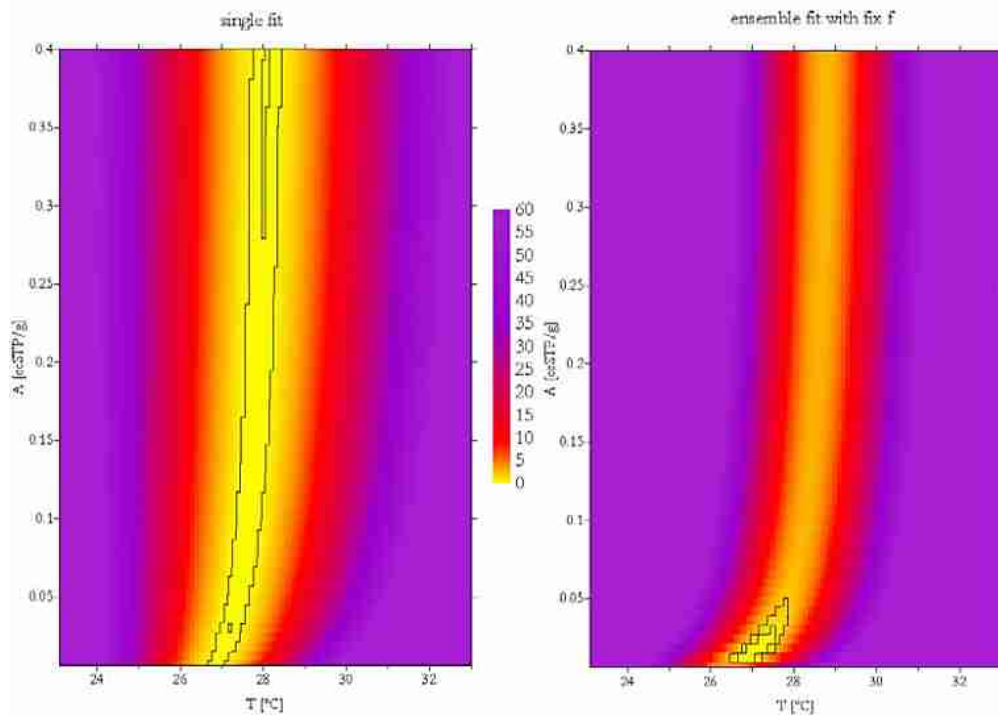


Figure 5.25.: Observed χ^2 valleys for sample 43. The left figure shows the results for normal fitting of A , F and T . The right figure shows the ensemble-fit results for a fixed F defined by the ensemble fit. While on the left no clear convergence can be found ($A = 0.3 \pm 3.4\text{ccSTP/g}$, $T = 28 \pm 3^\circ\text{C}$), the right figure clearly shows the result with $A = 0.017 \pm 0.019\text{ccSTP/g}$ and $T = 27.3 \pm 0.5^\circ\text{C}$.

Small deviations of the initial concentrations within the range of the measurement error have been made. As a result, a Monte Carlo simulation of a normal fitting result can provide the definitive statistical error of the fit to control whether a single fit shows the right uncertainty. This was e.g. achieved with sample 51.1 (Fig. 5.26). Moreover, Monte Carlo simulations help to find other local solutions of the fit. With the example of 25.1, Fig. 5.26 shows how the Monte Carlo simulation indicates the existence of two peaks in the propability distribution. This way, while a solution resulting from collinearity may be found by single fitting, the simulation shows the existence of an additional local solution, which corresponds in some cases to the physical solution. While Monte Carlo simulations could not provide definite solutions for all samples, they could show errors of the single fit method in other samples which had not been suspected (6.3, 11.3, 24.1b, 26.3, 24.2, 38.1 and 44.2).

Evaluation

With the knowledge provided by Monte Carlo simulations, solutions for some problematic samples can be found, while other non-solvable samples were sorted out. Well 19 as well as the doubtable thermal spring samples TS1 and TS2 persist to be without reasonable solution and will therefore be completely sorted out. Thermal spring samples may be corrupted due to their origin and makeshift sampling. Well 19 may be influenced by crystalline rock aquifer

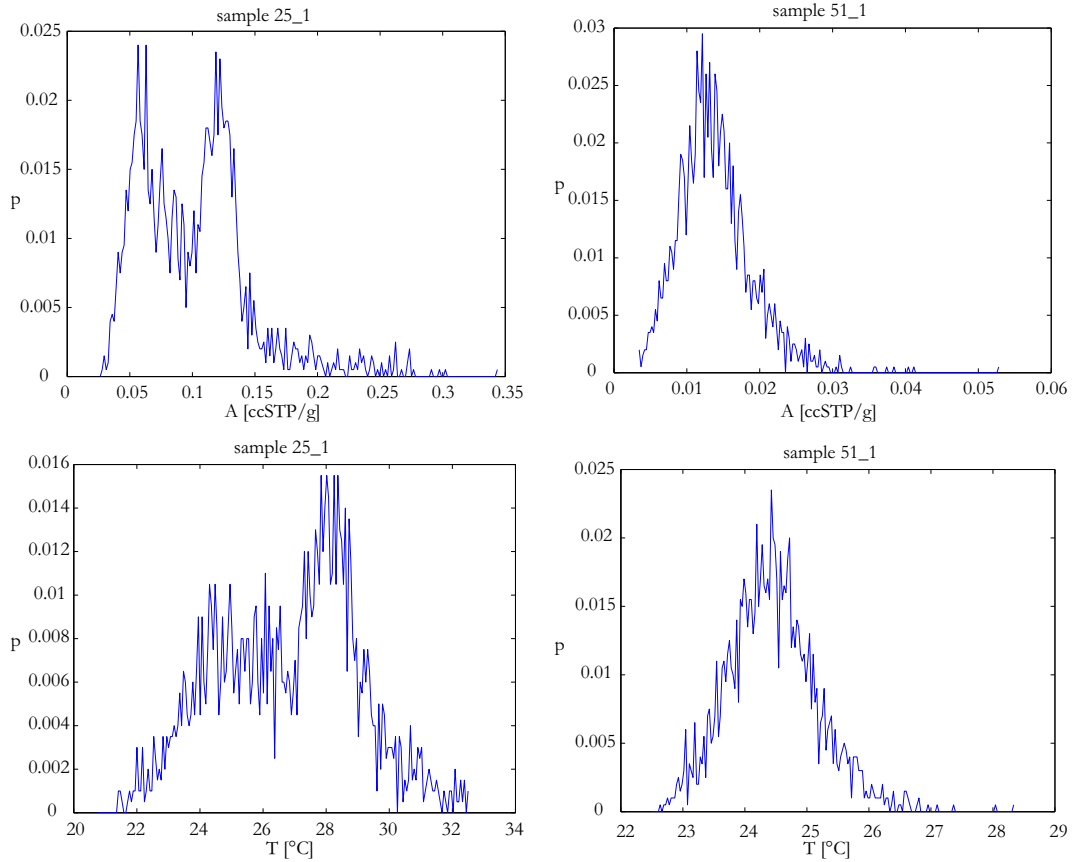


Figure 5.26.: Monte Carlo simulations of parameters A and T for the samples 25.1 and 51.1. 25 shows two peaks in excess air and temperature, indicating two possible solutions. The solution with physical relevance has a lower temperature and excess air component. Well 51 is, as already shown in Fig. 5.22, an example of a converging fit. The probability distribution has approximately the shape of a gauss curve, and the standard deviation match with the 1σ band of the curve. Results are physically relevant, no alternative solutions exist.

water and therefore is not solvable.

Furthermore, the problematic samples 25.2, 29.2, 32.1, 32.2 and 43.2 were sorted out as well for the final fit.

To sum it up, the used methods for the final evaluation are ensemble fits with fixed temperature for most wells, and ensemble fits with fixed fractionation for wells 25 and 43. In case of well 46, single fit results are better than ensemble fit results. Therefore, the single fit results are used and the weighted mean taken.

χ^2 values of the ensemble results are observed. For all wells besides four (with 0.9%, 0.95%, 0.74% and 0.63%), probabilities are above 1%. This is a good result, under the circumstances of an ensemble fit with a constraint solution. By calculating the weighted mean of the left samples for all other results independent of the fit such as the $^3\text{He}/^4\text{He}$ isotope ratio, a result for every well is finally found. Parameters, χ^2 and probability can be found in table D.12 & D.13.

Other models

The models CE (2.3.22), PR (2.3.21) and OD (2.3.23) were preliminarily fitted for comparison. Results are shown in table D.6 & D.7.

The PR model produced reasonable results with converging fits for most samples (sample 25_2 could not be fitted). Temperatures are slightly higher than results from the CE model. While some samples (such as 19_3, 27_3 or 44_3, which include outliers of the CE model) yield quite different temperatures relative to the CE model, most wells show a relatively similar temperature trend about 1 – 2°C warmer than the CE model.

The OD model was initially modelled with a free oxygen consumption parameter G . Only values of G between 1 and 1.26 are physically reasonable values. As a result, only 30% of the wells were able to generate a physically meaningful result. When fitted with a fixed value of G for all samples [Castro *et al.*, 2007], the resulting $G = 1.4$ lies above the physically allowed margin. Therefore, the OD results will not be further investigated.

For the palaeoclimatic discussion, final results of the CE model are used due to its physical significance.

5.3.3. Results of noble gas fitting

Table 5.4.: Summary of the palaeoclimate results for different palaeoclimate groups:

	$\delta^{18}\text{O}$ [‰]	err	NGT [°C]	err	ΔNe	err	D exc. [‰]	err
P MOD	-4.23	0.09	28.4	0.6	0.90	0.12	7.3	0.6
P LHO	-3.56	0.04	28.7	0.3	0.45	0.10	6.9	0.3
P OPT	-3.91	0.12	27.1	0.6	0.98	0.11	6.8	0.2
P TRA	-3.44	0.10	27.4	0.5	0.65	0.06	5.6	0.3
P GLA	-3.16	0.07	25.2	0.4	0.58	0.05	5.6	0.4
P PLE	-3.69	0.22	24.3	1.3	0.53	0.08	6.7	0.9
TS P PLE	-3.42	0.06	24.9	0.6	0.38	0.00	7.4	0.3

The NGT and therefore the MAST show as mean temperatures for the different groups 28.4°C for P MOD, 28.7°C for P LHO, 27.1°C for P OPT, 27.4°C for P TRA, 25.2°C for P GLA and 24.3°C for P PLE (summarised in table 5.4). This result is supported by the PR model results. The group CRY shows colder temperatures than wells of group P with similar ages. The MAAT of Ahmedabad is 27.5°C (shown in Fig. 2.6). Youngest and most shallow wells in the recharge show water temperatures of 29°C.

Another retrieved information of the noble gas measurements is the amount of excess air. The value is observed by neon excess above equilibrium concentration (math:deltaneon). Since neon is not very sensitive for temperature, the value of neon excess does not change much with different excess air models. Results (shown in Fig. 5.28) show low excess air in most groups.

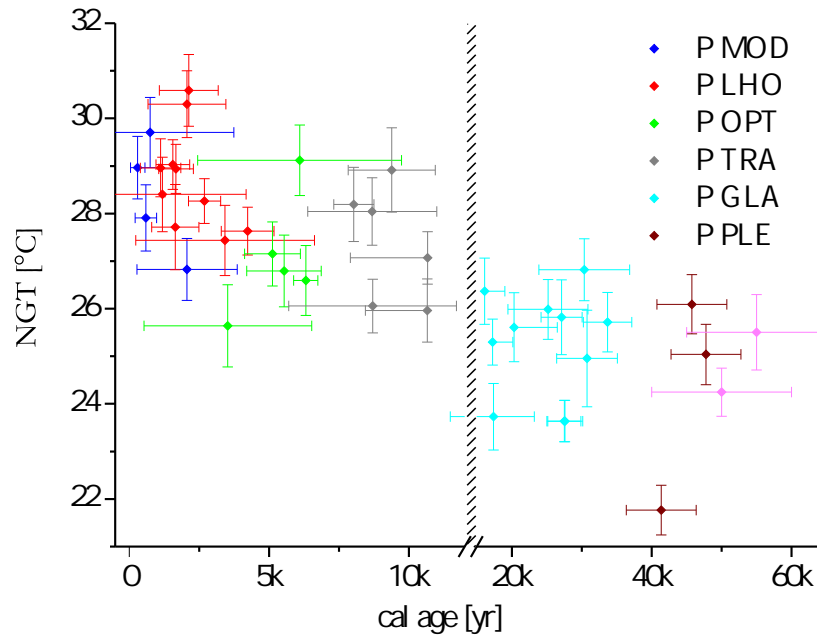


Figure 5.27.: A temperature drop of NGT can be observed over time. Youngest groups P MOD and P LHO show temperatures about 28.4 – 28.7°C, the glacial group P GLA shows a lower temperature of 25.2°C. A temperature change of $3.5 \pm 0.5^\circ\text{C}$ is observed. Both the CE and PR model show this trend. A temporal drop in NGT in group P OPT is observable.

Only groups P OPT (98%), confined wells of P MOD (90%) and CRY show high excess air (mean values shown in brackets, summarised in table 5.4). Wells east of the ECBBF show low excess air (shown in Fig. D.5).

Interpretation of group CRY

The wells of the CRY group show colder NGT than the P group, in three cases abnormally high excess air amounts with $\Delta\text{Ne} > 150\%$, on one hand due to bomb signature due to tritium signals and young ^{14}C ages, on the other hand extremely high amounts of ^4He of purely radiogenic origin. Moreover, very high ^{222}Rn concentrations and hot water temperature imply that the water originates from deep crystalline geologic regions. Stable isotopes show no distinct value but wide scattering. Variation on the LMWL (Fig. 5.20) due to water-rock interaction as shown by Frapet *et al.* [1984] is not observed. If anything, wells of group TS-CRY may show a slightly stronger oxygen enrichment. Panichi and Gonfiantini [1978] observed a pronounced shift towards enriched $\delta^{18}\text{O}$ values in geothermal waters. Finally, SF_6 concentrations three orders of magnitude above recent atmospheric equilibrium complete the picture.

A mixture of very young water and old formation water may explain high helium, radon and SF_6 together with occurring tritium and radiocarbon. Under the assumption of no isotopic fractionation, the observed isotope ratios indicate mixing of a modern (-3.9‰) with an old component enriched more than the most enriched samples of the P group (well TS2: -2.2‰).

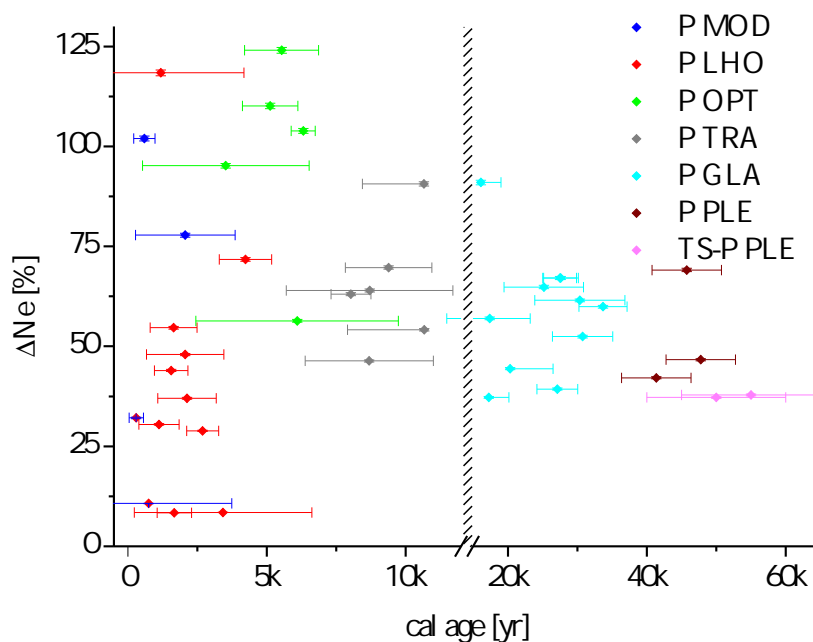


Figure 5.28.: Excess air versus age of the palaeogroup P. Old groups P PLE, P GLA and P TRA show low excess air amounts of 53 – 65%, P OPT and confined wells of group P MOD (compare to Fig. D.5) show high excess air amounts of 90 – 98%. Group P LHO shows the lowest excess air amount of the Holocene with 45%. Since high excess air indicates strong monsoon (see chapter 2.3.8), the Holocene appears to experience more precipitation than the late Pleistocene. For a period in the late Holocene, lower precipitation occurred.

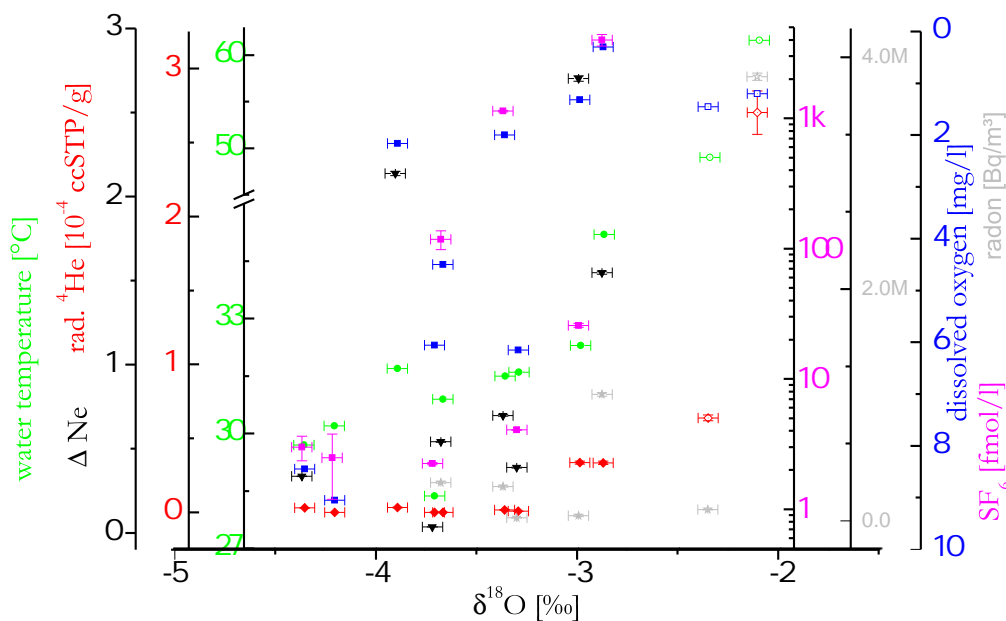


Figure 5.29.: Tracers are shown for the CRY group (and open symbols for TS-CRY). An indistinct mixing trend may be existent between a young water component and an old component with certain characteristics, such as high excess air, enriched isotopes and high SF₆ concentrations.

All concerned tracers are shown in Fig. 5.29. An unambiguous mixing behaviour is not visible, but in principle, mixture of a young and an old component may be indicated. In this case, some information about the old component is presumed. Besides the obvious characteristics of high temperature and radiogenic He, the old water component is enriched in stable isotopes and SF₆, and carries a high excess air component. The wells with high excess air all showed strong bubbling in spite of pressurising the well. This is consistent with the observed high dissolved gas pressure. Low oxygen readings argue against atmospheric contamination. Observed tracers lead to the assumption of a geothermal mixing endmember. Evidently, water of the group CRY is not suitable to be comprised for the palaeoclimate record, which is discussed in the following paragraph.

Interpretation of the palaeoclimate group P

High excess air signals are found in group P OPT and P MOD. Outliers of this trend are the wells 30 and 46 of group P MOD. These wells differ from others due to their position to the East of the ECBBF, positioning them in the unconfined zone [Deshpande, 2006]. Furthermore, the wells 30 and 46 tap very shallow layers of groundwater and show information of a water table few meters above the bottom of the well shaft (shown in Fig. 3.6 and table D.1). Pumping for irrigation depletes these shallow unconfined layers and erases the excess air information from the water as soon as the water table drops to the niveau of the pump.

Since all outliers are taken into account, appearance of high excess air amounts in P OPT and P MOD can be assumed. Coincidentally, the same groups show depleted stable isotope ratios, indicating an amount effect (as shown in Fig. 5.19). A correlation between depleted stable isotope ratios and high excess air amounts is confirmed. Since high excess air implies stronger seasonal rain events (see chapter 2.3.8), a monsoon signal is obtained. Stronger precipitation and massive rain events in these times are therefore strongly suggested and agree with numerous palaeoclimate studies of the region (to cite [Overpeck *et al.*, 1996] as an example). Contrary, P LHO and P GLA are groups with low excess air amounts. Weak monsoon and dry conditions are therefore expected in these ages and are confirmed by other studies such as the work of Enzel *et al.* [1999].

With exception of the late Holocene, a stronger monsoon and more precipitation for the epoch of the Holocene is therefore observed. As a humidity proxy is produced, the temperature proxy is examined.

The retrieved NGT information can be interpreted as a palaeoclimatic signal. Between P LHO and P GLA, a temperature drop of approximately $3.5 \pm 0.5^\circ\text{C}$ can be extracted from the mean results (shown in table 5.4). Furthermore, the mean of group P OPT shows a temperature change of $1.7 \pm 0.7^\circ\text{C}$ during the Holocene. These temperature changes took place in ground temperature at the depth of the water table. As discussed in chapter 2.1.3, MAST may differ from MAAT. For the study region, aridity has an influence on NGT. As found by Beyerle *et al.* [2003], strong changes in humidity and therefore vegetation and the soil moisture can

result in changes of the MAAT – MAST relationship. Drier periods may have relatively elevated MAST. This has an influence on temperature changes between the last Glacial and the Holocene.

MAAT of modern Ahmedabad shows temperatures of 27.5°C , which is slightly colder than the WTT obtained from young and shallow wells in the recharge and with it the MAST. While the P LHO group shows infiltration temperatures higher than the MAAT, the NGT of group P OPT is closer to air temperature. The obtained NGT of P MOD is comparable to modern WTT, showing that the NGT derived by the CE model equals the MAST. As a consequence, the NGT of the aquifer shows a record of MAST. The deviation between MAAT and MAST was less during humid phases such as P MOD and P OPT compared to arid phases such as P LHO or P GLA. Concluding, the temperature difference between modern times and the last glacial period is estimated by comparing temperatures of P LHO and P GLA, resulting in $\Delta T = 3.5 \pm 0.5^{\circ}\text{C}$. Furthermore, higher humidity reduces the deviation of MAST from MAAT in the soil.

A temperature change of 4.5°C for East Asia in northern China is observed by Kreuzer *et al.* [2009]. As shown by palaeotemperature studies in different latitudes [Aeschbach-Hertig *et al.*, 2002] [Johnsen *et al.*, 1995] [Stute *et al.*, 1995], temperature change from Holocene to the LGM was more pronounced in higher latitudes. In this study, a temperature change of $3.5 \pm 0.5^{\circ}\text{C}$ was found for the region of North-West India and fits into this pattern. This result is contradictory to the study of Weyhenmeyer *et al.* [2000] of Oman groundwater which suggests a temperature change between modern times and the LGM of 6.5°C in the vicinity of the Middle East and of South Asia. It may be crucial for all groundwater studies to take into account change of soil moisture conditions in the analysed regions. Moisture related tracers such as excess air amounts are similar for P GLA and P LHO in this study, giving reason to presume a similar humidity situation. Other studies of the region confirm weak monsoon conditions during both the last Glacial and the late Holocene [Juyal *et al.*, 2003]. Therefore, no evidence for differing humidity-evoked effects on soil temperature exist for a comparison of these times. The observed temperature change of 3.5°C is therefore likely to be comparable to the temperature change in MAAT of the region, and to have happened in the early Holocene, since colder NGT during P OPT result from changes in humidity.

6. Summary

6.1. Discussion of laboratory methods

In order to determine palaeoclimate information in this project, improvements in the noble gas analysis of the Heidelberg noble gas mass spectrometer were achieved. To understand and reduce offsets of absolute noble gas concentrations, I investigated and implemented new methods of gas separation. In this context, I established a measurement routine with high performance for the study of noble gas temperatures. Results of a laboratory water standard (shown in 4.6.1) showed a measurement uncertainty for water samples of

He : 0.4%, Ne : 0.5%, Ar : 0.6%, Kr : 1.9%, Xe : 1.4%

The reproducibility was

He : 0.2%, Ne : 0.6%, Ar : 0.3%, Kr : 0.7%, Xe : 1.2%

The deviation of the results from theoretical values¹ was

He : 2.7%, Ne : 0.5%, Ar : 0.6%, Kr : - 0.2%, Xe : 0.4%

which was a major improvement to the initial status.

For the first time, several approaches of thorough evaluation using the fitting software NOBLE2007 were implemented for interpretation of noble gas concentrations. In this regard, a familiar problem of the CE model was investigated and solutions were found in some cases.

6.2. Discussion of hydrogeology

For reasons of observation and dating of the aquifer system in the North Cambay Basin, I compared multiple carbon dating models for hydrology. Among others, the model created by Fohlmeister [2008] was applied for the first time and showed sound results. Calibrated radiocarbon as well as T-³He and He-Rn ages were determined. He-Rn ages proved useful as an independent supporting age tracer for carbon dating. The age pattern of a preceding study of the region (found in Agarwal *et al.* [2006] and Fig. 3.2) was confirmed. As shown in Fig. 5.17, ages of the water increase with distance to the recharge area in the North-East of the region. Ages range from modern samples showing bomb tritium up to the limit of radiocarbon

¹The helium abundance in the laboratory air exceeded atmospheric averages.

dating of about 40-50 kyr. By analysis of $^3\text{He}/^4\text{He}$ isotope ratios, influence of old water from deep layers with mantle origin was observed near characteristic fault zones of the region and in deep wells. Mixture of a young and an old component of groundwater with radiogenic influence from crystalline geology was observed in wells in the Aravalli Foothills (group CRY). In this group, SF_6 concentrations significantly higher than recent atmospheric equilibrium were observed but could not unambiguously be characterised (see 5.2.5). Nonetheless, natural production is strongly suggested. In the sedimentary aquifer, SF_6 concentrations still exceed modern atmospheric equilibrium and pool in distinct depths of the aquifer (Fig. 5.15 and 5.16).

6.3. Discussion of the palaeoclimate

A multitracer climate proxy is obtained from geochemistry, stable isotopes and noble gases. Alkalinity already showed high amounts in modern samples and low amounts in old samples. This indicates a comparatively greater soil CO_2 concentration in recent times and thus greater biologic activity compared to the LGM (Fig. 5.5). Stable isotopes during the last Glacial are enriched due to the global ice-volume effect. Deuterium excess indicates a glacial signature before 10 kyr (Fig. 5.19 and 5.28).

Numerous studies about the palaeoclimate of South Asia exist. For the time of the last Glacial, colder temperatures are assumed from global climate proxies. Stable isotopes cannot provide a temperature record for the region due to superimposing effects, while other tracers only provide trends by qualitative relations. For the times of the last Glacial and the late Holocene, weak monsoon and precipitation is postulated.

In my study, I could find a well-defined correlation of depleted stable isotope ratios, indicating an amount effect, and high excess air amounts, showing strong rainfall in modern times and the early Holocene. The data also shows comparatively weak precipitation and monsoon for late Holocene and glacial times. This way, I confirmed older studies with an independent tracer information and showed the significance of excess air data as a precipitation proxy.

In addition to this, I detected a change in MAST from noble gas measurements. The record shows a mean value of $(25.2 \pm 0.4)^\circ\text{C}$ in the last Glacial changing to $(28.7 \pm 0.5)^\circ\text{C}$ after the transition to Holocene times (Fig. 5.27). The temperature change sums up to $(3.5 \pm 0.5)^\circ\text{C}$. Modern NGT closely resemble the WTT of young shallow water. Temporal change in NGT in the early Holocene and modern times may be influenced by a change in humidity. According to excess air information, this influence is irrelevant when comparing temperatures of the last Glacial and the late Holocene. Hence, I can provide first quantitative data about changes in MAST in this region of South Asia.

6.4. Outlook

The achieved measurement routine of the noble gas mass spectrometer has to be further improved by reducing measurement time without loss of precision. This can be realised by overlapping of measurement cycles, or by omitting measurements of residual Ar in the Kr/Xe fraction.

Apart from routine measurements, the phenomenon of non-sample krypton (“ghost” krypton, see chap. B.2.3) may be further investigated.

The use of NOBLE2007 for extensive evaluation compared to basic fitting with NOBLE90 is suggested. Better user friendliness of the NOBLE2007 program and optional integration of all evaluation steps performed in this study should therefore be considered. With the help of this tool and more data from field sites or laboratory setups, the CE model’s problem of collinearity for some samples may be further investigated.

Open questions of the North Cambay Basin groundwater study are associated with discovered high SF₆ concentrations. A natural production is highly suggested, yet the involved processes and mechanisms are not understood completely. The ambiguous origin of the old mixing water situated in the crystalline rock aquifer is connected with this question. Pending rock sample analysis done by the Institute of Earth Sciences, Heidelberg, may provide some evidence. Moreover, analysis of drilling profiles may show more evidence in this context.

Exact proportions of the different fractionation effects in the record’s stable isotope data were in some cases not completely interpreted. Since the Physical Research Laboratory set up a nationwide stable isotope measurement network (National Programme on isotope fingerprinting of waters of India, IWIN), new evidence about correlations of the modern hydrological cycle can improve the perspective on results presented in this study. Future collaboration with PRL is highly advisable.

A. Monsoon

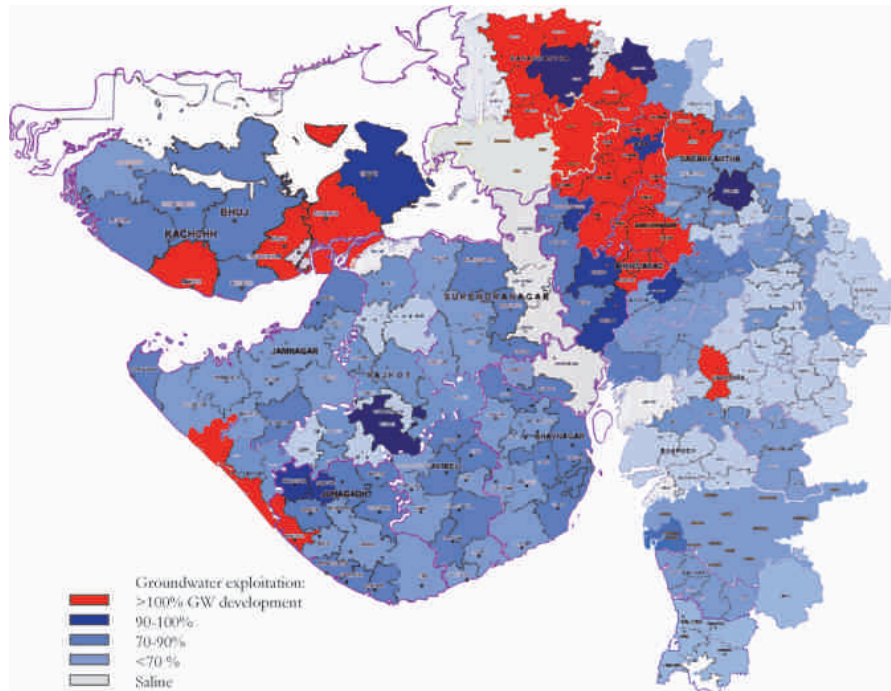


Figure A.1.: Groundwater exploitation map of Gujarat. Some regions show water mining in alarming dimensions. Data from [www.gwrdc.gujarat.gov.in, 2010].

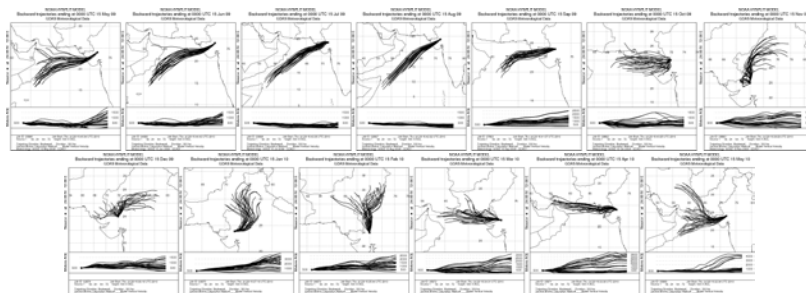
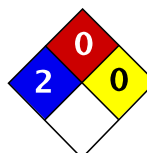


Figure A.2.: Monthly air trajectories in the region of Gujarat and their origin (simulated by NOAA HYSPLIT), beginning in May 2009 until May 2010. As a characteristic, the summer monsoon shows wind originating from the Arabian Sea. In the winter, the origin of the wind reverses with cold dry winds coming from the Tibetan plateau in January and February [[NOAA, 2010b](#)]. This behaviour is typical for the Indian summer monsoon.

B. Methods

B.1. Used field chemicals

To avoid biological alteration of the sample, silver nitrate was used to poison the samples for ^{14}C dating. As possibilities to poison water samples, [Clark and Fritz \[1997\]](#) suggest the use of mercury chloride. As the problems with transport through customs, the handling in the field and the disposal of samples sum up to alarming proportions, my predecessor in the group, Andreas Kreuzer, used sodium azide [[Kreuzer *et al.*, 2009](#)] to suppress biologic production. Sodium azide can be easily destroyed and the samples disposed. However, as addition of acids can produce hydrazoic acid, an extremely explosive liquid, treatment in the laboratory became more difficult than intended. Iodide had to be added to the sample before extraction to avoid destructive reactions. This increased difficulties of the extraction due to release of gaseous nitrogen and iodide spreading in the extraction line. It is therefore not suitable for this purpose. Since modern commercial water purifiers mostly use an organic chemical basis, they are not suitable for the purpose of treating samples for DIC analysis. As a result, I introduced a relatively weak poison, silver nitrate, which was the basis of old fashioned water purifiers for travelling. Silver nitrate (material safety data sheet shown in [Fig. B.1](#)) can easily be transported in solid state together with the sampling equipment, e.g. in the toolbox. It needs to be kept away from sunlight as it decomposes to silver or silver oxide exposed to solar radiation. It has a very high solubility in water, and is poisonous in dissolved state for virtually all water organisms. An amount of 25g of AgNO_3 was dissolved in a bottle of 500ml desalted water, and 2 ml were added to the 500 ml water samples intended for carbon analysis. Occurring precipitation of silver salts together with halogens was common, but even a weak concentration of dissolved metallic salts in water is poisonous for organisms. As a side information, samples for tritium analysis that were left untreated and stored in the lab in sunlight have not established any visual biologic activity after three years, indicating that biologic activity of Indian groundwater was low in the first place.



Health	3
Fire	0
Reactivity	0
Personal Protection	J

Material Safety Data Sheet Silver nitrate MSDS

Section 1: Chemical Product and Company Identification		
<p>Product Name: Silver nitrate</p> <p>Catalog Codes: SLS2122, SLS1327</p> <p>CAS#: 7761-88-8</p> <p>RTECS: VW4725000</p> <p>TSCA: TSCA 8(b) inventory: Silver nitrate</p> <p>Cf#: Not available.</p> <p>Synonym: Lunar caustic; Silver (1+) nitrate; Nitric acid, silver (1+) salt</p> <p>Chemical Name: Silver Nitrate</p> <p>Chemical Formula: AgNO₃</p>	<p>Contact Information:</p> <p>Sciencelab.com, Inc. 14025 Smith Rd. Houston, Texas 77396</p> <p>US Sales: 1-800-901-7247 International Sales: 1-281-441-4400</p> <p>Order Online: ScienceLab.com</p> <p>CHEMTREC (24HR Emergency Telephone), call: 1-800-424-9300</p> <p>International CHEMTREC, call: 1-703-527-3887</p> <p>For non-emergency assistance, call: 1-281-441-4400</p>	
Section 2: Composition and Information on Ingredients		
Composition:		
Name	CAS #	% by Weight
Silver nitrate	7761-88-8	100
<p>Toxicological Data on Ingredients: Silver nitrate: ORAL (LD50): Acute: 1173 mg/kg [Rat]. 50 mg/kg [Mouse]. 473 mg/kg [Guinea pig].</p>		
Section 3: Hazards Identification		
<p>Potential Acute Health Effects: Very hazardous in case of skin contact (irritant), of ingestion. Hazardous in case of skin contact (permeator), of eye contact (irritant), of inhalation. Slightly hazardous in case of skin contact (corrosive). The amount of tissue damage depends on length of contact. Eye contact can result in corneal damage or blindness. Skin contact can produce inflammation and blistering. Inhalation of dust will produce irritation to gastro-intestinal or respiratory tract, characterized by burning, sneezing and coughing. Severe over-exposure can produce lung damage, choking, unconsciousness or death. Prolonged exposure may result in skin burns and ulcerations. Over-exposure by inhalation may cause respiratory irritation.</p> <p>Potential Chronic Health Effects: CARCINOGENIC EFFECTS: Not available. MUTAGENIC EFFECTS: Not available. TERATOGENIC EFFECTS: Not available.</p>		

p. 1

Figure B.1.: The MSDS of silver nitrate.

<p>DEVELOPMENTAL TOXICITY: Not available. The substance is toxic to lungs. The substance may be toxic to mucous membranes, skin, eyes. Repeated or prolonged exposure to the substance can produce target organs damage. Repeated exposure of the eyes to a low level of dust can produce eye irritation. Repeated skin exposure can produce local skin destruction, or dermatitis. Repeated inhalation of dust can produce varying degree of respiratory irritation or lung damage.</p>
<p>Section 4: First Aid Measures</p>
<p>Eye Contact: Check for and remove any contact lenses. In case of contact, immediately flush eyes with plenty of water for at least 15 minutes. Cold water may be used. Get medical attention.</p> <p>Skin Contact: In case of contact, immediately flush skin with plenty of water for at least 15 minutes while removing contaminated clothing and shoes. Cover the irritated skin with an emollient. Cold water may be used. Wash clothing before reuse. Thoroughly clean shoes before reuse. Get medical attention immediately.</p> <p>Serious Skin Contact: Wash with a disinfectant soap and cover the contaminated skin with an anti-bacterial cream. Seek immediate medical attention.</p> <p>Inhalation: If inhaled, remove to fresh air. If not breathing, give artificial respiration. If breathing is difficult, give oxygen. Get medical attention.</p> <p>Serious Inhalation: Evacuate the victim to a safe area as soon as possible. Loosen tight clothing such as a collar, tie, belt or waistband. If breathing is difficult, administer oxygen. If the victim is not breathing, perform mouth-to-mouth resuscitation. WARNING: It may be hazardous to the person providing aid to give mouth-to-mouth resuscitation when the inhaled material is toxic, infectious or corrosive. Seek immediate medical attention.</p> <p>Ingestion: Do NOT induce vomiting unless directed to do so by medical personnel. Never give anything by mouth to an unconscious person. If large quantities of this material are swallowed, call a physician immediately. Loosen tight clothing such as a collar, tie, belt or waistband.</p> <p>Serious Ingestion: Not available.</p>
<p>Section 5: Fire and Explosion Data</p>
<p>Flammability of the Product: Non-flammable.</p> <p>Auto-Ignition Temperature: Not applicable.</p> <p>Flash Points: Not applicable.</p> <p>Flammable Limits: Not applicable.</p> <p>Products of Combustion: Not available.</p> <p>Fire Hazards in Presence of Various Substances: organic materials, combustible materials</p> <p>Explosion Hazards in Presence of Various Substances: Risks of explosion of the product in presence of mechanical impact: Not available. Risks of explosion of the product in presence of static discharge: Not available.</p> <p>Fire Fighting Media and Instructions: Not applicable.</p> <p>Special Remarks on Fire Hazards: Contact with combustible or organic materials may cause fire.</p>

p. 2

Figure B.2.: The MSDS of silver nitrate.

<p>Special Remarks on Explosion Hazards: Silver nitrate mixed with dry powdered magnesium may ignite explosively on contact with a drop of water. An explosive fulminate may be formed if silver nitrate is mixed with alcohols. Highly explosive is formed by the addition of calcium carbide to silver nitrate solution.</p>
Section 6: Accidental Release Measures
<p>Small Spill: Use appropriate tools to put the spilled solid in a convenient waste disposal container.</p> <p>Large Spill: Oxidizing material. Corrosive solid. Stop leak if without risk. Do not get water inside container. Avoid contact with a combustible material (wood, paper, oil, clothing...). Keep substance damp using water spray. Do not touch spilled material. Use water spray to reduce vapors. Prevent entry into sewers, basements or confined areas; dike if needed. Call for assistance on disposal. Be careful that the product is not present at a concentration level above TLV. Check TLV on the MSDS and with local authorities.</p>
Section 7: Handling and Storage
<p>Precautions: Keep container dry. Keep away from heat. Keep away from sources of ignition. Keep away from combustible material.. Do not ingest. Do not breathe dust. Never add water to this product. In case of insufficient ventilation, wear suitable respiratory equipment. If ingested, seek medical advice immediately and show the container or the label. Avoid contact with skin and eyes.</p> <p>Storage: Keep container tightly closed. Keep container in a cool, well-ventilated area. Separate from acids, alkalis, reducing agents and combustibles. See NFPA 43A, Code for the Storage of Liquid and Solid Oxidizers. Sensitive to light. Store in light-resistant containers.</p>
Section 8: Exposure Controls/Personal Protection
<p>Engineering Controls: Use process enclosures, local exhaust ventilation, or other engineering controls to keep airborne levels below recommended exposure limits. If user operations generate dust, fume or mist, use ventilation to keep exposure to airborne contaminants below the exposure limit.</p> <p>Personal Protection: Splash goggles. Synthetic apron. Vapor and dust respirator. Be sure to use an approved/certified respirator or equivalent. Gloves.</p> <p>Personal Protection in Case of a Large Spill: Splash goggles. Full suit. Vapor and dust respirator. Boots. Gloves. A self contained breathing apparatus should be used to avoid inhalation of the product. Suggested protective clothing might not be sufficient; consult a specialist BEFORE handling this product.</p> <p>Exposure Limits: TWA: 0.01 (mg/m) Ag) from ACGIH (TLV) [United States] TWA: 0.01 (mg/m) Ag) from OSHA (PEL) [United States]³ Consult local authorities for acceptable exposure limits.</p>
Section 9: Physical and Chemical Properties
<p>Physical state and appearance: Solid. (Crystals solid.)</p>

p. 3

Figure B.3.: The MSDS of silver nitrate.

<p>Odor: Not available.</p> <p>Taste: Bitter. Metallic</p> <p>Molecular Weight: 169.87 g/mole</p> <p>Color: Colorless. White.</p> <p>pH (1% soln/water): 6 - 7 [slightly acidic to neutral]</p> <p>Boiling Point: Decomposition temperature: 440°C (824°F)</p> <p>Melting Point: 212°C (413.6°F)</p> <p>Critical Temperature: Not available.</p> <p>Specific Gravity: 4.35 (Water = 1)</p> <p>Vapor Pressure: Not applicable.</p> <p>Vapor Density: 5.8 (Air = 1)</p> <p>Volatility: Not available.</p> <p>Odor Threshold: Not available.</p> <p>Water/Oil Dist. Coeff.: Not available.</p> <p>Ionicity (in Water): Not available.</p> <p>Dispersion Properties: See solubility in water, diethyl ether.</p> <p>Solubility: Easily soluble in cold water, hot water. Soluble in diethyl ether. Very slightly soluble in acetone. Solubility in water: 122 g/100 ml water @ 0 deg. C. Solubility in water: 952 g/100 ml water @ 190 deg. C Solubility in alcohol: 1 g/30 ml alcohol; 1g/ 6.5 ml boiling alcohol. Solubility in acetone: 1 g/ 253 ml acetone</p>
--

Section 10: Stability and Reactivity Data
<p>Stability: The product is stable.</p> <p>Instability Temperature: Not available.</p> <p>Conditions of Instability: Incompatible materials, light</p> <p>Incompatibility with various substances: Reactive with reducing agents, combustible materials, organic materials, alkalis.</p> <p>Corrosivity: Non-corrosive in presence of glass.</p> <p>Special Remarks on Reactivity: Sensitive to light. Incompatible with antimony salts, arsenites, bromides, carbonates, chlorides, iodides, thiocyanates, ferrous salts, hypophosphites, morphine salts, oils, creosote, phosphates, tannic acid, tartrates, vegetable decoctions, and extracts, sodium hydroxide, charcoal, thimerosal, benzalkonium chloride, halogenated acids and their salts. alcohols. Silver nitrate reacts with acetylene in presence of ammonia to form silver acetylide, a sensitive powerful detonator</p>

p. 4

Figure B.4.: The MSDS of silver nitrate.

<p>when dry. Reaction between silver nitrate and chlorosulfonic acid is violent. Silver nitrate is reduced by hydrogen sulfide in the dark. Silver nitrate is easily reduced to metallic silver by ferrous salts, arsenites, hypophosphites, tartrates, sugars, tannins, volatile oils.</p> <p>Special Remarks on Corrosivity: Not available.</p> <p>Polymerization: Will not occur.</p>
<p>Section 11: Toxicological Information</p>
<p>Routes of Entry: Absorbed through skin. Dermal contact. Eye contact. Inhalation. Ingestion.</p> <p>Toxicity to Animals: Acute oral toxicity (LD50): 50 mg/kg [Mouse].</p> <p>Chronic Effects on Humans: Causes damage to the following organs: lungs. May cause damage to the following organs: mucous membranes, skin, eyes.</p> <p>Other Toxic Effects on Humans: Very hazardous in case of skin contact (irritant), of ingestion. Hazardous in case of skin contact (permeator), of inhalation. Slightly hazardous in case of skin contact (corrosive).</p> <p>Special Remarks on Toxicity to Animals: Not available.</p> <p>Special Remarks on Chronic Effects on Humans: May affect genetic material (mutagenic). May cause cancer based on animal test data. May cause adverse reproductive effects.</p> <p>Special Remarks on other Toxic Effects on Humans: Acute Potential Health Effects: Skin: Causes severe irritation and burns. It may cause dermatitis. It may be absorbed through the skin. Eyes: Causes severe irritation, corneal opacification, bleeding conjunctiva, burns of conjunctiva, argyria, blindness Inhalation: Causes irritation of the respiratory tract and mucous membranes with possible chemical burns. Symptoms may include burning sensation, coughing, wheezing, laryngitis, shortness of breath, headache, nausea, vomiting. Ingestion: Severe gastrointestinal tract irritation and burns, pain and burning in the mouth, violent abdominal pain, argyria -grayish/blackening of skin and mucous membranes, throat and abdomen, salivation, vomiting of black material, diarrhea, hypermotility, ulcerative gingivitis . May affect kidneys (lesions of kidneys, anuria,), lungs</p>
<p>Section 12: Ecological Information</p>
<p>Ecotoxicity: Not available.</p> <p>BOD5 and COD: Not available.</p> <p>Products of Biodegradation: Possibly hazardous short term degradation products are not likely. However, long term degradation products may arise.</p> <p>Toxicity of the Products of Biodegradation: The products of degradation are less toxic than the product itself.</p> <p>Special Remarks on the Products of Biodegradation: Not available.</p>

Figure B.5.: The MSDS of silver nitrate.



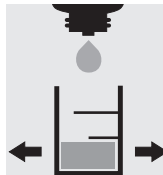
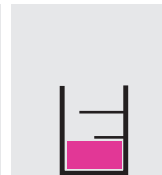
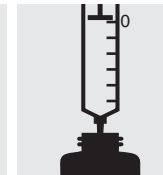
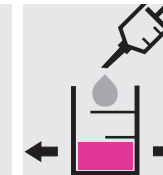
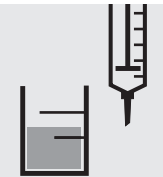
Section 13: Disposal Considerations
<p>Waste Disposal: Waste must be disposed of in accordance with federal, state and local environmental control regulations.</p>
Section 14: Transport Information
<p>DOT Classification: CLASS 5.1: Oxidizing material.</p> <p>Identification: : Silver nitrate UNNA: 1493 PG: II</p> <p>Special Provisions for Transport: Not available.</p>
Section 15: Other Regulatory Information
<p>Federal and State Regulations: Connecticut hazardous material survey.: Silver nitrate Illinois chemical safety act: Silver nitrate New York acutely hazardous substances: Silver nitrate Rhode Island RTK hazardous substances: Silver nitrate Pennsylvania RTK: Silver nitrate Massachusetts RTK: Silver nitrate Massachusetts spill list: Silver nitrate New Jersey: Silver nitrate New Jersey spill list: Silver nitrate Louisiana spill reporting: Silver nitrate California Director's List of Hazardous Substances: Silver nitrate TSCA 8(b) inventory: Silver nitrate</p> <p>Other Regulations: OSHA: Hazardous by definition of Hazard Communication Standard (29 CFR 1910.1200). EINECS: This product is on the European Inventory of Existing Commercial Chemical Substances.</p> <p>Other Classifications:</p> <p>WHMIS (Canada): CLASS C: Oxidizing material. CLASS E: Corrosive solid.</p> <p>DSCL (EEC): R8- Contact with combustible material may cause fire. R20/22- Harmful by inhalation and if swallowed. R34- Causes burns. R50/53- Very toxic to aquatic organisms, may cause long-term adverse effects in the aquatic environment. S24/25- Avoid contact with skin and eyes. S26- In case of contact with eyes, rinse immediately with plenty of water and seek medical advice. S28- After contact with skin, wash immediately with plenty of water S36/37/39- Wear suitable protective clothing, gloves and eye/face protection. S45- In case of accident or if you feel unwell,</p>

p. 6

Figure B.6.: The MSDS of silver nitrate.

<p>seek medical advice immediately (show the label where possible). S46- If swallowed, seek medical advice immediately and show this container or label. S60- This material and its container must be disposed of as hazardous waste. S61- Avoid release to the environment. Refer to special instructions/Safety data sheets.</p> <p>HMIS (U.S.A.):</p> <p>Health Hazard: 3</p> <p>Fire Hazard: 0</p> <p>Reactivity: 0</p> <p>Personal Protection: j</p> <p>National Fire Protection Association (U.S.A.):</p> <p>Health: 2</p> <p>Flammability: 0</p> <p>Reactivity: 0</p> <p>Specific hazard:</p> <p>Protective Equipment: Gloves (impervious). Synthetic apron. Wear appropriate respirator when ventilation is inadequate. Splash goggles.</p>
<p style="text-align: center;">Section 16: Other Information</p> <p>References: Not available.</p> <p>Other Special Considerations: Not available.</p> <p>Created: 10/10/2005 08:53 PM</p> <p>Last Updated: 11/06/2008 12:00 PM</p> <p><i>The information above is believed to be accurate and represents the best information currently available to us. However, we make no warranty of merchantability or any other warranty, express or implied, with respect to such information, and we assume no liability resulting from its use. Users should make their own investigations to determine the suitability of the information for their particular purposes. In no event shall ScienceLab.com be liable for any claims, losses, or damages of any third party or for lost profits or any special, indirect, incidental, consequential or exemplary damages, howsoever arising, even if ScienceLab.com has been advised of the possibility of such damages.</i></p>

Figure B.7.: The MSDS of silver nitrate.

	Alkalität (Säurekapazität bis pH 8,2 und pH 4,3) Alkalinity (Acid capacity to pH 8.2 and pH 4.3) Alcalinité (Capacité pour acides jusqu'à pH 8.2 et pH 4.3) Alcalinidad (Capacidad de ácido hasta pH 8.2 y pH 4.3)	111109 Aquamerck®		
Messbereich / Measuring range / Domaine de mesure / Intervalo de medida: 0.1 – 10 mmol/l mit 1 Pipettenfüllung / with 1 full pipette / avec 1 volume de pipette / con 1 carga de pipeta Abstufung / Graduation / Graduación 0.1 mmol/l				
Säurekapazität bis pH 8,2 ($K_{S8,2}$, „p-Wert“) Acid capacity to pH 8.2 ($K_{S8,2}$, “p-value”) Capacité pour acides jusqu'à pH 8,2 ($K_{S8,2}$, TA, «valeur p») Capacidad de ácido hasta pH 8,2 ($K_{S8,2}$, TA, “valor p”):				
<p>Die Bestimmung ist nur möglich, wenn die Wasserprobe einen pH über 8,2 besitzt. The determination is only possible if the water sample has a pH above 8.2. La détermination est possible uniquement si l'échantillon d'eau a un pH supérieur à 8,2. La determinación solamente es posible si la muestra de agua tiene un pH superior a 8,2.</p>				
				
5 ml Probe (A)	2 Tropfen Reagenz R-1 zugeben und umschwenken.	Farbe der Lösung: Rosa bis Rot	Tropfrohr der Titrierpipette mit Reagenz R-3 füllen.	Reagenz R-3 langsam und unter Umschwenken zur Probe tropfen, bis sich diese vollständig entfärbt hat.
5 ml of sample (A)	Add 2 drops of reagent R-1 and swirl.	Colour of the solution: pink to red	Fill the dropping tube of the titration pipette with reagent R-3.	Slowly add reagent R-3 dropwise to the sample while swirling until the sample becomes entirely colourless .
5 ml d'échantillon (A)	Ajouter 2 gouttes de réactif R-1 et agiter légèrement.	Couleur de la solution: de rose à rouge	Remplir le tube compte-gouttes de la pipette de titrage avec du réactif R-3.	Ajouter lentement , goutte à goutte et en agitant légèrement , le réactif R-3 à l'échantillon jusqu'à décoloration totale .
5 ml de muestra (A)	Añadir 2 gotas de reactivo R-1 y agitar por balanceo.	Color de la solución: de rosa a rojo	Llenar el tubo cuentagotas de la pipeta de valoración con reactivo R-3.	Lentamente y agitando por balanceo , gotear el reactivo R-3 a la muestra hasta décoloración total .
		Messwert für $K_{S8,2}$ in mmol/l auf der Skala der Titrierpipette ablesen. Read off the result for $K_{S8,2}$ in mmol/l from the scale of the titration pipette. Lire le résultat pour $K_{S8,2}$ en mmol/l sur l'échelle de la pipette de titrage. Leer el valor de medición para $K_{S8,2}$ en mmol/l en la escala de la pipeta de valoración.		

Ausgabedatum / Release / Version / Fecha de emisión 03/2010

Figure B.8.: Manual of the aquamerck alkalinity titration quicktest.


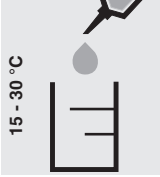
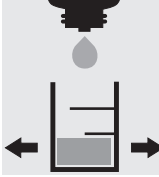
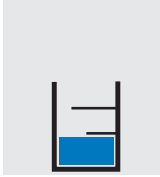
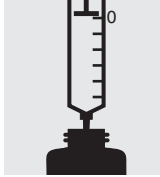
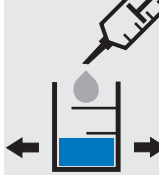
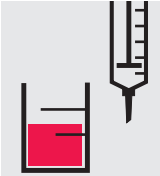
	Alkalität (Säurekapazität bis pH 8,2 und pH 4,3) Alkalinity (Acid capacity to pH 8.2 and pH 4.3) Alcalinité (Capacité pour acides jusqu'à pH 8.2 et pH 4.3) Alcalinidad (Capacidad de ácido hasta pH 8.2 y pH 4.3)	111109 Aquamerck®		
Messbereich / Measuring range / Domaine de mesure / Intervalo de medida: 0.1 – 10 mmol/l mit 1 Pipettenfüllung / with 1 full pipette / avec 1 volume de pipette / con 1 carga de pipeta Abstufung / Graduation / Graduación 0.1 mmol/l				
Säurekapazität bis pH 4,3 (K_{S4,3}, Gesamtalkalität, „m-Wert“) Acid capacity to pH 4.3 (K_{S4,3}, total alkalinity, “m-value”) Capacité pour acides jusqu'à pH 4,3 (K_{S4,3}, alcalinité totale, TAC, «valeur m») Capacidad de ácido hasta pH 4,3 (K_{S4,3}, alcalinidad total, TAC, “valor m”):				
Die Bestimmung ist nur möglich, wenn die Wasserprobe einen pH über 4,3 besitzt. The determination is only possible if the water sample has a pH above 4.3. La détermination est possible uniquement si l'échantillon d'eau a un pH supérieur à 4,3. La determinación solamente es posible si la muestra de agua tiene un pH superior a 4,3.				
				
15 - 30 °C 5 ml Probe (B)	2 Tropfen Reagenz R-2 zugeben und umschwenken.	Farbe der Lösung: Blau	Tropfrohr der Titrierpipette mit Reagenz R-3 füllen.	Reagenz R-3 langsam und unter Umschwenken zur Probe tropfen, bis deren Farbe von Blau nach Rot umschlägt.
5 ml of sample (B)	Add 2 drops of reagent R-2 and swirl.	Colour of the solution: blue	Fill the dropping tube of the titration pipette with reagent R-3.	Slowly add reagent R-3 dropwise to the sample while swirling until its colour changes from blue to red .
5 ml d'échantillon (B)	Ajouter 2 gouttes de réactif R-2 et agiter légèrement.	Couleur de la solution: bleue	Remplir le tube compte-gouttes de la pipette de titrage avec du réactif R-3.	Ajouter lentement , goutte à goutte et en agitant légèrement , le réactif R-3 à l'échantillon jusqu'à ce que sa couleur vire du bleu au rouge .
5 ml de muestra (B)	Añadir 2 gotas de reactivo R-2 y agitar por balanceo.	Color de la solución: azul	Llenar el tubo cuentagotas de la pipeta de valoración con reactivo R-3.	Lentamente y agitando por balanceo , gotear el reactivo R-3 a la muestra, hasta que su color vire de azul a rojo .
	Messwert für K _{S4,3} in mmol/l auf der Skala der Titrierpipette ablesen. Read off the result for K _{S4,3} in mmol/l from the scale of the titration pipette. Lire le résultat pour K _{S4,3} en mmol/l sur l'échelle de la pipette de titrage. Leer el valor de medición para K _{S4,3} en mmol/l en la escala de la pipeta de valoración.			
4.3 < pH < 8.2: SBV / ANC / TAC / K_{S4,3} = mmol/l HCO₃⁻ (mmol/l HCO ₃ ⁻ x 61.02 = mg/l HCO ₃ ⁻)				
pH > 8.2: (K_{S4,3} - K_{S8,2}) x 12.01 = TIC (CIT) [mg/l C]				
TIC / CIT: Gesamter anorganisch gebundener Kohlenstoff / total inorganic carbon / carbone inorganique total / carbono inorgánico total				
Ausgabedatum / Release / Version / Fecha de emisión 03/2010				

Figure B.9.: Manual of the aquamerck alkalinity titration quicktest.

B.2. Noble gas measurement

B.2.1. Heidelberg MS

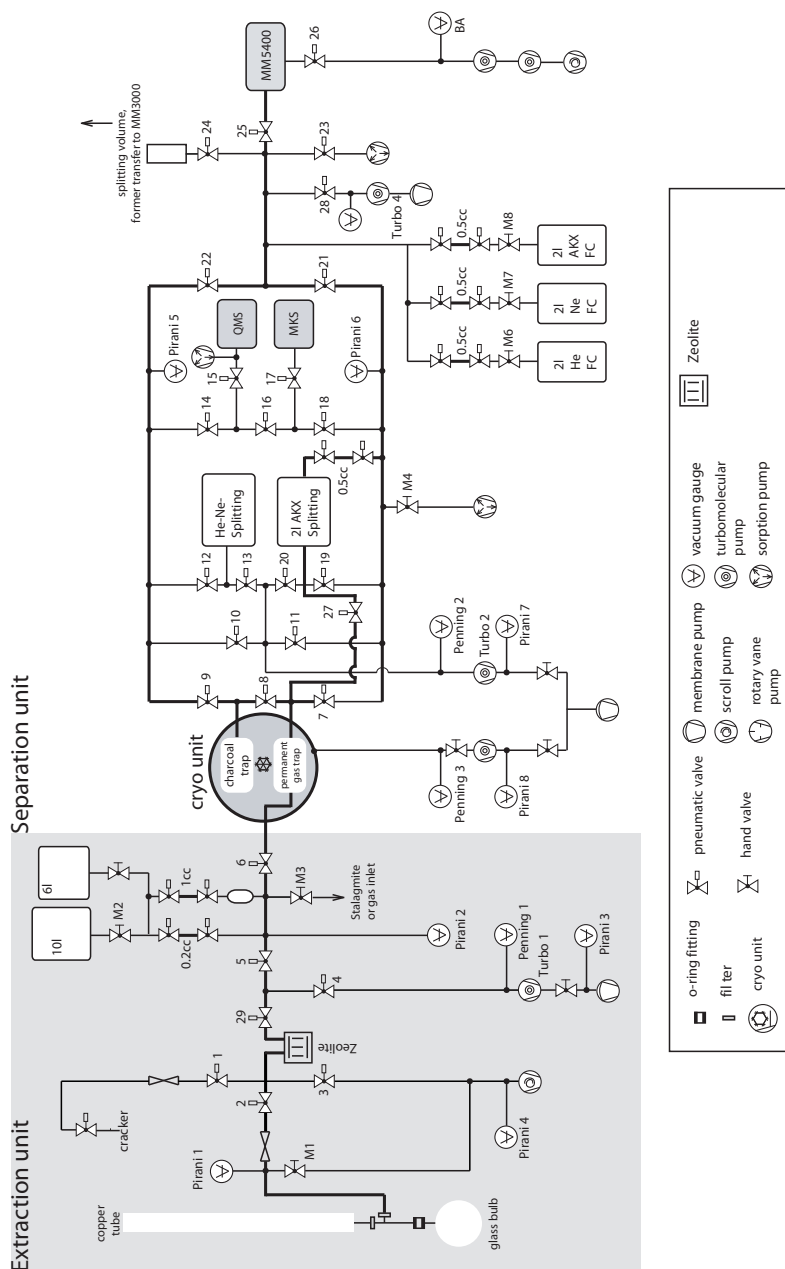


Figure B.10.: A detailed diagram of the line. The whole setup as well as the mass spectrometric unit are in detail described in Friedrich [2007].

B.2.2. Desorption curves

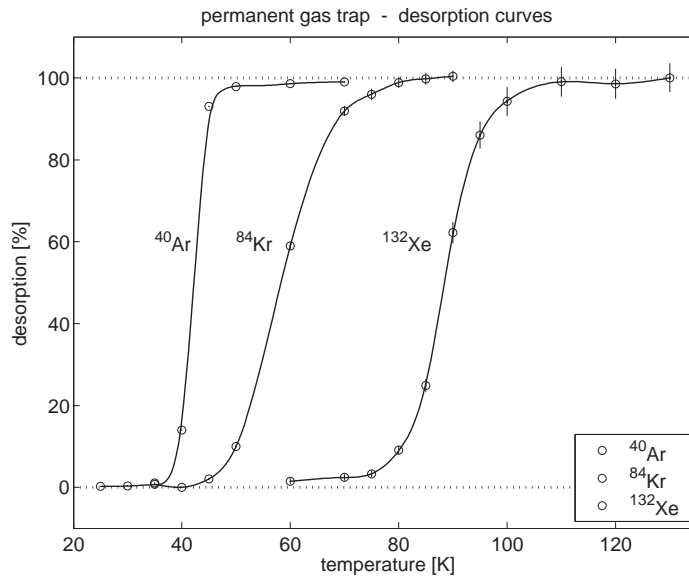


Figure B.11.: Desorption curves measured by Friedrich [2007] and Träumner [2005]. The curves show that a clear-cut separation of Kr and Ar is not possible.

When the Heidelberg noble gas mass spectrometer was established, Friedrich [2007] and Träumner [2005] measured desorption curves of Ar, Kr and Xe in the SST using 1 cc of atmospheric gas (shown in Fig. B.11). However, physical adsorption on surfaces is pressure dependent.

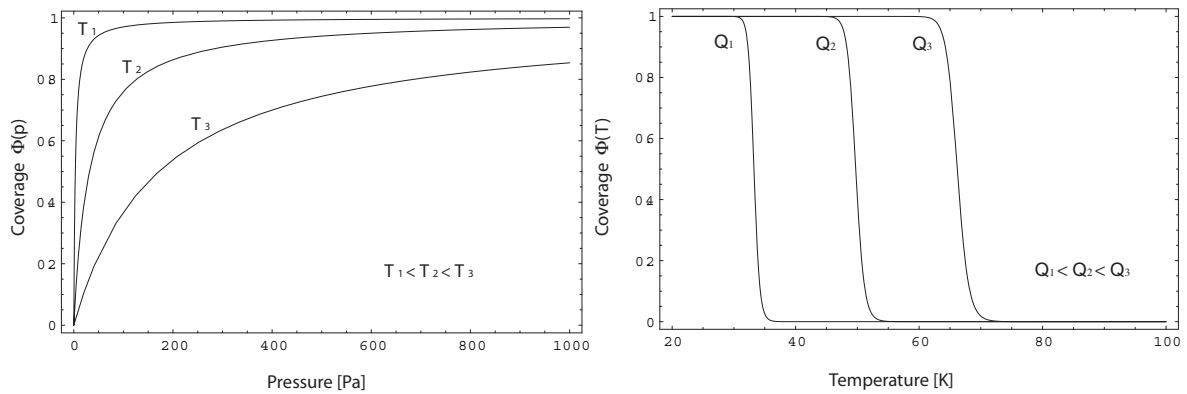


Figure B.12.: Langmuir isotherms and isobars show that higher pressure increases the coverage, lower pressure decreases it [Wutz, 2010].

A simple model of Langmuir estimating the coverage of a surface with one layer of particles produces isotherms and isobars shown in Fig. B.12. The plot shows that for constant temperatures, higher pressure increases the coverage and lower pressure decreases it. The dependency was studied for this specific setup by Wonneberger [2008] and is shown in Fig. B.13.

Therefore, the amount of gas plays a major role in the separation of gases in the cryo. For small gas amounts, a very narrow range exists for the separation of argon from krypton and xenon. Separation needed to be proved to be independent from used gas amounts. Therefore,

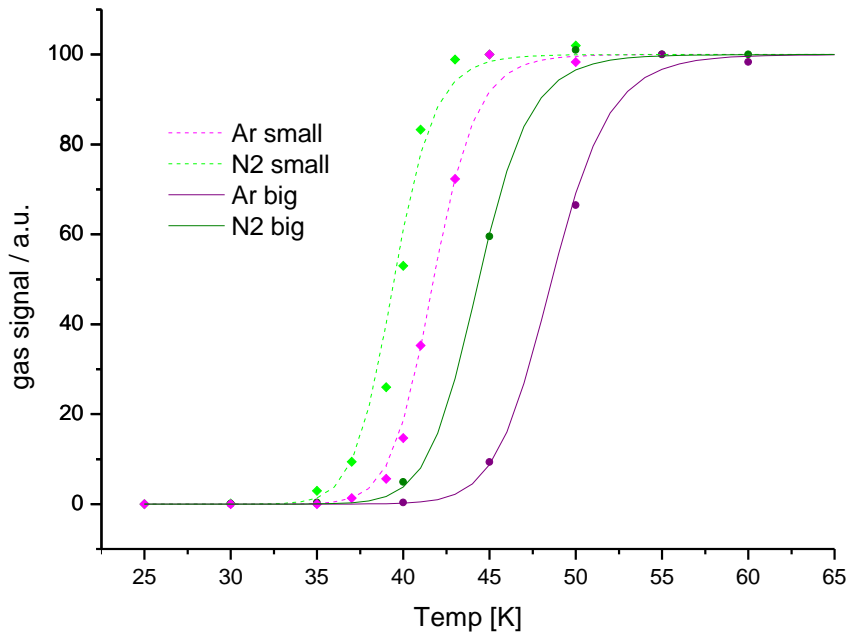
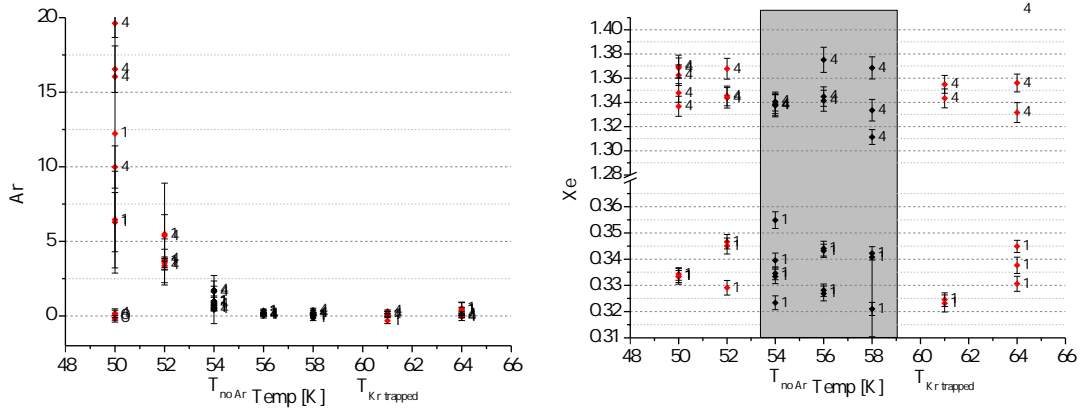


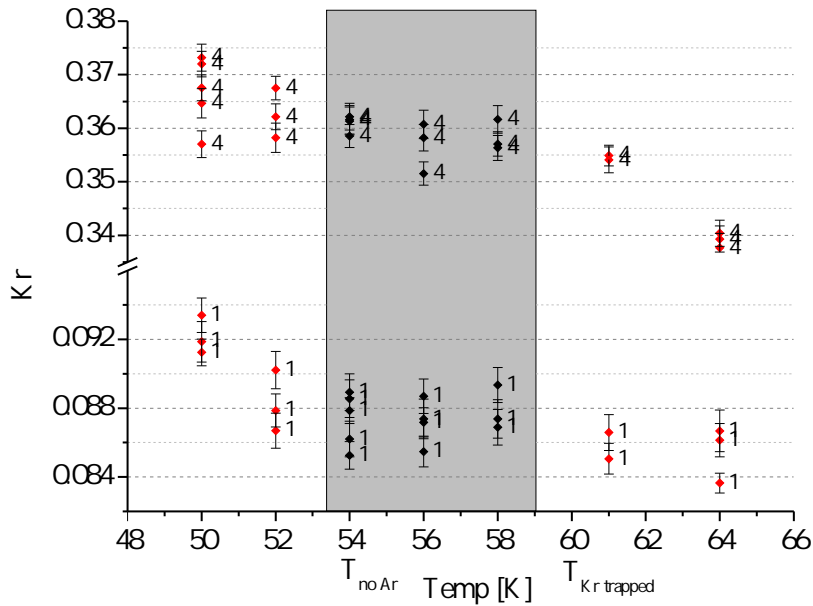
Figure B.13.: Theoretical relation of desorption [Langmuir, 1916], and observed pressure dependency of desorbed argon and nitrogen (data from Wonneberger [2008]). The desorption curves for small calibrations are situated at lower temperatures, and have a higher slope. Bigger calibrations have higher desorption temperatures and a smaller slope. Then again, the gap between Ar and N₂ is bigger.

desorption curves were measured. As methods changed over time, desorption curves were done several times. Some interesting phenomena about mass spectrometric measurements could be gathered from these experiments. The experiment was to separate Ar from Kr & Xe in the SST at a given temperature and afterwards measure the residual Ar, Kr and Xe which was trapped in the cryo. Fig. B.14 shows the residual concentrations for different tested separation temperatures. For Ar, it is noted that above a temperature of $T_{\text{no Ar}} = 54\text{K}$ no argon is left in the Kr Xe fraction, while below this temperature, a significant residual of Ar rests in the Kr/Xe fraction.

Krypton shows the most interesting behaviour. For temperatures higher than $T_{\text{no Ar}}$, the Kr signal is constant. Above a certain temperature $T_{\text{Kr trapped}} \approx 60\text{K}$, the signal deteriorates. As a matter of fact, above a certain temperature, not all Kr atoms can be trapped in the cryo anymore, and Kr begins to desorb from the surface during pumping. To ensure complete measurement of Kr, the separation temperature needs to be lower than $T_{\text{Kr trapped}}$. As different calibration sizes indicate, $T_{\text{Kr trapped}}$ is changing for different gas pressures, since higher pressures raise the threshold temperature. Between $T_{\text{no Ar}}$ and $T_{\text{Kr trapped}}$, a stable and constant plateau can be observed. The other end of the scale shows a curious aspect: Kr signal increases at temperatures below $T_{\text{no Ar}}$. An additional Kr component is therefore suspected. Due to weaker count rates, the xenon signals show scattering. Nonetheless, xenon shows a very homogeneous behaviour at all temperatures above $T_{\text{no Ar}}$, since the desorption temperature of Xe is higher than the observed temperature range. Below $T_{\text{no Ar}}$, xenon does not show significant changes.



(a) Argon shows no signals above $T_{\text{no Ar}}$. Signals below $T_{\text{no Ar}}$ increase with less temperature. (b) Xenon shows relatively constant signals for all temperatures.

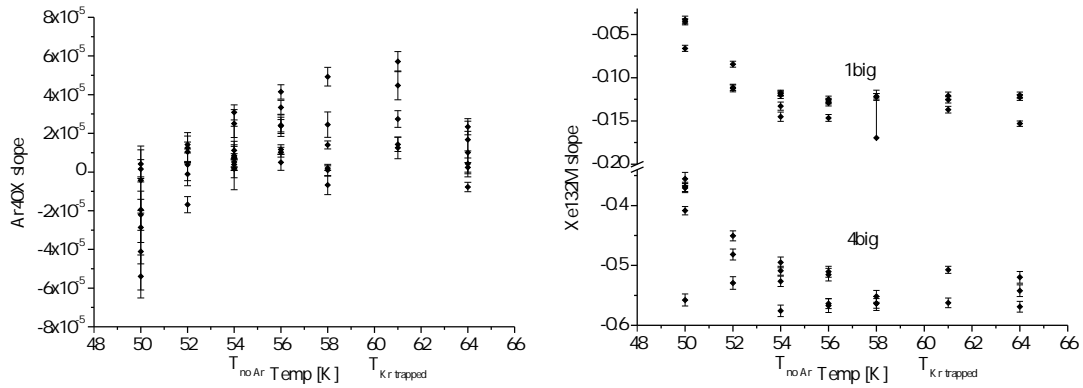


(c) Krypton shows a plateau of constant values between $T_{\text{no Ar}}$ and $T_{\text{Kr trapped}}$. The plateau is independent from sample size. At higher temperatures, Kr is lost due to pumping. Colder temperatures show an additional Kr component emitted by the mass spectrometer.

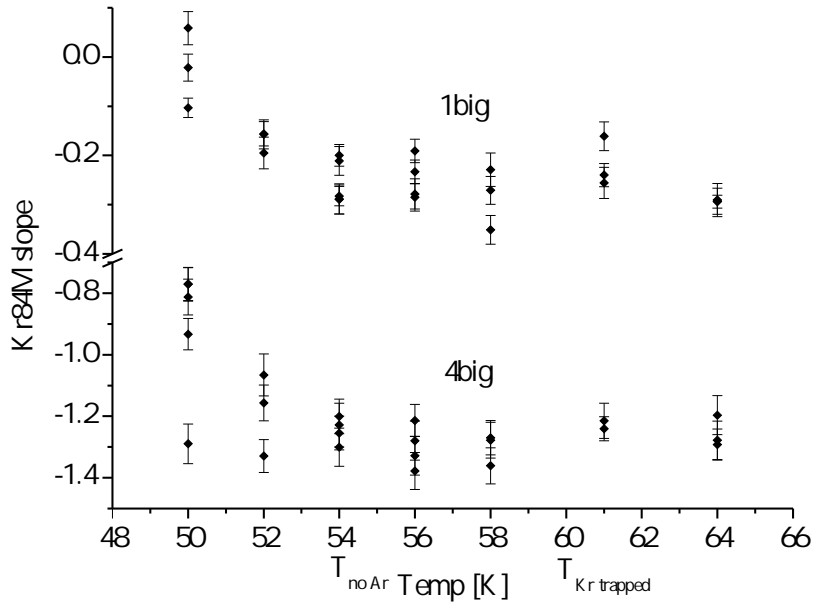
Figure B.14.: Gas concentrations in the Kr/Xe fraction for different separation temperatures.

To better understand the additional gas species, the slopes of these gases have to be observed (see Fig. B.15). For temperatures above $T_{\text{no Ar}}$, all argon which occurs in the MS originates from the machine's background. Therefore, as long as the MS is not pumped, the concentration rises over time, and the peak trends have a positive slope. For temperatures below $T_{\text{no Ar}}$, the prevailing fraction of argon consists of injected Ar gas originating from the cryo. As this gas has a higher concentration than the background, actual consumption takes place and the slope is negative.

For Kr and Xe, the slopes of the peak trends are constant for all temperatures above $T_{\text{no Ar}}$. This is a normal behaviour for gas injected into a mass spectrometer. For temperatures below $T_{\text{no Ar}}$, the value of this slope begins to increase and reaches positive values. The normal Kr or Xe background of the MS which is known from blank measurements cannot be responsible for this: Firstly, the background is completely independent from the cryo separation temperature or the injected amount of argon. Secondly, the dimension of this additional component is orders of magnitude higher than the line blank.



(a) Argon slope is negative for cold temperatures (b) Xenon slope shows the same behaviour as the indicating real gas depletion. For temperatures above $T_{\text{no Ar}}$, a positive slope results from background signals. Kr slope. Therefore, an additional component of Xe is produced as well.



(c) Krypton slope is constant and negative above $T_{\text{no Ar}}$ indicating gas depletion from measurement. Below $T_{\text{no Ar}}$, an additional component of krypton is produced in the mass spec.

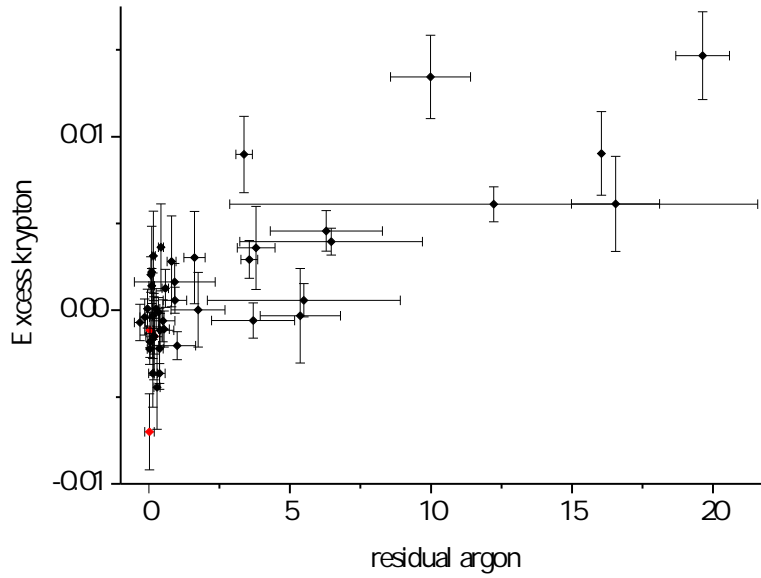
Figure B.15.: Slopes of the peak trends of noble gases in the Kr/Xe fraction for different separation temperatures.

B.2.3. “Ghost” krypton

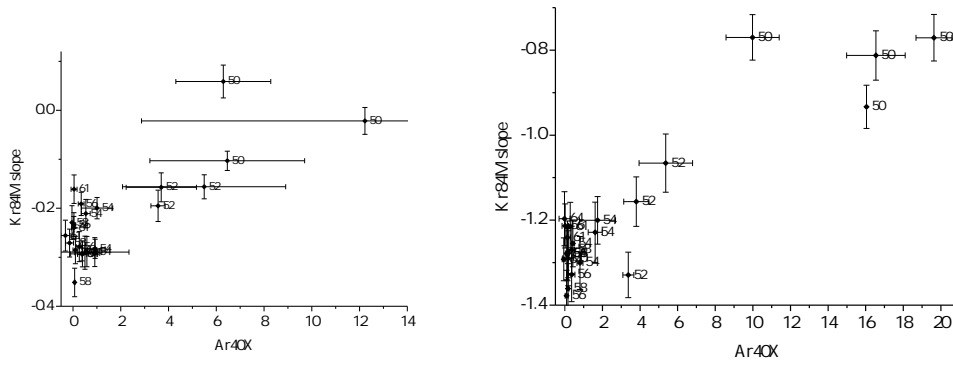
Before interpreting the additional Kr/Xe component shown in Fig. B.14, some facts have to be observed. When a peak trend of a MS measurement has a positive slope, gas is produced in the mass spectrometer. Nonetheless, gas is still consumed by the ionisation and detection process. For this reason, the additional component can grow faster than the consumption rate. Experiments done by Kluge and Marx (personal comm.) showed that the additional component can also be shown when no injected Kr or Xe is present. Some correlations can be found in Fig. B.16. Firstly, it can be seen (Fig. B.16(b)) that the slope of Kr and therefore the production rate of “ghost” krypton is correlated with the amount of residual argon. Secondly, when the plateau of Kr at temperatures between $T_{\text{no Ar}}$ and $T_{\text{Kr trapped}}$ is defined as 100 %, the excess Kr is correlated with the amount of residual argon (Fig. B.16(a)). These two correlations do not explain why the extrapolation of krypton back to the time of inlet does not nullify the additional component. Its behaviour must be more complicated. As the phenomenon depends on the amount of residual argon, it has different dimensions for noble gas ratios in air compared to ratios in water. It may therefore have caused offset problems from 2005–2008.

A preliminary interpretation of this phenomenon was done in the workgroup. The observations may result from krypton desorbed on the metallic surfaces of the mass spectrometer. Though only a small fraction of this krypton participates in the measured blank of the machine, a significant amount of this gas is mobilised when argon is in the mass spectrometer. The argon beam generated in the source hits the metallic surface and desorbs Kr. However, this assumption needs to be extensively checked by experiments. Another idea to explain the “ghost” krypton fraction may involve reactions and behaviour of the source which may have a different efficiency for krypton when high amounts of argon are present.

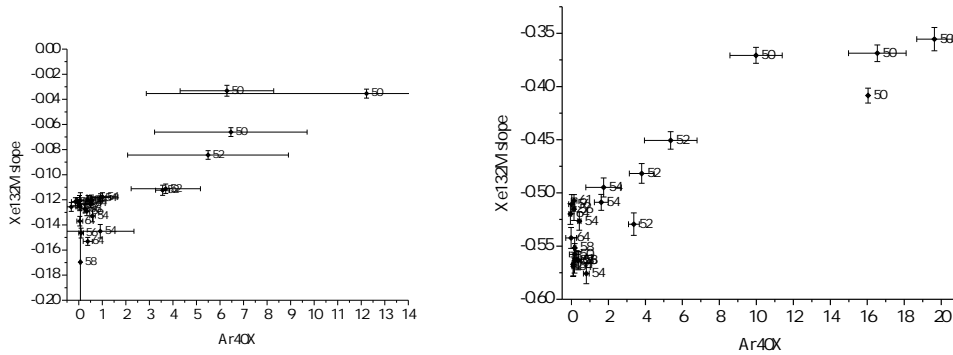
The proven origin of “ghost” krypton is still unknown and will be a topic of future studies. Independent from its origin, its presence prevents thorough measurements. Therefore, the temperature used for gas separation of samples and calibrations has to be between $T_{\text{no Ar}}$ and $T_{\text{Kr trapped}}$. This can be achieved, since the desorption curves for small and the biggest calibration sizes show no relevant difference (see Fig. B.14).



(a) Excess Kr above the expected Kr signal shows a correlation with the signal of residual Ar.



(b) Krypton slopes for both calibration sizes are displayed and show a correlation with the signal of residual argon. Numbers indicate the separation temperature.



(c) Xenon slopes for both calibration sizes are displayed and show a correlation with the signal of residual argon. Numbers indicate the separation temperature.

Figure B.16.: Excess Kr and the slope of Kr shown versus residual Ar in the Kr Xe load. Correlations can be seen in both cases.

B.2.4. Performance tests of the current method

Table B.1.: Measurement of 18 samples of air equilibrated water was done. For the particular noble gases, the offset (deviation between the measured and the theoretical value) and the measurement uncertainty for every single measurement is shown. The mean of the offset and the measurement uncertainty is calculated as well as the standard deviation of the measured offsets. The distribution of results is shown in Fig. B.17.

meas. no	He		Ne		Ar		Kr		Xe		
	offset	meas. uncert.	offset	meas. uncert.	offset	meas. uncert.	offset	meas. uncert.	offset	meas. uncert.	
AEW 2177	3.0%	0.4%	0.4%	0.5%	0.8%	0.5%	0.8%	1.9%	1.3%	1.4%	
AEW 2193	2.5%	0.4%	0.4%	0.4%	0.3%	0.4%	0.7%	2.1%	-0.6%	1.5%	
AEW 2194	2.5%	0.4%	-0.9%	0.6%	0.0%	0.5%	0.0%	1.8%	0.6%	1.4%	
AEW 2195	2.6%	0.4%	0.1%	0.5%	0.3%	0.5%	-0.8%	1.6%	0.9%	1.5%	
AEW 2198	2.5%	0.4%	1.2%	0.5%	0.4%	0.5%	-1.5%	2.4%	1.2%	1.3%	
AEW 2199	2.7%	0.4%	0.7%	0.5%	0.6%	0.5%	-0.3%	2.0%	0.8%	1.2%	
AEW 2251	2.8%	0.4%	1.3%	0.5%	0.9%	0.5%	0.5%	1.9%	2.3%	1.7%	
AEW 2252	2.8%	0.4%	0.6%	0.5%	1.0%	0.5%	-0.9%	2.0%	-1.5%	1.5%	
AEW 2257	2.7%	0.4%	0.4%	0.4%	1.2%	0.5%	-0.3%	1.7%	-0.9%	1.4%	
AEW 2258	2.6%	0.4%	0.3%	0.5%	0.6%	0.5%	-1.5%	1.9%	0.3%	1.3%	
AEW 2268	2.7%	0.4%	0.2%	0.5%	0.7%	0.5%	0.1%	2.0%	-2.3%	1.3%	
AEW 2269	2.6%	0.4%	0.5%	0.5%	0.5%	0.5%	0.0%	2.0%	0.1%	1.3%	
AEW 2283	2.8%	0.4%	0.7%	0.5%	0.8%	0.5%	-0.2%	1.8%	-0.4%	1.5%	
AEW 2287	2.8%	0.4%	1.7%	0.4%	0.2%	0.5%	-0.4%	1.8%	2.3%	1.2%	
AEW 2288	3.1%	0.4%	0.9%	0.5%	0.7%	0.5%	-0.2%	2.0%	1.9%	1.2%	
AEW 2289	2.2%	0.4%	0.9%	0.5%	0.3%	0.5%	-0.6%	1.9%	0.8%	1.4%	
AEW 2298	2.6%	0.4%	-0.1%	0.5%	0.7%	0.5%	1.2%	1.7%	0.3%	1.2%	
AEW 2299	2.7%	0.4%	0.2%	0.5%	1.2%	0.5%	0.4%	2.0%	0.8%	1.3%	
μ offset	μ meas. uncert.	μ 2.7%	μ 0.4%	μ 0.5%	μ 0.5%	μ 0.6%	μ 0.5%	μ -0.2%	μ 1.9%	μ 0.4%	μ 1.4%
σ reproducibility		σ 0.2%		σ 0.6%		σ 0.3%		σ 0.7%		σ 1.2%	

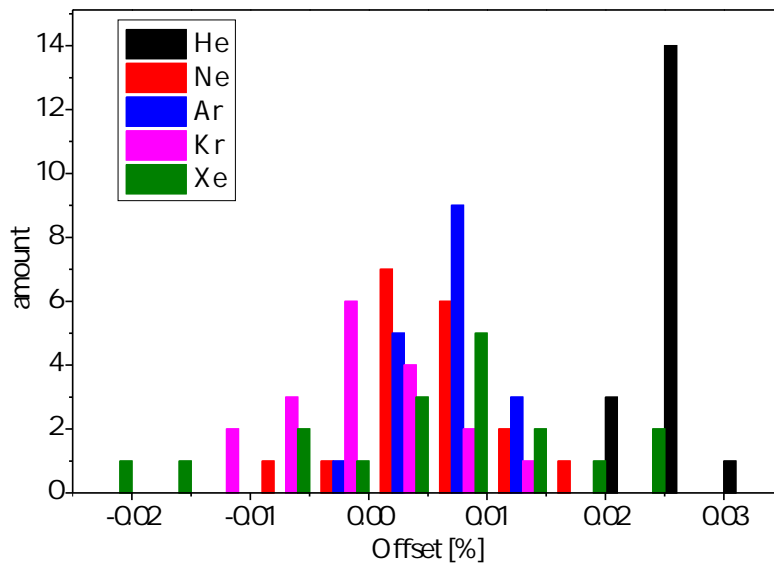


Figure B.17.: A histogram shows the measured offsets for particular noble gases. All results apart from He approximately show standard distributions. For He, a higher amount of helium gas in the laboratory standard is suspected.

B.2.5. Measurement in the mass spectrometer

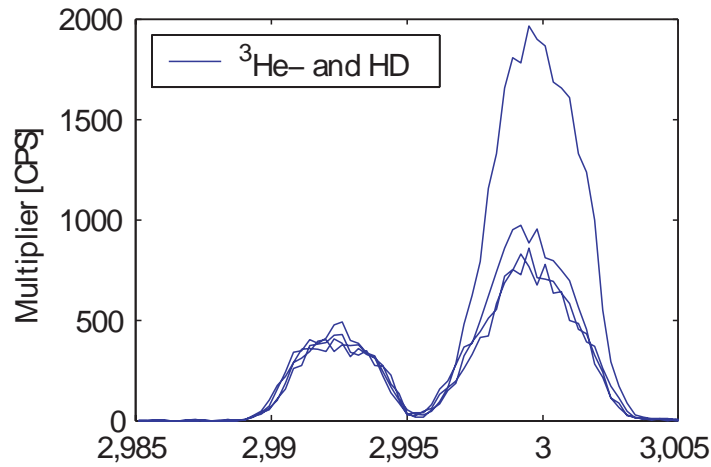


Figure B.18.: Peak shapes of ^3He and HD measured at the HD MS 5400 observed by Friedrich [2007].

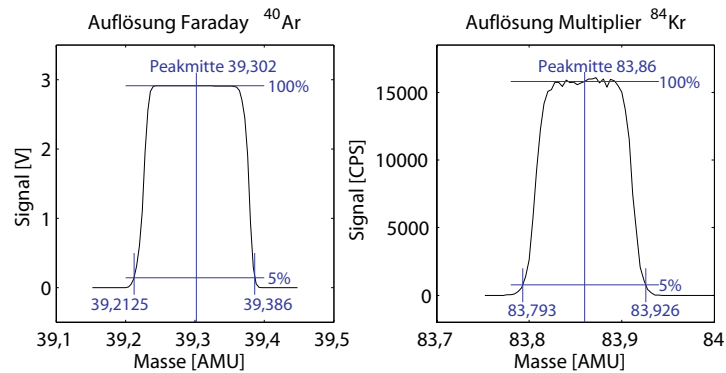


Figure B.19.: Peak resolution of a faraday detector and a multiplier detector peak observed by Friedrich [2007]. The observed resolutions are $\frac{39.302}{39.386-39.2125} = 227$ for ^{40}Ar on the faraday and $\frac{83.86}{83.926-83.793} = 631$ for ^{84}Kr on the multiplier. Obviously, the sizes cannot be compared directly.

B.2.6. Run54 evaluation

Nonlinearity corrections of the measured noble gas isotopes for run54 are shown in Fig. B.20. Fitting curves are of constant order for most isotopes and all ratios. A first order fit was used for ^3He , and a second order fit for ^4He .

B.2.7. Preparing for fitting software

For the NOBLE90 software, input data has to be a tab-separated textfile with the columns

Sample — Nr — He — err He — Ne — err Ne — Ar — err Ar — Kr — err Kr —

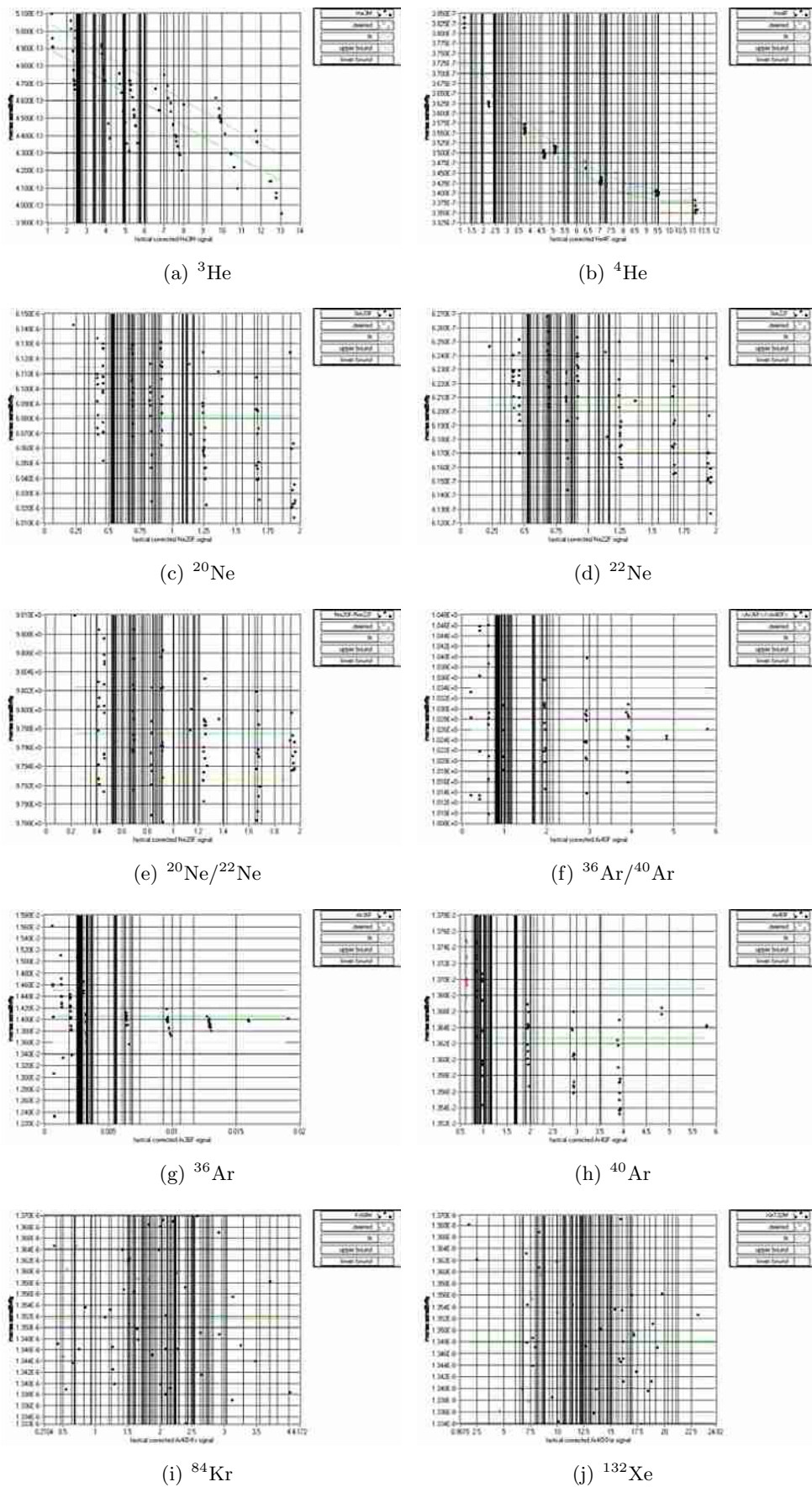


Figure B.20.: Nonlinearity fitting curves of run54.

Xe — err Xe — ^3He — err ^3He — $^3\text{He}/^4\text{He}$ — err $^3\text{He}/^4\text{He}$ — $^{20}\text{Ne}/^{22}\text{Ne}$ — err
 $^{20}\text{Ne}/^{22}\text{Ne}$ — $^{36}\text{Ar}/^{40}\text{Ar}$ — err $^{36}\text{Ar}/^{40}\text{Ar}$ — T — S — P — A — F — N — X
 — H — R

While T, S, P, A, F should be familiar by now, “N” represents a scaling factor for the values, “X” is used for tritogenic ^3He , “H” for radiogenic ^4He , and “R” for the radiogenic $^3\text{He}/^4\text{He}$ ratio.

For NOBLE2007 the columns have to be

Sample — Nr — He — err He — ^3He — err ^3He — Ne — err Ne — Ar — err Ar
 — Kr — err Kr — Xe — err Xe — A — F/B — P — S — T — A low — F/B
 low — T low — A high — F/B high — T high — useconstraint

“useconstraint” needs to be set as the value “1”.

Better input options for NOBLE2007 exist in principle and will be implemented in the future.

C. Fieldbook entries of the sampling sites

APPENDIX C. FIELDBOOK ENTRIES OF THE SAMPLING SITES

Probenahmestelle: 01

Alt. Bezeichnung: *Kampuch*

Datum & Uhrzeit: *16.02.09 15:15*

Länge | 29° 12' 20" O | Breite | 2° 02' 20" N | Höhe a.s.l. | 62 m

Parameter des Brunnen:
Tiefe | 20 m | Wasserpegel | 4,35 m | Pumprate | 100 l/min

Vor Ort gemessene Parameter:
Temperatur (°C) | *32,4°C (100)* | *30,1 (100)*
Leitfähigkeit (µS/cm) | *4,77 mS/cm (100)* | *4,23 mS/cm (100)*
O₂-Gehalt: *0,58 mg/l (100)* | *0,18 mg/l (100)*
pH-Wert: *6,25 (100)*
Alkalinität: *Wasserhärte im Calcium-Äquivalent*

Lufttemp. (°C) | *24,9°C (100)*
Luftdruck (mbar)
Wetter: *Wärm. bew. clouds, sunny*

NG	08.0	IND. 01.1	Kupferschöne
NG	08.0	IND. 01.2	Kupferschöne
NG	08.0	IND. 01.3	Kupferschöne
TC	08.0	IND. 01.1	500 ml Glas
TC	08.0	IND. 01.2	500 ml Glas
TC	08.0	IND. 01.3	500 ml Glas
CO ₂ -H	08.0	IND. 01.1	30 ml Glas
CO ₂ -H	08.0	IND. 01.2	30 ml Glas
CO ₂ -H	08.0	IND. 01.3	30 ml Glas
STa	08.0	IND. 01.1	500 ml Stahl
STa	08.0	IND. 01.2	500 ml Stahl
STa	08.0	IND. 01.3	500 ml Stahl
STb	08.0	IND. 01.1	500 ml Stahl
STb	08.0	IND. 01.2	500 ml Stahl
STb	08.0	IND. 01.3	500 ml Stahl
STc	08.0	IND. 01.1	250 ml Glas
STc	08.0	IND. 01.2	250 ml Glas
STc	08.0	IND. 01.3	250 ml Glas
Re			Datensatznummer

Bemerkungen: *Brunnen hat wenig Druck & O₂-Gehalt, Wasser warm, kein Sauerstoff, kein Chlorid, kein Nitrat, kein Ammonium, kein Phosphat, kein Kalium, kein Natrium, kein Magnesium, kein Calcium, kein Eisen, kein Mangan, kein Zink, kein Kupfer, kein Nickel, kein Cadmium, kein Blei, kein Chrom, kein Silber, kein Gold, kein Platin, kein Quecksilber, kein Arsen, kein Antimon, kein Zinn, kein Titan, kein Vanadium, kein Selen, kein Tellur, kein Bismut, kein Polonium, kein Astat, kein Francium, kein Radium, kein Actin, kein Thorium, kein Protactinium, kein Uran, kein Neptunium, kein Plutonium, kein Americium, kein Curium, kein Berkelevium, kein Californium, kein Einsteinium, kein Fermium, kein Mendelevium, kein Nobelium, kein Lawrencium, kein Rutherfordium, kein Dubnium, kein Seaborgium, kein Bohrium, kein Hassium, kein Meitnerium, kein Darmstadtium, kein Roentgenium, kein Copernicium, kein Flerovium, kein Oganesson*

Probennehmer: *T.H.H.*

Datenerfassung: *T.H.H.*

(a) sampling site 01

Probenahmestelle: 02

Alt. Bezeichnung: *Kampuch*

Datum & Uhrzeit: *17.02.09 9:00*

Länge | 29° 04' 10" O | Breite | 2° 02' 20" N | Höhe a.s.l. | 62 m

Parameter des Brunnen:
Tiefe | 20 m | Wasserpegel | 4,35 m | Pumprate | 100 l/min

Vor Ort gemessene Parameter:
Temperatur (°C) | *31,8°C (100)* | *30,0 (100)*
Leitfähigkeit (µS/cm) | *3,77 mS/cm (100)* | *3,83 (100)*
O₂-Gehalt: *0,15 mg/l (100)* | *0,63 (100)*
pH-Wert: *7,01 (100)* | *6,98 (100)*
Alkalinität: *5,5 mS/cm*

Lufttemp. (°C) | *27,2°C (100)* | *25,8°C*
Luftdruck (mbar)
Wetter: *Wärm.*

NG	08.0	IND. 02.1	Kupferschöne
NG	08.0	IND. 02.2	Kupferschöne
NG	08.0	IND. 02.3	Kupferschöne
TC	08.0	IND. 02.1	500 ml Glas
TC	08.0	IND. 02.2	500 ml Glas
TC	08.0	IND. 02.3	500 ml Glas
CO ₂ -H	08.0	IND. 02.1	30 ml Glas
CO ₂ -H	08.0	IND. 02.2	30 ml Glas
CO ₂ -H	08.0	IND. 02.3	30 ml Glas
STa	08.0	IND. 02.1	500 ml Stahl
STa	08.0	IND. 02.2	500 ml Stahl
STa	08.0	IND. 02.3	500 ml Stahl
STb	08.0	IND. 02.1	250 ml Glas
STb	08.0	IND. 02.2	250 ml Glas
STb	08.0	IND. 02.3	250 ml Glas
Re			Datensatznummer

Bemerkungen: *Wasser warm, kein Sauerstoff, kein Chlorid, kein Nitrat, kein Ammonium, kein Phosphat, kein Kalium, kein Natrium, kein Magnesium, kein Calcium, kein Eisen, kein Mangan, kein Zink, kein Kupfer, kein Nickel, kein Cadmium, kein Blei, kein Chrom, kein Silber, kein Gold, kein Platin, kein Quecksilber, kein Arsen, kein Antimon, kein Zinn, kein Titan, kein Vanadium, kein Selen, kein Tellur, kein Bismut, kein Polonium, kein Astat, kein Francium, kein Radium, kein Actin, kein Thorium, kein Protactinium, kein Uran, kein Neptunium, kein Plutonium, kein Americium, kein Curium, kein Berkelevium, kein Californium, kein Einsteinium, kein Fermium, kein Mendelevium, kein Nobelium, kein Lawrencium, kein Rutherfordium, kein Dubnium, kein Seaborgium, kein Bohrium, kein Hassium, kein Meitnerium, kein Darmstadtium, kein Roentgenium, kein Copernicium, kein Flerovium, kein Oganesson*

Probennehmer: *T.H.H.*

Datenerfassung: *T.H.H.*

(b) sampling site 02

Probenahmestelle: 03

Alt. Bezeichnung: *Gangjoral*

Datum & Uhrzeit: *17.02.09 15:30*

Länge | 27° 07' 20" O | Breite | 2° 02' 20" N | Höhe a.s.l. | 62 m

Parameter des Brunnen:
Tiefe | 20 m | Wasserpegel | 4,35 m | Pumprate | 100 l/min

Vor Ort gemessene Parameter:
Temperatur (°C) | *32,8°C (100)* | *32,6°C (100)*
Leitfähigkeit (µS/cm) | *5,57 mS/cm (100)* | *3,4 mS/cm (100)*
O₂-Gehalt: *0,36 mg/l (100)* | *0,18 (100)*
pH-Wert: *6,99 (100)* | *7,5 (100)*
Alkalinität: *6,9 mS/cm (100)*

Lufttemp. (°C) | *30°C*
Luftdruck (mbar)
Wetter: *Wärm. bew. sunny*

NG	08.0	IND. 03.1	Kupferschöne
NG	08.0	IND. 03.2 <td>Kupferschöne</td>	Kupferschöne
NG	08.0	IND. 03.3 <td>Kupferschöne</td>	Kupferschöne
TC	08.0	IND. 03.1 <td>500 ml Glas</td>	500 ml Glas
TC	08.0	IND. 03.2 <td>500 ml Glas</td>	500 ml Glas
TC	08.0	IND. 03.3 <td>500 ml Glas</td>	500 ml Glas
CO ₂ -H	08.0	IND. 03.1 <td>30 ml Glas</td>	30 ml Glas
CO ₂ -H	08.0	IND. 03.2 <td>30 ml Glas</td>	30 ml Glas
CO ₂ -H	08.0	IND. 03.3 <td>30 ml Glas</td>	30 ml Glas
STa	08.0	IND. 03.1 <td>500 ml Stahl</td>	500 ml Stahl
STa	08.0	IND. 03.2 <td>500 ml Stahl</td>	500 ml Stahl
STa	08.0	IND. 03.3 <td>500 ml Stahl</td>	500 ml Stahl
STb	08.0	IND. 03.1 <td>250 ml Glas</td>	250 ml Glas
STb	08.0	IND. 03.2 <td>250 ml Glas</td>	250 ml Glas
STb	08.0	IND. 03.3 <td>250 ml Glas</td>	250 ml Glas
Re			Datensatznummer

Bemerkungen: *Wasser warm, kein Sauerstoff, kein Chlorid, kein Nitrat, kein Ammonium, kein Phosphat, kein Kalium, kein Natrium, kein Magnesium, kein Calcium, kein Eisen, kein Mangan, kein Zink, kein Kupfer, kein Nickel, kein Cadmium, kein Blei, kein Chrom, kein Silber, kein Gold, kein Platin, kein Quecksilber, kein Arsen, kein Antimon, kein Zinn, kein Titan, kein Vanadium, kein Selen, kein Tellur, kein Bismut, kein Polonium, kein Astat, kein Francium, kein Radium, kein Actin, kein Thorium, kein Protactinium, kein Uran, kein Neptunium, kein Plutonium, kein Americium, kein Curium, kein Berkelevium, kein Californium, kein Einsteinium, kein Fermium, kein Mendelevium, kein Nobelium, kein Lawrencium, kein Rutherfordium, kein Dubnium, kein Seaborgium, kein Bohrium, kein Hassium, kein Meitnerium, kein Darmstadtium, kein Roentgenium, kein Copernicium, kein Flerovium, kein Oganesson*

Probennehmer: *T.H.H.*

Datenerfassung: *T.H.H.*

(c) sampling site 03

Probenahmestelle: 04

Alt. Bezeichnung: *Kampuch*

Datum & Uhrzeit: *18.02.09 14:15*

Länge | 29° 04' 10" O | Breite | 2° 02' 20" N | Höhe a.s.l. | 62 m

Parameter des Brunnen:
Tiefe | 20 m | Wasserpegel | 4,35 m | Pumprate | 100 l/min

Vor Ort gemessene Parameter:
Temperatur (°C) | *31,8°C (100)* | *31,2°C (100)*
Leitfähigkeit (µS/cm) | *6,7 mS/cm (100)* | *6,75 mS/cm*
O₂-Gehalt: *0,15 mg/l (100)*
pH-Wert: *7,2 (100)* | *7,0 (100)*
Alkalinität: *6,9 mS/cm (100)*

Lufttemp. (°C) | *34,2°C*
Luftdruck (mbar)
Wetter: *Wärm. bew. sunny*

NG	08.0	IND. 04.1	Kupferschöne
NG	08.0	IND. 04.2 <td>Kupferschöne</td>	Kupferschöne
NG	08.0	IND. 04.3 <td>Kupferschöne</td>	Kupferschöne
TC	08.0	IND. 04.1 <td>500 ml Glas</td>	500 ml Glas
TC	08.0	IND. 04.2 <td>500 ml Glas</td>	500 ml Glas
TC	08.0	IND. 04.3 <td>500 ml Glas</td>	500 ml Glas
CO ₂ -H	08.0	IND. 04.1 <td>30 ml Glas</td>	30 ml Glas
CO ₂ -H	08.0	IND. 04.2 <td>30 ml Glas</td>	30 ml Glas
CO ₂ -H	08.0	IND. 04.3 <td>30 ml Glas</td>	30 ml Glas
STa	08.0	IND. 04.1 <td>500 ml Stahl</td>	500 ml Stahl
STa	08.0	IND. 04.2 <td>500 ml Stahl</td>	500 ml Stahl
STa	08.0	IND. 04.3 <td>500 ml Stahl</td>	500 ml Stahl
STb	08.0	IND. 04.1 <td>250 ml Glas</td>	250 ml Glas
STb	08.0	IND. 04.2 <td>250 ml Glas</td>	250 ml Glas
STb	08.0	IND. 04.3 <td>250 ml Glas</td>	250 ml Glas
Re			Datensatznummer

Bemerkungen: *Wasser warm, kein Sauerstoff, kein Chlorid, kein Nitrat, kein Ammonium, kein Phosphat, kein Kalium, kein Natrium, kein Magnesium, kein Calcium, kein Eisen, kein Mangan, kein Zink, kein Kupfer, kein Nickel, kein Cadmium, kein Blei, kein Chrom, kein Silber, kein Gold, kein Platin, kein Quecksilber, kein Arsen, kein Antimon, kein Zinn, kein Titan, kein Vanadium, kein Selen, kein Tellur, kein Bismut, kein Polonium, kein Astat, kein Francium, kein Radium, kein Actin, kein Thorium, kein Protactinium, kein Uran, kein Neptunium, kein Plutonium, kein Americium, kein Curium, kein Berkelevium, kein Californium, kein Einsteinium, kein Fermium, kein Mendelevium, kein Nobelium, kein Lawrencium, kein Rutherfordium, kein Dubnium, kein Seaborgium, kein Bohrium, kein Hassium, kein Meitnerium, kein Darmstadtium, kein Roentgenium, kein Copernicium, kein Flerovium, kein Oganesson*

Probennehmer: *T.H.H.*

Datenerfassung: *T.H.H.*

(d) sampling site 04

Figure C.1.: Fieldbook scans 1-4

APPENDIX C. FIELDBOOK ENTRIES OF THE SAMPLING SITES

Probenahmestelle: 05

Alt. Bezeichnung: *Waldbach*

Datum & Uhrzeit: *21.02.2010*

Länge | *52° 21' 20" O* | Breite | *49° 01' 10" N* | Höhe a.s.l. | *410 m*

Parameter des Brandens:
Tiefe | *0.5 m* | Wasserpegel | *1.0 m* | Pumpe | *100 l/min*

Vor Ort gemessene Parameter:
Temperatur: (°C) *25.3°C (100)* | *35.2°C (100)*
Leitfähigkeit: (κ²⁵ μS/cm) *2,85 mS/cm (100)* | *3,26 mS/cm (100)*
O₂-Gehalt: *13.5 ml/l (100)* | *14.5 ml/l (100)*
pH-Wert: *7.14 (100)* | *7.18 (100)*
Alkalinität: *3.6 mmol/l (100)* | *3.6 mmol/l (100)*

Lufttemp.: (°C) *20.8°C (100)*
Luftdruck: (mbar)
Wetter: *Wolklos*

Genommene Proben:	INDEXTYP	Material
NO	08.0 2.22 IND 05 1	Kupferschneide
NI	08.0 2.22 IND 05 2	Kupferschneide
NO	08.0 2.22 IND 05 3	Kupferschneide
NC	08.0 2.22 IND 05 1	500 ml Glas
NC	08.0 2.22 IND 05 2	500 ml Glas
NO, HI	08.0 2.22 IND 05 1	30 ml Glas
SF ₁	08.0 2.22 IND 05 1	500 ml Stahl
SF ₂	08.0 2.22 IND 05 2	500 ml Stahl
HI	08.0 2.22 IND 05 1	250 ml Glas
***Rn		Datensatznummer

Bemerkungen: *2 Liter ausgefüllt 100 Sek nach*
SH durch Stoffe, die bei Regen aus dem
Grundwasser in den Bach fließen

Probennehmer: *T. B. B.*
Datenerfassung: *T. B. B.*

(a) sampling site 05

Probenahmestelle: 06

Alt. Bezeichnung: *Dörfels (Wasserdamm)*

Datum & Uhrzeit: *21.02.2010*

Länge | *52° 21' 20" O* | Breite | *49° 01' 10" N* | Höhe a.s.l. | *410 m*

Parameter des Brandens:
Tiefe | *0.5 m* | Wasserpegel | *1.0 m* | Pumpe | *100 l/min*

Vor Ort gemessene Parameter:
Temperatur: (°C) *20.7°C (100)* | *29.8°C (100)*
Leitfähigkeit: (κ²⁵ μS/cm) *2,36 mS/cm (100)* | *2,85 mS/cm (100)*
O₂-Gehalt: *6,62 ml/l (100)* | *6,28 ml/l (100)*
pH-Wert: *7,45 (100)* | *7,27 (100)*
Alkalinität: *3,0 mmol/l (100)*

Lufttemp.: (°C) *28,9°C (100)*
Luftdruck: (mbar)
Wetter: *Wolklos*

Genommene Proben:	INDEXTYP	Material
NO	08.0 2.22 IND 06 1	Kupferschneide
NI	08.0 2.22 IND 06 2	Kupferschneide
NO	08.0 2.22 IND 06 3	Kupferschneide
NC	08.0 2.22 IND 06 1	500 ml Glas
NC	08.0 2.22 IND 06 2	500 ml Glas
NO, HI	08.0 2.22 IND 06 1	30 ml Glas
SF ₁	08.0 2.22 IND 06 1	500 ml Stahl
SF ₂	08.0 2.22 IND 06 2	500 ml Stahl
HI	08.0 2.22 IND 06 1	250 ml Glas
***Rn		Datensatznummer

Bemerkungen: *Wasser H₂O, aber kein Dreck im Wasser durch*
den Pumpen. 2 x 100 ml ausgefüllt. Wasser
schon im Wasser, aber kein Dreck

Probennehmer: *T. B. B.*
Datenerfassung: *T. B. B.*

(b) sampling site 06

Probenahmestelle: 07

Alt. Bezeichnung: *Graf (Wasserdamm)*

Datum & Uhrzeit: *24.02.2010*

Länge | *52° 21' 20" O* | Breite | *49° 01' 10" N* | Höhe a.s.l. | *410 m*

Parameter des Brandens:
Tiefe | *0.5 m* | Wasserpegel | *1.0 m* | Pumpe | *100 l/min*

Vor Ort gemessene Parameter:
Temperatur: (°C) *22,2°C (100)* | *22,3°C (100)* | *22,5°C (100)*
Leitfähigkeit: (κ²⁵ μS/cm) *2,72 mS/cm (100)* | *2,72 mS/cm (100)*
O₂-Gehalt: *7,30 ml/l (100)* | *7,80 ml/l (100)*
pH-Wert: *7,20 (100)* | *7,21 (100)*
Alkalinität: *2,9 mmol/l (100)*

Lufttemp.: (°C) *23,6°C (100)*
Luftdruck: (mbar)
Wetter: *Schön, Sonne*

Genommene Proben:	INDEXTYP	Material
NO	08.0 2.22 IND 07 1	Kupferschneide
NI	08.0 2.22 IND 07 2	Kupferschneide
NO	08.0 2.22 IND 07 3	Kupferschneide
NC	08.0 2.22 IND 07 1	500 ml Glas
NC	08.0 2.22 IND 07 2	500 ml Glas
NO, HI	08.0 2.22 IND 07 1	30 ml Glas
SF ₁	08.0 2.22 IND 07 1	500 ml Stahl
SF ₂	08.0 2.22 IND 07 2	500 ml Stahl
HI	08.0 2.22 IND 07 1	250 ml Glas
***Rn		Datensatznummer

Bemerkungen: *Wasser aus Brunnen gefüllt, 100 Sek nach*
H₂O, aber kein Dreck im Wasser durch
den Pumpen. 2 x 100 ml ausgefüllt. Wasser
schon im Wasser, aber kein Dreck

Probennehmer: *T. B. B.*
Datenerfassung: *T. B. B.*

(c) sampling site 07

Probenahmestelle: 08

Alt. Bezeichnung: *Nafsta*

Datum & Uhrzeit: *24.02.2010*

Länge | *52° 21' 20" O* | Breite | *49° 01' 10" N* | Höhe a.s.l. | *410 m*

Parameter des Brandens:
Tiefe | *0.5 m* | Wasserpegel | *1.0 m* | Pumpe | *100 l/min*

Vor Ort gemessene Parameter:
Temperatur: (°C) *22,3°C (100)*
Leitfähigkeit: (κ²⁵ μS/cm) *3,2 mS/cm (100)*
O₂-Gehalt: *2,7 ml/l (100)*
pH-Wert: *7,6 (100)*
Alkalinität: *2,3 mmol/l (100)*

Lufttemp.: (°C) *18,4°C (100)*
Luftdruck: (mbar)
Wetter: *Wolklos, Sonne*

Genommene Proben:	INDEXTYP	Material
NO	08.0 2.22 IND 08 1	Kupferschneide
NI	08.0 2.22 IND 08 2	Kupferschneide
NO	08.0 2.22 IND 08 3	Kupferschneide
NC	08.0 2.22 IND 08 1	500 ml Glas
NC	08.0 2.22 IND 08 2	500 ml Glas
NO, HI	08.0 2.22 IND 08 1	30 ml Glas
SF ₁	08.0 2.22 IND 08 1	500 ml Stahl
SF ₂	08.0 2.22 IND 08 2	500 ml Stahl
HI	08.0 2.22 IND 08 1	250 ml Glas
***Rn		Datensatznummer

Bemerkungen: *Wasser aus Brunnen gefüllt, 100 Sek nach*
H₂O, aber kein Dreck im Wasser durch
den Pumpen. 2 x 100 ml ausgefüllt. Wasser
schon im Wasser, aber kein Dreck

Probennehmer: *T. B. B.*
Datenerfassung: *T. B. B.*

(d) sampling site 08

Figure C.2.: Fieldbook scans 5-8

APPENDIX C. FIELDBOOK ENTRIES OF THE SAMPLING SITES

Probenahmestelle: 09

Alt. Bezeichnung: Laxmpawa (Daman)

Datum & Uhrzeit: 24. 2. 08 16:00

Länge | 2° 32' 44" O | Breite | 74° 25' 45" N | Höhe a.s.l. | 98 m

Parameter des Brunnens:
 Tiefe | 100 ft | Wasserspiegel | 100 ft | Pumpe | 100 ft

Vor Ort gemessene Parameter:
 Temperatur (°C) 30,2°C
 Leitfähigkeit (µS/cm) 2,62
 O₂-Gehalt 2,73
 pH-Wert 7,19
 Alkalinität 85

Lufttemp. (°C) 30,5°C
 Luftdruck (mbar)
 Wetter: schön, warm, wind

Gemessene Proben:
 NG 08.0 1.22 IND. 09.1 Kupferschne
 NG 08.0 1.22 IND. 09.2 Kupferschne
 NG 08.0 1.22 IND. 09.3 Kupferschne
 TC 08.0 1.22 IND. 09.1 500 ml Glas
 TC 08.0 1.22 IND. 09.2 500 ml Glas
 TC 08.0 1.22 IND. 09.3 500 ml Glas
 O₂/H 08.0 1.22 IND. 09.1 30 ml Glas
 SF₆ 08.0 1.22 IND. 09.1 500 ml Stahl
 SF₆ 08.0 1.22 IND. 09.2 500 ml Stahl
 H₂ 08.0 1.22 IND. 09.1 250 ml Glas
 H₂ 08.0 1.22 IND. 09.2 250 ml Glas
 H₂ 08.0 1.22 IND. 09.3 250 ml Glas

Bemerkungen: Test von Bohrer, auch von 12 m über der Bohrer...
 Probennehmer: TSM
 Datenerfassung: TSM

(a) sampling site 09

Probenahmestelle: 10

Alt. Bezeichnung: Nava

Datum & Uhrzeit: 18. 2. 08 19:00

Länge | 2° 32' 44" O | Breite | 74° 25' 45" N | Höhe a.s.l. | 98 m

Parameter des Brunnens:
 Tiefe | 100 ft | Wasserspiegel | 100 ft | Pumpe | 100 ft

Vor Ort gemessene Parameter:
 Temperatur (°C) 25,7°C
 Leitfähigkeit (µS/cm) 4,85
 O₂-Gehalt 0,38
 pH-Wert 7,05
 Alkalinität 4,5

Lufttemp. (°C) 23,3
 Luftdruck (mbar)
 Wetter: bewölkt/wald, schöner wilder Tag

Gemessene Proben:
 NG 08.0 1.22 IND. 10.1 Kupferschne
 NG 08.0 1.22 IND. 10.2 Kupferschne
 NG 08.0 1.22 IND. 10.3 Kupferschne
 TC 08.0 1.22 IND. 10.1 500 ml Glas
 TC 08.0 1.22 IND. 10.2 500 ml Glas
 TC 08.0 1.22 IND. 10.3 500 ml Glas
 O₂/H 08.0 1.22 IND. 10.1 30 ml Glas
 SF₆ 08.0 1.22 IND. 10.1 500 ml Stahl
 SF₆ 08.0 1.22 IND. 10.2 500 ml Stahl
 H₂ 08.0 1.22 IND. 10.1 250 ml Glas
 H₂ 08.0 1.22 IND. 10.2 250 ml Glas
 H₂ 08.0 1.22 IND. 10.3 250 ml Glas

Bemerkungen: von Bohrer, an 12 m über Bohrer...
 Probennehmer: TSM
 Datenerfassung: TSM

(b) sampling site 10

Probenahmestelle: 11

Alt. Bezeichnung: Nava Manva

Datum & Uhrzeit: 27. 02. 08 05:00

Länge | 2° 32' 44" O | Breite | 74° 25' 45" N | Höhe a.s.l. | 98 m

Parameter des Brunnens:
 Tiefe | 100 ft | Wasserspiegel | 100 ft | Pumpe | 100 ft

Vor Ort gemessene Parameter:
 Temperatur (°C) 35,8°C
 Leitfähigkeit (µS/cm) 7,52
 O₂-Gehalt 0,46
 pH-Wert 6,82
 Alkalinität 5

Lufttemp. (°C) 22,5°C
 Luftdruck (mbar)
 Wetter: warm, windig, windig (aufsteigend)

Gemessene Proben:
 NG 08.0 1.22 IND. 11.1 Kupferschne
 NG 08.0 1.22 IND. 11.2 Kupferschne
 NG 08.0 1.22 IND. 11.3 Kupferschne
 TC 08.0 1.22 IND. 11.1 500 ml Glas
 TC 08.0 1.22 IND. 11.2 500 ml Glas
 TC 08.0 1.22 IND. 11.3 500 ml Glas
 O₂/H 08.0 1.22 IND. 11.1 30 ml Glas
 SF₆ 08.0 1.22 IND. 11.1 500 ml Stahl
 SF₆ 08.0 1.22 IND. 11.2 500 ml Stahl
 H₂ 08.0 1.22 IND. 11.1 250 ml Glas
 H₂ 08.0 1.22 IND. 11.2 250 ml Glas
 H₂ 08.0 1.22 IND. 11.3 250 ml Glas

Bemerkungen: Tests unter Beobachtung...
 Probennehmer: TSM
 Datenerfassung: TSM

(c) sampling site 11

Probenahmestelle: 12

Alt. Bezeichnung: Sonar

Datum & Uhrzeit: 27. 02. 08 14:00

Länge | 2° 32' 44" O | Breite | 74° 25' 45" N | Höhe a.s.l. | 98 m

Parameter des Brunnens:
 Tiefe | 100 ft | Wasserspiegel | 100 ft | Pumpe | 100 ft

Vor Ort gemessene Parameter:
 Temperatur (°C) 33,1°C
 Leitfähigkeit (µS/cm) 4,22
 O₂-Gehalt 0,37
 pH-Wert 7,32
 Alkalinität 4,4

Lufttemp. (°C) 35,8°C
 Luftdruck (mbar)
 Wetter: warm, windig

Gemessene Proben:
 NG 08.0 1.22 IND. 12.1 Kupferschne
 NG 08.0 1.22 IND. 12.2 Kupferschne
 NG 08.0 1.22 IND. 12.3 Kupferschne
 TC 08.0 1.22 IND. 12.1 500 ml Glas
 TC 08.0 1.22 IND. 12.2 500 ml Glas
 TC 08.0 1.22 IND. 12.3 500 ml Glas
 O₂/H 08.0 1.22 IND. 12.1 30 ml Glas
 SF₆ 08.0 1.22 IND. 12.1 500 ml Stahl
 SF₆ 08.0 1.22 IND. 12.2 500 ml Stahl
 H₂ 08.0 1.22 IND. 12.1 250 ml Glas
 H₂ 08.0 1.22 IND. 12.2 250 ml Glas
 H₂ 08.0 1.22 IND. 12.3 250 ml Glas

Bemerkungen: Zur Luftmessung...
 Probennehmer: TSM
 Datenerfassung: TSM

(d) sampling site 12

Figure C.3.: Fieldbook scans 9-12

APPENDIX C. FIELDBOOK ENTRIES OF THE SAMPLING SITES

Probenahmestelle: 13

Alt. Bezeichnung: *Zinnwala*

Datum & Uhrzeit: *27.2.2008 17:00-17:15*

Länge | 22° 21' 30" O | Breite | 55° 45' 45" N | Höhe a.s.l. | 10 m

Parameter des Brunnen:
 Tiefe | 112.4 | Wasserpegel | *100-101.1* | Pumprate | *3000/1000*

Vor Ort gemessene Parameter:
 Temperatur (°C) | *28.2* | Leitfähigkeit (µS/cm) | *1.58* | O₂-Gehalt | *0.13* | pH-Wert | *7.62* | Alkalinität | *35*

Lufttemp. (°C) | *29.02*
 Luftdruck (mbar)
 Wetter: *Wolkenlos, Sonne, klar*

Genommene Proben:	INDEXTYP	Material
NO ₃	08.0 - 1.3	IND 1.3.1 Kupferschiene
NO ₂	08.0 - 1.3	IND 1.3.2 Kupferschiene
NO ₃	08.0 - 1.3	IND 1.3.3 Kupferschiene
PC	08.0 - 1.3	IND 1.3.1 500 ml Glas
PC	08.0 - 1.3	IND 1.3.2 500 ml Glas
O ₂ /H	08.0 - 1.3	IND 1.3.1 30 ml Glas
SF ₆	08.0 - 1.3	IND 1.3.1 500 ml Stahl
SF ₆	08.0 - 1.3	IND 1.3.2 500 ml Stahl
H	08.0 - 1.3	IND 1.3.1 250 ml Glas
Ro		Datensatznummer

Bemerkungen: *Plastikflaschen, keine Wasserprobe durch Verunreinigung der Schichtkappe (aufbewahren)*

Probennehmer: *Marin & Tim*
 Datenerfassung: *Marin & Tim*

(a) sampling site 13

Probenahmestelle: 14

Alt. Bezeichnung: *Kumbhasan*

Datum & Uhrzeit: *28.2.08 18:00*

Länge | 22° 12' 37" O | Breite | 24° 09' 18" N | Höhe a.s.l. | 122 m

Parameter des Brunnen:
 Tiefe | 215.1 | Wasserpegel | *200-205.1* | Pumprate | *1000/1000*

Vor Ort gemessene Parameter:
 Temperatur (°C) | *32.5* | Leitfähigkeit (µS/cm) | *1.99* | O₂-Gehalt | *2.9* | pH-Wert | *6.73* | Alkalinität | *6.2*

Lufttemp. (°C) | *23.7*
 Luftdruck (mbar)
 Wetter: *sehr Dunstig, klar*

Genommene Proben:	INDEXTYP	Material
NO ₃	08.0 - 1.4	IND 1.4.1 Kupferschiene
NO ₂	08.0 - 1.4	IND 1.4.2 Kupferschiene
NO ₃	08.0 - 1.4	IND 1.4.3 Kupferschiene
PC	08.0 - 1.4	IND 1.4.1 500 ml Glas
PC	08.0 - 1.4	IND 1.4.2 500 ml Glas
O ₂ /H	08.0 - 1.4	IND 1.4.1 30 ml Glas
SF ₆	08.0 - 1.4	IND 1.4.1 500 ml Stahl
SF ₆	08.0 - 1.4	IND 1.4.2 500 ml Stahl
H	08.0 - 1.4	IND 1.4.2 250 ml Glas
Ro		Datensatznummer

Bemerkungen: *bei ca. 10m unterirdischer Wasserschicht, O₂ Wert ist durch Brunnenluft sehr gut, keine Wasserprobe durch Verunreinigung der Schichtkappe (aufbewahren)*

Probennehmer: *Tim*
 Datenerfassung: *Tim*

(b) sampling site 14

Probenahmestelle: 15

Alt. Bezeichnung: *Akesan*

Datum & Uhrzeit: *28.2.08 18:45*

Länge | 22° 21' 30" O | Breite | 24° 42' 25" N | Höhe a.s.l. | 200 m

Parameter des Brunnen:
 Tiefe | 100.4 | Wasserpegel | *500-505.4* | Pumprate | *1000/1000*

Vor Ort gemessene Parameter:
 Temperatur (°C) | *28.7* | Leitfähigkeit (µS/cm) | *0.85* | O₂-Gehalt | *8.6* | pH-Wert | *6.82* | Alkalinität | *9.1*

Lufttemp. (°C)
 Luftdruck (mbar)
 Wetter:

Genommene Proben:	INDEXTYP	Material
NO ₃	08.0 - 1.5	IND 1.5.1 Kupferschiene
NO ₂	08.0 - 1.5	IND 1.5.2 Kupferschiene
NO ₃	08.0 - 1.5	IND 1.5.3 Kupferschiene
PC	08.0 - 1.5	IND 1.5.1 500 ml Glas
PC	08.0 - 1.5	IND 1.5.2 500 ml Glas
O ₂ /H	08.0 - 1.5	IND 1.5.1 30 ml Glas
SF ₆	08.0 - 1.5	IND 1.5.1 500 ml Stahl
SF ₆	08.0 - 1.5	IND 1.5.2 500 ml Stahl
H	08.0 - 1.5	IND 1.5.1 250 ml Glas
Ro		Datensatznummer

Bemerkungen: *bei ca. 10m unterirdischer Wasserschicht, O₂ Wert ist durch Brunnenluft sehr gut, keine Wasserprobe durch Verunreinigung der Schichtkappe (aufbewahren)*

Probennehmer: *Marin & Tim*
 Datenerfassung: *Marin & Tim*

(c) sampling site 15

Probenahmestelle: 16

Alt. Bezeichnung: *Vadu*

Datum & Uhrzeit: *28.2.08 18:25*

Länge | 22° 09' 22" O | Breite | 23° 53' 25" N | Höhe a.s.l. | 100 m

Parameter des Brunnen:
 Tiefe | 100.4 | Wasserpegel | *500-505.4* | Pumprate | *1000/1000*

Vor Ort gemessene Parameter:
 Temperatur (°C) | *38.0* | Leitfähigkeit (µS/cm) | *4.62* | O₂-Gehalt | *0.75* | pH-Wert | *6.74* | Alkalinität | *9.1*

Lufttemp. (°C) | *23.7*
 Luftdruck (mbar)
 Wetter: *sehr feucht, warm, klar*

Genommene Proben:	INDEXTYP	Material
NO ₃	08.0 - 1.6	IND 1.6.1 Kupferschiene
NO ₂	08.0 - 1.6	IND 1.6.2 Kupferschiene
NO ₃	08.0 - 1.6	IND 1.6.3 Kupferschiene
PC	08.0 - 1.6	IND 1.6.1 500 ml Glas
PC	08.0 - 1.6	IND 1.6.2 500 ml Glas
O ₂ /H	08.0 - 1.6	IND 1.6.1 30 ml Glas
SF ₆	08.0 - 1.6	IND 1.6.1 500 ml Stahl
SF ₆	08.0 - 1.6	IND 1.6.2 500 ml Stahl
H	08.0 - 1.6	IND 1.6.1 250 ml Glas
Ro		Datensatznummer

Bemerkungen: *bei ca. 10m unterirdischer Wasserschicht, O₂ Wert ist durch Brunnenluft sehr gut, keine Wasserprobe durch Verunreinigung der Schichtkappe (aufbewahren)*

Probennehmer: *Marin & Tim*
 Datenerfassung: *Marin & Tim*

(d) sampling site 16

Figure C.4.: Fieldbook scans 13-16

APPENDIX C. FIELDBOOK ENTRIES OF THE SAMPLING SITES

Probenahmestelle: 17

Alt. Bezeichnung: *Dumwalden*

Datum & Uhrzeit: *29.01.08 12:00 - 13:30*

Länge | 2° 17' 10" O | Breite | 47° 11' 00" N | Höhe a.s.l. | 43 m

Parameter des Brunnen:
 Tiefe | 2,2 m | Wasserpegel | 1,0 m | Pumprate | 10 l/min

Vor Ort gemessene Parameter:
 Temperatur (°C) | 32,6°C (12:00) | 33,0°C (13:30)
 Leitfähigkeit (µS/cm) | 4,32 $\frac{\mu S}{cm}$ (12:00) | 5,3 $\frac{\mu S}{cm}$ (13:30)
 O₂-Gehalt | 0,75 $\frac{mg}{l}$ (12:00)
 pH-Wert | 5,96 (12:00) | 7,1 (13:30)
 Alkalinität | 7,3 mmol/l (13:30)

Lufttemp. (°C) | 34,9
 Luftdruck (mbar)
 Wetter: *Hitz, bew. bis*

Genommene Proben:			
NG	08.0 2.03 IND 17.1	Kupferschiene	
NG	08.0 2.03 IND 17.1	Kupferschiene	
NG	08.0 2.03 IND 17.1	Kupferschiene	
TC	08.0 2.03 IND 17.1	500 ml Glas	
TC	08.0 2.03 IND 17.1	500 ml Glas	
TC, H	08.0 2.03 IND 17.1	30 ml Glas	
SF ₁	08.0 2.03 IND 17.1	500 ml Stahl	2,8
SF ₂	08.0 2.03 IND 17.1	500 ml Stahl	2,4
H	08.0 2.03 IND 17.1	250 ml Glas	
Rn		Dosisratenzähler	

Bemerkungen: *Niedrige Leitfähigkeit durch hohen Gehalt an gelösten organischen Stoffen (Dünger) und hohen Gehalt an gelösten organischen Stoffen.*

Probennehmer: *M. H. & T. M.*

Datenerfassung: *M. H. & T. M.*

(a) sampling site 17

Probenahmestelle: 18

Alt. Bezeichnung: *Sengsdorf*

Datum & Uhrzeit: *30.08 12:00 - 13:30*

Länge | 2° 25' 00" O | Breite | 47° 07' 00" N | Höhe a.s.l. | 129 m

Parameter des Brunnen:
 Tiefe | 2,2 m | Wasserpegel | 1,0 m | Pumprate | 10 l/min

Vor Ort gemessene Parameter:
 Temperatur (°C) | 29,6°C (12:00) | 31,2°C (12:30) | 29,8°C (13:00)
 Leitfähigkeit (µS/cm) | 0,912 $\frac{\mu S}{cm}$ (12:00) | 0,944 $\frac{\mu S}{cm}$ (12:30) | 1,13 (13:00)
 O₂-Gehalt | 8,30 $\frac{mg}{l}$ (12:00) | 8,77 $\frac{mg}{l}$ (13:00)
 pH-Wert | 7,07 (12:00) | 6,87 (12:30) | 7,0 (13:00)
 Alkalinität | 6,5 mmol/l

Lufttemp. (°C) | 30,9°C (12:00)
 Luftdruck (mbar)
 Wetter: *hit. bis, bew.*

Genommene Proben:			
NG	08.0 2.03 IND 18.1	Kupferschiene	
NG	08.0 2.03 IND 18.2	Kupferschiene	
NG	08.0 2.03 IND 18.3	Kupferschiene	
TC	08.0 2.03 IND 18.1	500 ml Glas	
TC	08.0 2.03 IND 18.2	500 ml Glas	
TC, H	08.0 2.03 IND 18.1	30 ml Glas	
SF ₁	08.0 2.03 IND 18.1	500 ml Stahl	2,7
SF ₂	08.0 2.03 IND 18.2	500 ml Stahl	2,7
H	08.0 2.03 IND 18.1	250 ml Glas	
Rn		Dosisratenzähler	

Bemerkungen: *O₂ Gehalt stark (7-8) auf Luftniveau, weil Antriebsleistung im Eigenantriebsfeld von Grundbrunnen nicht durch Strom.*

Probennehmer: *M. H. & T. M.*

Datenerfassung: *M. H. & T. M.*

(b) sampling site 18

Probenahmestelle: 19

Alt. Bezeichnung: *Chudwin*

Datum & Uhrzeit: *01.01.08 10:00 - 14:00*

Länge | 2° 15' 20" O | Breite | 47° 11' 00" N | Höhe a.s.l. | 43 m

Parameter des Brunnen:
 Tiefe | 2,2 m | Wasserpegel | 1,0 m | Pumprate | 10 l/min

Vor Ort gemessene Parameter:
 Temperatur (°C) | 30,2°C (10:00) | 30,2°C (10:20) | 31,1°C (14:00)
 Leitfähigkeit (µS/cm) | 2,80 $\frac{\mu S}{cm}$ (10:00) | 0,956 $\frac{\mu S}{cm}$ (10:20) | 1,13 (14:00)
 O₂-Gehalt | 8,60 $\frac{mg}{l}$ (10:00) | 9,50 $\frac{mg}{l}$ (10:20)
 pH-Wert | 7,30 (10:00) | 7,02 (10:20) | 7,0 (14:00)
 Alkalinität | 5,9 mmol/l

Lufttemp. (°C) | 33,7°C
 Luftdruck (mbar)
 Wetter: *hit. bis, bew.*

Genommene Proben:			
NG	08.0 2.03 IND 19.1	Kupferschiene	
NG	08.0 2.03 IND 19.2	Kupferschiene	
NG	08.0 2.03 IND 19.3	Kupferschiene	
TC	08.0 2.03 IND 19.1	500 ml Glas	
TC	08.0 2.03 IND 19.2	500 ml Glas	
TC, H	08.0 2.03 IND 19.1	30 ml Glas	
SF ₁	08.0 2.03 IND 19.1	500 ml Stahl	2,8
SF ₂	08.0 2.03 IND 19.2	500 ml Stahl	2,7
H	08.0 2.03 IND 19.1	250 ml Glas	
Rn		Dosisratenzähler	

Bemerkungen: *Guter Druck beim Bohren.*

Probennehmer: *M. H. & T. M.*

Datenerfassung: *M. H. & T. M.*

(c) sampling site 19

Probenahmestelle: 20

Alt. Bezeichnung: *Sujaniplatz*

Datum & Uhrzeit: *30.08 17:00 - 17:30*

Länge | 2° 26' 10" O | Breite | 47° 07' 00" N | Höhe a.s.l. | 129 m

Parameter des Brunnen:
 Tiefe | 2,2 m | Wasserpegel | 1,0 m | Pumprate | 10 l/min

Vor Ort gemessene Parameter:
 Temperatur (°C) | 35,3°C (17:00) | 36,5°C (17:30)
 Leitfähigkeit (µS/cm) | 2,80 $\frac{\mu S}{cm}$ (17:00) | 2,91 $\frac{\mu S}{cm}$ (17:30)
 O₂-Gehalt | 1,25 $\frac{mg}{l}$ (17:00) | 1,21 $\frac{mg}{l}$ (17:30)
 pH-Wert | 7,22 (17:00) | 7,13 (17:30)
 Alkalinität | 6,9 mmol/l

Lufttemp. (°C) | 30,9°C → 34,2°C
 Luftdruck (mbar)
 Wetter: *hit. bis, bew.*

Genommene Proben:			
NG	08.0 2.03 IND 20.1	Kupferschiene	
NG	08.0 2.03 IND 20.2	Kupferschiene	
NG	08.0 2.03 IND 20.3	Kupferschiene	
TC	08.0 2.03 IND 20.1	500 ml Glas	
TC	08.0 2.03 IND 20.2	500 ml Glas	
TC, H	08.0 2.03 IND 20.1	30 ml Glas	
SF ₁	08.0 2.03 IND 20.1	500 ml Stahl	2,7
SF ₂	08.0 2.03 IND 20.2	500 ml Stahl	2,7
H	08.0 2.03 IND 20.1	250 ml Glas	
Rn		Dosisratenzähler	

Bemerkungen: *am Ende des F7-Rohrs, Luftdrucke höher als beim Bohren.*

Probennehmer: *M. H. & T. M.*

Datenerfassung: *M. H. & T. M.*

(d) sampling site 20

Figure C.5.: Fieldbook scans 17-20

APPENDIX C. FIELDBOOK ENTRIES OF THE SAMPLING SITES

Probenahmestelle: 21

Alt. Bezeichnung: Güavada

Datum & Uhrzeit: 27.1.09 11⁴⁷ - 13⁰⁰

Länge | 12° 07' 22" O | Breite | 13° 31' 41" N | Höhe absl. | 147 m

Parameter des Brunnens:
 Tiefe | 3,5 m | Wasserpegel | 100% | Pumpe | 100%

Vor Ort gemessene Parameter:
 Temperatur (°C) | 27,4 (1200) | 27,2 (12:35) | 26,9 (12:45) | 57,0 E 12:00
 Leitfähigkeit (µS/cm) | 1788 (12:00) | 1800 (12:10) | 1790 (12:20)
 O₂-Gehalt: 0,22 (12:00) | 0,59 (12:35)
 pH-Wert: 7,07 (12:00) | 7,07 (12:35)
 Alkalinität: 4,1 mmol/L (12:00)

Lufttemp: (°C) 29,3°C
 Luftdruck: (mbar)
 Wetter: Höf. klar

Gemessene Proben:

NG	08.0	IND 21.1	Kupferschöne
NG	08.0	IND 21.2	Kupferschöne
NG	08.0	IND 21.3	Kupferschöne
TC	08.0	IND 21.1	500 ml Glas
TC	08.0	IND 21.2	500 ml Glas
TC	08.0	IND 21.3	500 ml Glas
Sf ₁	08.0	IND 21.1	500 ml Stahl
Sf ₂	08.0	IND 21.2	500 ml Stahl
Sf ₃	08.0	IND 21.3	500 ml Stahl
H	08.0	IND 21.1	250 ml Glas
Rn	08.0	IND 21.1	Datensatznummer

Bemerkungen: Gar keine Böden, keine Austüte, UT Druck nach Auslösch (12:49) geod. ab.

Probennummer: 121

Datenerfassung:

(a) sampling site 21

Probenahmestelle: 22

Alt. Bezeichnung: Holpl. (T) MEDUSA (Tibaki)

Datum & Uhrzeit: 27.1. 16²⁰ - 15⁰⁰

Länge | 22° 31' 22" O | Breite | 13° 32' 17" N | Höhe absl. | 112 m

Parameter des Brunnens:
 Tiefe | 7,5 m | Wasserpegel | 100% | Pumpe | 100%

Vor Ort gemessene Parameter:
 Temperatur (°C) | 23,32 (14:40) | 23,8 (15:00)
 Leitfähigkeit (µS/cm) | 1300 | 0,53 (14:40) | 1300 (15:00)
 O₂-Gehalt: 3,9632 (14:40) | 3,98, 3,98 (15:00)
 pH-Wert: 6,39 (14:40) | 6,92 (15:00)
 Alkalinität: 7,0 mmol/L | TDS 900 µg/l

Lufttemp: (°C) 26,3°C
 Luftdruck: (mbar)
 Wetter: 100% bew. wolky, sample in shade

Gemessene Proben:

NG	08.0	IND 22.1	Kupferschöne
NG	08.0	IND 22.2	Kupferschöne
NG	08.0	IND 22.3	Kupferschöne
TC	08.0	IND 22.1	500 ml Glas
TC	08.0	IND 22.2	500 ml Glas
TC	08.0	IND 22.3	500 ml Glas
Sf ₁	08.0	IND 22.1	500 ml Stahl
Sf ₂	08.0	IND 22.2	500 ml Stahl
Sf ₃	08.0	IND 22.3	500 ml Stahl
H	08.0	IND 22.1	250 ml Glas
Rn	08.0	IND 22.1	Datensatznummer

Bemerkungen: Druck auf, kein (T) Boden (15:00)

Probennummer:

Datenerfassung:

(b) sampling site 22

Probenahmestelle: 23

Alt. Bezeichnung: Ubl. (UT)

Datum & Uhrzeit: 28.1.09 11⁰⁰ - 12⁰⁰

Länge | 12° 07' 22" O | Breite | 13° 31' 41" N | Höhe absl. | 147 m

Parameter des Brunnens:
 Tiefe | 3,5 m | Wasserpegel | 100% | Pumpe | 100%

Vor Ort gemessene Parameter:
 Temperatur (°C) | 29,5 (12:00) | 30,7 (12:00) | 30,6 (12:00)
 Leitfähigkeit (µS/cm) | 813 (12:00) | 812 (12:00) | 806 (12:00)
 O₂-Gehalt: 4,66 (12:00) | 4,69 (12:00) | 4,39 (12:00)
 pH-Wert: 7,07 (12:00) | 7,09 (12:00) | 7,06 (12:00)
 Alkalinität: 5,5 mmol/L (12:00)

Lufttemp: (°C) 29,2
 Luftdruck: (mbar)
 Wetter: Dunkel bew. sample in shade

Gemessene Proben:

NG	08.0	IND 23.1	Kupferschöne
NG	08.0	IND 23.2	Kupferschöne
NG	08.0	IND 23.3	Kupferschöne
TC	08.0	IND 23.1	500 ml Glas
TC	08.0	IND 23.2	500 ml Glas
TC	08.0	IND 23.3	500 ml Glas
Sf ₁	08.0	IND 23.1	500 ml Stahl
Sf ₂	08.0	IND 23.2	500 ml Stahl
Sf ₃	08.0	IND 23.3	500 ml Stahl
H	08.0	IND 23.1	250 ml Glas
Rn	08.0	IND 23.1	Datensatznummer

Bemerkungen: im 1. und 2. Brunnen, im 1. soll kein Wasser rauskommen. Druck wurde abgelesen keine Druck gibt, keine Bohrer

Probennummer:

Datenerfassung:

(c) sampling site 23

Probenahmestelle: 24

Alt. Bezeichnung: Santos SANTOL (Gehaus)

Datum & Uhrzeit: 28.1.09 16⁰⁰ | 18⁰⁰ (18:00)

Länge | 17° 51' 21" O | Breite | 13° 31' 21" N | Höhe absl. | 107 m

Parameter des Brunnens:
 Tiefe | 14,5 m | Wasserpegel | 100% | Pumpe | 100%

Vor Ort gemessene Parameter:
 Temperatur (°C) | 29,7 (16:00) | 31,2 (16:20)
 Leitfähigkeit (µS/cm) | 1209 (16:00) | 1217 (16:20)
 O₂-Gehalt: 5,92 (16:00) | 6,00 (16:20) | 3,60 (16:20) | 1,8 (16:30)
 pH-Wert: 7,07 (16:00) | 7,20 (16:20)
 Alkalinität: 11,6 mmol/L (16:00)

Lufttemp: (°C)
 Luftdruck: (mbar)
 Wetter: Dunkel bew. sample in shade

Gemessene Proben:

NG	08.0	IND 24.1	Kupferschöne
NG	08.0	IND 24.2	Kupferschöne
NG	08.0	IND 24.3	Kupferschöne
TC	08.0	IND 24.1	500 ml Glas
TC	08.0	IND 24.2	500 ml Glas
TC	08.0	IND 24.3	500 ml Glas
Sf ₁	08.0	IND 24.1	500 ml Stahl
Sf ₂	08.0	IND 24.2	500 ml Stahl
Sf ₃	08.0	IND 24.3	500 ml Stahl
H	08.0	IND 24.1	250 ml Glas
Rn	08.0	IND 24.1	Datensatznummer

Bemerkungen: 16:50 Stromausfall bis ca. 17:00. 2. Seite v. 2. H. Probe gelöst. 18:00 Abbruch, umgeben mit Gasampel. O₂-Sättigung wurde abgelesen. (Schauen auf O₂)

Probennummer:

Datenerfassung:

(d) sampling site 24

Figure C.6.: Fieldbook scans 21-24

APPENDIX C. FIELDBOOK ENTRIES OF THE SAMPLING SITES

Probenahmestelle: 25

Alt. Bezeichnung: *Chitara*

Datum & Uhrzeit: *29.1.08 1^h 2⁰⁰*

Länge | 72° 49,17' O | Breite | 2° 40,88' N | Höhe a.s.l. | 194 m

Parameter des Brunnen:
 Tiefe | 320 ft | Wasserpiegel | 160 | Pumpe | 200
bei 300 ft / Hand max. 100 ft

Vor Ort gemessene Parameter:
 Temperatur (°C) | *31,1 (1^h) 30,9 (1^h) 29,5 (1^h) 29,2 (1^h)* | *10/10h*
 Leitfähigkeit (κ^m μS/cm) | *594 (1^h) 578 (1^h) 601 (1^h)*
 O₂-Gehalt: | *5,63 (1^h) 5,28 (1^h) 4,08 (1^h)*
 pH-Wert: | *6,95 (1^h) 7,02 (1^h) 6,97 (1^h)*
 Alkalinität: | *4,6 mmol/L*

Lufttemp. (°C) | *28,5 ca. 15*
 Luftdruck (mbar)
 Wetter: *Dau...*

Gemessene Proben:			
NO ₃	08.0	IND 25.1	Kupferschne
NO ₂	08.0	IND 25.2	Kupferschne
NO	08.0	IND 25.3	Kupferschne
TC	08.0	IND 25.4	500 ml Glas
TC	08.0	IND 25.2	500 ml Glas
TC	08.0	IND 25.5	500 ml Glas
TC	08.0	IND 25.1	500 ml Stahl
TC	08.0	IND 25.2	500 ml Stahl
TC	08.0	IND 25.3	250 ml Glas
TC	08.0	IND 25.4	Datensatznummer

Bemerkungen: *Diesel zur höchsten Probe (ca. 100m) durch Schichten, oben werden alle anfangs 100 m liegen so auch nicht ge...*

Probennehmer:
 Datenerfassung:

(a) sampling site 25

Probenahmestelle: 26

Alt. Bezeichnung: *Menyar*

Datum & Uhrzeit: *29.1.08 18^h 18⁰⁰*

Länge | 72° 57,35' O | Breite | 2° 19,325' N | Höhe a.s.l. | 1781 m

Parameter des Brunnen:
 Tiefe | 1800 ft | Wasserpiegel | 100 ft | Pumpe | 1500 ft
10 ft schief

Vor Ort gemessene Parameter:
 Temperatur (°C) | *34,4 (18^h) 35,5 (18^h)*
 Leitfähigkeit (κ^m μS/cm) | *255 (18^h) 2,55 (18^h) 2,55 (18^h)*
 O₂-Gehalt: | *1,48 (18^h) 0,81 (18^h) 0,25 (18^h)*
 pH-Wert: | *7,05 (18^h) 6,98 (18^h) 6,97 (18^h)*
 Alkalinität: | *2 mmol/L (in. alkalinität)*

Lufttemp. (°C) | *28,1*
 Luftdruck (mbar)
 Wetter: *Dau, ab...*

Gemessene Proben:			
NO ₃	08.0	IND 26.1	Kupferschne
NO ₂	08.0	IND 26.2	Kupferschne
NO	08.0	IND 26.3	Kupferschne
TC	08.0	IND 26.1	500 ml Glas
TC	08.0	IND 26.2	500 ml Glas
TC	08.0	IND 26.3	500 ml Glas
TC	08.0	IND 26.4	30 ml Glas
TC	08.0	IND 26.5	500 ml Stahl
TC	08.0	IND 26.6	500 ml Stahl
TC	08.0	IND 26.7	250 ml Glas
TC	08.0	IND 26.8	Datensatznummer

Bemerkungen: *selb. Vordruck! Falsche Daten, wie viel Wasser...*

Probennehmer:
 Datenerfassung:

(b) sampling site 26

Probenahmestelle: 27

Alt. Bezeichnung: *Umikbar UMEGADU*

Datum & Uhrzeit: *30.1.08 16.05 - 18⁰⁰*

Länge | 72° 49,17' O | Breite | 2° 40,88' N | Höhe a.s.l. | 194 m

Parameter des Brunnen:
 Tiefe | 320 ft | Wasserpiegel | 320 ft | Pumpe |
300 ft 200 ft, 50 ft 100 ft

Vor Ort gemessene Parameter:
 Temperatur (°C) | *32,8 (16^h) 31,6 (16^h) 31,3 (16^h) 31,2 (16^h)*
 Leitfähigkeit (κ^m μS/cm) | *4,03 (16^h) 3,98 (16^h) 3,98 (16^h) 3,38 (16^h)*
 O₂-Gehalt: | *1,76 (16^h) 0,77 (16^h) 2,40 (16^h) 1,32 (16^h)*
 pH-Wert: | *7,18 (16^h) 6,91 (16^h) 6,93 6,87 (16^h)*
 Alkalinität: | *6,1 mmol/L (ca.)*

Lufttemp. (°C) | *27,5*
 Luftdruck (mbar)
 Wetter: *Dau, some. Sample in some*

Gemessene Proben:			
NO ₃	08.0	IND 27.1	Kupferschne
NO ₂	08.0	IND 27.2	Kupferschne
NO	08.0	IND 27.3	Kupferschne
TC	08.0	IND 27.1	500 ml Glas
TC	08.0	IND 27.2	500 ml Glas
TC	08.0	IND 27.3	500 ml Glas
TC	08.0	IND 27.4	30 ml Glas
TC	08.0	IND 27.5	500 ml Stahl
TC	08.0	IND 27.6	500 ml Stahl
TC	08.0	IND 27.7	250 ml Glas
TC	08.0	IND 27.8	Datensatznummer

Bemerkungen: *Gem. Stoffe, Sample Glas nicht ordentlich Druck?*

Probennehmer:
 Datenerfassung:

(c) sampling site 27

Probenahmestelle: 28

Alt. Bezeichnung: *Naripura*

Datum & Uhrzeit: *31.1.08 18^h 18⁰⁰*

Länge | 72° 49,17' O | Breite | 2° 40,88' N | Höhe a.s.l. | 194 m

Parameter des Brunnen:
 Tiefe | 320 ft | Wasserpiegel | 320 ft | Pumpe | ca. 150 m

Vor Ort gemessene Parameter:
 Temperatur (°C) | *33,5 (18^h) 33,3 (18^h) 33,3 (18^h)*
 Leitfähigkeit (κ^m μS/cm) | *1,85 (18^h) 1,85 (18^h) 1,85 (18^h)*
 O₂-Gehalt: | *1,36 (18^h) 1,50 (18^h) 1,87 (18^h)*
 pH-Wert: | *7,28 (18^h) 7,37 (18^h) 7,25 (18^h)*
 Alkalinität: | *6,5 mmol/L*

Lufttemp. (°C) | *27,6*
 Luftdruck (mbar)
 Wetter: *Dau, ab... (hochste)*

Gemessene Proben:			
NO ₃	08.0	IND 28.1	Kupferschne
NO ₂	08.0	IND 28.2	Kupferschne
NO	08.0	IND 28.3	Kupferschne
TC	08.0	IND 28.1	500 ml Glas
TC	08.0	IND 28.2	500 ml Glas
TC	08.0	IND 28.3	500 ml Glas
TC	08.0	IND 28.4	30 ml Glas
TC	08.0	IND 28.5	500 ml Stahl
TC	08.0	IND 28.6	500 ml Stahl
TC	08.0	IND 28.7	250 ml Glas
TC	08.0	IND 28.8	Datensatznummer

Bemerkungen: *selb. Vordruck! Falsche Daten, wie viel Wasser...*

Probennehmer:
 Datenerfassung:

(d) sampling site 28

Figure C.7.: Fieldbook scans 25-28

APPENDIX C. FIELDBOOK ENTRIES OF THE SAMPLING SITES

Probenahmestelle: 29

Alt. Bezeichnung: Melaj

Datum & Uhrzeit: 29.09 14⁰⁰-15⁰⁰

Länge | 72° 18' 29" O | Breite | 2° 01' 45" N | Höhe aal | 29 m

Parameter des Brunnens: Tiefe | 682 m | Wasserpegel | des Br. | Pumprate | 27 l/min |
Wasserpegel des Br. 3001 (15.15)

Vor Ort gemessene Parameter:

Temperatur (°C)	23.5 (14 ⁰⁰)	23.5 (15 ⁰⁰)	23.4 (15 ¹⁵)
Luftfeuchtigkeit (a ³ w/cm)	33.7 (14 ⁰⁰)	33.7 (15 ⁰⁰)	32.5 (15 ¹⁵)
O ₂ -Gehalt	0.27 (14 ⁰⁰)	0.28 (15 ⁰⁰)	0.40 (15 ¹⁵)
pH-Wert	7.49 (14 ⁰⁰)	7.50 (15 ⁰⁰)	7.51 (15 ¹⁵)
Alkalinität	8.5 mmol/l		

Lufttemp.: (°C) 20.1
 Luftdruck: (mbar)
 Wetter: Sonnig, heiß, PN in Sonne

NG	08.0	IND 29.1	Kupferschneide
NG	08.0	IND 29.2	Kupferschneide
NG	08.0	IND 29.3	Kupferschneide
TC	08.0	IND 29.1	500 ml Glas
TC	08.0	IND 29.2	500 ml Glas
TC	08.0	IND 29.3	500 ml Glas
CO ₂ H	08.0	IND 29.1	30 ml Glas
SF ₆	08.0	IND 29.1	300 ml Stahl
SF ₆	08.0	IND 29.2	300 ml Stahl
SF ₆	08.0	IND 29.3	300 ml Stahl
H	08.0	IND 29.1	250 ml Glas
H	08.0	IND 29.2	250 ml Glas
H	08.0	IND 29.3	250 ml Glas
Dn	08.0	IND 29.1	Datensatznummer

Bemerkungen: Müllsäcke, Metall Fässer/Aggregat, Luftdruck 40
 at ca. 10m Höhe Turm in den Sonne war aufsteigend

Probennehmer:
 Datenerfassung:

(a) sampling site 29

Probenahmestelle: 30

Alt. Bezeichnung: Lardol

Datum & Uhrzeit: 1.2.09 12⁰⁰-13⁰⁰ Pump seit 10⁰⁰

Länge | 72° 45' 15" O | Breite | 2° 03' 32" N | Höhe aal | 30 m

Parameter des Brunnens: Tiefe | 300 m | Wasserpegel | 270 m | Pumprate | 9 l/min
Wasserpegel des Br. 270 m

Vor Ort gemessene Parameter:

Temperatur (°C)	36.0 (12 ⁰⁰)	30.7 (12 ⁰⁰)	27.9 (12 ⁰⁰)
Luftfeuchtigkeit (a ³ w/cm)	1004 (12 ⁰⁰)	1035 (12 ⁰⁰)	1035 (12 ⁰⁰)
O ₂ -Gehalt	6.95 (12 ⁰⁰)	7.39 (12 ⁰⁰)	7.35 (12 ⁰⁰)
pH-Wert	7.06 (12 ⁰⁰)	7.05 (12 ⁰⁰)	7.04 (12 ⁰⁰)
Alkalinität	7 mmol/l		

Lufttemp.: (°C) 29.0 (12⁰⁰)
 Luftdruck: (mbar)
 Wetter: Schön, warm, sample in Sonne

NG	08.0	IND 30.1	Kupferschneide
NG	08.0	IND 30.2	Kupferschneide
NG	08.0	IND 30.3	Kupferschneide
TC	08.0	IND 30.1	500 ml Glas
TC	08.0	IND 30.2	500 ml Glas
TC	08.0	IND 30.3	500 ml Glas
CO ₂ H	08.0	IND 30.1	30 ml Glas
SF ₆	08.0	IND 30.1	300 ml Stahl
SF ₆	08.0	IND 30.2	300 ml Stahl
SF ₆	08.0	IND 30.3	300 ml Stahl
H	08.0	IND 30.1	250 ml Glas
H	08.0	IND 30.2	250 ml Glas
H	08.0	IND 30.3	250 ml Glas
Dn	08.0	IND 30.1	Datensatznummer

Bemerkungen: Pump seit 10 schiffen ins dieht mit Comert
 an Druck. warm, keine Blasen

Probennehmer:
 Datenerfassung:

(b) sampling site 30

Probenahmestelle: 31

Alt. Bezeichnung: Pedhanti

Datum & Uhrzeit: 1.2.09 14⁰⁰-15⁰⁰

Länge | 72° 45' 45" O | Breite | 2° 03' 24" N | Höhe aal | 31 m

Parameter des Brunnens: Tiefe | 270 m | Wasserpegel | 240 m | Pumprate | 20 l/min
Wasserpegel des Br. 240 m

Vor Ort gemessene Parameter:

Temperatur (°C)	31.6 (14 ⁰⁰)	31.6 (15 ⁰⁰)	31.5 (15 ⁰⁰)
Luftfeuchtigkeit (a ³ w/cm)	1165 (14 ⁰⁰)	1163 (15 ⁰⁰)	1165 (15 ⁰⁰)
O ₂ -Gehalt	6.21 (14 ⁰⁰)	6.08 (15 ⁰⁰)	6.24 (15 ⁰⁰)
pH-Wert	7.01 (14 ⁰⁰)	7.05 (15 ⁰⁰)	7.01 (15 ⁰⁰)
Alkalinität	8.5 mmol/l		

Lufttemp.: (°C) 32.2°C
 Luftdruck: (mbar)
 Wetter: Schön, warm, s. in Sonne

NG	08.0	IND 31.1	Kupferschneide
NG	08.0	IND 31.2	Kupferschneide
NG	08.0	IND 31.3	Kupferschneide
TC	08.0	IND 31.1	500 ml Glas
TC	08.0	IND 31.2	500 ml Glas
TC	08.0	IND 31.3	500 ml Glas
CO ₂ H	08.0	IND 31.1	30 ml Glas
SF ₆	08.0	IND 31.1	300 ml Stahl
SF ₆	08.0	IND 31.2	300 ml Stahl
SF ₆	08.0	IND 31.3	300 ml Stahl
H	08.0	IND 31.1	250 ml Glas
H	08.0	IND 31.2	250 ml Glas
H	08.0	IND 31.3	250 ml Glas
Dn	08.0	IND 31.1	Datensatznummer

Bemerkungen: Br. läuft seit 10⁰⁰ Comert. Druck 40, keine Blasen

Probennehmer:
 Datenerfassung:

(c) sampling site 31

Probenahmestelle: 32

Alt. Bezeichnung: Langhøj

Datum & Uhrzeit: 4.2.09 11⁰⁰-12⁰⁰

Länge | 72° 12' 22" O | Breite | 2° 03' 26" N | Höhe aal | 32 m

Parameter des Brunnens: Tiefe | 280 m | Wasserpegel | 270 m | Pumprate | 23 l/min
Wasserpegel des Br. 270 m

Vor Ort gemessene Parameter:

Temperatur (°C)	31.8 (11 ⁰⁰)	31.9 (11 ⁰⁰)	31.8 (12 ⁰⁰)
Luftfeuchtigkeit (a ³ w/cm)	2.20 (11 ⁰⁰)	2.20 (11 ⁰⁰)	2.20 (12 ⁰⁰)
O ₂ -Gehalt	4.07 (11 ⁰⁰)	4.25 (11 ⁰⁰)	4.28 (12 ⁰⁰)
pH-Wert	6.88 (11 ⁰⁰)	6.92 (11 ⁰⁰)	6.87 (12 ⁰⁰)
Alkalinität	9.5 mmol/l		

Lufttemp.: (°C) 22.9°C
 Luftdruck: (mbar)
 Wetter: Schön, warm

NG	08.0	IND 32.1	Kupferschneide
NG	08.0	IND 32.2	Kupferschneide
NG	08.0	IND 32.3	Kupferschneide
TC	08.0	IND 32.1	500 ml Glas
TC	08.0	IND 32.2	500 ml Glas
TC	08.0	IND 32.3	500 ml Glas
CO ₂ H	08.0	IND 32.1	30 ml Glas
SF ₆	08.0	IND 32.1	300 ml Stahl
SF ₆	08.0	IND 32.2	300 ml Stahl
SF ₆	08.0	IND 32.3	300 ml Stahl
H	08.0	IND 32.1	250 ml Glas
H	08.0	IND 32.2	250 ml Glas
H	08.0	IND 32.3	250 ml Glas
Dn	08.0	IND 32.1	Datensatznummer

Bemerkungen: Drip System; Comert. Druck 5 - höherer Druck, keine Blasen mehr. Gut bei Druck 8

Probennehmer:
 Datenerfassung:

(d) sampling site 32

Figure C.8.: Fieldbook scans 29-32

APPENDIX C. FIELDBOOK ENTRIES OF THE SAMPLING SITES

Probenahmestelle: 33

All. Bezeichnung: GORWARIA

Datum & Uhrzeit: 04.02.09 12:30 - 13:00

Länge: 72° 35.41' O | Breite: 2° 23.48' N | Höhe a.s.l.: 1078 m

Parameter des Brunnens:
 Tiefe: 46.2 ft | Wasserpegel: 45.00 ft | Pumpenrate: 3.2 GPM

Vor Ort gemessene Parameter:
 Temperatur (°C): 32.5 (90.5) | 32.5 (90.5) | 32.6 (90.7)
 Leitfähigkeit (µS/cm): 1276 (0.45 (µM)) | 1270 (0.45) | 1287 (0.46)
 O₂-Gehalt: 5.38 (0.17) | 5.35 (0.17) | 5.38 (0.17)
 pH-Wert: 7.01 (0.15) | 7.05 (0.15) | 7.04 (0.15)
 Alkalinität: 7.6 mmol/L (2.1)

Lufttemp. (°C): 30.2 (86.4 F)
 Luftdruck (mbar):
 Wetter: w/m, leicht, 30-35°C in der Sonne

Genommene Proben:	IND	Material
NG	08.0	IND_3.3.1 Kupferschiene
NG	08.0	IND_3.3.2 Kupferschiene
NG	08.0	IND_3.3.3 Kupferschiene
TC	08.0	IND_3.3.1 500 ml Glas
TC	08.0	IND_3.3.2 500 ml Glas
CO ₂ H	08.0	IND_3.3 30 ml Glas
SF ₆	08.0	IND_3.3.1 500 ml Stahl
SF ₆	08.0	IND_3.3.2 500 ml Stahl
H	08.0	IND_3.3 250 ml Glas
Rn	2.8.3	16.20 Datumsnummer

Bemerkungen: Zentraler Brunnen am Aussichtspunkt - 20 m über Meeresspiegel, kein Druck, aber wenig Brunnen (am Ende von P-14) sind im Gange, Brunnen stehen nun frisch geborenen Mineral (K-30)

Probennehmer:
 Datumerfassung:

(a) sampling site 33

Probenahmestelle: 34

All. Bezeichnung: Doragath

Datum & Uhrzeit: 5.2.09 12:00 - 13:00

Länge: 72° 36.59' O | Breite: 2° 23.47' N | Höhe a.s.l.: 1078 m

Parameter des Brunnens:
 Tiefe: 46.2 ft | Wasserpegel: 45.00 ft | Pumpenrate: 3.2 GPM

Vor Ort gemessene Parameter:
 Temperatur (°C): 34.6 (94.3) | 34.1 (93.4) | 34.2 (93.6)
 Leitfähigkeit (µS/cm): 1524 (0.50 (µM)) | 1529 (0.50) | 1530 (0.50)
 O₂-Gehalt: 3.42 (0.12) | 3.71 (0.12) | 3.72 (0.12)
 pH-Wert: 7.78 (0.15) | 7.89 (0.15) | 7.88 (0.15)
 Alkalinität: 6.0 mmol/L

Lufttemp. (°C): 29.4 (85.0 F)
 Luftdruck (mbar):
 Wetter: leicht, warm, Sonne; Sample in Sonne

Genommene Proben:	IND	Material
NG	08.0	IND_3.4.1 Kupferschiene
NG	08.0	IND_3.4.2 Kupferschiene
NG	08.0	IND_3.4.3 Kupferschiene
TC	08.0	IND_3.4.1 500 ml Glas
TC	08.0	IND_3.4.2 500 ml Glas
CO ₂ H	08.0	IND_3.4 30 ml Glas
SF ₆	08.0	IND_3.4.1 500 ml Stahl
SF ₆	08.0	IND_3.4.2 500 ml Stahl
H	08.0	IND_3.4 250 ml Glas
Rn	2.8.3	16.20 Datumsnummer

Bemerkungen: Das angeschlossene für eine Computer, oder Druck, keine Brunnen; LWP; spülen lassen am Anfang

Probennehmer:
 Datumerfassung:

(b) sampling site 34

Probenahmestelle: 35

All. Bezeichnung: Wandasan (Schnee)

Datum & Uhrzeit: 5.2.09 16:00 - 17:00

Länge: 72° 35.49' O | Breite: 2° 23.47' N | Höhe a.s.l.: 75 m

Parameter des Brunnens:
 Tiefe: 40 ft | Wasserpegel: 39.25 ft | Pumpenrate: 1.5 GPM

Vor Ort gemessene Parameter:
 Temperatur (°C): 31.2 (88.2) | 31.4 (88.5) | 31.1 (88.0)
 Leitfähigkeit (µS/cm): 1283 (0.45 (µM)) | 1300 (0.45) | 1297 (0.45)
 O₂-Gehalt: 4.28 (0.15) | 4.17 (0.15) | 4.20 (0.15)
 pH-Wert: 7.23 (0.15) | 7.20 (0.15) | 7.44 (0.15)
 Alkalinität: 7.0 mmol/L | 7.5 (0.12) | 7.76

Lufttemp. (°C): 28.0
 Luftdruck (mbar):
 Wetter: leicht, warm, e. in Sonne/Schatten

Genommene Proben:	IND	Material
NG	08.0	IND_3.5.1 Kupferschiene
NG	08.0	IND_3.5.2 Kupferschiene
NG	08.0	IND_3.5.3 Kupferschiene
TC	08.0	IND_3.5.1 500 ml Glas
TC	08.0	IND_3.5.2 500 ml Glas
CO ₂ H	08.0	IND_3.5 30 ml Glas
SF ₆	08.0	IND_3.5.1 500 ml Stahl
SF ₆	08.0	IND_3.5.2 500 ml Stahl
H	08.0	IND_3.5 250 ml Glas
Rn	2.8.3	16.20 Datumsnummer

Bemerkungen: Sehr starker Druck pH-Sensor wurde hier, keine Brunnen, Alkalinität

Probennehmer:
 Datumerfassung:

(c) sampling site 35

Probenahmestelle: 36

All. Bezeichnung: Kherpur

Datum & Uhrzeit: 6.2.09 13:00 - 14:00

Länge: 73° 33.67' O | Breite: 2° 23.57' N | Höhe a.s.l.: 23 m

Parameter des Brunnens:
 Tiefe: 20 ft | Wasserpegel: 19.20 ft | Pumpenrate: 1.5 GPM

Vor Ort gemessene Parameter:
 Temperatur (°C): 31.6 (88.9) | 31.8 (89.2) | 31.7 (89.1)
 Leitfähigkeit (µS/cm): 1276 (0.45 (µM)) | 1277 (0.45) | 1279 (0.45)
 O₂-Gehalt: 5.41 (0.17) | 5.10 (0.17) | 5.02 (0.17)
 pH-Wert: 7.23 (0.15) | 7.26 (0.15) | 7.25 (0.15)
 Alkalinität: 8.9 mmol/L

Lufttemp. (°C): 31.2
 Luftdruck (mbar):
 Wetter: leicht, warm, Sonne; Sample in Schatten

Genommene Proben:	IND	Material
NG	08.0	IND_3.6.1 Kupferschiene
NG	08.0	IND_3.6.2 Kupferschiene
NG	08.0	IND_3.6.3 Kupferschiene
TC	08.0	IND_3.6.1 500 ml Glas
TC	08.0	IND_3.6.2 500 ml Glas
CO ₂ H	08.0	IND_3.6 30 ml Glas
SF ₆	08.0	IND_3.6.1 500 ml Stahl
SF ₆	08.0	IND_3.6.2 500 ml Stahl
H	08.0	IND_3.6 250 ml Glas
Rn	2.8.3	16.20 Datumsnummer

Bemerkungen: Guter Druck, warm, keine Brunnen

Probennehmer:
 Datumerfassung:

(d) sampling site 36

Figure C.9.: Fieldbook scans 33-36

APPENDIX C. FIELDBOOK ENTRIES OF THE SAMPLING SITES

Probenahmestelle: 37

Alt. Bezeichnung: Hansselpur

Datum & Uhrzeit: 12.09 12⁰⁰ - 13⁰⁰

Länge | 72° 0' 20" O | Breite | 13° 28' 2" N | Höhe a.s.l. | 37 m

Parameter des Brunnens:
Tiefe | 30,3 m | Wasserpegel | 250 cm | Pumpe | 50 cm

Vor Ort gemessene Parameter:
Temperatur (°C) | 37,7 (12⁰⁰) | 37,2 (12⁰⁰) | 37,2 (12⁰⁰) | 37,2 (12⁰⁰)
Leitfähigkeit (µS/cm) | 2,38 (12⁰⁰) | 2,38 (12⁰⁰) | 2,32 (12⁰⁰) | 2,33 (12⁰⁰)
O₂-Gehalt | 0,28 (12⁰⁰) | 0,36 (12⁰⁰) | 0,37 (12⁰⁰)
pH-Wert | 8,00 (12⁰⁰) | 8,03 (12⁰⁰) | 8,04 (12⁰⁰)
Alkalinität | 5,1 mmol/l | 1,5

Lufttemp. (°C) | 31,2°C
Luftdruck (mbar)
Wetter: Hagel, bew., Sample in Sand

NG	08.0	IND 37.1	Kupferschne
NG	08.0	IND 37.2	Kupferschne
NG	08.0	IND 37.3	Kupferschne
TC	08.0	IND 37.1	500 ml Glas
TC	08.0	IND 37.2	500 ml Glas
TC	08.0	IND 37.3	500 ml Glas
O ₂ /H	08.0	IND 37.1	30 ml Glas
S ₂	08.0	IND 37.1	500 ml Stahl
S ₂	08.0	IND 37.2	500 ml Stahl
H	08.0	IND 37.1	250 ml Glas
Re	12.09	12.09	Datensatznummer

Bemerkungen: Cometer, WP, - mit Sand in der Leitung, Guter Druck
mit Wasserprobe ausgeführt

Probennehmer:
Datumfassung:

(a) sampling site 37

Probenahmestelle: 38

Alt. Bezeichnung: TUMM DINGHOVI

Datum & Uhrzeit: 10.09 9⁰⁰ - 10⁰⁰

Länge | 72° 35' 15" O | Breite | 13° 35' 00" N | Höhe a.s.l. | 38 m

Parameter des Brunnens:
Tiefe | 75,6 m | Wasserpegel | 420 cm | Pumpe | 35 cm

Vor Ort gemessene Parameter:
Temperatur (°C) | 35,4 (09⁰⁰) | 35,2 (09⁰⁰) | 35,4 (10⁰⁰)
Leitfähigkeit (µS/cm) | 1442 (09⁰⁰) | 1443 (09⁰⁰) | 1443 (10⁰⁰)
O₂-Gehalt | 3,02 (09⁰⁰) | 3,11 (09⁰⁰) | 3,11 (10⁰⁰)
pH-Wert | 7,02 (09⁰⁰) | 7,05 (09⁰⁰) | 7,10 (10⁰⁰)
Alkalinität | 0,01 mmol/l (ca)

Lufttemp. (°C) | 40,3
Luftdruck (mbar)
Wetter: Dawn, 20°C, Sample in Sediment

NG	08.0	IND 38.1	Kupferschne
NG	08.0	IND 38.2	Kupferschne
NG	08.0	IND 38.3	Kupferschne
TC	08.0	IND 38.1	500 ml Glas
TC	08.0	IND 38.2	500 ml Glas
TC	08.0	IND 38.3	500 ml Glas
O ₂ /H	08.0	IND 38.1	30 ml Glas
S ₂	08.0	IND 38.1	500 ml Stahl
S ₂	08.0	IND 38.2	500 ml Stahl
H	08.0	IND 38.1	250 ml Glas
Re	10.09	10.09	Datensatznummer

Bemerkungen: Pumpen, TUM, bew., WP, Kompletter, mit
ausgeführt, keine Probe, Druck ab 40cm, Geringe
Fluss in Richtung

Probennehmer:
Datumfassung:

(b) sampling site 38

Probenahmestelle: 39

Alt. Bezeichnung: Altesan

Datum & Uhrzeit: 11.09 10⁰⁰ - 11⁰⁰

Länge | 72° 0' 20" O | Breite | 13° 28' 2" N | Höhe a.s.l. | 37 m

Parameter des Brunnens:
Tiefe | 30,3 m | Wasserpegel | 250 cm | Pumpe | 50 cm

Vor Ort gemessene Parameter:
Temperatur (°C) | 35,3 (10⁰⁰) | 35,2 (10⁰⁰) | 35,4 (10⁰⁰) | 35,7 (10⁰⁰)
Leitfähigkeit (µS/cm) | 162 (10⁰⁰) | 5,07 (10⁰⁰) | 162 (10⁰⁰) | 162 (10⁰⁰)
O₂-Gehalt | 3,25 (10⁰⁰) | 3,30 (10⁰⁰) | 3,11 (10⁰⁰) | 3,98 (10⁰⁰)
pH-Wert | 7,26 (10⁰⁰) | 7,21 (10⁰⁰) | 7,10 (10⁰⁰) | 7,28 (10⁰⁰)
Alkalinität | 9,5 mmol/l

Lufttemp. (°C) | 29,3°C
Luftdruck (mbar)
Wetter: Dawn, (hagel), Sonne, Sample in Sediment

NG	08.0	IND 39.1	Kupferschne
NG	08.0	IND 39.2 <th>Kupferschne</th>	Kupferschne
NG	08.0	IND 39.3 <th>Kupferschne</th>	Kupferschne
TC	08.0	IND 39.1 <td>500 ml Glas</td>	500 ml Glas
TC	08.0	IND 39.2 <td>500 ml Glas</td>	500 ml Glas
TC	08.0	IND 39.3 <td>500 ml Glas</td>	500 ml Glas
O ₂ /H	08.0	IND 39.1 <td>30 ml Glas</td>	30 ml Glas
S ₂	08.0	IND 39.1 <td>500 ml Stahl</td>	500 ml Stahl
S ₂	08.0	IND 39.2 <td>500 ml Stahl</td>	500 ml Stahl
H	08.0	IND 39.1 <td>250 ml Glas</td>	250 ml Glas
Re	11.09	11.09	Datensatznummer

Bemerkungen: Sediment, WP, oder keine Probe, Temperaturmessung nur in
10⁰⁰ und 11⁰⁰; Cometer, WP, Kompletter, mit Wasser
probe ausgeführt

Probennehmer: St. Wasser (hagel, Bewölkung) → mit WP nicht möglich
Datumfassung:

(c) sampling site 39

Probenahmestelle: 40

Alt. Bezeichnung: Kappel KAYAL

Datum & Uhrzeit: 16.09 10⁰⁰ - 11⁰⁰

Länge | 72° 0' 20" O | Breite | 13° 28' 2" N | Höhe a.s.l. | 37 m

Parameter des Brunnens:
Tiefe | 30,3 m | Wasserpegel | 300 cm | Pumpe | 35 cm

Vor Ort gemessene Parameter:
Temperatur (°C) | 32,1 (10⁰⁰) | 32,2 (10⁰⁰) | 32,7 (10⁰⁰) | 32,8 (10⁰⁰)
Leitfähigkeit (µS/cm) | 222 (10⁰⁰) | 5,07 (10⁰⁰) | 222 (10⁰⁰) | 222 (10⁰⁰)
O₂-Gehalt | 2,26 (10⁰⁰) | 2,46 (10⁰⁰) | 2,20 (10⁰⁰)
pH-Wert | 7,14 (10⁰⁰) | 7,18 (10⁰⁰) | 7,17 (10⁰⁰)
Alkalinität | 6,5

Lufttemp. (°C) | 24,8°C (10⁰⁰)
Luftdruck (mbar)
Wetter: Hagel, bew., Sonne, Sample in Sediment

NG	08.0	IND 40.1	Kupferschne
NG	08.0	IND 40.2 <th>Kupferschne</th>	Kupferschne
NG	08.0	IND 40.3 <th>Kupferschne</th>	Kupferschne
TC	08.0	IND 40.1 <td>500 ml Glas</td>	500 ml Glas
TC	08.0	IND 40.2 <td>500 ml Glas</td>	500 ml Glas
TC	08.0	IND 40.3 <td>500 ml Glas</td>	500 ml Glas
O ₂ /H	08.0	IND 40.1 <td>30 ml Glas</td>	30 ml Glas
S ₂	08.0	IND 40.1 <td>500 ml Stahl</td>	500 ml Stahl
H	08.0	IND 40.1 <td>250 ml Glas</td>	250 ml Glas
Re	16.09	16.09	Datensatznummer

Bemerkungen: Druckmessung, Kompletter, Kompletter, Kompletter
Kompletter

Probennehmer:
Datumfassung:

(d) sampling site 40

Figure C.10.: Fieldbook scans 37-40

APPENDIX C. FIELDBOOK ENTRIES OF THE SAMPLING SITES

Probenahmestelle: 43¹

Alt. Bezeichnung: Charade

Datum & Uhrzeit: 16.7.09 12:20 - 12:40

Länge [W: 2° 35' 50" O] Breite [33° 23' 23" N] Höhe a.s.l. [104 m]

Parameter des Brunnens:
 Tiefe: [] Wasserpfeil: [] Pumprate: []

Vor Ort gemessene Parameter:
 Temperatur (°C): 32.7 (12:20)
 Leitfähigkeit (κ²⁵ μS/cm): 17.4 (12:20)
 O₂-Gehalt: 3.99 / 6.66 (12:20) / 6.72 (12:20)
 pH-Wert: 7.91 (12:20)
 Alkalinität: []

Lufttemp. (°C): []
 Luftdruck (mbar): []
 Wetter: hazy, some sun, some shadows

Gemessene Proben:

NO ₃	08.0	IND -4.1.1	Kupferschne	3 1/2 Liter
NO ₂	08.0	IND -4.1.2	Kupferschne	3
NO	08.0	IND -4.1.3	Kupferschne	3
PC	08.0	IND -4.1.2	500 ml Glas	
PC	08.0	IND -4.1.2	500 ml Glas	
CO ₂ -H	08.0	IND -4.1.1	30 ml Glas	
Fe	08.0	IND -4.1.1	500 ml Stahl	
Fe	08.0	IND -4.1.2	500 ml Stahl	
H	08.0	IND -4.1	250 ml Glas	
Pa	0	IND -4.1	Datensatznummer	

Bemerkungen: Luftdruck & Temperatur gemessen. Wasser mit Druck Brunnen steht. Leitfähigkeit & keine Nitro / kein CO₂

Probennummer: []
 Datumerfassung: []

(a) sampling site 41

Probenahmestelle: 44²

Alt. Bezeichnung: Santol (Sand)

Datum & Uhrzeit: 18.7.09 12:45 - 13:30

Länge [W: 2° 37' 35" O] Breite [23° 40' 34" N] Höhe a.s.l. [113 m]

Parameter des Brunnens:
 Tiefe: 165 ft | Wasserpfeil: [] | Pumprate: 10 L/min

Vor Ort gemessene Parameter:
 Temperatur (°C): 28.3 / 28.4 (13:00)
 Leitfähigkeit (κ²⁵ μS/cm): 15.97 / 0.55 / 13.8 / 0.55
 O₂-Gehalt: 6.99 / 6.66 (12:20) / 6.72 (12:20)
 pH-Wert: 7.15 / 7.20 (13:00)
 Alkalinität: []

Lufttemp. (°C): []
 Luftdruck (mbar): []
 Wetter: []

Gemessene Proben:

NO ₃	08.0	IND -4.4.1	Kupferschne	
NO ₂	08.0	IND -4.4.2	Kupferschne	
NO	08.0	IND -4.4.3	Kupferschne	
PC	08.0	IND -4.4.1	500 ml Glas	
PC	08.0	IND -4.4.2	500 ml Glas	
CO ₂ -H	08.0	IND -4.4	30 ml Glas	
Fe	08.0	IND -4.4.1	500 ml Stahl	
Fe	08.0	IND -4.4.2	500 ml Stahl	
H	08.0	IND -4.4	250 ml Glas	
Pa	0	IND -4.4	Datensatznummer	

Bemerkungen: 2. Prob. mit Wasser aus Brunnen. 1st aber Druck zu hoch. Keine Nitro / kein CO₂

Probennummer: []
 Datumerfassung: []

(b) sampling site 42

Probenahmestelle: 43³

Alt. Bezeichnung: Santol (North)

Datum & Uhrzeit: 19.7.09 12:55 - 13:30

Länge [W: 2° 37' 52" O] Breite [23° 40' 22" N] Höhe a.s.l. [102 m]

Parameter des Brunnens:
 Tiefe: 75 ft | Wasserpfeil: [] | Pumprate: 10 L/min

Vor Ort gemessene Parameter:
 Temperatur (°C): 28.2 / 28.5 / 28.4 (13:00)
 Leitfähigkeit (κ²⁵ μS/cm): 13.09 / 0.55 / 13.09 / 0.55 (13:00) / 13.10 (13:00)
 O₂-Gehalt: 5.30 / 5.65 / 6.42 (13:00) / 6.00 (13:00)
 pH-Wert: 6.97 / 7.02 / 6.96 (13:00)
 Alkalinität: 7.9 mmol/L

Lufttemp. (°C): 33.2°C
 Luftdruck (mbar): []
 Wetter: hot, sun, some in shade

Gemessene Proben:

NO ₃	08.0	IND -4.3.1	Kupferschne	
NO ₂	08.0	IND -4.3.2	Kupferschne	
NO	08.0	IND -4.3.3	Kupferschne	
PC	08.0	IND -4.3.2	500 ml Glas	
PC	08.0	IND -4.3.2	500 ml Glas	
CO ₂ -H	08.0	IND -4.3.1	30 ml Glas	
Fe	08.0	IND -4.3.1	500 ml Stahl	
Fe	08.0	IND -4.3.2	500 ml Stahl	
H	08.0	IND -4.3	250 ml Glas	
Pa	0	IND -4.3	Datensatznummer	

Bemerkungen: Druck ist höher und Pumpen Brunnen an. Prob. aber normal. Keine Nitro / kein CO₂. 1st aber Druck zu hoch. Keine Nitro / kein CO₂

Probennummer: []
 Datumerfassung: []

(c) sampling site 43

Probenahmestelle: 44⁴

Alt. Bezeichnung: Manjer

Datum & Uhrzeit: 19.7.09 14:55 - 15:30

Länge [W: 2° 37' 22" O] Breite [23° 42' 22" N] Höhe a.s.l. [120 m]

Parameter des Brunnens:
 Tiefe: 250 ft | Wasserpfeil: 200 ft | Pumprate: 10 L/min

Vor Ort gemessene Parameter:
 Temperatur (°C): 31.8 (15:00) / 31.8 (15:00) / 31.5 (15:00)
 Leitfähigkeit (κ²⁵ μS/cm): 10.19 / 5.03 (15:00) / 10.10 (15:00) / 10.12 (15:00)
 O₂-Gehalt: 1.25 (15:00) / 2.10 (15:00) / 2.29 (15:00)
 pH-Wert: 7.12 (15:00) / 7.11 (15:00) / 7.10 (15:00)
 Alkalinität: 7 mmol/L

Lufttemp. (°C): 31.2°C
 Luftdruck (mbar): []
 Wetter: sun, some in shade

Gemessene Proben:

NO ₃	08.0	IND -2.2.1	Kupferschne	
NO ₂	08.0	IND -2.2.2	Kupferschne	
NO	08.0	IND -2.2.3	Kupferschne	
PC	08.0	IND -2.2.1	500 ml Glas	
PC	08.0	IND -2.2.2	500 ml Glas	
CO ₂ -H	08.0	IND -2.2	30 ml Glas	
Fe	08.0	IND -2.2.1	500 ml Stahl	
Fe	08.0	IND -2.2.2	500 ml Stahl	
H	08.0	IND -2.2	250 ml Glas	
Pa	0	IND -2.2	Datensatznummer	

Bemerkungen: Voll Wasser, Druck geht; Leitfähigkeit an Wasser. Leitfähigkeit ist 5% höher. Keine Nitro / kein CO₂

Probennummer: []
 Datumerfassung: []

(d) sampling site 44

Figure C.11.: Fieldbook scans 41-44

APPENDIX C. FIELDBOOK ENTRIES OF THE SAMPLING SITES

Probenahmestelle: 45

Alt. Bezeichnung: *Garada*

Datum & Uhrzeit: *3.7.20 11:30 - 14:30*

Länge: *27° 52' 45" O* | Breite: *12° 35' 42" N* | Höhe a.s.l.: *117 m*

Parameter des Brunnen:

Tiefe	500 ft	Wasserspiegel / Pumpiefe	350 ft / 650 ft	Pumptrate	10 cm
Screen	300 ft			cm o sec	30 sec

Vor Ort gemessene Parameter:

Temperatur (°C): *36,5°C (114°) (117m) 31,65 (114°) 36,4°C (114m)*

Leitfähigkeit (µS/cm): *925,25 (15m) 925,25 (15m) 925,25 (15m) 925,25 (15m) 925,25 (15m)*

O₂-Gehalt: *2,2 (114m) (17) 2,30 (114m) (17) 2,2 (114m) (17) 2,2 (114m) (17) 2,2 (114m) (17)*

pH-Wert: *6,87 (114m) (17) 6,88 (114m) (17) 6,88 (114m) (17) 6,88 (114m) (17) 6,88 (114m) (17)*

Alkalinität:

Lufttemp. (°C): *32 / 33°C (114m) 27,0°C*

Luftdruck (mbar): *1000,1 mbar (1000) 998,9 mbar (114m)*

Wetter: *Sonnig, klar, warm*

Gemessene Proben:

NO ₃	10.0 2. 3	IND -45.1	Kupferschneide	mit 50 ml
NO ₂	10.0 2. 3	IND -45.2	Kupferschneide	mit 50 ml
CO ₃ H ₂ O	10.0 2. 3	IND -45.3	50 ml Glas	
SO ₄	10.0 2. 3	IND -45.4	500 ml Stahl	
SO ₄	10.0 2. 3	IND -45.5	500 ml Stahl	

Bemerkungen: *Sehr viele Blasen aufsteigen. Sie nicht gut fließen. Keine Blasen, immer Blasen. Sample in Sonne.*

Probennehmer:

Datenerfassung:

(a) sampling site 45

Probenahmestelle: 46

Alt. Bezeichnung: *Sardata Malakoppara*

Datum & Uhrzeit: *3.7.20 15:35 - 15:55*

Länge: *27° 52' 30" O* | Breite: *12° 35' 42" N* | Höhe a.s.l.: *117 m*

Parameter des Brunnen:

Tiefe	210	Wasserspiegel / Pumpiefe	140	Pumptrate	15 cm
Screen	110		280	cm o sec	13 sec

Vor Ort gemessene Parameter:

Temperatur (°C): *27,9 (15m) 27,7 (15m) 27,9 (15m)*

Leitfähigkeit (µS/cm): *925,25 (15m) 925,25 (15m) 925,25 (15m) 925,25 (15m) 925,25 (15m)*

O₂-Gehalt: *6,15 (15m) 6,13 (15m) 6,22 (15m) 6,22 (15m) 6,22 (15m)*

pH-Wert: *6,84 (15m) 6,85 (15m) 6,84 (15m) 6,84 (15m) 6,84 (15m)*

Alkalinität:

Lufttemp. (°C):

Luftdruck (mbar): *997,3 (15m)*

Wetter: *Wolken, Sonnig*

Gemessene Proben:

NO ₃	10.0 2. 3	IND -46.1	Kupferschneide	mit 50 ml
NO ₂	10.0 2. 3	IND -46.2	Kupferschneide	mit 50 ml
CO ₃ H ₂ O	10.0 2. 3	IND -46.3	50 ml Glas	
SO ₄	10.0 2. 3	IND -46.4	500 ml Stahl	
SO ₄	10.0 2. 3	IND -46.5	500 ml Stahl	

Bemerkungen: *keine Blasen, 4. Sample, tolle Samples s. im Feldbuch Teil 2*

Probennehmer:

Datenerfassung:

(b) sampling site 46

Probenahmestelle: (47) 11:2

Alt. Bezeichnung: *Nava Hauka*

Datum & Uhrzeit: *5.2.20 7:35 - 7:45*

Länge: *27° 52' 45" O* | Breite: *12° 35' 42" N* | Höhe a.s.l.: *117 m*

Parameter des Brunnen:

Tiefe	200 ft	Wasserspiegel / Pumpiefe	140 ft / 640 ft	Pumptrate	11 cm
Screen	700 ft			cm o sec	16 sec

Vor Ort gemessene Parameter:

Temperatur (°C): *36,1°C (114m) 36,4°C (114m) 36,2°C (114m)*

Leitfähigkeit (µS/cm): *3,34 (114m) 3,34 (114m) 3,34 (114m) 3,34 (114m) 3,34 (114m)*

O₂-Gehalt: *0,22 (114m) 0,22 (114m) 0,22 (114m) 0,22 (114m) 0,22 (114m)*

pH-Wert: *6,87 (114m) 6,87 (114m) 6,87 (114m) 6,87 (114m) 6,87 (114m)*

Alkalinität:

Lufttemp. (°C): *30° (114m) 38,5° (114m)*

Luftdruck (mbar): *1009,2 (114m) 1009,5 (114m)*

Wetter: *Warm, klar, sonnig*

Gemessene Proben:

NO ₃	10.0 2. 3	IND -47.1	Kupferschneide	mit 50 ml
NO ₂	10.0 2. 3	IND -47.2	Kupferschneide	mit 50 ml
CO ₃ H ₂ O	10.0 2. 3	IND -47.3	50 ml Glas	
SO ₄	10.0 2. 3	IND -47.4	500 ml Stahl	
SO ₄	10.0 2. 3	IND -47.5	500 ml Stahl	

Bemerkungen: *Silberplattensystem → schwer zusammenzusetzen. Blasen, da Druckluft sehr selten. Letzte Entgasung. Etwas Sand im Wasser. Wenn sich 2. Werten um Entgasung. Blasen aus System zu kommen. Wenige Blasen in Silbersystem. Sample in Sonne.*

Probennehmer:

Datenerfassung:

(c) sampling site 47

Probenahmestelle: 48

Alt. Bezeichnung: *Medha*

Datum & Uhrzeit: *8.7.20 11:30 (Sonne) - 12:30*

Länge: *27° 52' 45" O* | Breite: *12° 35' 42" N* | Höhe a.s.l.: *117 m*

Parameter des Brunnen:

Tiefe	200 ft	Wasserspiegel / Pumpiefe	275 ft	Pumptrate	17 cm
Screen	100 ft		410 ft	cm o sec	200 ft / 150

Vor Ort gemessene Parameter:

Temperatur (°C): *36,7°C (114m) 36,5°C (114m) 36,2°C (114m)*

Leitfähigkeit (µS/cm): *925,25 (15m) 925,25 (15m) 925,25 (15m) 925,25 (15m) 925,25 (15m)*

O₂-Gehalt: *0,22 (114m) 0,22 (114m) 0,22 (114m) 0,22 (114m) 0,22 (114m)*

pH-Wert: *7,48 (114m) 7,36 (114m) 7,23 (114m)*

Alkalinität:

Lufttemp. (°C): *36,29,7°C (114m)*

Luftdruck (mbar): *1009,2 mbar (114m) 1009,5 mbar (114m)*

Wetter: *Warm, (sonnig), klar, Sample in halbschatten*

Gemessene Proben:

NO ₃	10.0 2. 3	IND -48.1	Kupferschneide	mit 50 ml
NO ₂	10.0 2. 3	IND -48.2	Kupferschneide	mit 50 ml
CO ₃ H ₂ O	10.0 2. 3	IND -48.3	50 ml Glas	
SO ₄	10.0 2. 3	IND -48.4	500 ml Stahl	
SO ₄	10.0 2. 3	IND -48.5	500 ml Stahl	

Bemerkungen: *Sand im Druck, etwas Entgasung, (mit) keine Blasen von vorher, etwas Sand im Wasser*

Probennehmer:

Datenerfassung:

(d) sampling site 48

Figure C.12.: Fieldbook scans 45-48

APPENDIX C. FIELDBOOK ENTRIES OF THE SAMPLING SITES

Probenahmestelle: 49

Alt. Bezeichnung: *Rampura*

Datum & Uhrzeit: *08.02.10 15:30*

Länge | 21° 22' 22" O | Breite | 27° 16' 43" N | Höhe a.s.l. | 102 m

Parameter des Brunnens:
 Tiefe / Screen: 1200 ft / 1200 ft
 Wasserpiegel / Pumpiefe: /
 Pumprate / Cm o sec: 2.0 m³ / 1.5

Vor Ort gemessene Parameter:
 Temperatur: (°C) *40.4°C* / *40.1°C* / *39.4°C*
 Leitfähigkeit: (µS/cm) *1550 µS* / *500 µS*
 O-Gehalt: *0.25* / *0.25* / *0.25*
 pH-Wert: *7.66* / *7.06* / *7.01*
 Alkalinität: / /

Lufttemp: (°C) *30.0°C* / *29.0°C*
 Luftdruck: (mbar) *1004.7 mbar* / *1004.1 mbar*
 Wetter: *überwiegend bewölkt*

Gemessene Proben:
 NG: 10.0 2. 3 IND-49.1 Kupferschne
 NG: 10.0 2. 3 IND-49.2 Kupferschne
 10 ml H₂O: 10.0 2. 3 IND-49 50 ml Glas
 SF₁: 10.0 2. 3 IND-49.1 500 ml Stahl
 SF₂: 10.0 2. 3 IND-49.2 500 ml Stahl

Bemerkungen: *Leichte - in Zukunft vom Rohr leichtes Wasser... in Wasser... in Wasser... in Wasser...*

Probennehmer:
 Durchmesser:

(a) sampling site 49

Probenahmestelle: 50

Alt. Bezeichnung: *Vansa*

Datum & Uhrzeit: *07.10 13:45*

Länge | 72° 42' 33" O | Breite | 21° 16' 22" N | Höhe a.s.l. | 50 m

Parameter des Brunnens:
 Tiefe / Screen: 200 ft / 200 ft
 Wasserpiegel / Pumpiefe: 1.00 ft / 2.50 ft
 Pumprate / Cm o sec: 10.00 / 2.0

Vor Ort gemessene Parameter:
 Temperatur: (°C) *37.0°C* / *36.8°C*
 Leitfähigkeit: (µS/cm) *4.60 µS* / *1.75 µS*
 O-Gehalt: *0.43* / *0.42*
 pH-Wert: *6.91* / *6.95*
 Alkalinität: / /

Lufttemp: (°C) *28.0°C*
 Luftdruck: (mbar) *1005.4 mbar* / *1006.2 mbar*
 Wetter: *heiß, klar, sonnig, 5. in Sonne*

Gemessene Proben:
 NG: 10.0 2. 3 IND-50.1 Kupferschne
 NG: 10.0 2. 3 IND-50.2 Kupferschne
 10 ml H₂O: 10.0 2. 3 IND-50 50 ml Glas
 SF₁: 10.0 2. 3 IND-50.1 500 ml Stahl
 SF₂: 10.0 2. 3 IND-50.2 500 ml Stahl

Bemerkungen: *Leichte - in Rohr mit Wasser... Leichte - in Rohr mit Wasser... Leichte - in Rohr mit Wasser...*

Probennehmer:
 Durchmesser:

(b) sampling site 50

Probenahmestelle: 51

Alt. Bezeichnung: *Sarala* *Dharam*

Datum & Uhrzeit: *10.10 11:00*

Länge | 22° 42' 22" O | Breite | 21° 40' 50" N | Höhe a.s.l. | 100 m

Parameter des Brunnens:
 Tiefe / Screen: 750 ft / 750 ft
 Wasserpiegel / Pumpiefe: 100 ft / 100 ft
 Pumprate / Cm o sec: 2.0 m³ / 1.5

Vor Ort gemessene Parameter:
 Temperatur: (°C) *44.0°C* / *41.3°C*
 Leitfähigkeit: (µS/cm) *3.52 µS* / *32.7 µS*
 O-Gehalt: *0.16* / *0.7*
 pH-Wert: *7.6* / *7.25*
 Alkalinität: / /

Lufttemp: (°C) *25° in Schatten*
 Luftdruck: (mbar) *1014.2 mbar*
 Wetter: *heiß, klar, sonnig, 5. in Sonne*

Gemessene Proben:
 NG: 10.0 2. 3 IND-51.1 Kupferschne
 NG: 10.0 2. 3 IND-51.2 Kupferschne
 10 ml H₂O: 10.0 2. 3 IND-51 50 ml Glas
 SF₁: 10.0 2. 3 IND-51.1 500 ml Stahl
 SF₂: 10.0 2. 3 IND-51.2 500 ml Stahl

Bemerkungen: *Keine (?) Ausguss... Blasen... (Gold) mit... Blasen... Blasen... Blasen...*

Probennehmer:
 Durchmesser:

(c) sampling site 51

Probenahmestelle: 52

Alt. Bezeichnung: *Shival*

Datum & Uhrzeit: *10.10 12:30*

Länge | 72° 42' 22" O | Breite | 21° 40' 50" N | Höhe a.s.l. | 100 m

Parameter des Brunnens:
 Tiefe / Screen: 650 ft / 650 ft
 Wasserpiegel / Pumpiefe: 100 ft / 100 ft
 Pumprate / Cm o sec: 4.5 m³ / 1.5

Vor Ort gemessene Parameter:
 Temperatur: (°C) *40.8°C* / *40.3°C*
 Leitfähigkeit: (µS/cm) *3.8 µS* / *2.6 µS*
 O-Gehalt: *0.19* / *0.40*
 pH-Wert: *7.43* / *7.51*
 Alkalinität: / /

Lufttemp: (°C) *29.7*
 Luftdruck: (mbar) *1011.0 mbar*
 Wetter: *heiß, klar, sonnig, 5. in Sonne / Schatten*

Gemessene Proben:
 NG: 10.0 2. 3 IND-52.1 Kupferschne
 NG: 10.0 2. 3 IND-52.2 Kupferschne
 10 ml H₂O: 10.0 2. 3 IND-52 50 ml Glas
 SF₁: 10.0 2. 3 IND-52.1 500 ml Stahl
 SF₂: 10.0 2. 3 IND-52.2 500 ml Stahl

Bemerkungen: *Hilfs-Hof... Blasen... Blasen... Blasen... Blasen...*

Probennehmer:
 Durchmesser:

(d) sampling site 52

Figure C.13.: Fieldbook scans 51-52

APPENDIX C. FIELDBOOK ENTRIES OF THE SAMPLING SITES

Probenahmestelle: 53

Alt. Bezeichnung: *Dharampur*

Datum & Uhrzeit: *12.7.09 13⁰⁰ - 14⁰⁰*

Länge | 52° 4' 00" O | Breite | 12° 32' N | Höhe a.s.l. | 46 m

Parameter des Brunnen:

Tiefe | 700 m | Wasserpel. | Pumprate | 12 cm³/s

Vor Ort gemessene Parameter:

Temperatur (°C) *22.6 (13⁰⁰) / 21.7 (14⁰⁰) / 21.6 (15⁰⁰)*

Leitfähigkeit (µS/cm) *146.4 (13⁰⁰) / 141.1 (14⁰⁰) / 141.6 (15⁰⁰)*

O₂-Gehalt: *0.55 (13⁰⁰) / 0.46 (14⁰⁰) / 0.40 (15⁰⁰)*

pH-Wert: *7.20 (13⁰⁰) / 7.18 (14⁰⁰) / 7.19 (15⁰⁰)*

Alkalinität:

Lufttemp. (°C) *29° 28.9°C*

Luftdruck (mbar) *1019.6 mbar (13⁰⁰)*

Wetter: *heiß, klar, Sonne, 5.1. Sonne*

Gesammelte Proben:

NG	08.0	IND-53.1	Kupferschne
NG	08.0	IND-53.2	Kupferschne
TC	08.0	IND-53.1	500 ml Glas
TC	08.0	IND-53.2	500 ml Glas
SP	08.0	IND-53.1	500 ml Stahl
SP	08.0	IND-53.2	500 ml Stahl

Bemerkungen: *Oliven in der Leitung & Essig-Gehörgang, Chlor-Bleichen im Schalen*

Probennummer: *WTU auch mit Diodol gemacht*

Datenerfassung: *A. V. U.*

(a) sampling site 53

Probenahmestelle: 24*

Alt. Bezeichnung: *Santal 16⁰⁰*

Datum & Uhrzeit: *29.7.09 16⁰⁰ - 17⁰⁰*

Länge | 29° 33' 30" O | Breite | 12° 47' 22" N | Höhe a.s.l. | 29.9 m

Parameter des Brunnen:

Tiefe | 315 m | Wasserpel. | Pumprate

Vor Ort gemessene Parameter:

Temperatur (°C) *29.8 (16⁰⁰) / 31.5 (16³⁰) / 31.2 (16⁵⁰) / 31.7 (16⁵⁰)*

Leitfähigkeit (µS/cm) *174.4 (16⁰⁰) / 175.0 (16³⁰) / 175.5 (16⁵⁰) / 178.2 (16⁵⁰)*

O₂-Gehalt: *5.94 (16⁰⁰) / 4.4 (16³⁰) / 2.5 (16⁵⁰) / 2.0 (16⁵⁰)*

pH-Wert: *7.16 (16⁰⁰) / 7.20 (16³⁰) / 7.3 (16⁵⁰) / 7.29 (16⁵⁰)*

Alkalinität:

Lufttemp. (°C)

Luftdruck (mbar)

Wetter: *warm, sonnig, wolkig im Halbschatten*

Gesammelte Proben:

NG	08.0	IND-24.1	Kupferschne
NG	08.0	IND-24.2	Kupferschne
NG	08.0	IND-24.3	Kupferschne
TC	08.0	IND-24.1	500 ml Glas
TC	08.0	IND-24.2	500 ml Glas
TC	08.0	IND-24.3	500 ml Glas
SP	08.0	IND-24.1	500 ml Stahl
SP	08.0	IND-24.2	500 ml Stahl
SP	08.0	IND-24.3	250 ml Glas
Rn	2	IND-24	Datensatznummer

Bemerkungen: *Samstags*

Probennummer:

Datenerfassung:

(b) sampling site 24*

Probenahmestelle: 40

Alt. Bezeichnung: *Personal Spring (LAWANSA)*

Datum & Uhrzeit: *16.2.09 13⁰⁰ - 13⁴⁰*

Länge | O | Breite | N | Höhe a.s.l. | m

Parameter des Brunnen:

Tiefe | 26.5 m | Wasserpel. | Pumprate

Vor Ort gemessene Parameter:

Temperatur (°C) *4.2 (13⁰⁰)*

Leitfähigkeit (µS/cm) *10.44 (13⁰⁰) / 6.42 (13⁴⁰)*

O₂-Gehalt: *1.45 (13⁰⁰)*

pH-Wert: *6.72 (13⁰⁰)*

Alkalinität: *1.6 mmol/L (13⁰⁰)*

Lufttemp. (°C) *30.5*

Luftdruck (mbar)

Wetter: *Heiß, Sonne*

Gesammelte Proben:

NG	08.0	IND-40.1	Kupferschne
NG	08.0	IND-40.2	Kupferschne
NG	08.0	IND-40.3	Kupferschne
TC	08.0	IND-40.1	500 ml Glas
TC	08.0	IND-40.2	500 ml Glas
TC	08.0	IND-40.3	500 ml Glas
SP	08.0	IND-40.1	500 ml Stahl
SP	08.0	IND-40.2	500 ml Stahl
SP	08.0	IND-40.3	250 ml Glas
Rn	2	IND-40	Datensatznummer

Bemerkungen: *2. Foto T1/1 Eimer messung; 1. Schritt nach H₂S 2. Fe₂O₃ & Fe₂(OH)₂ H₂O*

Probennummer:

Datenerfassung:

(c) sampling site TS1

Probenahmestelle: 41

Alt. Bezeichnung: *Personal Spring 2 Tana*

Datum & Uhrzeit: *16.2.09 16⁰⁰ - 17⁰⁰*

Länge | O | Breite | N | Höhe a.s.l. | m

Parameter des Brunnen:

Tiefe | | Wasserpel. | Pumprate

Vor Ort gemessene Parameter:

Temperatur (°C) *65.6 (16⁰⁰)*

Leitfähigkeit (µS/cm) *5.3 - 5.1 (16⁰⁰)*

O₂-Gehalt: *7.2 (16⁰⁰) -> 0.1, 17°C (16⁰⁰) (17⁰⁰)*

pH-Wert: *6.52 (16⁰⁰)*

Alkalinität: *2.1 mmol/L (16⁰⁰)*

Lufttemp. (°C) *29.2*

Luftdruck (mbar)

Wetter: *Heiß, Sonne, im Schatten*

Gesammelte Proben:

NG	08.0	IND-41.1	Kupferschne
NG	08.0	IND-41.2	Kupferschne
NG	08.0	IND-41.3	Kupferschne
TC	08.0	IND-41.1	500 ml Glas
TC	08.0	IND-41.2	500 ml Glas
TC	08.0	IND-41.3	500 ml Glas
SP	08.0	IND-41.1	500 ml Stahl
SP	08.0	IND-41.2	500 ml Stahl
SP	08.0	IND-41.3	250 ml Glas
Rn	2	IND-41	Datensatznummer

Bemerkungen: *weiße Platte; Schienen & Schilde unter Wasser gehalten...*

Probennummer:

Datenerfassung:

(d) sampling site TS2

Figure C.14.: Fieldbook scans 53, repetition of 24, and TS1 and TS2

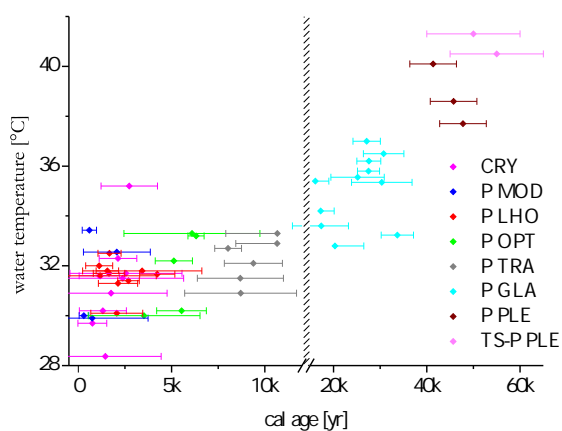
APPENDIX C. FIELDBOOK ENTRIES OF THE SAMPLING SITES

Date/Time	WTW Ind. T	WTW Ind. pH	WTW Ind. Salin.	WTW Ind. Conduct.	WTW Ind. Diss. O ₂	WTW Ind. Turb.	WTW Ind. Chlorophyll	WTW Ind. Chl. a	WTW Ind. Chl. b	WTW Ind. Chl. c	WTW Ind. Chl. d	WTW Ind. Chl. e	WTW Ind. Chl. f	WTW Ind. Chl. g	WTW Ind. Chl. h	WTW Ind. Chl. i	WTW Ind. Chl. j	WTW Ind. Chl. k	WTW Ind. Chl. l	WTW Ind. Chl. m	WTW Ind. Chl. n	WTW Ind. Chl. o	WTW Ind. Chl. p	WTW Ind. Chl. q	WTW Ind. Chl. r	WTW Ind. Chl. s	WTW Ind. Chl. t	WTW Ind. Chl. u	WTW Ind. Chl. v	WTW Ind. Chl. w	WTW Ind. Chl. x	WTW Ind. Chl. y	WTW Ind. Chl. z		
29.7.10	20.62	7.06	19.25	58.5	0.475	1.35	20.62	7.06	19.25	58.5	0.475	1.35	20.62	7.06	19.25	58.5	0.475	1.35	20.62	7.06	19.25	58.5	0.475	1.35	20.62	7.06	19.25	58.5	0.475	1.35	20.62	7.06	19.25	58.5	0.475
30.7.10	20.50	7.00	14.24	58.6	0.472	1.85	20.50	7.00	14.24	58.6	0.472	1.85	20.50	7.00	14.24	58.6	0.472	1.85	20.50	7.00	14.24	58.6	0.472	1.85	20.50	7.00	14.24	58.6	0.472	1.85	20.50	7.00	14.24	58.6	0.472
31.7.10	20.6	7.02	14.37	58.7	0.468	1.85	20.6	7.02	14.37	58.7	0.468	1.85	20.6	7.02	14.37	58.7	0.468	1.85	20.6	7.02	14.37	58.7	0.468	1.85	20.6	7.02	14.37	58.7	0.468	1.85	20.6	7.02	14.37	58.7	0.468
1.8.10	20.8	7.00	14.23	58.7	0.468	1.85	20.8	7.00	14.23	58.7	0.468	1.85	20.8	7.00	14.23	58.7	0.468	1.85	20.8	7.00	14.23	58.7	0.468	1.85	20.8	7.00	14.23	58.7	0.468	1.85	20.8	7.00	14.23	58.7	0.468
2.8.10	20.7	7.02	14.21	58.7	0.468	1.85	20.7	7.02	14.21	58.7	0.468	1.85	20.7	7.02	14.21	58.7	0.468	1.85	20.7	7.02	14.21	58.7	0.468	1.85	20.7	7.02	14.21	58.7	0.468	1.85	20.7	7.02	14.21	58.7	0.468
3.8.10	20.9	7.00	14.25	58.7	0.468	1.85	20.9	7.00	14.25	58.7	0.468	1.85	20.9	7.00	14.25	58.7	0.468	1.85	20.9	7.00	14.25	58.7	0.468	1.85	20.9	7.00	14.25	58.7	0.468	1.85	20.9	7.00	14.25	58.7	0.468
4.8.10	21.0	7.02	14.27	58.7	0.468	1.85	21.0	7.02	14.27	58.7	0.468	1.85	21.0	7.02	14.27	58.7	0.468	1.85	21.0	7.02	14.27	58.7	0.468	1.85	21.0	7.02	14.27	58.7	0.468	1.85	21.0	7.02	14.27	58.7	0.468
5.8.10	21.1	7.00	14.28	58.7	0.468	1.85	21.1	7.00	14.28	58.7	0.468	1.85	21.1	7.00	14.28	58.7	0.468	1.85	21.1	7.00	14.28	58.7	0.468	1.85	21.1	7.00	14.28	58.7	0.468	1.85	21.1	7.00	14.28	58.7	0.468
6.8.10	21.2	7.02	14.29	58.7	0.468	1.85	21.2	7.02	14.29	58.7	0.468	1.85	21.2	7.02	14.29	58.7	0.468	1.85	21.2	7.02	14.29	58.7	0.468	1.85	21.2	7.02	14.29	58.7	0.468	1.85	21.2	7.02	14.29	58.7	0.468
7.8.10	21.3	7.00	14.30	58.7	0.468	1.85	21.3	7.00	14.30	58.7	0.468	1.85	21.3	7.00	14.30	58.7	0.468	1.85	21.3	7.00	14.30	58.7	0.468	1.85	21.3	7.00	14.30	58.7	0.468	1.85	21.3	7.00	14.30	58.7	0.468
8.8.10	21.4	7.02	14.31	58.7	0.468	1.85	21.4	7.02	14.31	58.7	0.468	1.85	21.4	7.02	14.31	58.7	0.468	1.85	21.4	7.02	14.31	58.7	0.468	1.85	21.4	7.02	14.31	58.7	0.468	1.85	21.4	7.02	14.31	58.7	0.468
9.8.10	21.5	7.00	14.32	58.7	0.468	1.85	21.5	7.00	14.32	58.7	0.468	1.85	21.5	7.00	14.32	58.7	0.468	1.85	21.5	7.00	14.32	58.7	0.468	1.85	21.5	7.00	14.32	58.7	0.468	1.85	21.5	7.00	14.32	58.7	0.468
10.8.10	21.6	7.02	14.33	58.7	0.468	1.85	21.6	7.02	14.33	58.7	0.468	1.85	21.6	7.02	14.33	58.7	0.468	1.85	21.6	7.02	14.33	58.7	0.468	1.85	21.6	7.02	14.33	58.7	0.468	1.85	21.6	7.02	14.33	58.7	0.468
11.8.10	21.7	7.00	14.34	58.7	0.468	1.85	21.7	7.00	14.34	58.7	0.468	1.85	21.7	7.00	14.34	58.7	0.468	1.85	21.7	7.00	14.34	58.7	0.468	1.85	21.7	7.00	14.34	58.7	0.468	1.85	21.7	7.00	14.34	58.7	0.468
12.8.10	21.8	7.02	14.35	58.7	0.468	1.85	21.8	7.02	14.35	58.7	0.468	1.85	21.8	7.02	14.35	58.7	0.468	1.85	21.8	7.02	14.35	58.7	0.468	1.85	21.8	7.02	14.35	58.7	0.468	1.85	21.8	7.02	14.35	58.7	0.468

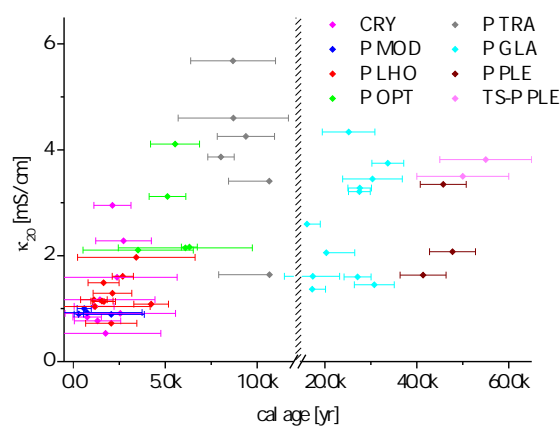
Figure C.15.: Fieldbook scans WTW protocol 2009 and 2010

D. Further results

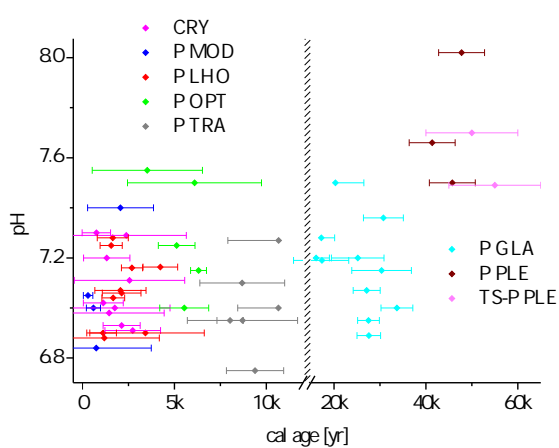
D.1. Figures



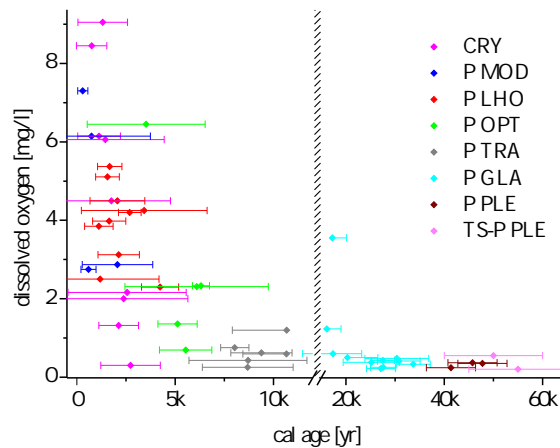
(a) Water temperature increases with age.



(b) Specific conductivity of the water grows with age.



(c) pH changes from acid to basic milieu with age.



(d) Dissolved oxygen becomes depleted with age.

Figure D.1.: The most important measured parameters of the wells plotted versus age.

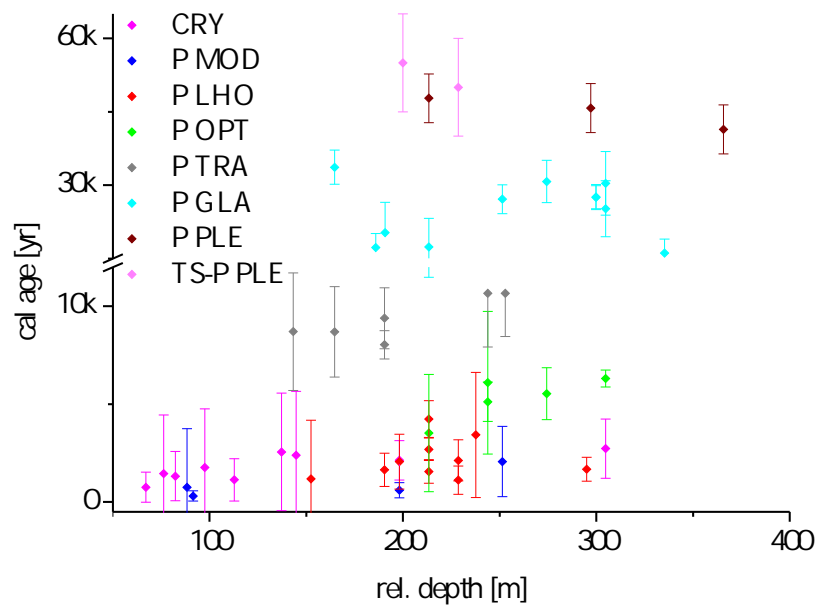
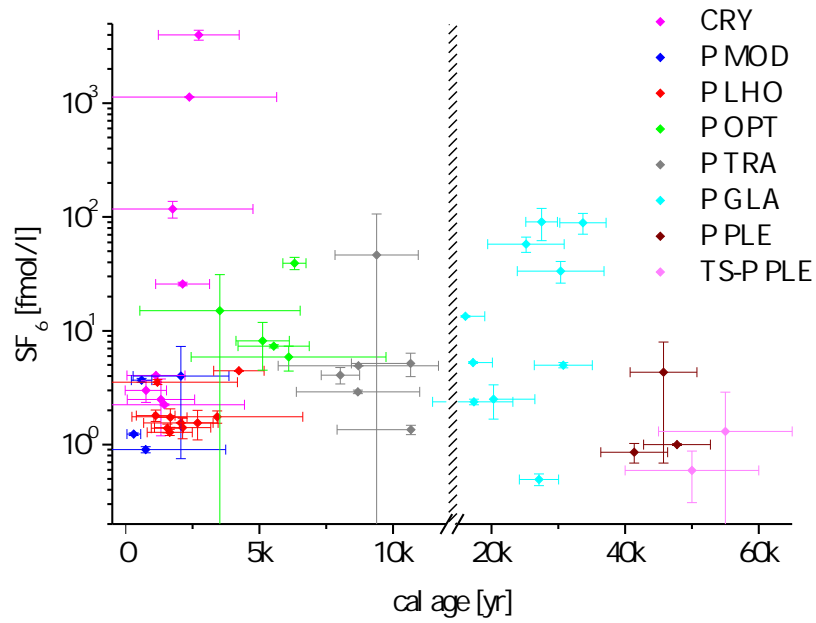
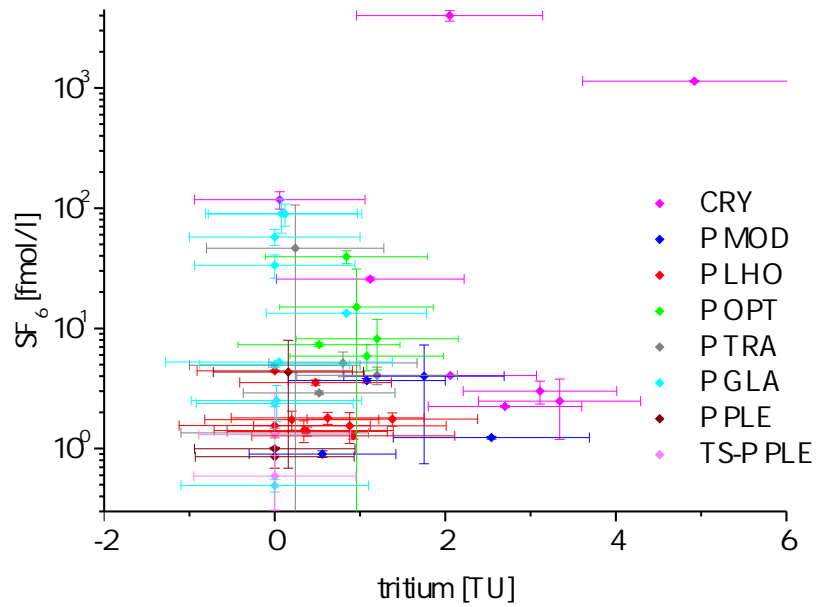


Figure D.2.: Calibrated age is plotted versus relative depth of the well. A connection between relative depth and age of the water is not existent.



(a) SF_6 versus age. Group CRY shows values several orders of magnitude higher than modern atmospheric equilibrium.



(b) SF_6 versus tritium. Wells with tritium show no significance in SF_6 .

Figure D.3.: SF_6 versus age and tritium. No distinct trend can be observed.

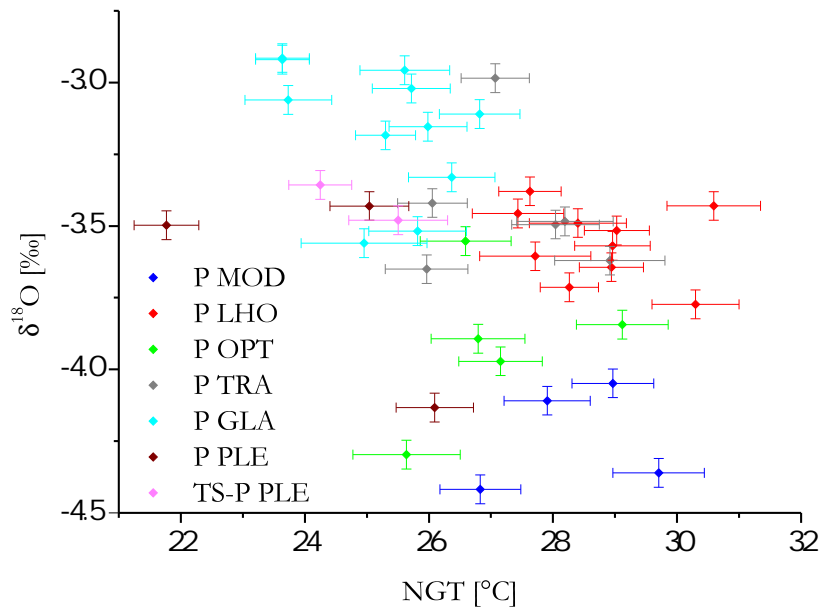


Figure D.4.: Stable isotopes versus NGT show no trend. A significant temperature effect in precipitation is therefore unlikely.

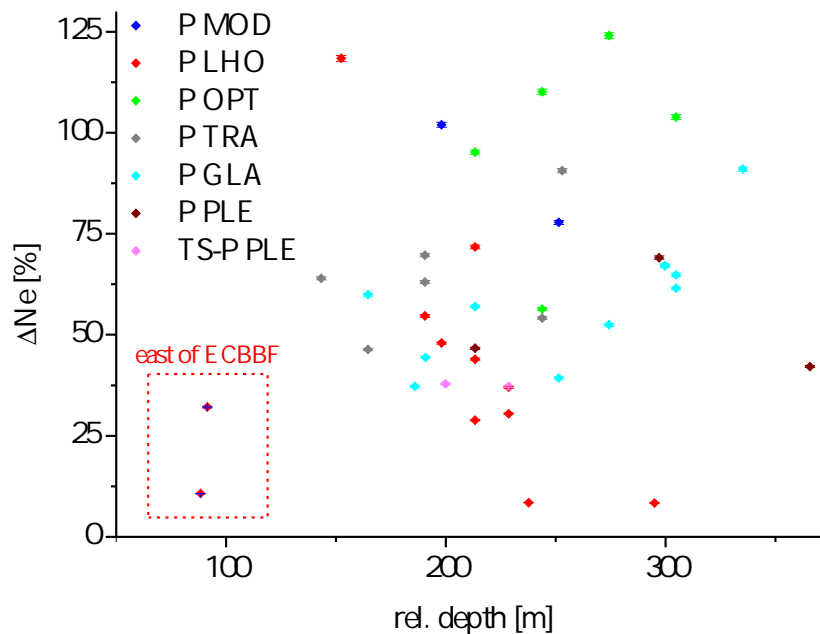


Figure D.5.: Excess air is plotted versus relative depth of the tubewell. Shallow young wells which are situated east of the ECBBF in the recharge area show comparatively low excess air amounts. This may result from unconfined conditions in this region combined with strong seasonal irrigation.

D.2. Tables

Table D.1.: Mastertable (1):

No	Altitude			Rock	abs. depth	screen bottom edge	Latitude	Longitude	Dist. Recharge	water temp.	κ20	S	pH	diss. ox.	
	m asl	Water level	screen top edge												m asl
1	67		-78		191	-124	23.87	71.98	61	08/02/14	32.1	4253	4	6.75	0.62
2	80		-103		253	-173	23.93	72.08	50	08/02/17	32.9	3408	3	7.00	0.60
3	103	12	-80		244	-141	24.03	72.16	36	08/02/17	32.2	3117	3	7.25	1.36
4	46		-76		165	-119	23.85	71.89	70	08/02/18	31.5	5680	5	7.10	0.25
5	40	-82	-106		305	-265	23.72	71.84	83	08/02/19	35.4	3448	3	7.15	0.48
6	134	43	12		213	-79	24.09	72.23	26	08/02/21	30.0	2107	2	7.55	6.45
7	156		49		198	-42	24.13	72.27	20	08/02/21	33.4	1003	1	7.00	2.75
8	77	1	-109		244	-167	23.96	72.08	47	08/02/24	33.3	2147	2	7.50	2.31
9	98	-54	-115		305	-207	24.02	72.17	36	08/02/24	33.2	2165	2	7.15	2.33
10	53		-160		305	-252	23.79	71.90	73	08/02/25	35.6	4338	4	7.20	0.38
11	44	-79	-164		300	-256	23.75	71.88	77	08/02/27	35.8	3211	3	6.95	0.43
12	33		-58		165	-132	23.66	71.74	95	08/02/27	33.2	3748	3	7.00	0.33
13	35	-72	-178		297	-262	23.72	71.81	85	08/02/27	38.6	3345	3	7.50	0.37
14	172	142	81		251	-79	24.16	72.31	15	08/02/28	32.6	893	1	7.40	2.87
15	220								8	08/02/28	28.7	764	1	6.80	8.60
16	91	-49	-61		274	-183	23.96	72.16	40	08/02/28	30.2	4110	4	7.00	0.69
17	69	-41	-53		191	-122	23.87	71.97	62	08/02/29	32.7	3864	3	6.95	0.75
18	229		192	165	67	162	24.22	72.45	0	08/03/03	29.7	841	1	7.30	8.45
19	202	156	165		82	120	24.21	72.38	6	08/03/03	30.2	768	1	7.20	9.05
20	90	-38	-62		335	-245	23.89	72.11	49	08/03/03	35.4	2598	2	7.20	1.23
21	127	51	36		251	-124	23.59	72.69	37	09/01/27	37.0	1599	1	7.07	0.22
22	112		-10		229	-117	23.54	72.60	47	09/01/27	32.0	1167	1	6.90	3.85
23	121	-31	45		198	-77	23.57	72.63	43	09/01/28	30.1	725	1	7.07	4.50
24	149		138	140	145	4	23.76	72.86	12	09/01/28-29	31.5	1592	1	7.29	2.00
25	146	103	146	123	98	48	23.75	72.81	17	09/01/29	30.9	535	0	7.00	4.50
26	181		169	169	305	-124	23.81	72.96	0	09/01/29	35.2	2281	2	6.91	0.30
27	182		167	161	198	-16	23.80	72.93	3	09/01/30	32.3	2952	3	6.93	1.32
28	59	-69	-32		244	-185	23.27	72.30	90	09/01/31	33.3	1640	1	7.27	1.20
29	37		-54		191	-154	23.16	72.17	108	09/02/01	32.8	2057	2	7.50	0.50
30	138	62	62		91	47	23.63	72.75	30	09/02/01	30.0	897	1	7.05	7.30
31	133	72	--	63	113	20	23.67	72.82	21	09/02/04	31.6	1042	1	7.02	6.15
32	95		34		238	-143	23.44	72.51	62	09/02/04	31.8	1968	2	6.90	4.25
33	116		24		295	-179	23.49	72.57	53	09/02/04	32.5	1136	1	7.04	5.37
34	60		-31		186	-126	23.26	72.28	93	09/02/05	34.2	1366	1	7.28	3.55
35	92		31		213	-121	23.37	72.39	75	09/02/05	31.4	1610	1	7.16	4.20
36	83	-39	-1		213	-130	23.36	72.38	78	09/02/06	31.8	1142	1	7.25	5.11
37	31		-45		213	-182	23.09	72.07	121	09/02/08	37.7	2075	2	8.02	0.35
38	91		0		229	-138	23.42	72.44	69	09/02/10	31.3	1291	1	7.06	3.12
39	71		-51		191	-120	23.33	72.34	83	09/02/11	31.7	1488	1	7.28	3.98
40	88		-19		213	-125	23.41	72.42	71	09/02/16	31.7	1084	1	7.16	2.30
41									59	09/02/16	32.7	1140	1	7.11	11.40
42									11	09/02/19	28.4	1248	1	7.08	6.84
43	154	--		143	76	78	23.77	72.87	11	09/02/19	28.4	1171	1	6.98	6.06
44	180	95	171	171	137	43	23.80	72.96	1	09/02/19	31.7	911	1	7.11	2.16
45	127	20	36		152	-25	23.57	72.70	37	10/02/03	31.6	1040	1	6.88	2.50
46	133	60	69		88	45	23.57	72.71	37	10/02/03	29.9	925	1	6.84	6.15
47	44	-88	-164		300	-256	23.75	71.88	78	10/02/05	36.2	3280	3	6.89	0.25
48	43	-71	-94		274	-231	23.13	72.30	99	10/02/08	36.5	1450	1	7.36	0.41
49	42	--			366	-324	23.27	72.13	101	10/02/08	40.1	1633	1	7.66	0.24
50	56	-5	-57		143	-87	23.85	71.94	65	10/02/09	30.9	4600	4	6.95	0.43
51	10	-8	-112		229	-219	22.67	72.20	145	10/02/10	41.3	3500	3	7.70	0.55
52	12	-22	-110		200	-188	22.68	72.15	145	10/02/10	40.5	3815	3	7.49	0.20
53	46	-76	-70		213	-167	23.22	72.23	100	10/02/12	33.6	1610	1	7.19	0.60
TS1							22.91	73.14	-10	09/02/14	49.0	9383	8	6.74	1.45
TS2							22.80	73.46	-12	09/02/14	61.6	4741	4	6.57	1.20

Table D.2.: Mastertable (2):

No	Alk. err	Fluoride	Chloride	NO ₃	SO ₄	Tritium	ΔT	$\delta^{13}C$	err	Act.	err	Category	q	err	cal. Age	σ age	
	mmol/l	ppm	ppm	ppm	ppm	TU		‰		pmC					yr		
1	6	0.1		412	3.9	41.9	0.2	1.0	-7.6	0.1	30.9	0.2	P TRA	0.8	0.1	9391	1558
2	5.5	0.1	0.66	805	3.2	76.8	0.8	0.9	-7.6	0.1	28.2	0.2	P TRA	0.8	0.2	10657	2205
3	6.9	0.1	0.83	529		44.6	1.2	1.0	-9.1	0.1	47.5	0.3	P OPT	0.8	0.1	5124	1000
4	5.9	0.1	0.35	1617	39.2	252	0.5	0.9	-7.6	0.1	35.4	0.2	P TRA	0.8	0.2	8693	2308
5	3.6	0.1		884	45.9	333	0.0	0.9	-7.6	0.1	6.2	0.1	P GLA	1.0	0.4	30361	6499
6	8	0.1	0.62	374	12.3	91	1.0	0.9	-10.2	0.1			P OPT			3526	3000
7	7.1	0.1	0.74	186	63.3	38.3	1.1	0.9	-8.4	0.1	77.5	0.3	P MOD	0.8	0.05	596	388
8	7.3	0.1	0.72	630	61.8	44.6	1.1	0.9	-7.7	0.1	43.6	0.3	P OPT	0.7	0.2	6096	3649
9	8.5	0.1	1.16	495	4.7	168	0.8	1.0	-8.3	0.1	38.5	0.2	P OPT	0.8	0.04	6316	432
10	4.5	0.1	0.33	1575	53.3	365	0.0	1.0	-6.9	0.1	8.9	0.1	P GLA	0.9	0.3	25160	5718
11	5	0.1	0.39	878	4	346	0.1	0.9	-6.1	0.1	5.1	0.1	P GLA	0.8	0.2	27509	2355
12	4.1	0.1	0.31	1163	3.2	354	0.1	0.9	-7.9	0.1	3.2	0.1	P GLA	1.0	0.3	33676	3465
13	3.5	0.1	0.75	1054		86.8	0.2	0.9	-12.1	0.1	0.6	0.1	P PLE-TS	1.1	0.5	45762	5000
14	6.7	0.1	0.68	100	39.2	31.2	1.8	0.9	-8.8	0.1	78.7	0.3	P MOD	0.8	0.2	2068	1793
15			0.85	1292	45.9	115											
16	9.1	0.1	0.51	1291	12.3	130	0.5	1.0	-8.5	0.1	42.8	0.2	P OPT	0.8	0.1	5537	1329
17	7.3	0.1	0.74	88.9	61.1	13.9	1.2	0.9	-8.1	0.1	33.7	0.2	P TRA	0.8	0.1	8035	722
18	6.5	0.1	0.78	86.1	63	11.2	3.1	0.9	-9.7	0.1	107.3	0.5	CRY	0.9	0.1	756	771
19	5.9	0.1	0.44	619	4.7	276	3.3	1.0	-9.1	0.1	95.6	0.4	CRY	0.9	0.1	1324	1260
20	6.1	0.1	0.72	64.2	49.4	11.1	0.8	0.9	-7.0	0.1	15.6	0.1	P GLA	0.8	0.2	16103	2891
21	4.1	0.1					0.0	1.1	-10.4	0.1	6.8	0.1	P GLA	1.0	0.3	27122	2934
22	7	0.1					0.6	1.1	-9.2	0.1	77.3	0.3	P LHO	0.9	0.1	1120	721
23	5.8	0.1					0.0	1.1	-8.3	0.1	74.2	0.3	P LHO	0.9	0.1	2063	1394
24	11.6	0.1					4.9	1.3	-10.3	0.1	99.3	0.4	CRY	0.7	0.2	2386	3270
25	4.6	0.1					0.1	1.0	-10.9	0.1			CRY			1760	3000
26	8	0.1					2.1	1.1	-10.0	0.1	65.7	0.3	CRY	0.9	0.1	2731	1512
27	6.1	0.1					1.1	1.1	-10.4	0.1	74.1	0.4	CRY	0.9	0.1	2131	1009
28	6.5	0.1					0.0	1.1	-7.5	0.1	27.8	0.2	P TRA	0.8	0.2	10668	2755
29	8.5	0.1					0.0	1.0	-6.1	0.1	10.5	0.2	P GLA	0.6	0.2	20322	6151
30	7	0.1					2.5	1.2	-9.7	0.1	101.8	0.4	P MOD	0.9	0.1	305	261
31	8.5	0.1					2.1	1.0	-10.0	0.1	91.8	0.4	CRY	0.8	0.1	1134	1083
32	9.5	0.1					1.4	1.0	-10.5	0.1	76.5	0.3	P LHO	0.8	0.2	3427	3195
33	7.6	0.1					0.2	1.0	-9.4	0.1	68.5	0.3	P LHO	0.8	0.1	1676	618
34	6	0.1					0.1	1.3	-7.6	0.1	14.1	0.1	P GLA	0.8	0.2	17256	2873
35	7	0.1					0.9	1.1	-9.1	0.1	60.7	0.3	P LHO	0.8	0.05	2694	574
36	8.9	0.1					0.4	0.9	-9.1	0.1	63.6	0.3	P LHO	0.8	0.1	1559	606
37	5.1	0.1					0.0	0.9	-14.2	0.1	0.4	0.04	P PLE-TS	1.0	0.3	47746	5000
38	8	0.1					0.3	1.1	-9.8	0.1	66.9	0.3	P LHO	0.8	0.1	2130	1052
39	9.5	0.1					0.9	1.2	-9.1	0.1	62.7	0.3	P LHO	0.7	0.1	1647	847
40	6.5	0.1					0.0	0.9	-9.5	0.1	54.7	0.3	P LHO	0.9	0.1	4241	942
41																	
42																	
43	7.9	0.1					2.7	0.9	-10.7	0.1			CRY			1447	3000
44	7	0.1					2.4	0.9	-11.8	0.1			CRY			2559	3000
45							0.5	0.9					P LHO			1184	3000
46							0.6	0.9					P MOD			745	3000
47							0.0	0.9	-6.1	0.1	5.1	0.1	P GLA	0.8	0.3	27577	2563
48							0.0	0.9	-10.3	0.1	4.8	0.02	P GLA	1.0	0.3	30743	4330
49							0.0	0.9	-12.4	0.1	1.2	0.1	P PLE-TS	1.0	0.4	41375	5000
50							0.0	1.0					P TRA			8706	3000
51							0.0	1.0					TS-P PLE			50000	10000
52							0.0	0.9					TS-P PLE			55000	10000
53							0.0	0.9	-5.6	0.1	15.4	0.01	P GLA	0.7	0.2	17351	5870
TS1	1.5	0.1											TS-CRY				
TS2	2.9	0.1											TS-CRY				

Table D.3.: Mastertable (3):

No	ALK	ALK mod	CMB calc	CMB meas	C13 17‰	C13 Mün	C13 mod 17‰	F&G Alk 17‰	F&G mod 17‰	C13 22‰	C13 mod 22‰	F&G Alk 22‰	F&G mod 22‰
	yr	yr	yr	yr	yr	yr	yr	yr	yr	yr	yr	yr	yr
1	5816	9719	8522	8951	3028	9259	6698	-2980	6771	1131	3813	-7279	2779
2	5936	9595	8334	11401	3784	10015	7615	-71	7560	1887	4569	-4220	3614
3	1170	3455	5281	5710	1026	7258	4697	861	4137	-897	1786	-3233	114
4	3872	7053	8748	9178	1896	8128	5567	-1696	5210	0	2682	-5918	1176
5	18109	22000	24826	27893	16235	22467	20067	13339	20210	14339	17021	9365	16398
6													
7	-2438	1236	434	863	-3746	2485	-75	-5703	336	-5656	-2974	-9764	-3589
8	1576	2111	5837	6266	261	6492	3932	-1670	-156	-1637	1045	-5727	-4169
9	3054	5993	5042	5471	1936	8167	5607	314	5228	28	2710	-3749	1278
10	15116	18815	20120	23187	12589	18821	16421	8183	16030	10704	13386	4173	12230
11	20229	24678	23239	26306	16146	22378	19978	5133	20094	14275	16957	715	16329
12	23963	28320	28865	31932	22153	28385	25985	19164	26920	20251	22933	15063	23001
13	36444	38562	44393	47460	37990	43297	42742	39151	40661	36219	39620	36005	37539
14	-3190	-2120	1592	2021	-3438	2793	232	-3730	-1870	-5356	-2674	-7801	-5897
15													
16	2482	6132	3155	3584	1260	7492	4931	-753	5672	-651	3695	-5015	1562
17	4549	8429	6904	7333	2890	9122	6561	175	7153	984	3667	-3951	3193
18	-5617	-3710	-877	-447	-5200	1032	-1529	-4630	-1970	-7132	-4450	-8869	-6152
19	-4518	-2075	728	1158	-4841	1391	-1170	-5281	-1461	-6762	-4080	-9504	-5598
20	10430	13073	12836	15903	8063	14295	11895	4051	10030	6176	8858	47	6195
21	17573	21750	22880	25947	18194	24425	22025	18846	22945	16249	18931	15007	19177
22	-2178	1865	228	658	-2905	3327	766	-3941	1890	-4830	-2148	-8074	-2122
23	-2179	1130	2678	3107	-3429	2802	242	-5504	559	-5339	-2657	-9773	-3563
24	-4993	-2982	-5236	-4806	-4099	2133	-428	-3033	-655	-6042	-3360	-7158	-4734
25													
26	-893	3168	517	946	-879	5353	2792	-854	3793	-2817	-135	-4792	-60
27	-1899	2034	1863	2292	-1588	4643	2083	-1198	3356	-3533	-851	-5295	-655
28	5555	7705	10255	10684	3798	10029	7469	955	5556	1902	4584	-3130	1596
29	13345	13881	16292	16722	10209	16440	13880	3144	6346	8335	11017	-1150	2214
30	-4766	-1351	-1609	-1180	-4754	1478	-1083	-4723	-119	-6687	-4005	-8958	-4261
31	-3876	-295	-2485	-2055	-3682	2549	-12	-3424	998	-5620	-2938	-7558	-3051
32	-2107	1948	-2311	-1882	-1767	4465	1904	-1336	3343	-3713	-1031	-5463	-696
33	-1503	1986	962	1391	-1786	4445	1885	-2147	2553	-3714	-1032	-6234	-1438
34	11180	13256	13968	17035	9613	15844	13445	7243	11366	7714	10396	3222	7452
35	-710	2150	2948	3377	-1077	5155	2594	-1567	2650	-2999	-317	-5717	-1410
36	-1252	1037	669	1098	-1437	4794	2233	-1660	1685	-3360	-678	-5779	-2362
37	41115	41823	46349	49416	44220	49526	48971	46304	46667	42413	45814	43108	43477
38	-1330	2053	763	1192	-1209	5023	2462	-1037	3289	-3144	-462	-5189	-777
39	-1166	906	285	715	-1265	4966	2406	-1370	1663	-3189	-507	-5493	-2394
40	147	2978	4456	4885	215	6446	3886	321	4085	-1715	967	-3806	36
41													
42													
43													
44													
45													
46													
47	20464	24680	23644	26711	16148	22380	19980	3563	19490	14275	16957	-1004	15733
48	19975	22890	25209	29250	20897	54541	24728	21847	24691	18953	21636	17991	20886
49	31107	31926	36957	40998	32960	65963	37711	34264	34869	31900	34583	32319	32930
50													
51													
52													
53	10652	13281	15147	14472	6302	44948	9973	-9421	6530	4436	7119	-14647	n.a.n.
TS1													
TS2													

Stat. Model used 80% pmC. Isotope models used a soil CO₂ isotope amount of -17‰ (and -22‰ which was not used for the mean). Recharge water for young wells was simulated using 4% pCO₂, 29°C, pH=7, old water used 2.8%, 25°C, ph=7.

Table D.4.: Mastertable (4):

No	radon Bq/l	err	³ He/ ⁴ He	err	Ne/He	err	n.a. ⁴ He ccSTP/g	err	rad. ⁴ He ccSTP/g	err	T- ³ He Age yr	err	He-Rn age k yr	err
1			7.6E-07	1E-08	4.18E-01	3.5E-03	6.25E-07	5.4E-09	5.83E-07	1.3E-08				
2			7.8E-07	1E-08	5.80E-01	4.6E-03	4.86E-07	4.0E-09	4.54E-07	1.1E-08				
3			8.4E-07	1E-08	5.86E-01	4.7E-03	5.27E-07	4.4E-09	4.88E-07	1.1E-08				
4			6.6E-07	1E-08	2.92E-01	2.3E-03	7.95E-07	6.1E-09	7.49E-07	1.4E-08				
5			3.1E-07	5E-09	1.45E-01	1.6E-03	1.89E-06	2.0E-08	1.84E-06	4.4E-08				
6			6.2E-07	2E-08	2.25E-01	3.1E-03	1.54E-06	2.1E-08	1.46E-06	5.4E-08				
7			1.1E-06	2E-08	1.01E+00	8.1E-03	2.54E-07	2.4E-09	2.29E-07	6.3E-09				
8			7.9E-07	1E-08	5.12E-01	4.1E-03	4.53E-07	3.7E-09	4.22E-07	8.8E-09				
9			7.4E-07	1E-08	6.28E-01	5.1E-03	4.74E-07	4.0E-09	4.46E-07	1.1E-08				
10			2.8E-07	4E-09	1.34E-01	1.1E-03	2.08E-06	1.5E-08	2.03E-06	4.1E-08				
11			2.2E-07	5E-09	1.38E-01	9.1E-04	2.08E-06	1.2E-08	2.05E-06	6.7E-08				
12			2.3E-07	4E-09	1.65E-01	1.3E-03	1.66E-06	1.2E-08	1.64E-06	3.9E-08				
13			3.3E-07	5E-09	9.34E-02	7.5E-04	3.10E-06	2.2E-08	3.01E-06	6.4E-08				
14			1.2E-06	2E-08	2.71E+00	2.2E-02	3.37E-08	8.1E-10	3.14E-08	2.6E-09	33	8		
15														
16			9.9E-07	2E-08	2.50E+00	2.0E-02	5.35E-08	1.1E-09	5.20E-08	8.2E-09				
17			5.6E-07	9E-09	2.66E-01	2.4E-03	9.83E-07	8.7E-09	9.35E-07	2.0E-08				
18			3.2E-07	1E-08	9.26E-02	1.1E-03	3.12E-06	3.6E-08	3.03E-06	1.2E-07	85	5		
19											?	?		
20			5.7E-07	8E-09	1.95E-01	1.6E-03	1.63E-06	1.2E-08	1.55E-06	2.8E-08	No noble gas information exists for well 19.			
21	65	3	1.3E-07	2E-09	2.15E-01	1.7E-03	1.08E-06	8.1E-09	1.08E-06	4.8E-08			91	77
22	8	2	6.6E-07	1E-08	7.49E-01	6.0E-03	2.42E-07	2.1E-09	2.31E-07	7.6E-09			166	140
23	37	2	4.8E-07	8E-09	8.13E-01	6.5E-03	2.46E-07	2.2E-09	2.40E-07	1.1E-08			36	30
24	294	6	8.7E-08	1E-09	1.63E-01	1.1E-03	1.74E-06	1.0E-08	1.73E-06	1.7E-07	17	3	33	28
25	330	6	5.0E-07	9E-09	1.51E+00	1.2E-02	1.12E-07	1.3E-09	1.12E-07	1.3E-09			2	2
26	1090	14	1.0E-07	2E-09	1.31E-02	1.0E-04	3.38E-05	2.4E-07	3.35E-05	1.1E-06	111	9	170	144
27	42	6	1.2E-07	3E-09	1.93E-02	1.6E-04	3.39E-05	2.4E-07	3.36E-05	1.0E-06			4385	3720
28	20	3	9.0E-07	1E-08	2.55E+00	1.7E-02	3.80E-08	6.2E-10	3.79E-08	3.6E-08			11	13
29	31	2	5.9E-07	9E-09	1.69E+00	1.4E-02	8.56E-08	1.1E-09	8.56E-08	1.1E-09			15	13
30	8	2	1.4E-06	2E-08	3.84E+00	2.5E-02	1.42E-09	3.4E-10	1.01E-09	4.6E-10	9	4	1	1
31	24	2	1.6E-07	2E-09	2.97E-01	1.9E-03	7.54E-07	4.7E-09	7.51E-07	3.7E-08	36	8	171	145
32	9	1	1.3E-06	4E-08	3.63E+00	4.2E-02	4.21E-09	5.2E-10	4.16E-09	1.9E-08			3	12
33	10	1	1.1E-06	3E-08	3.11E+00	2.6E-02	1.28E-08	4.2E-10	1.27E-08	9.8E-09			7	8
34	12	1	7.0E-07	2E-08	1.91E+00	1.6E-02	6.51E-08	9.0E-10	6.48E-08	4.1E-08			29	31
35	13	1	1.4E-06	2E-08	3.70E+00	2.4E-02	3.53E-09	3.5E-10	3.08E-09	9.1E-10			1	1
36	9	1	1.3E-06	2E-08	3.65E+00	2.4E-02	3.66E-09	3.9E-10	3.38E-09	1.4E-09			2	2
37	14	1	9.7E-07	1E-08	4.89E-02	3.2E-04	5.28E-06	3.1E-08	4.78E-06	7.1E-08			1845	1565
38	14	1	1.3E-06	2E-08	3.53E+00	2.8E-02	6.15E-09	4.7E-10	5.68E-09	1.8E-09			2	2
39	13	1	1.2E-06	4E-08	3.48E+00	4.0E-02	7.45E-09	7.7E-10	7.34E-09	2.1E-08			3	9
40	10	3	1.1E-06	2E-08	3.02E+00	2.0E-02	2.12E-08	5.7E-10	2.12E-08	5.7E-10			12	10
41	--	--												
42	--	--												
43	--	--	1.4E-06	3E-08	3.86E+00	3.1E-02	1.46E-09	3.3E-10	1.13E-09	5.3E-10	7	3		
44	--	--	1.3E-07	2E-09	1.60E-01	1.4E-03	3.32E-06	2.4E-08	3.30E-06	1.3E-07	63	7		
45	--	--	1.1E-06	4E-08	2.94E+00	3.4E-02	2.84E-08	1.3E-09	2.83E-08	1.9E-07				
46	--	--	1.4E-06	3E-08	3.86E+00	3.1E-02	6.16E-10	3.5E-10	5.56E-10	1.5E-09				
47	--	--	2.2E-07	5E-09	1.38E-01	9.1E-04	2.08E-06	1.2E-08	2.05E-06	6.7E-08				
48	--	--	3.2E-07	1E-08	5.71E-01	6.5E-03	4.03E-07	4.7E-09	3.98E-07	4.2E-08				
49	--	--	6.6E-07	2E-08	2.22E-01	1.8E-03	1.10E-06	8.3E-09	1.04E-06	2.9E-08				
50	--	--	7.8E-07	2E-08	2.23E-01	1.8E-03	1.22E-06	9.1E-09	1.13E-06	3.2E-08				
51			4.5E-07	1E-08	1.12E-02	9.1E-05	2.17E-05	1.5E-07	2.08E-05	5.4E-07				
52			3.4E-07	1E-08	7.90E-03	9.1E-05	3.06E-05	3.1E-07	2.97E-05	1.2E-06				
53			6.3E-07	2E-08	1.74E+00	2.0E-02	8.90E-08	1.6E-09	8.89E-08	1.6E-07				
TS1	95	3	5.5E-08	1E-09	1.91E-03	1.5E-05	6.41E-05	4.5E-07	6.39E-05	2.0E-06				
TS2	3834	31	6.9E-08	3E-09	1.59E-03	1.8E-05	2.72E-04	2.7E-06	2.70E-04	1.5E-05				

Table D.5.: Mastertable (5):

No	SF ₆	err	δ ¹⁸ O	err	δD	err	D excess	err	NGT	err	Δ Ne	err
	fmol/l		‰		‰		‰		°C		%	
1	46.4	59.7	-3.62	0.05	-24.0	0.1	4.9	0.09	28.9	0.9	69.7%	0.4%
2	5.2	1.2	-3.65	0.05	-22.7	0.1	6.5	0.09	26.0	0.7	90.6%	0.5%
3	8.2	3.7	-3.97	0.05	-24.6	0.1	7.1	0.09	27.2	0.7	110.1%	0.7%
4	2.9	0.1	-3.49	0.05	-22.5	0.1	5.5	0.09	28.0	0.7	46.4%	0.3%
5	33.5	7.3	-3.11	0.05	-20.3	0.1	4.6	0.09	26.8	0.7	61.5%	0.4%
6	15.1	16.0	-4.30	0.05	-27.4	0.1	6.9	0.09	25.6	0.9	95.2%	0.6%
7	3.7	0.1	-4.11	0.05	-26.6	0.1	6.3	0.09	27.9	0.7	102.0%	0.6%
8	5.9	1.4	-3.84	0.05	-23.8	0.1	6.9	0.09	29.1	0.7	56.4%	0.3%
9	39.3	4.9	-3.55	0.05	-22.2	0.1	6.3	0.09	26.6	0.7	103.9%	0.6%
10	57.6	8.8	-3.15	0.05	-20.3	0.1	4.9	0.09	26.0	0.6	64.8%	0.4%
11	90.4	28.4	-2.91	0.05	-18.4	0.1	4.9	0.09	23.6	0.4	67.1%	0.4%
12	89.2	18.6	-3.02	0.05	-19.2	0.1	4.9	0.09	25.7	0.6	59.9%	0.4%
13	4.3	3.6	-4.13	0.05	-27.2	0.1	5.8	0.09	26.1	0.6	69.1%	0.4%
14	4.0	3.3	-4.42	0.05	-28.7	0.1	6.7	0.09	26.8	0.7	77.8%	0.5%
15												
16	7.3	0.2	-3.89	0.05	-24.6	0.1	6.5	0.09	26.8	0.8	124.0%	0.7%
17	4.1	0.7	-3.48	0.05	-23.3	0.1	4.6	0.09	28.2	0.8	63.1%	0.4%
18	3.0	0.6	-4.35	0.05	-28.1	0.1	6.7	0.09	24.8	0.8	33.6%	0.2%
19	2.5	1.3	-4.20	0.05	-27.6	0.1	6.0	0.09				
20	13.4	0.2	-3.33	0.05	-21.6	0.1	5.1	0.09	26.4	0.7	91.0%	0.5%
21	0.5	0.1	-3.52	0.05	-21.4	0.1	6.7	0.09	25.8	0.8	39.3%	0.2%
22	1.8	0.2	-3.57	0.05	-22.3	0.1	6.2	0.09	29.0	0.6	30.5%	0.2%
23	1.6	0.0	-3.77	0.05	-23.1	0.1	7.1	0.09	30.3	0.7	48.0%	0.3%
24	1135.7	13.7	-3.36	0.05	-22.8	0.1	4.1	0.09	26.9	0.7	69.8%	0.4%
25	117.7	19.5	-3.67	0.05	-22.5	0.1	6.9	0.09	25.1	1.1	54.2%	0.3%
26	3994.8	400.0	-2.87	0.05	-16.3	0.1	6.7	0.09	27.2	0.8	154.8%	0.9%
27	25.8	0.9	-2.99	0.05	-18.4	0.1	5.5	0.09	24.2	0.7	270.2%	1.6%
28	1.4	0.1	-2.98	0.05	-18.0	0.1	5.9	0.09	27.1	0.6	54.1%	0.3%
29	2.5	0.8	-2.96	0.05	-18.4	0.1	5.3	0.09	25.6	0.7	44.4%	0.3%
30	1.2	0.0	-4.05	0.05	-23.3	0.1	9.1	0.09	29.0	0.7	32.1%	0.2%
31	4.1	0.0	-3.29	0.05	-20.7	0.1	5.6	0.09	28.2	0.6	38.8%	0.2%
32	1.8	0.2	-3.46	0.05	-20.6	0.1	7.1	0.09	27.4	0.7	8.5%	0.1%
33	1.7	0.3	-3.64	0.05	-21.7	0.1	7.5	0.09	28.9	0.5	8.4%	0.1%
34	5.3	0.1	-3.18	0.05	-17.9	0.1	7.5	0.09	25.3	0.5	37.3%	0.2%
35	1.5	0.4	-3.71	0.05	-22.2	0.1	7.5	0.09	28.3	0.5	28.9%	0.2%
36	1.4	0.1	-3.52	0.05	-22.2	0.1	6.0	0.09	29.0	0.5	44.0%	0.3%
37	1.0	0.0	-3.43	0.05	-21.7	0.1	5.7	0.09	25.0	0.6	46.7%	0.3%
38	1.4	0.3	-3.43	0.05	-21.2	0.1	6.3	0.09	30.6	0.8	37.0%	0.2%
39	1.3	0.1	-3.61	0.05	-20.8	0.1	8.0	0.09	27.7	0.9	54.7%	0.3%
40	4.4	0.0	-3.38	0.05	-19.1	0.1	7.9	0.09	27.6	0.5	71.7%	0.4%
41												
42												
43	2.2	0.0	-3.71	0.05	-26.2	0.1	3.5	0.09	27.3	0.5	3.5%	0.0%
44			-3.89	0.05	-24.5	0.1	6.6	0.09	30.2	1.1	213.8%	1.3%
45	3.5	0.2	-3.49	0.05	-22.7	0.1	5.2	0.09	28.4	0.8	118.4%	0.7%
46	0.9	0.1	-4.36	0.05	-27.7	0.1	7.2	0.09	29.7	0.7	10.7%	0.1%
47			-2.92	0.05	-19.5	0.1	3.9	0.09	23.6	0.4	67.1%	0.4%
48	5.0	0.3	-3.56	0.05	-20.1	0.1	8.4	0.09	25.0	1.0	52.4%	0.3%
49	0.9	0.2	-3.50	0.05	-19.5	0.1	8.5	0.09	21.8	0.5	42.1%	0.3%
50	4.9	0.0	-3.42	0.05	-21.4	0.1	6.0	0.09	26.1	0.6	64.0%	0.4%
51	0.6	0.3	-3.36	0.05	-19.8	0.1	7.1	0.09	24.2	0.5	37.2%	0.2%
52	1.3	1.6	-3.48	0.05	-20.2	0.1	7.6	0.09	25.5	0.8	37.8%	0.2%
53	2.4	0.1	-3.06	0.05	-18.8	0.1	5.7	0.09	23.7	0.7	57.0%	0.3%
TS1	0.7	0.0	-2.35	0.05	-16.8	0.1	2.0	0.09				
TS2	24.9	0.2	-2.10	0.05	-11.9	0.1	5.0	0.09				

D.2.1. Noble 2007

Table D.6.: Preliminary fit (1):

No.	ACE								APR							
	ccSTP /l	σ A	F _{CE}	σ F	T _{CE} °C	σ T	Chi ²	Prob	ccSTP /l	σ A	F _{PR}	σ F	T _{PR} °C	σ T	Chi ²	Prob
01_3	17	4	0.38	0.05	25.9	1.3	2.2	0.14	26	10	1.35	0.36	29.0	2.6	0.3	0.57
01_4	28	5	0.44	0.02	30.1	1.2	0.1	0.74	37	9	1.66	0.23	33.0	1.9	0.7	0.41
02_2	18	3	0.25	0.04	26.2	1.2	0.3	0.57	22	6	0.89	0.24	27.9	1.9	0.0	0.91
02_3	16	2	0.25	0.04	25.8	0.8	0.4	0.52	18	4	0.78	0.20	26.9	1.2	0.0	0.88
03_2	19	3	0.21	0.03	26.9	1.0	4.6	0.03	21	4	0.70	0.19	27.8	1.4	7.1	0.01
03_3	19	2	0.21	0.03	27.4	0.9	0.7	0.39	23	4	0.76	0.17	28.7	1.3	0.1	0.78
04_2	9	4	0.35	0.12	26.6	1.0	3.3	0.07	11	5	0.86	0.42	27.8	1.6	2.2	0.14
04_3	19	5	0.54	0.04	28.9	1.0	1.4	0.24	21	7	1.57	0.33	30.7	1.6	0.2	0.64
05_2	9	3	0.22	0.12	24.5	1.0	0.1	0.77	9	3	0.45	0.35	25.0	1.4	0.0	0.94
05_3	15	3	0.36	0.05	27.9	0.9	0.1	0.77	17	4	0.98	0.25	29.0	1.3	0.1	0.81
06_1	17	3	0.18	0.05	26.0	1.2	0.0	0.88	21	5	0.65	0.25	27.6	2.1	0.2	0.67
06_2	17	3	0.27	0.05	25.1	1.2	2.6	0.11	25	7	1.04	0.28	27.9	2.3	0.6	0.43
07_2	14	2	0.16	0.06	26.0	1.1	2.3	0.13	14	4	0.40	0.24	26.4	1.5	3.4	0.06
07_3	19	2	0.23	0.03	28.9	0.9	1.0	0.32	23	4	0.85	0.18	30.4	1.3	0.1	0.72
08_2	10	3	0.32	0.10	27.4	1.1	0.3	0.57	10	4	0.67	0.38	28.1	1.6	0.8	0.36
08_3	19	4	0.46	0.04	30.0	1.0	1.0	0.32	22	6	1.38	0.28	31.8	1.6	0.1	0.78
09_2	19	3	0.24	0.04	25.0	1.2	0.0	0.86	24	6	0.88	0.23	26.6	1.8	0.3	0.58
09_3	23	3	0.27	0.03	27.4	0.9	0.5	0.48	30	5	1.08	0.17	29.5	1.5	0.0	0.87
10_2	6	2	0.00	0.24	23.3	0.9	0.4	0.54	6	2	0.00	0.36	23.3	1.2	0.4	0.54
10_3	15	3	0.35	0.05	27.3	0.8	1.7	0.19	18	5	1.03	0.24	28.7	1.3	0.6	0.45
11_2	10	3	0.20	0.11	24.3	1.0	1.1	0.30	10	3	0.38	0.33	24.5	1.4	1.6	0.21
11_3	19	3	0.37	0.04	28.4	0.9	0.0	0.88	22	5	1.14	0.22	29.9	1.4	0.3	0.58
12_2	10	3	0.27	0.10	24.1	1.0	0.4	0.55	10	4	0.53	0.35	24.5	1.4	0.8	0.38
12_3	13	3	0.32	0.06	26.5	0.8	0.0	0.83	14	4	0.81	0.25	27.3	1.1	0.0	0.83
13_2	8	3	0.12	0.14	24.2	1.0	0.0	0.93	8	3	0.23	0.33	24.4	1.3	0.0	0.83
13_3	14	3	0.31	0.05	27.0	0.8	0.4	0.52	16	4	0.85	0.23	28.0	1.2	0.0	0.86
14_2	11	3	0.19	0.08	25.3	1.0	0.1	0.74	12	4	0.48	0.29	25.9	1.4	0.0	0.97
14_3	16	3	0.30	0.04	27.8	0.9	1.4	0.24	19	4	0.93	0.21	29.1	1.3	0.4	0.54
16_2	21	3	0.20	0.03	26.9	1.3	1.3	0.25	26	5	0.77	0.20	28.3	1.9	3.6	0.06
16_3	22	2	0.21	0.02	26.7	0.9	1.9	0.17	30	5	0.91	0.16	28.7	1.4	0.4	0.55
17_2	22	4	0.45	0.03	29.0	1.0	2.1	0.15	27	7	1.50	0.25	31.2	1.6	0.3	0.58
17_3	14	4	0.36	0.07	26.3	1.2	1.6	0.20	19	8	1.14	0.38	28.6	2.4	0.4	0.54
18_1	10	3	0.22	0.10	25.4	1.0	0.8	0.38	12	4	0.59	0.36	26.4	1.7	0.3	0.58
18_3	41	10	0.54	0.02	24.0	1.2	2.0	0.15	57	17	2.26	0.27	27.9	2.3	0.1	0.82
19_2	147	643	0.76	0.01	19.1	10.7	7.7	0.01	83	46	3.26	0.47	22.2	3.7	12.6	0.00
19_3	143	751	0.75	0.01	20.5	13.4	34.5	0.00	180	102	3.89	0.47	30.0	6.3	31.6	0.00
20_2	19	3	0.29	0.04	25.9	1.2	2.8	0.10	27	7	1.10	0.24	28.4	2.0	0.6	0.43
20_3	19	3	0.27	0.03	26.5	0.8	1.4	0.24	23	5	0.95	0.19	28.0	1.3	0.3	0.61
21_1	18	6	0.56	0.05	24.7	1.0	0.0	0.99	17	7	1.43	0.39	25.9	1.5	0.4	0.55
21_2	26	9	0.61	0.03	26.8	1.3	0.7	0.42	23	10	1.80	0.40	28.2	2.0	2.5	0.11
22_1	10	5	0.56	0.10	28.9	0.8	0.1	0.74	7	4	0.98	0.49	29.4	1.1	0.0	0.93
22_2b	12	5	0.57	0.08	29.1	1.0	0.3	0.57	10	5	1.21	0.47	30.0	1.5	0.1	0.81
23_1	14	4	0.45	0.06	29.2	0.9	0.2	0.63	13	4	1.03	0.32	30.0	1.3	0.9	0.35
23_2	21	6	0.52	0.04	31.6	1.2	0.0	0.94	22	8	1.56	0.32	33.4	1.9	0.4	0.53
24*_2	28	6	0.44	0.02	27.3	1.2	0.1	0.77	38	10	1.69	0.25	30.1	2.0	0.7	0.40
24_2	30	6	0.46	0.02	27.4	1.2	0.1	0.72	40	11	1.78	0.25	30.4	2.1	0.6	0.44
24_3	25	5	0.43	0.03	26.0	1.1	0.2	0.70	31	8	1.51	0.25	28.3	1.8	0.7	0.39
25_1	101	135	0.61	0.02	27.2	7.0	0.1	0.75	85	32	2.73	0.34	30.0	3.6	5.8	0.02
25_2	132	444	0.59	0.01	29.6	18.2	6.9	0.01	0	0						
25_3	140	404	0.61	0.01	28.9	14.6	0.1	0.75	103	39	2.89	0.34	31.8	4.0	3.2	0.07
26_1	35	3	0.23	0.01	27.3	1.1	0.4	0.51	54	8	1.28	0.14	31.1	1.8	0.4	0.54
26_2	36	4	0.23	0.01	27.1	1.2	0.0	0.96	57	9	1.32	0.15	31.1	2.1	1.7	0.19
	0	0							113	22	2.04	0.18	42.1	3.9	0.0	1.00
27_1	37	2	0.08	0.01	23.2	0.9	0.1	0.77	47	5	0.56	0.10	25.1	1.3	1.1	0.29
27_2	41	2	0.09	0.01	25.8	1.2	2.0	0.16	55	6	0.73	0.11	28.6	1.8	4.5	0.03
27_3	50	4	0.12	0.01	32.0	1.8	5.7	0.02	83	11	1.11	0.12	39.5	3.3	0.4	0.55
28_1	13	3	0.38	0.07	25.2	0.8	0.1	0.80	13	4	0.89	0.30	26.0	1.2	0.1	0.81
28_2	19	4	0.45	0.04	27.9	1.1	0.6	0.43	20	6	1.26	0.29	29.2	1.6	2.1	0.15
28_3	19	4	0.44	0.04	28.1	1.0	0.5	0.48	21	6	1.33	0.28	29.8	1.6	0.0	0.93
29_1	31	10	0.60	0.03	27.2	1.4	0.0	0.83	33	13	2.03	0.37	29.5	2.2	0.8	0.38
29_2	117	783	0.78	0.02	26.1	15.6	24.4	0.00	92	61	3.50	0.55	31.6	5.0	29.6	0.00

Table D.7.: Preliminary fit (2):

No.	ACE								APR							
	ccSTP /l	σ_A	F _{CE}	σ_F	T _{CE} °C	σ_T	Chi ²	Prob	ccSTP /l	σ_A	F _{PR}	σ_F	T _{PR} °C	σ_T	Chi ²	Prob
29_3	16	4	0.49	0.05	24.4	0.9	1.6	0.20	17	6	1.31	0.34	25.7	1.4	0.5	0.47
30_1	20	8	0.65	0.04	28.3	0.9	3.2	0.07	14	6	1.55	0.43	28.9	1.4	5.5	0.02
30_2	49	33	0.70	0.02	31.8	2.4	0.4	0.54	35	17	2.35	0.44	33.5	2.7	3.1	0.08
30_3	16	6	0.61	0.05	27.6	0.9	0.0	0.87	13	6	1.39	0.43	28.5	1.4	0.6	0.44
31_1	21	7	0.59	0.04	28.0	1.1	1.0	0.32	18	8	1.56	0.40	29.1	1.7	2.7	0.10
31_2	28	10	0.60	0.03	29.8	1.4	0.7	0.40	27	11	1.87	0.38	31.5	2.1	2.8	0.09
31_3	18	6	0.58	0.04	27.1	0.8	0.3	0.58	17	6	1.53	0.36	28.3	1.4	0.0	0.92
32_1	115	2018	0.90	0.02	30.3	16.4	0.9	0.35	38	51	3.57	1.10	32.7	4.5	0.3	0.59
32_2	100	1915	0.91	0.04	30.5	17.1	7.3	0.01	29	42	3.41	1.22	32.3	4.1	8.2	0.00
32_3	1	9	0.01	9.67	27.4	0.7	2.6	0.11	1	2	0.20	1.90	27.5	0.9	2.5	0.11
33_1	38	66	0.89	0.03	30.4	1.7	0.5	0.50	14	18	2.68	1.18	31.5	2.4	0.1	0.80
33_2	86	799	0.90	0.03	31.7	9.7	2.2	0.14	15	21	2.73	1.24	32.1	2.8	3.7	0.05
33_3	1	8	0.00	8.91	28.4	0.7	1.1	0.30	1	2	0.00	1.81	28.4	0.8	1.1	0.30
34_1	7	3	0.33	0.18	24.6	0.6	6.8	0.01	5	2	0.32	0.41	24.6	0.8	7.5	0.01
34_2	23	8	0.61	0.04	28.0	1.2	2.1	0.15	19	8	1.62	0.41	28.9	1.8	4.7	0.03
34_3	16	5	0.55	0.05	26.3	0.8	0.2	0.65	13	5	1.28	0.37	27.1	1.2	1.0	0.32
35_1	9	4	0.52	0.11	28.1	0.7	0.1	0.71	7	3	0.86	0.46	28.5	1.0	0.0	0.84
35_2	17	7	0.64	0.05	29.4	1.1	0.1	0.72	13	7	1.51	0.49	30.3	1.6	0.7	0.42
35_3	10	5	0.56	0.10	27.6	0.8	2.2	0.14	9	5	1.14	0.50	28.5	1.3	1.3	0.25
36_1	15	4	0.50	0.05	30.0	0.9	0.0	0.95	14	5	1.22	0.34	31.1	1.4	0.3	0.59
36_2	12	4	0.46	0.08	29.5	1.0	9.0	0.00	9	4	0.81	0.39	29.6	1.3	11.1	0.00
36_3	6	3	0.17	0.26	27.5	0.8	1.6	0.20	6	2	0.31	0.42	27.8	1.1	1.4	0.23
37_1	22	6	0.54	0.04	23.8	0.9	0.4	0.52	24	8	1.62	0.32	25.4	1.5	0.0	0.88
37_2	28	8	0.56	0.03	26.2	1.2	2.8	0.09	27	10	1.74	0.34	27.6	1.9	6.9	0.01
37_3	22	6	0.52	0.04	25.0	1.1	0.0	0.83	22	8	1.53	0.34	26.5	1.8	1.3	0.25
38_1	5	3	0.27	0.31	26.6	0.7	0.0	0.85	4	2	0.30	0.49	26.7	0.9	0.1	0.81
38_2	24	9	0.63	0.03	31.1	1.3	0.3	0.56	21	9	1.77	0.41	32.5	1.9	1.8	0.18
38_3	18	6	0.58	0.04	30.3	1.0	0.0	0.95	16	6	1.49	0.37	31.5	1.5	0.3	0.58
39_2	38	11	0.54	0.02	33.5	1.8	8.9	0.00	57	19	2.30	0.30	38.8	3.2	3.0	0.08
39_3	11	3	0.35	0.08	27.7	0.9	0.0	1.00	11	4	0.76	0.31	28.4	1.3	0.1	0.75
40_1	17	3	0.35	0.04	27.9	0.8	2.3	0.13	21	5	1.09	0.22	29.5	1.3	0.7	0.40
40_2	14	3	0.30	0.06	27.0	0.9	0.7	0.40	15	4	0.77	0.26	27.7	1.3	1.5	0.22
40_4	16	3	0.33	0.04	27.9	0.9	1.4	0.24	17	4	0.89	0.23	28.8	1.2	2.9	0.09
43_1	102	4362	0.96	0.03	28.1	15.6	4.0	0.05	12	36	3.40	2.55	28.8	3.4	4.4	0.04
43_2	96	2207	0.94	0.03	29.4	12.9	9.7	0.00	13	29	3.14	1.92	30.0	3.1	11.1	0.00
43_3	304	3372	0.96	0.01	27.9	2.8	0.0	0.86	6	21	2.87	2.94	27.7	2.5	0.0	0.99
44_1	40	3	0.15	0.01	29.2	1.4	1.0	0.31	62	8	1.06	0.12	33.7	2.3	0.1	0.79
44_2	34	3	0.16	0.01	34.1	1.5	0.1	0.77	49	7	1.00	0.13	37.7	2.3	1.8	0.18
44_3	50	5	0.19	0.01	31.5	1.8	10.7	0.00	94	14	1.52	0.14	40.3	3.4	1.2	0.28
45_1	19	2	0.19	0.03	28.4	0.8	0.9	0.33	22	3	0.66	0.15	29.4	1.1	2.3	0.13
46_1	1	7	0.00	5.75	29.7	0.7	0.3	0.62	1	2	0.00	1.45	29.7	0.9	0.3	0.62
46_2	1	7	0.00	6.42	29.7	0.7	1.2	0.28	1	2	0.00	1.58	29.7	0.9	1.2	0.28
47_1	7	2	0.07	0.15	23.2	0.7	0.0	0.96	7	2	0.11	0.27	23.2	0.8	0.0	0.93
47_2	9	2	0.17	0.10	23.8	0.7	0.3	0.61	9	2	0.33	0.26	24.0	0.9	0.4	0.51
48_1	25	6	0.52	0.03	25.0	1.0	0.5	0.48	27	8	1.65	0.29	26.6	1.6	2.8	0.09
49_1	11	4	0.43	0.09	21.7	0.8	11.4	0.00	8	3	0.65	0.40	21.7	1.1	13.6	0.00
49_2	15	4	0.50	0.05	21.8	0.7	0.8	0.38	13	4	1.10	0.33	22.4	1.0	1.9	0.17
50_1	18	3	0.39	0.04	26.9	0.8	0.3	0.61	19	5	1.12	0.24	28.1	1.3	1.1	0.28
50_2	14	3	0.33	0.06	25.2	0.7	0.4	0.51	14	4	0.80	0.25	25.9	1.1	1.1	0.29
51_1	14	5	0.55	0.06	24.5	0.7	0.0	0.98	12	5	1.19	0.38	25.2	1.1	0.2	0.70
51_2	11	4	0.48	0.08	24.0	0.7	0.5	0.49	10	4	0.93	0.39	24.5	1.0	1.0	0.32
52_1	14	5	0.53	0.06	25.5	0.8	0.9	0.35	13	5	1.25	0.38	26.5	1.2	0.3	0.60
53_1	12	3	0.33	0.07	23.7	0.7	4.0	0.05	11	3	0.65	0.28	24.0	0.9	5.4	0.02
53_2	123	1790	0.93	0.01	19.7	9.5	111.1	0.00	25	31	3.45	1.04	20.7	2.3	117.7	0.00
TS1	12	3	0.91	0.01	23.7	0.7			11	3	0.84	0.27	23.5	0.9		
TS1_1	0	0	0.00	1.41	51.5	0.6	2795.6	0.00	0	0	0.00	1.41	51.5	0.6	2795.6	0.00
TS1_2	0	0	0.00	1.41	57.3	0.8	2144.9	0.00	0	0	0.00	1.41	57.3	0.8	2144.9	0.00
TS2	0	0	0.00	1.00	53.5	0.5			0	0	0.00	1.00	53.5	0.5		
TS2_1	53	6	0.28	0.01	31.6	1.6	1.1	0.29	92	14	1.83	0.15	38.3	2.6	10.4	0.00
TS2_3	0	89	1.82	571.60	25.8	1.1	8.6	0.00	0	52	5.61	1.41	26.2	2.7	11.5	0.00

Table D.8.: Collinearities of Cef (1)

No.	A ccSTP /l	σ A	F	σ F	T °C	σ T	Chi ²	Prob	res Ne %	res Ar %	res Kr %	res Xe %	coll (A,F)	coll (A,T)	coll (F,T)	coll (A,F,T)
01_3	17	4	0.38	0.05	25.9	1.3	2.2	0.1	0.0	-0.4	1.0	-1.1	6.6	2.0	1.6	18.3
01_4	28	5	0.44	0.02	30.1	1.2	0.1	0.7	0.0	-0.1	0.3	-0.1	4.6	2.3	1.6	11.0
02_2	18	3	0.25	0.04	26.2	1.2	0.3	0.6	0.0	-0.1	0.5	-0.3	6.7	1.9	1.5	15.9
02_3	16	2	0.25	0.04	25.8	0.8	0.4	0.5	0.0	-0.1	0.6	-0.2	7.8	1.7	1.4	15.2
03_2	19	3	0.21	0.03	26.9	1.0	4.6	0.0	0.0	0.5	-2.0	0.7	6.6	1.8	1.5	13.5
03_3	19	2	0.21	0.03	27.4	0.9	0.7	0.4	0.0	-0.2	0.8	-0.3	7.1	1.7	1.4	14.1
04_2	9	4	0.35	0.12	26.6	1.0	3.3	0.1	0.0	-0.4	1.4	-1.1	10.5	1.7	1.5	24.9
04_3	19	5	0.54	0.04	28.9	1.0	1.4	0.2	0.0	-0.3	1.1	-0.3	5.8	2.1	1.6	13.0
05_2	9	3	0.22	0.12	24.5	1.0	0.1	0.8	0.0	-0.1	0.2	-0.2	11.1	1.6	1.4	25.6
05_3	15	3	0.36	0.05	27.9	0.9	0.1	0.8	0.0	-0.1	0.3	-0.1	7.5	1.8	1.5	15.2
06_1	17	3	0.18	0.05	26.0	1.2	0.0	0.9	0.0	0.0	0.1	-0.1	7.4	1.7	1.4	19.7
06_2	17	3	0.27	0.05	25.1	1.2	2.6	0.1	0.0	-0.4	1.0	-1.1	6.9	1.8	1.5	18.4
06_3	212	513	0.82	0.01	35.2	3.9	5.2	0.0	0.0	-0.5	2.1	-0.7	2.2	14.1	2.4	16.9
07_2	14	2	0.16	0.06	26.0	1.1	2.3	0.1	0.0	0.4	-1.2	0.9	8.2	1.6	1.4	19.2
07_3	19	2	0.23	0.03	28.9	0.9	1.0	0.3	0.0	-0.2	0.9	-0.3	6.8	1.7	1.4	13.6
08_2	10	3	0.32	0.10	27.4	1.1	0.3	0.6	0.0	0.2	-0.5	0.3	9.6	1.7	1.5	23.2
08_3	19	4	0.46	0.04	30.0	1.0	1.0	0.3	0.0	-0.2	0.9	-0.3	6.1	2.0	1.6	13.4
09_2	19	3	0.24	0.04	25.0	1.2	0.0	0.9	0.0	0.0	0.1	-0.1	6.1	1.9	1.5	14.1
09_3	23	3	0.27	0.03	27.4	0.9	0.5	0.5	0.0	-0.2	0.7	-0.2	5.8	1.9	1.5	12.0
10_2	6	2	0.00	0.24	23.3	0.9	0.4	0.5	0.0	0.1	-0.5	0.4	18.0	1.5	1.4	41.0
10_3	15	3	0.35	0.05	27.3	0.8	1.7	0.2	0.0	-0.3	1.2	-0.4	7.4	1.8	1.5	15.1
11_2	10	3	0.20	0.11	24.3	1.0	1.1	0.3	0.0	0.2	-0.8	0.6	10.8	1.6	1.4	25.0
11_3	19	3	0.37	0.04	28.4	0.9	0.0	0.9	0.0	0.0	0.1	0.0	6.4	1.9	1.5	13.2
12_2	10	3	0.27	0.10	24.1	1.0	0.4	0.5	0.0	0.1	-0.5	0.4	10.2	1.6	1.5	23.9
12_3	13	3	0.32	0.06	26.5	0.8	0.0	0.8	0.0	0.0	0.2	-0.1	8.6	1.7	1.5	17.0
13_2	8	3	0.12	0.14	24.2	1.0	0.0	0.9	0.0	0.0	-0.1	0.1	13.1	1.5	1.4	30.1
13_3	14	3	0.31	0.05	27.0	0.8	0.4	0.5	0.0	-0.1	0.6	-0.2	8.1	1.7	1.5	16.1
14_2	11	3	0.19	0.08	25.3	1.0	0.1	0.7	0.0	-0.1	0.3	-0.2	9.9	1.6	1.4	22.7
14_3	16	3	0.30	0.04	27.8	0.9	1.4	0.2	0.0	-0.3	1.1	-0.4	7.4	1.7	1.5	14.7
16_2	21	3	0.20	0.03	26.9	1.3	1.3	0.2	0.0	0.3	-0.9	0.6	6.0	1.9	1.5	14.2
16_3	22	2	0.21	0.02	26.7	0.9	1.9	0.2	0.0	-0.3	1.3	-0.4	6.2	1.8	1.5	12.3
17_2	22	4	0.45	0.03	29.0	1.0	2.1	0.1	0.0	-0.4	1.3	-0.4	5.5	2.1	1.6	12.0
17_3	14	4	0.36	0.07	26.3	1.2	1.6	0.2	0.0	-0.3	0.8	-0.9	7.8	1.9	1.6	21.3
18_1	10	3	0.22	0.10	25.4	1.0	0.8	0.4	0.0	-0.2	0.5	-0.7	10.6	1.6	1.4	27.7
18_3	41	10	0.54	0.02	24.0	1.2	2.0	0.2	0.0	-0.4	1.3	-0.3	3.6	3.0	1.7	9.7
19_2	147	643	0.76	0.01	19.1	10.7	7.7	0.0	-0.6	1.4	0.3	-2.3	2.3	51.5	2.3	52.5
19_3	143	751	0.75	0.01	20.5	13.4	34.5	0.0	-1.4	4.1	1.2	-3.8	2.2	65.9	2.1	70.8
20_2	19	3	0.29	0.04	25.9	1.2	2.8	0.1	0.0	-0.4	1.3	-0.9	6.1	1.9	1.5	14.7
20_3	19	3	0.27	0.03	26.5	0.8	1.4	0.2	0.0	-0.3	1.1	-0.3	6.8	1.7	1.5	13.4
21_1	18	6	0.56	0.05	24.7	1.0	0.0	1.0	0.0	0.0	0.0	0.0	6.5	2.1	1.6	14.3
21_2	26	9	0.61	0.03	26.8	1.3	0.7	0.4	0.0	0.2	-0.7	0.2	4.8	2.5	1.8	12.1
22_1	10	5	0.56	0.10	28.9	0.8	0.1	0.7	0.0	-0.1	0.3	-0.1	9.5	1.7	1.5	19.0
22_2b	12	5	0.57	0.08	29.1	1.0	0.3	0.6	0.0	-0.1	0.5	-0.2	8.5	1.9	1.6	18.6
23_1	14	4	0.45	0.06	29.2	0.9	0.2	0.6	0.0	0.1	-0.4	0.1	7.3	1.8	1.5	14.9
23_2	21	6	0.52	0.04	31.6	1.2	0.0	0.9	0.0	0.0	0.1	0.0	5.6	2.2	1.7	13.1
24*_2	28	6	0.44	0.02	27.3	1.2	0.1	0.8	0.0	-0.1	0.3	-0.1	4.7	2.4	1.7	11.2
24_1b	18	3	0.37	0.04	23.7	0.8	7.0	0.0	0.0	-0.7	2.4	-0.8	6.2	1.8	1.5	12.4
24_2	30	6	0.46	0.02	27.4	1.2	0.1	0.7	0.0	-0.1	0.3	-0.1	4.5	2.5	1.7	10.9
24_3	25	5	0.43	0.03	26.0	1.1	0.2	0.7	0.0	-0.1	0.3	-0.2	4.6	2.2	1.6	10.6
25_1	101	135	0.61	0.02	27.2	7.0	0.1	0.8	0.0	0.2	-0.2	0.0	2.6	11.5	2.1	33.0
25_2	132	444	0.59	0.01	29.6	18.2	6.9	0.0	-0.5	1.4	1.0	-1.9	2.4	26.7	2.2	78.8
25_3	140	404	0.61	0.01	28.9	14.6	0.1	0.8	-0.1	0.1	0.2	-0.2	2.3	37.4	2.2	63.1
26_1	35	3	0.23	0.01	27.3	1.1	0.4	0.5	0.0	-0.2	0.6	-0.2	4.3	2.1	1.5	9.0
26_2	36	4	0.23	0.01	27.1	1.2	0.0	1.0	0.0	0.0	0.0	0.0	4.5	2.2	1.6	10.1
26_3	58	9	0.30	0.01	32.5	2.3	6.1	0.0	0.1	-0.9	2.2	-0.7	3.2	3.8	1.8	10.8
27_1	37	2	0.08	0.01	23.2	0.9	0.1	0.8	0.0	0.1	-0.3	0.1	4.5	1.7	1.3	8.2
27_2	41	2	0.09	0.01	25.8	1.2	2.0	0.2	0.0	0.3	-1.4	0.3	5.0	1.8	1.4	9.8
27_3	50	4	0.12	0.01	32.0	1.8	5.7	0.0	0.1	-0.8	2.0	-1.0	3.9	2.4	1.6	9.9
28_1	13	3	0.38	0.07	25.2	0.8	0.1	0.8	0.0	-0.1	0.2	-0.1	8.0	1.7	1.5	16.7

Table D.9.: Collinearities of CEf (2)

No.	A ccSTP /l	σ_A	F	σ_F	T °C	σ_T	Chi ²	Prob	res Ne %	res Ar %	res Kr %	res Xe %	coll (A,F)	coll (A,T)	coll (F,T)	coll (A,F,T)
28_2	19	4	0.45	0.04	27.9	1.1	0.6	0.4	0.0	0.2	-0.7	0.3	6.3	2.0	1.6	14.1
28_3	19	4	0.44	0.04	28.1	1.0	0.5	0.5	0.0	-0.2	0.6	-0.2	5.9	2.0	1.6	12.9
29_1	31	10	0.60	0.03	27.2	1.4	0.0	0.8	0.0	-0.1	0.2	-0.1	4.2	2.8	1.8	11.4
29_2	117	783	0.78	0.02	26.1	15.6	24.4	0.0	-1.2	3.8	-1.1	-2.8	2.4	22.7	2.2	75.6
29_3	16	4	0.49	0.05	24.4	0.9	1.6	0.2	0.0	-0.3	1.2	-0.4	6.7	1.9	1.5	13.9
30_1	20	8	0.65	0.04	28.3	0.9	3.2	0.1	0.0	0.5	-1.7	0.4	5.0	2.2	1.6	11.2
30_2	49	33	0.70	0.02	31.8	2.4	0.4	0.5	0.0	0.2	-0.6	0.1	3.3	4.4	2.0	14.3
30_3	16	6	0.61	0.05	27.6	0.9	0.0	0.9	0.0	0.0	-0.1	0.1	5.8	2.0	1.6	13.1
31_1	21	7	0.59	0.04	28.0	1.1	1.0	0.3	0.0	0.2	-0.9	0.3	5.6	2.3	1.7	13.2
31_2	28	10	0.60	0.03	29.8	1.4	0.7	0.4	0.0	0.2	-0.8	0.2	4.6	2.7	1.8	12.1
31_3	18	6	0.58	0.04	27.1	0.8	0.3	0.6	0.0	-0.1	0.5	-0.2	5.6	2.0	1.6	11.9
32_1	115	2018	0.90	0.02	30.3	16.4	0.9	0.4	-0.2	0.4	0.5	-0.6	2.4	26.4	2.2	75.9
32_2	100	1915	0.91	0.04	30.5	17.1	7.3	0.0	-0.6	2.0	-0.9	-1.4	2.5	16.1	2.2	81.7
32_3	1	9	0.01	9.67	27.4	0.7	2.6	0.1	0.0	-0.3	1.5	-0.5	105.9	1.5	1.5	212.6
33_1	38	66	0.89	0.03	30.4	1.7	0.5	0.5	0.0	-0.2	0.6	-0.1	3.4	3.7	1.9	11.9
33_2	86	799	0.90	0.03	31.7	9.7	2.2	0.1	-0.2	1.0	-1.1	-0.2	2.6	11.4	2.2	48.1
33_3	1	8	0.00	8.91	28.4	0.7	1.1	0.3	0.1	-0.3	-0.6	0.7	98.7	1.4	1.4	193.1
34_1	7	3	0.33	0.18	24.6	0.6	6.8	0.0	0.0	0.7	-2.4	0.8	13.4	1.5	1.4	24.8
34_2	23	8	0.61	0.04	28.0	1.2	2.1	0.1	0.0	0.4	-1.3	0.5	5.2	2.4	1.7	12.7
34_3	16	5	0.55	0.05	26.3	0.8	0.2	0.6	0.0	0.1	-0.4	0.1	6.3	1.9	1.5	13.1
35_1	9	4	0.52	0.11	28.1	0.7	0.1	0.7	0.0	-0.1	0.4	-0.1	10.7	1.6	1.5	20.1
35_2	17	7	0.64	0.05	29.4	1.1	0.1	0.7	0.0	0.1	-0.3	0.1	6.3	2.1	1.7	14.4
35_3	10	5	0.56	0.10	27.6	0.8	2.2	0.1	0.0	-0.4	1.3	-0.5	9.1	1.7	1.5	19.0
36_1	15	4	0.50	0.05	30.0	0.9	0.0	0.9	0.0	0.0	-0.1	0.0	6.7	1.9	1.5	14.0
36_2	12	4	0.46	0.08	29.5	1.0	9.0	0.0	0.0	0.7	-2.7	1.1	8.8	1.8	1.6	19.4
36_3	6	3	0.17	0.26	27.5	0.8	1.6	0.2	0.0	-0.3	1.1	-0.6	17.4	1.5	1.4	36.2
37_1	22	6	0.54	0.04	23.8	0.9	0.4	0.5	0.0	-0.2	0.6	-0.2	4.9	2.2	1.6	10.4
37_2	28	8	0.56	0.03	26.2	1.2	2.8	0.1	0.0	0.4	-1.5	0.5	4.6	2.6	1.7	11.5
37_3	22	6	0.52	0.04	25.0	1.1	0.0	0.8	0.0	0.1	-0.2	0.1	5.2	2.2	1.6	12.5
38_1	5	3	0.27	0.31	26.6	0.7	0.0	0.9	0.0	0.0	-0.2	0.0	19.3	1.5	1.4	37.3
38_2	24	9	0.63	0.03	31.1	1.3	0.3	0.6	0.0	0.2	-0.5	0.2	4.8	2.5	1.7	12.5
38_3	18	6	0.58	0.04	30.3	1.0	0.0	1.0	0.0	0.0	-0.1	0.0	5.7	2.1	1.6	12.4
39_2	38	11	0.54	0.02	33.5	1.8	8.9	0.0	0.1	-0.8	2.8	-0.7	3.9	3.2	1.9	12.1
39_3	11	3	0.35	0.08	27.7	0.9	0.0	1.0	0.0	0.0	0.0	0.0	9.2	1.7	1.5	19.1
40_1	17	3	0.35	0.04	27.9	0.8	2.3	0.1	0.0	-0.4	1.4	-0.5	6.4	1.8	1.5	12.9
40_2	14	3	0.30	0.06	27.0	0.9	0.7	0.4	0.0	0.2	-0.8	0.3	8.6	1.7	1.5	17.6
40_4	16	3	0.33	0.04	27.9	0.9	1.4	0.2	0.0	0.3	-1.1	0.4	6.9	1.8	1.5	13.9
43_1	102	4362	0.96	0.03	28.1	15.6	4.0	0.0	-0.5	1.5	-0.7	-1.0	2.5	17.8	2.2	77.3
43_2	96	2207	0.94	0.03	29.4	12.9	9.7	0.0	-0.6	2.3	-1.7	-1.1	2.5	14.7	2.2	64.3
43_3	304	3370	0.96	0.01	27.9	2.8	0.0	0.9	0.0	-0.1	0.2	-0.1	2.1	8.8	2.5	12.4
44_1	40	3	0.15	0.01	29.2	1.4	1.0	0.3	0.0	-0.3	0.9	-0.3	4.6	2.1	1.5	10.1
44_2	34	3	0.16	0.01	34.1	1.5	0.1	0.8	0.0	0.1	-0.3	0.1	5.0	2.1	1.5	11.1
44_3	50	5	0.19	0.01	31.5	1.8	10.7	0.0	0.1	-1.1	2.8	-1.2	3.6	2.7	1.7	9.7
45_1	19	2	0.19	0.03	28.4	0.8	0.9	0.3	0.0	0.2	-0.9	0.3	6.3	1.6	1.4	12.1
46_1	1	7	0.00	5.75	29.7	0.7	0.3	0.6	0.1	-0.3	-0.2	0.4	83.2	1.4	1.4	161.5
46_2	1	7	0.00	6.42	29.7	0.7	1.2	0.3	0.0	-0.4	1.0	-0.3	87.3	1.5	1.4	177.7
47_1	7	2	0.07	0.15	23.2	0.7	0.0	1.0	0.0	0.0	0.0	0.0	15.1	1.4	1.3	27.4
47_2	9	2	0.17	0.10	23.8	0.7	0.3	0.6	0.0	0.1	-0.5	0.2	11.9	1.5	1.4	22.3
48_1	25	6	0.52	0.03	25.0	1.0	0.5	0.5	0.0	0.2	-0.6	0.2	4.6	2.3	1.6	10.4
49_1	11	4	0.43	0.09	21.7	0.8	11.4	0.0	0.0	0.8	-2.9	1.5	9.1	1.7	1.5	19.1
49_2	15	4	0.50	0.05	21.8	0.7	0.8	0.4	0.0	0.2	-0.8	0.3	7.0	1.8	1.5	13.5
50_1	18	3	0.39	0.04	26.9	0.8	0.3	0.6	0.0	0.1	-0.5	0.1	6.2	1.8	1.5	12.3
50_2	14	3	0.33	0.06	25.2	0.7	0.4	0.5	0.0	0.1	-0.6	0.2	7.8	1.7	1.4	15.0
51_1	14	5	0.55	0.06	24.5	0.7	0.0	1.0	0.0	0.0	0.0	0.0	7.0	1.8	1.5	13.5
51_2	11	4	0.48	0.08	24.0	0.7	0.5	0.5	0.0	0.2	-0.6	0.2	8.8	1.7	1.5	17.3
52_1	14	5	0.53	0.06	25.5	0.8	0.9	0.3	0.0	-0.2	0.9	-0.3	7.2	1.8	1.5	14.4
53_1	12	3	0.33	0.07	23.7	0.7	4.0	0.0	0.0	0.4	-1.8	0.6	9.1	1.6	1.4	17.5
53_2	123	1790	0.93	0.01	19.7	9.5	111.1	0.0	-3.1	8.5	-3.2	-4.3	2.2	37.6	2.1	53.1
													393.3	309.2	94.0	1171.2

Table D.10.: Collinearities of CEb (1):

No.	A ccSTP		B ccSTP		σ B	T °C	σ T	Chi ²	Prob	res Ne %	res Ar %	res Kr %	res Xe %	coll (A,B)	coll (A,T)	coll (B,T)	coll (A,B,T)
01_3	20	5	7	3	25.9	1.3	2.2	0.1	0.0	-0.4	1.0	-1.1	16.7	1.8	1.7	48.8	
01_4	33	6	14	4	30.1	1.2	0.1	0.7	0.0	-0.1	0.3	-0.1	16.8	1.9	1.7	43.5	
02_2	21	4	5	2	26.2	1.2	0.3	0.6	0.0	-0.1	0.5	-0.3	12.6	1.9	1.7	31.4	
02_3	18	3	5	1	25.8	0.8	0.4	0.5	0.0	-0.1	0.6	-0.2	14.3	1.7	1.6	28.8	
03_2	22	3	5	1	26.9	1.0	4.6	0.0	0.0	0.5	-2.0	0.7	11.3	1.8	1.6	24.2	
03_3	21	3	4	1	27.4	0.9	0.7	0.4	0.0	-0.2	0.8	-0.3	12.1	1.8	1.6	25.1	
04_2	11	4	4	3	26.6	1.0	3.3	0.1	0.0	-0.4	1.4	-1.0	21.0	1.7	1.6	51.3	
04_3	22	6	12	4	28.9	1.0	1.4	0.2	0.0	-0.3	1.1	-0.4	24.2	1.8	1.7	57.3	
05_2	10	3	2	2	24.5	1.0	0.1	0.8	0.0	-0.1	0.2	-0.2	16.8	1.7	1.5	39.4	
05_3	18	4	6	2	27.9	0.9	0.1	0.8	0.0	-0.1	0.3	-0.1	17.6	1.7	1.6	37.2	
06_1	19	3	3	1	26.1	1.2	0.0	0.9	0.0	0.0	0.1	-0.1	11.4	1.8	1.6	31.8	
06_2	20	4	5	2	25.1	1.2	2.6	0.1	0.0	-0.4	1.0	-1.1	13.4	1.8	1.6	37.3	
06_3	251	619	204	504	35.1	4.0	5.2	0.0	0.0	-0.5	2.1	-0.7	112.8	2.4	2.4	808.4	
07_2	16	3	2	1	26.0	1.1	2.3	0.1	0.0	0.4	-1.2	0.9	11.7	1.8	1.6	28.1	
07_3	22	3	5	1	28.9	0.9	1.0	0.3	0.0	-0.2	0.9	-0.3	12.5	1.8	1.6	26.2	
08_2	12	4	4	3	27.5	1.1	0.3	0.6	0.0	0.1	-0.4	0.3	18.7	1.7	1.6	46.6	
08_3	22	5	10	3	30.0	1.0	1.0	0.3	0.0	-0.2	0.9	-0.3	19.9	1.8	1.7	46.3	
09_2	22	4	5	2	25.0	1.2	0.0	0.9	0.0	0.0	0.1	-0.1	11.2	1.9	1.6	27.3	
09_3	26	3	7	2	27.4	0.9	0.5	0.5	0.0	-0.2	0.7	-0.2	12.4	1.8	1.6	27.0	
10_2	7	3	0	2	23.3	0.9	0.4	0.5	0.0	0.1	-0.5	0.4	18.1	1.6	1.5	41.4	
10_3	18	4	6	2	27.3	0.8	1.7	0.2	0.0	-0.3	1.2	-0.4	17.4	1.7	1.6	36.7	
11_2	11	3	2	2	24.3	1.0	1.1	0.3	0.0	0.2	-0.8	0.6	16.1	1.7	1.6	38.1	
11_3	21	4	8	2	28.4	0.9	0.0	0.9	0.0	0.0	0.1	0.0	16.2	1.8	1.6	35.4	
12_2	12	4	3	2	24.1	1.0	0.4	0.5	0.0	0.1	-0.5	0.4	17.4	1.7	1.6	41.7	
12_3	15	3	5	2	26.5	0.8	0.0	0.8	0.0	0.0	0.2	-0.1	17.6	1.7	1.6	36.0	
13_2	9	3	1	2	24.2	1.0	0.0	0.9	0.0	0.0	-0.1	0.1	16.4	1.6	1.5	38.2	
13_3	16	3	5	2	27.0	0.8	0.4	0.5	0.0	-0.1	0.6	-0.2	16.6	1.7	1.6	34.0	
14_2	13	3	2	2	25.3	1.0	0.1	0.7	0.0	-0.1	0.3	-0.2	14.7	1.7	1.6	34.7	
14_3	19	3	6	2	27.8	0.9	1.4	0.2	0.0	-0.3	1.1	-0.4	15.2	1.7	1.6	31.7	
16_2	25	3	5	1	26.9	1.3	1.3	0.2	0.0	0.3	-0.9	0.6	10.2	1.9	1.7	25.6	
16_3	26	3	5	1	26.7	0.9	1.9	0.2	0.0	-0.3	1.3	-0.4	11.2	1.8	1.6	23.5	
17_2	25	5	11	3	29.0	1.0	2.1	0.1	0.0	-0.4	1.3	-0.4	18.4	1.8	1.7	43.1	
17_3	16	5	6	3	26.3	1.2	1.6	0.2	0.0	-0.3	0.8	-0.9	17.7	1.8	1.7	50.7	
18_1	12	3	3	2	25.4	1.0	0.8	0.4	0.0	-0.2	0.5	-0.7	16.5	1.7	1.6	43.9	
18_3	45	11	25	7	24.0	1.2	2.0	0.2	0.0	-0.4	1.3	-0.4	20.8	1.9	1.8	60.9	
19_2	163	720	124	548	19.1	10.6	7.7	0.0	-0.6	1.4	0.3	-2.3	59.5	2.4	2.3	1266.3	
19_3	159	846	119	636	20.5	13.4	34.5	0.0	-1.4	4.1	1.2	-3.8	52.7	2.2	2.1	1631.3	
20_2	22	4	6	2	25.9	1.2	2.8	0.1	0.0	-0.4	1.3	-0.9	12.7	1.9	1.7	32.2	
20_3	21	3	6	2	26.5	0.8	1.4	0.2	0.0	-0.3	1.1	-0.3	13.6	1.7	1.6	28.2	
21_1	20	7	11	5	24.7	1.0	0.0	1.0	0.0	0.0	0.0	0.0	27.2	1.8	1.7	64.2	
21_2	30	11	18	7	26.8	1.3	0.7	0.4	0.0	0.2	-0.7	0.2	28.7	1.9	1.8	78.4	
22_1	11	5	6	4	28.9	0.8	0.1	0.7	0.0	-0.1	0.3	-0.1	32.1	1.6	1.5	66.2	
22_2b	14	6	8	5	29.1	1.0	0.3	0.6	0.0	-0.1	0.5	-0.2	32.3	1.7	1.7	73.8	
23_1	16	4	7	3	29.2	0.9	0.2	0.6	0.0	0.1	-0.4	0.1	20.6	1.7	1.6	44.2	
23_2	25	7	13	5	31.6	1.2	0.0	0.9	0.0	0.0	0.1	0.0	23.1	1.9	1.7	58.7	
24*_2	33	7	14	4	27.3	1.2	0.1	0.8	0.0	-0.1	0.3	-0.1	17.4	1.9	1.8	45.0	
24_1b	20	4	8	2	23.7	0.8	7.0	0.0	0.0	-0.7	2.4	-0.8	15.7	1.7	1.6	32.8	
24_2	34	7	16	4	27.4	1.2	0.1	0.7	0.0	-0.1	0.3	-0.1	18.2	1.9	1.8	47.6	
24_3	28	6	12	3	26.0	1.1	0.2	0.7	0.0	-0.1	0.3	-0.2	14.7	1.8	1.7	36.4	
25_1	119	182	72	113	27.3	7.7	0.1	0.8	0.0	0.2	-0.3	0.0	30.9	2.3	2.2	449.6	
25_2	153	534	91	319	29.6	18.3	6.9	0.0	-0.5	1.4	1.0	-1.9	32.4	2.4	2.2	1058.2	
25_3	161	492	98	300	28.8	15.0	0.1	0.8	0.0	0.1	0.2	-0.2	31.8	2.4	2.2	855.3	
26_1	40	4	9	1	27.3	1.1	0.4	0.5	0.0	-0.2	0.6	-0.2	9.2	1.9	1.6	20.8	
26_2	41	4	10	2	27.1	1.2	0.0	1.0	0.0	0.0	0.0	0.0	10.2	2.0	1.7	24.5	
26_3	68	11	20	4	32.5	2.3	6.1	0.0	0.1	-0.9	2.2	-0.7	10.1	2.3	1.9	38.2	
27_1	42	2	3	1	23.3	0.9	0.1	0.8	0.0	0.1	-0.3	0.1	6.0	1.8	1.5	11.5	
27_2	46	3	4	1	25.9	1.2	2.0	0.2	0.0	0.2	-1.4	0.3	7.4	2.1	1.7	15.7	
27_3	59	5	7	1	32.0	1.8	5.7	0.0	0.1	-0.8	2.0	-1.0	6.7	2.4	1.8	19.1	
28_1	14	4	6	2	25.2	0.8	0.1	0.8	0.0	-0.1	0.2	-0.1	18.7	1.6	1.5	40.3	

Table D.11.: Collinearities of CEb (2):

No.	A ccSTP		B ccSTP		T °C	σ T	Chi ²	Prob	res Ne %	res Ar %	res Kr %	res Xe %	coll (A,B)	coll (A,T)	coll (B,T)	coll (A,B,T)
28_2	21	5	10	3	27.9	1.1	0.6	0.4	0.0	0.2	-0.7	0.3	20.1	1.8	1.7	47.4
28_3	21	5	9	3	28.1	1.0	0.5	0.5	0.0	-0.2	0.6	-0.2	18.1	1.8	1.6	42.2
29_1	35	12	21	8	27.2	1.4	0.0	0.8	0.0	0.0	0.2	-0.1	26.7	1.9	1.8	78.6
29_2	134	915	104	717	26.1	15.8	24.4	0.0	-1.2	3.8	-1.1	-2.8	65.4	2.3	2.2	2064.7
29_3	18	5	9	3	24.4	0.9	1.6	0.2	0.0	-0.3	1.2	-0.4	22.0	1.7	1.6	47.8
30_1	23	9	15	7	28.3	0.9	3.2	0.1	0.0	0.5	-1.7	0.4	30.5	1.7	1.6	73.3
30_2	58	40	40	29	31.8	2.4	0.4	0.5	0.0	0.2	-0.6	0.1	37.3	2.1	2.0	179.9
30_3	18	7	11	5	27.6	0.9	0.0	0.9	0.0	0.0	-0.1	0.1	27.5	1.7	1.6	65.2
31_1	24	8	14	6	28.0	1.1	1.0	0.3	0.0	0.2	-0.9	0.3	27.7	1.8	1.7	70.6
31_2	33	11	20	8	29.8	1.4	0.7	0.4	0.0	0.2	-0.8	0.2	27.5	1.9	1.8	79.8
31_3	21	7	12	5	27.1	0.8	0.3	0.6	0.0	-0.1	0.5	-0.2	25.3	1.7	1.6	57.1
32_1	134	2353	121	2128	30.3	16.3	0.9	0.4	-0.2	0.4	0.5	-0.6	160.2	2.3	2.3	4890.4
32_2	117	2301	107	2097	30.5	17.4	7.3	0.0	-0.6	2.0	-0.9	-1.4	176.6	2.2	2.2	5889.0
32_3	1	10	0	9	27.4	0.7	2.6	0.1	0.0	-0.3	1.5	-0.6	107.7	1.5	1.5	216.2
33_1	28	39	25	35	30.1	1.2	0.5	0.5	0.0	0.0	0.7	-0.3	94.4	1.8	1.8	270.5
33_2	85	447	76	403	31.6	5.6	2.2	0.1	-0.2	1.0	-1.0	-0.3	137.6	2.2	2.1	1512.8
33_3	1	9	0	9	28.4	0.7	1.1	0.3	0.1	-0.3	-0.6	0.7	98.7	1.5	1.4	193.1
34_1	8	3	3	3	24.6	0.6	6.8	0.0	0.0	0.6	-2.4	0.9	24.0	1.5	1.4	45.2
34_2	26	10	16	7	28.0	1.2	2.1	0.1	0.0	0.4	-1.3	0.5	29.0	1.9	1.8	76.9
34_3	18	6	10	4	26.3	0.8	0.2	0.6	0.0	0.1	-0.4	0.1	24.7	1.7	1.6	53.9
35_1	10	5	5	4	28.1	0.7	0.1	0.7	0.0	-0.1	0.4	-0.1	31.4	1.6	1.5	60.6
35_2	20	9	13	7	29.4	1.1	0.1	0.7	0.0	0.1	-0.3	0.1	34.8	1.8	1.7	84.8
35_3	11	6	6	4	27.6	0.8	2.2	0.1	0.0	-0.3	1.3	-0.6	31.5	1.6	1.6	67.9
36_1	18	5	9	4	30.0	0.9	0.0	0.9	0.0	0.0	-0.1	0.0	22.4	1.7	1.6	49.6
36_2	14	5	6	3	29.5	1.0	9.0	0.0	0.0	0.7	-2.7	1.1	24.9	1.8	1.7	57.2
36_3	6	3	1	2	27.5	0.8	1.6	0.2	0.0	-0.3	1.1	-0.6	23.0	1.6	1.5	48.3
37_1	24	7	13	4	23.8	0.9	0.4	0.5	0.0	-0.1	0.6	-0.2	20.2	1.8	1.6	46.0
37_2	32	9	18	6	26.2	1.2	2.8	0.1	0.0	0.4	-1.5	0.5	24.1	1.9	1.8	65.5
37_3	25	7	13	5	25.0	1.1	0.0	0.8	0.0	0.1	-0.2	0.1	21.4	1.8	1.7	55.0
38_1	6	4	2	3	26.6	0.7	0.0	0.9	0.0	0.0	-0.2	0.1	29.8	1.6	1.5	58.3
38_2	28	11	18	8	31.1	1.3	0.3	0.6	0.0	0.2	-0.5	0.2	29.9	1.9	1.8	84.2
38_3	21	7	12	5	30.3	1.0	0.0	1.0	0.0	0.0	-0.1	0.0	26.0	1.7	1.6	59.8
39_2	45	14	24	8	33.5	1.8	8.9	0.0	0.1	-0.8	2.8	-0.7	22.2	2.1	1.9	76.9
39_3	13	4	5	2	27.7	0.9	0.0	1.0	0.0	0.0	0.0	0.0	19.5	1.7	1.6	41.6
40_1	20	4	7	2	27.9	0.8	2.3	0.1	0.0	-0.4	1.4	-0.5	15.0	1.7	1.6	31.9
40_2	16	3	5	2	27.0	0.9	0.7	0.4	0.0	0.2	-0.8	0.3	17.2	1.7	1.6	36.6
40_4	18	3	6	2	27.9	0.9	1.4	0.2	0.0	0.3	-1.1	0.4	15.1	1.7	1.6	31.8
43_1	117	4880	112	4692	28.1	15.2	4.0	0.0	-0.5	1.5	-0.7	-1.0	411.5	2.2	2.2	12562.0
43_2	109	2322	103	2189	29.3	11.9	9.7	0.0	-0.6	2.3	-1.7	-1.1	265.6	2.2	2.2	6354.9
43_3	313	3541	301	3401	27.9	3.0	0.0	0.9	0.0	-0.1	0.2	-0.1	632.3	2.5	2.5	3492.2
44_1	46	4	7	1	29.2	1.4	1.0	0.3	0.0	-0.3	0.9	-0.3	8.2	2.2	1.8	19.7
44_2	40	4	7	1	34.1	1.5	0.1	0.8	0.0	0.1	-0.3	0.1	8.9	2.2	1.8	21.9
44_3	59	6	11	2	31.5	1.8	10.7	0.0	0.1	-1.1	2.8	-1.2	7.8	2.3	1.8	23.3
45_1	22	2	4	1	28.4	0.8	0.9	0.3	0.0	0.2	-0.9	0.3	10.2	1.7	1.5	20.3
46_1	1	8	0	7	29.8	0.7	0.3	0.6	0.1	-0.3	-0.1	0.4	83.0	1.5	1.5	161.3
46_2	1	8	0	7	29.7	0.7	1.2	0.3	0.0	-0.4	1.0	-0.2	87.1	1.5	1.5	177.4
47_1	8	2	1	1	23.2	0.7	0.0	1.0	0.0	0.0	0.0	0.0	16.9	1.5	1.4	31.0
47_2	11	3	2	1	23.8	0.7	0.3	0.6	0.0	0.1	-0.5	0.2	16.5	1.6	1.5	31.4
48_1	29	7	15	5	25.0	1.0	0.5	0.5	0.0	0.2	-0.6	0.2	20.1	1.8	1.7	49.0
49_1	13	4	6	3	21.8	0.8	11.4	0.0	0.0	0.8	-2.9	1.5	22.9	1.7	1.6	49.9
49_2	16	5	8	3	21.8	0.7	0.8	0.4	0.0	0.2	-0.8	0.3	22.8	1.6	1.5	45.8
50_1	20	4	8	2	26.9	0.8	0.3	0.6	0.0	0.1	-0.5	0.1	16.2	1.7	1.6	33.9
50_2	15	3	5	2	25.2	0.7	0.4	0.5	0.0	0.1	-0.6	0.2	16.5	1.6	1.5	32.6
51_1	16	5	8	4	24.5	0.7	0.0	1.0	0.0	0.0	0.0	0.0	25.2	1.6	1.5	51.0
51_2	13	5	6	3	24.0	0.7	0.5	0.5	0.0	0.1	-0.6	0.2	25.7	1.6	1.5	52.0
52_1	16	5	8	4	25.5	0.8	0.9	0.3	0.0	-0.2	0.9	-0.3	25.3	1.7	1.6	53.0
53_1	13	3	4	2	23.7	0.7	4.0	0.0	0.0	0.4	-1.8	0.6	18.6	1.6	1.5	36.5
53_2	137	2015	127	1865	19.7	9.6	111.1	0.0	-3.1	8.5	-3.2	-4.3	164.7	2.2	2.2	3810.8
													4675.2	215.2	199.3	52140.3

Table D.12.: Final fit (1):

No	A	err A	F	err F	NGT	err	Chi ²	Prob	How	C _{equ} He	C _{equ} Ne	C _{equ} Ar	C _{equ} Kr	C _{equ} Xe
	ccSTP/g				°C					ccSTP/g	ccSTP/g	ccSTP/g	ccSTP/g	ccSTP/g
1	0.026	0.003	0.44	0.01	28.9	0.9	7.77	0.05	Tfix	4.31E-08	1.71E-07	2.61E-04	5.58E-08	7.29E-09
2	0.017	0.001	0.25	0.02	26.0	0.7	0.81	0.85	Tfix	4.34E-08	1.75E-07	2.75E-04	5.96E-08	7.90E-09
3	0.019	0.001	0.21	0.02	27.2	0.7	5.47	0.14	Tfix	4.33E-08	1.73E-07	2.69E-04	5.80E-08	7.64E-09
4	0.015	0.002	0.48	0.03	28.0	0.7	7.03	0.07	Tfix	4.32E-08	1.72E-07	2.65E-04	5.69E-08	7.46E-09
5	0.014	0.002	0.35	0.03	26.8	0.7	6.67	0.08	Tfix	4.33E-08	1.74E-07	2.71E-04	5.85E-08	7.71E-09
6	0.017	0.002	0.24	0.02	25.6	0.9	2.75	0.43	Tfix	4.35E-08	1.75E-07	2.77E-04	6.01E-08	7.97E-09
7	0.017	0.001	0.22	0.02	27.9	0.7	7.23	0.06	Tfix	4.32E-08	1.72E-07	2.66E-04	5.70E-08	7.49E-09
8	0.016	0.002	0.42	0.03	29.1	0.7	4.00	0.26	Tfix	4.31E-08	1.71E-07	2.60E-04	5.55E-08	7.25E-09
9	0.022	0.002	0.27	0.02	26.6	0.7	3.22	0.36	Tfix	4.33E-08	1.74E-07	2.72E-04	5.88E-08	7.76E-09
10	0.012	0.002	0.30	0.04	26.0	0.6	11.57	0.01	Tfix	4.34E-08	1.75E-07	2.75E-04	5.96E-08	7.89E-09
11	0.009	0.001	0.15	0.05	23.6	0.4	2.52	0.77	Tfix	4.37E-08	1.78E-07	2.87E-04	6.29E-08	8.43E-09
12	0.013	0.002	0.35	0.03	25.7	0.6	3.59	0.31	Tfix	4.34E-08	1.75E-07	2.76E-04	5.99E-08	7.95E-09
13	0.013	0.001	0.28	0.04	26.1	0.6	5.03	0.17	Tfix	4.34E-08	1.75E-07	2.74E-04	5.94E-08	7.87E-09
14	0.014	0.001	0.27	0.03	26.8	0.7	4.85	0.18	Tfix	4.33E-08	1.74E-07	2.71E-04	5.84E-08	7.71E-09
15														
16	0.022	0.001	0.21	0.02	26.8	0.8	3.12	0.37	Tfix	4.33E-08	1.74E-07	2.71E-04	5.85E-08	7.72E-09
17	0.020	0.002	0.43	0.02	28.2	0.8	6.32	0.10	Tfix	4.32E-08	1.72E-07	2.64E-04	5.67E-08	7.43E-09
18	0.012	0.002	0.55	0.01	24.8	0.8	3.61	0.31	Tfix	4.35E-08	1.76E-07	2.81E-04	6.12E-08	8.15E-09
19														
20	0.019	0.002	0.29	0.02	26.4	0.7	4.01	0.26	Tfix	4.34E-08	1.74E-07	2.73E-04	5.91E-08	7.81E-09
21	0.022	0.004	0.59	0.02	25.8	0.8	2.35	0.50	Tfix	4.36E-08	1.76E-07	2.77E-04	6.00E-08	7.96E-09
22	0.011	0.003	0.56	0.05	29.0	0.6	0.46	0.93	Tfix	4.32E-08	1.72E-07	2.62E-04	5.59E-08	7.30E-09
23	0.017	0.002	0.49	0.03	30.3	0.7	2.83	0.42	Tfix	4.31E-08	1.70E-07	2.56E-04	5.43E-08	7.05E-09
24	0.028	0.002	0.45	0.01	26.9	0.7	1.22	0.94	Tfix	4.35E-08	1.74E-07	2.71E-04	5.85E-08	7.72E-09
25	0.066	0.012	0.60	0.01	25.1	1.1	1.93	0.59	Ffix	4.37E-08	1.76E-07	2.80E-04	6.10E-08	8.12E-09
26	0.036	0.002	0.23	0.01	27.2	0.8	0.43	0.93	Tfix	4.34E-08	1.74E-07	2.70E-04	5.82E-08	7.66E-09
27	0.038	0.001	0.08	0.01	24.2	0.7	5.38	0.15	Tfix	4.38E-08	1.78E-07	2.85E-04	6.24E-08	8.34E-09
28	0.016	0.002	0.44	0.02	27.1	0.6	7.51	0.19	Tfix	4.35E-08	1.74E-07	2.71E-04	5.83E-08	7.69E-09
29	0.021	0.003	0.55	0.02	25.6	0.7	5.07	0.17	Tfix	4.36E-08	1.76E-07	2.78E-04	6.03E-08	8.01E-09
30	0.025	0.004	0.66	0.01	29.0	0.7	9.49	0.09	Tfix	4.32E-08	1.72E-07	2.62E-04	5.59E-08	7.30E-09
31	0.021	0.003	0.60	0.01	28.2	0.6	5.24	0.39	Tfix	4.33E-08	1.73E-07	2.66E-04	5.69E-08	7.46E-09
32	0.001	0.009	0.01	9.67	27.4	0.7	2.55	0.11	single	4.34E-08	1.74E-07	2.69E-04	5.79E-08	7.61E-09
33	0.005	0.006	0.76	0.20	28.9	0.5	5.27	0.15	Tfix	4.32E-08	1.72E-07	2.62E-04	5.60E-08	7.31E-09
34	0.010	0.002	0.47	0.05	25.3	0.5	9.43	0.02	Tfix	4.37E-08	1.76E-07	2.79E-04	6.07E-08	8.08E-09
35	0.011	0.002	0.58	0.03	28.3	0.5	4.34	0.50	Tfix	4.33E-08	1.73E-07	2.65E-04	5.68E-08	7.44E-09
36	0.010	0.001	0.42	0.04	29.0	0.5	15.20	0.01	Tfix	4.32E-08	1.72E-07	2.62E-04	5.59E-08	7.29E-09
37	0.024	0.003	0.55	0.01	25.0	0.6	5.39	0.37	Tfix	4.37E-08	1.77E-07	2.81E-04	6.11E-08	8.13E-09
38	0.020	0.004	0.60	0.02	30.6	0.8	0.65	0.88	Tfix	4.31E-08	1.70E-07	2.55E-04	5.40E-08	7.00E-09
39	0.011	0.003	0.35	0.08	27.7	0.9	0.01	0.93	single	4.34E-08	1.73E-07	2.68E-04	5.75E-08	7.55E-09
40	0.016	0.001	0.33	0.02	27.6	0.5	5.20	0.39	Tfix	4.34E-08	1.73E-07	2.68E-04	5.76E-08	7.57E-09
41														
42														
43	0.017	0.019	0.95	0.03	27.3	0.5	5.79	0.12	Ffix	4.34E-08	1.74E-07	2.70E-04	5.81E-08	7.65E-09
44	0.047	0.003	0.18	0.01	30.2	1.1	12.36	0.01	Tfix	4.31E-08	1.70E-07	2.56E-04	5.45E-08	7.07E-09
45	0.019	0.002	0.19	0.03	28.4	0.8	1.00	0.32	single	4.33E-08	1.73E-07	2.64E-04	5.66E-08	7.42E-09
46	0.001	0.005	0.00	4.28	29.7	0.7	1.64	0.65	single	4.32E-08	1.71E-07	2.59E-04	5.50E-08	7.16E-09
47	0.009	0.001	0.15	0.05	23.6	0.4	2.52	0.77	Tfix	4.37E-08	1.78E-07	2.87E-04	6.29E-08	8.43E-09
48	0.025	0.006	0.52	0.03	25.0	1.0	0.55	0.46	single	4.37E-08	1.77E-07	2.81E-04	6.12E-08	8.15E-09
49	0.013	0.002	0.47	0.04	21.8	0.5	12.00	0.01	Tfix	4.41E-08	1.81E-07	2.98E-04	6.60E-08	8.94E-09
50	0.016	0.002	0.37	0.03	26.1	0.6	2.87	0.41	Tfix	4.34E-08	1.75E-07	2.75E-04	5.95E-08	7.88E-09
51	0.013	0.002	0.52	0.04	24.2	0.5	0.63	0.89	Tfix	4.38E-08	1.78E-07	2.85E-04	6.23E-08	8.32E-09
52	0.014	0.005	0.53	0.06	25.5	0.8	0.97	0.32	single	4.36E-08	1.76E-07	2.78E-04	6.05E-08	8.03E-09
53	0.012	0.003	0.33	0.07	23.7	0.7	4.22	0.04	single	4.38E-08	1.78E-07	2.88E-04	6.30E-08	8.44E-09
TS1														
TS2														

Table D.13.: Final fit (2):

No	$C_{\text{mod Ne}}$	$C_{\text{mod Ar}}$	$C_{\text{mod Kr}}$	$C_{\text{mod Xe}}$	n.a. ^4He	err	n.a. ^3He	err
	ccSTP/g	ccSTP/g	ccSTP/g	ccSTP/g	ccSTP/g		ccSTP/g	
1	2.91E-07	3.57E-04	6.91E-08	8.39E-09	6.25E-07	5.37E-09	4.32E-13	7.41E-15
2	3.33E-07	3.78E-04	7.29E-08	8.94E-09	4.86E-07	4.05E-09	3.26E-13	6.68E-15
3	3.64E-07	3.91E-04	7.37E-08	8.87E-09	5.27E-07	4.40E-09	3.92E-13	6.90E-15
4	2.52E-07	3.22E-04	6.45E-08	8.07E-09	7.95E-07	6.08E-09	4.77E-13	7.16E-15
5	2.81E-07	3.41E-04	6.76E-08	8.44E-09	1.89E-06	1.96E-08	5.11E-13	8.74E-15
6	3.42E-07	3.84E-04	7.39E-08	9.06E-09	1.54E-06	2.13E-08	8.85E-13	2.66E-14
7	3.48E-07	3.77E-04	7.13E-08	8.61E-09	2.54E-07	2.45E-09	2.55E-13	5.89E-15
8	2.67E-07	3.28E-04	6.46E-08	7.97E-09	4.53E-07	3.69E-09	3.19E-13	5.36E-15
9	3.55E-07	3.97E-04	7.51E-08	9.07E-09	4.74E-07	4.01E-09	2.94E-13	5.79E-15
10	2.88E-07	3.47E-04	6.88E-08	8.62E-09	2.08E-06	1.52E-08	4.97E-13	7.84E-15
11	2.97E-07	3.54E-04	7.12E-08	9.07E-09	2.08E-06	1.24E-08	3.68E-13	1.04E-14
12	2.80E-07	3.45E-04	6.89E-08	8.66E-09	1.66E-06	1.23E-08	3.01E-13	5.58E-15
13	2.95E-07	3.50E-04	6.91E-08	8.63E-09	3.10E-06	2.24E-08	9.30E-13	1.58E-14
14	3.09E-07	3.57E-04	6.95E-08	8.58E-09	3.37E-08	8.08E-10	2.33E-14	1.66E-15
15								
16	3.89E-07	4.12E-04	7.68E-08	9.16E-09	5.35E-08	1.10E-09	1.54E-14	2.21E-15
17	2.81E-07	3.46E-04	6.77E-08	8.32E-09	9.83E-07	8.66E-09	4.94E-13	7.98E-15
18	2.35E-07	3.23E-04	6.67E-08	8.59E-09	3.12E-06	3.60E-08	9.41E-13	3.23E-14
19								
20	3.33E-07	3.82E-04	7.33E-08	8.94E-09	1.63E-06	1.21E-08	8.53E-13	1.22E-14
21	2.45E-07	3.34E-04	6.81E-08	8.63E-09	1.08E-06	8.08E-09	6.35E-14	1.80E-15
22	2.24E-07	2.98E-04	6.08E-08	7.69E-09	2.42E-07	2.12E-09	1.21E-13	3.54E-15
23	2.52E-07	3.17E-04	6.25E-08	7.72E-09	2.46E-07	2.20E-09	6.01E-14	2.36E-15
24	2.96E-07	3.72E-04	7.27E-08	8.89E-09	1.74E-06	1.05E-08	5.43E-14	1.86E-15
25	2.72E-07	3.88E-04	7.84E-08	9.74E-09	1.12E-07	1.27E-09	-3.46E-15	1.56E-15
26	4.43E-07	4.70E-04	8.52E-08	9.85E-09	3.38E-05	2.40E-07	3.28E-12	8.06E-14
27	6.58E-07	5.82E-04	1.00E-07	1.13E-08	3.39E-05	2.41E-07	3.85E-12	8.96E-14
28	2.68E-07	3.39E-04	6.74E-08	8.42E-09	3.80E-08	6.18E-10	2.31E-15	1.45E-15
29	2.54E-07	3.42E-04	6.92E-08	8.74E-09	8.56E-08	1.06E-09	1.66E-15	1.18E-15
30	2.27E-07	3.11E-04	6.30E-08	7.91E-09	1.42E-09	3.42E-10	4.08E-15	1.20E-15
31	2.40E-07	3.21E-04	6.48E-08	8.12E-09	7.54E-07	4.71E-09	4.75E-14	1.56E-15
32	1.88E-07	2.77E-04	5.88E-08	7.68E-09	4.21E-09	5.19E-10	5.42E-16	2.12E-15
33	1.86E-07	2.71E-04	5.71E-08	7.40E-09	1.28E-08	4.25E-10	2.22E-15	1.51E-15
34	2.42E-07	3.23E-04	6.64E-08	8.52E-09	6.51E-08	8.96E-10	4.47E-15	2.00E-15
35	2.23E-07	3.00E-04	6.14E-08	7.81E-09	3.53E-09	3.49E-10	4.53E-15	1.15E-15
36	2.47E-07	3.11E-04	6.22E-08	7.79E-09	3.66E-09	3.91E-10	2.87E-15	1.09E-15
37	2.59E-07	3.50E-04	7.08E-08	8.94E-09	5.28E-06	3.08E-08	5.07E-12	6.06E-14
38	2.33E-07	3.06E-04	6.11E-08	7.59E-09	6.15E-09	4.67E-10	4.79E-15	1.35E-15
39	2.68E-07	3.28E-04	6.53E-08	8.17E-09	7.45E-09	7.70E-10	1.31E-15	3.26E-15
40	2.98E-07	3.51E-04	6.85E-08	8.43E-09	2.12E-08	5.70E-10	-4.32E-17	1.94E-15
41								
42								
43	1.80E-07	2.75E-04	5.89E-08	7.71E-09	1.46E-09	3.29E-10	3.26E-15	1.11E-15
44	5.35E-07	5.30E-04	9.16E-08	1.01E-08	3.32E-06	2.45E-08	2.69E-13	7.76E-15
45	3.77E-07	3.92E-04	7.30E-08	8.70E-09	2.84E-08	1.28E-09	1.24E-15	4.41E-15
46	1.89E-07	2.68E-04	5.62E-08	7.25E-09	6.16E-10	3.47E-10	6.12E-16	1.51E-15
47	2.97E-07	3.54E-04	7.12E-08	9.07E-09	2.08E-06	1.24E-08	3.68E-13	1.04E-14
48	2.69E-07	3.60E-04	7.23E-08	9.08E-09	4.03E-07	4.71E-09	5.67E-14	5.06E-15
49	2.57E-07	3.51E-04	7.30E-08	9.49E-09	1.10E-06	8.26E-09	6.88E-13	1.75E-14
50	2.86E-07	3.52E-04	6.96E-08	8.68E-09	1.22E-06	9.13E-09	9.02E-13	2.32E-14
51	2.44E-07	3.31E-04	6.84E-08	8.81E-09	2.17E-05	1.54E-07	9.71E-12	2.23E-13
52	2.43E-07	3.27E-04	6.69E-08	8.55E-09	3.06E-05	3.07E-07	1.05E-11	3.56E-13
53	2.80E-07	3.52E-04	7.13E-08	9.10E-09	8.90E-08	1.61E-09	3.56E-15	3.20E-15
TS1				measured	6.41E-05	4.53E-07	3.53E-12	6.20E-14
TS2				measured	2.72E-04	2.72E-06	1.88E-11	6.87E-13

Bibliography

- [Aeschbach-Hertig 2005] Aeschbach-Hertig, W.: A comment on “Helium sources in passive margin aquifers – new evidence for a significant mantle ^3He source in aquifers with unexpectedly low in situ $^3\text{He}/^4\text{He}$ production by M. C. Castro”. *Earth Planet Sci. Lett.* 240 , p. 827–829. 2005
- [Aeschbach-Hertig *et al.* 2008] Aeschbach-Hertig, W. ; El-Gamal, H. ; Wieser, M. ; Palcsu, L.: Modeling excess air and degassing in groundwater by equilibrium partitioning with a gas phase. *Water Resour. Res.* 44 , p. doi:10.1029/2007WR006454. 2008
- [Aeschbach-Hertig *et al.* 1999] Aeschbach-Hertig, W. ; Peeters, F. ; Beyerle, U. ; Kipfer, R.: Interpretation of dissolved atmospheric noble gases in natural waters. *Water Resour. Res.* 35(9) , p. 2779–2792. 1999
- [Aeschbach-Hertig *et al.* 2000] Aeschbach-Hertig, W. ; Peeters, F. ; Beyerle, U. ; Kipfer, R.: Palaeotemperature reconstruction from noble gases in ground water taking into account equilibration with entrapped air. *Nature* 405 , p. 1040–1044. 2000
- [Aeschbach-Hertig *et al.* 2002] Aeschbach-Hertig, W. ; Stute, M. ; Clark, J. ; Reuter, R. ; Schlosser, P.: A paleotemperature record derived from dissolved noble gases in groundwater of the Aquia Aquifer (Maryland, USA). *Geochim. Cosmochim. Acta* 66(5) , p. 797–817. 2002
- [Agarwal *et al.* 2006] Agarwal, M. ; Gupta, S. K. ; Deshpande, R. D. ; Yadava, M. G.: Helium, radon and radiocarbon studies on a regional aquifer system of the North Gujarat-Cambay region, India. *Chem. Geol.* 228 , p. 209–232. 2006
- [Anderson *et al.* 2002] Anderson, D. M. ; Overpeck, J. T. ; Gupta, A. K.: Increase in the Asian Southwest Monsoon During the Past Four Centuries. *Science* 297 , p. 596–599. 2002
- [Andrews and Lee 1979] Andrews, J. N. ; Lee, D. J.: Inert Gases in Groundwater from the Bunter Sandstone of England as Indicators of Age and Palaeoclimatic Trends. *J. Hydrol.* 41 , p. 233–252. 1979
- [Ballentine and Burnard 2002] Ballentine, C. J. ; Burnard, P. G.: Production, Release and Transport of Noble Gases in the Continental Crust. Porcelli, D. (ed.) ; Ballentine, C. (ed.) ; Wieler, R. (ed.): *Noble gases in geochemistry and cosmochemistry* Vol. 47. Mineralogical Society of America, Geochemical Society, 2002, chap. 14, p. 481–538
- [Ballentine and Hall 1999] Ballentine, C. J. ; Hall, C. M.: Determining paleotemperature and other variables by using an error-weighted, nonlinear inversion of noble gas concentrations in water. *Geochim. Cosmochim. Acta* 63(16) , p. 2315–2336. 1999
- [Barnett *et al.* 1988] Barnett, T. P. ; Dümenil, L. ; Schlese, U. ; Roeckner, E.: The Effect of Eurasian Snow Cover on Global Climate. *Science* 239 , p. 504–507. 1988
- [Battino 1979] Battino, R.: Xenon in Water. Clever, H. L. (ed.): *Solubility data series: Krypton, Xenon and Radon – Gas Solubilities* Vol. 2. Pergamon Press, 1979, chap. 2, p. 134
- [Baver *et al.* 1972] Baver, L. D. ; Gardner, W. H. ; Gardner, W. R.: Soil physics. John Wiley & Sons, Inc., New York, 1972
- [Bayer *et al.* 1989] Bayer, R. ; Schlosser, P. ; Bönisch, G. ; Rupp, H. ; Zaucker, F. ; Zimmek, G.: Performance and Blank Components of a Mass Spectrometric System for Routine Measurement of Helium Isotopes and Tritium by the ^3He In-growth Method. *Sitzungsberichte der Heidelberger Akademie der Wissenschaften*, Springer-Verlag Heidelberg, 1989
- [Becker and Kromer 1993] Becker, B. ; Kromer, B.: The continental tree-ring record – absolute chronology, calibration and climatic change at 11 ka. *Palaeogeog. Palaeoclim. Palaeoec.* 103 , p. 67–71. 1993
- [Beiser 1957] Beiser, A.: Variations in the Geomagnetic Dipole in the Past 15,000 Years. *J. Geophys. Res.* 62(2) , p. 235–239. 1957

- [Benson and Krause 1980] Benson, B. B. ; Krause, D.: Isotopic fractionation of helium during solution: A probe for the liquid state. *J. Solution Chem.* 9(12) , p. 895–909. 1980
- [Beyerle *et al.* 2000] Beyerle, U. ; Aeschbach-Hertig, W. ; Imboden, D. M. ; Baur, H. ; Graf, T. ; Kipfer, R.: A Mass Spectrometric System for the Analysis of Noble Gases and Tritium from Water Samples. *Environ. Sci. Technol.* 34 , p. 2042–2050. 2000
- [Beyerle *et al.* 2003] Beyerle, U. ; Rüedi, J. ; Leuenberger, M. ; Aeschbach-Hertig, W. ; F., Peeters. ; Kipfer, R. ; Dodo, A.: Evidence for periods of wetter and cooler climate in the Sahel between 6 and 40 kyr BP derived from groundwater. *Geophys. Res. Lett.* 30(4) , p. doi:10.1029/2002GL016310. 2003
- [Bhattacharya and Subrahmanyam 1986] Bhattacharya, G. C. ; Subrahmanyam, V.: Extension of the Narmada-Son Lineament on the Continental Margin off Saurashtra, Western India as Obtained from Magnetic Measurements. *Mar. Geophys. Res.* 8 , p. 329–344. 1986
- [Bührer and Ambühl 1975] Bührer, H. ; Ambühl, H.: Die Einleitung von gereinigtem Abwasser in Seen. *Aquatic Sci.* 37(2) , p. 347–369. 1975
- [Bischof 1837] Bischof, G.: Die Wärmelehre des Innern unsers Erdkörpers. Verlag von Joh. Ambros. Barth., Leipzig, 1837
- [Bottinga 1968] Bottinga, Y.: Calculation of Fractionation Factors for Carbon and Oxygen Isotopic Exchange in the System Calcite-Carbon Dioxide-Water. *J. Phys. Chem.* 72(8) , p. 800–808. 1968
- [Bottinga 1969] Bottinga, Y.: Calculated fractionation factors for carbon and hydrogen isotope exchange in the system calcite-carbon dioxide-graphite-methane-hydrogen-water vapor. *Geochim. Cosmochim. Acta* 33 , p. 49–64. 1969
- [Bourg and Sposito 2008] Bourg, I. C. ; Sposito, G.: Isotopic fractionation of noble gases by diffusion in liquid water: Molecular dynamics simulations and hydrologic applications. *Geochim. Cosmochim. Acta* 72 , p. 2237–2247. 2008
- [Breddam and Kurz 2001] Breddam, K. ; Kurz, M. D.: Helium Isotopic Signatures of Icelandic Alkaline Lavas. 2001. – AGU Fall Meeting
- [Bronk Ramsey 2009] Bronk Ramsey, C.: Bayesian Analysis of Radiocarbon Dates. *Radiocarbon* 51(1) , p. 337–360. 2009
- [Brook *et al.* 1983] Brook, G. A. ; Folkoff, M. E. ; Box, E. O.: A world model of soil carbon dioxide. *Earth Surf. Proc. Land.* 8 , p. 79–88. 1983
- [Brun *et al.* 2001] Brun, R. ; Reichert, P. ; Künsch, H. R.: Practical identifiability analysis of large environmental simulation models. *Water Resour. Res.* 37(4) , p. 1015–1030. 2001
- [Bundesministerium für Justiz 2001] Bundesministerium für Justiz: Verordnung über die Qualität von Wasser für den menschlichen Gebrauch. 2001
- [Burroughs 1969] Burroughs, E. G.: Collection Efficiency of Continuous Dynode Electron Multiple Arrays. *Rev. Sci. Instr.* 40(1) , p. 35–37. 1969
- [Busenberg and Plummer 2000] Busenberg, E. ; Plummer, L. N.: Dating young groundwater with sulfur hexafluoride: Natural and anthropogenic sources of sulfur hexafluoride. *Water Resour. Res.* 36(10) , p. 3011–3030. 2000
- [Castro *et al.* 2007] Castro, M. C. ; Hall, C. M. ; Patriarche, D. ; Goblet, P. ; Ellis, B. R.: A new noble gas paleoclimate record in Texas – Basic assumptions revisited. *Earth Planet Sci. Lett.* 257 , p. 170–187. 2007
- [Cerling 1984] Cerling, T. E.: The stable isotopic composition of modern soil carbonate and its relationship to climate. *Earth Planet Sci. Lett.* 71 , p. 229–240. 1984
- [Cey 2009] Cey, B. D.: On the accuracy of noble gas recharge temperatures as a paleoclimate proxy. *J. Geophys. Res.* 114 , p. doi:10.1029/2008JD010438. 2009
- [Clark and Fritz 1997] Clark, I. D. ; Fritz, P.: Environmental Isotopes in Hydrogeology. Lewis Publishers, New York, 1997
- [Clarke *et al.* 1969] Clarke, W. B. ; Beg, M. A. ; Craig, H.: Excess ^3He in the Sea: Evidence for Terrestrial Primordial Helium. *Earth Planet. Sci. Lett.* 6 , p. 213–220. 1969

- [Clarke *et al.* 1976] Clarke, W. B. ; Jenkins, W. J. ; Top, Z.: Determination of Tritium by Mass Spectrometric Measurement of ^3He . *Internat. J. Appl. Radiation Iso.* 27 , p. 515–522. 1976
- [Class and Goldstein 2005] Class, C. ; Goldstein, S. L.: Evolution of helium isotopes in the Earth's mantle. *Nature* 436 , p. 1107–1112. 2005
- [Coleman *et al.* 1982] Coleman, M. L. ; Shepherd, T. J. ; Durham, J. J. ; Rouse, J. E. ; Moore, G. R.: Reduction of water with zinc for hydrogen isotope analysis. *Anal. Chem.* 54(6) , p. 993–995. 1982
- [Craig 1954] Craig, H.: Carbon 13 in Plants and the Relationships between Carbon 13 and Carbon 14 Variations in Nature. *J. Geology* 62(2) , p. 115–149. 1954
- [Craig 1961] Craig, H.: Isotopic Variations in Meteoric Waters. *Science* 133 , p. 1702–1703. 1961
- [Craig and Lupton 1976] Craig, H. ; Lupton, J. E.: Primordial Neon, Helium, and Hydrogen in Oceanic Basalts. *Earth Planet. Sci. Lett.* 31 , p. 369–385. 1976
- [Craig *et al.* 1978] Craig, H. ; Lupton, J. E. ; Welhan, J. A. ; Poreda, R.: Helium Isotope Ratios in Yellowstone and Lassen Park Volcanic Gases. *Geophys. Res. Lett.* 5(11) , p. 897–900. 1978
- [Criss 1991] Criss, R. E.: Temperature dependence of isotopic fractionation factors. Taylor, Hugh P. (ed.) ; O'Neil, James R. (ed.) ; Kaplan, Isaac R. (ed.): *Stable isotope geochemistry*, Geochemical Society, USA, 1991, p. 11–16
- [Crowe 1958] Crowe, C.: Carbon-14 Activity During the Past 5,000 Years. *Nature* 182 , p. 470–471. 1958
- [Dansgaard 1964] Dansgaard, W.: Stable Isotopes in Precipitation. *Tellus* 16(4) , p. 436–468. 1964
- [Deines *et al.* 1974] Deines, P. ; Langmuir, D. ; Harmon, R. S.: Stable carbon isotope ratios and the existence of a gas phase in the evolution of carbonate ground waters. *Geochim. Cosmochim. Acta* 38 , p. 1147–1164. 1974
- [Deshpande 2006] Deshpande, R. D.: Groundwater in and Around Cambay Basin, Gujarat: Some Geochemical and Isotopic Investigations, Physical Research Laboratory, Ahmedabad, PhD Thesis, 2006
- [Deshpande *et al.* 2010] Deshpande, R. D. ; Maurya, A. S. ; Kumar, B. ; Sarkar, A. ; Gupta, S. K.: Rain-Vapor Interaction and Vapor Source Identification using Stable Isotopes from Semi-Arid Western India. *J. Geophys. Res.* in press , p. DOI:10.1029/2010JD014458. 2010
- [Drever 1997] Drever, J. I.: The geochemistry of natural waters. Prentice Hall, New Jersey, 1997
- [Dreybrodt 1988] Dreybrodt, W.: Processes in Karst Systems – Physics, Chemistry and Geology. Springer Verlag, Berlin, Heidelberg, New York, London, Paris, Tokyo, 1988
- [Durrige Co 2000] Durrige Co: RAD7 radon detector – Owner's manual. <http://www.durrige.com/Manuals.htm>. 2000
- [Durrige Co 2001] Durrige Co: RAD7 RAD-H₂O – Radon in water accessory – Owner's manual. 2001
- [Ehleringer *et al.* 1991] Ehleringer, J. R. ; Phillips, S. L. ; Schuster, W. S. F. ; Sandquist, D. R.: Differential utilization of summer rains by desert plants. *Oecologia* 88 , p. 430–434. 1991
- [Enzel *et al.* 1999] Enzel, Y. ; Ely, L. L. ; Hishra, S. ; Ramesh, R. ; Amit, R. ; Lazar, B. ; Rajaguru, S. N. ; Baker, V. R. ; Sandler, A.: High-Resolution Holocene Environmental Changes in the Thar Desert, Northwestern India. *Science* 284 , p. 125–128. 1999
- [Fabryka-Martin *et al.* 1994] Fabryka-Martin, J. ; Curtis, D. B. ; Dixon, P. ; Rokop, D. ; Roensch, F. ; Aguilar, R. ; Attrep, M. ; Cramer (ed), J. J. ; Smellie (ed), J. A. T.: Natural nuclear products in the Cigar Lake Deposit. Final Report of the AECL SKB Cigar Lake Analog Study. *AECL* 10851 , p. 268–291. 1994
- [Fairbanks *et al.* 2005] Fairbanks, R. G. ; Mortlock, R. A. ; Chiu, T.-C. ; Cao, L. ; Kaplan, A. ; Guilderson, T. P. ; Fairbanks, T. W. ; Bloom, A. L. ; Grootes, P. M. ; Nadeau, M.-J.: Radiocarbon calibration curve spanning 0 to 50,000 years BP based on paired $^{230}\text{Th}/^{234}\text{U}/^{238}\text{U}$ and ^{14}C dates on pristine corals. *Quatern. Sci. Rev.* 24 , p. 1781–1796. 2005
- [Fleitmann *et al.* 2007] Fleitmann, D. ; Burns, S. J. ; Mangini, A. ; Mudelsee, M. ; Kramers, J. ; Villa, I. ; Neff, U. ; Al-Subbary, A. A. ; Buettner, A. ; Hippler, D. ; Matter, A.: Holocene ITCZ and Indian monsoon dynamics recorded in stalagmites from Oman and Yemen (Socotra). *Quaternary Sci. Rev.* 26(1-2) , p. 170–188. 2007

- [Fleitmann *et al.* 2003a] Fleitmann, D. ; Burns, S. J. ; Mudelsee, M. ; Neff, U. ; Kramers, J. ; Mangini, A. ; Matter, A.: Holocene Forcing of the Indian Monsoon Recorded in a Stalagmite from Southern Oman. *Science* 300(5626) , p. 1737–1739. 2003
- [Fleitmann *et al.* 2003b] Fleitmann, D. ; Burns, S. J. ; Neff, U. ; Mangini, A. ; Matter, A.: Changing moisture sources over the last 330,000 years in Northern Oman from fluid-inclusion evidence in speleothems. *Quatern. Res.* 60 , p. 223–232. 2003
- [Florkowski 1985] Florkowski, T.: Sample preparation for hydrogen isotope analysis by mass spectrometry. *J. Appl. Rad. Iso.* 36(12) , p. 991–992. 1985
- [Fohlmeister 2008] Fohlmeister, J.: Carbon isotopes in stalagmites and drip water – Tracers of soil processes, Ruprecht-Karls-Universität Heidelberg, PhD thesis, 2008
- [Fontes and Garnier 1979] Fontes, J.-C. ; Garnier, J.-M.: Determination of the Initial ^{14}C Activity of the Total Dissolved Carbon: A Review of the Existing Models and a New Approach. *Water Resour. Res.* 15(2) , p. 399–413. 1979
- [Frape *et al.* 1984] Frape, S. K. ; Fritz, P. ; McNutt, R. H.: Water-rock interaction and chemistry of groundwaters from the Canadian Shield. *Geochim. Cosmochim. Acta* 48 , p. 1617–1627. 1984
- [Fricke and O'Neil 1999] Fricke, H. C. ; O'Neil, J. R.: The Correlation between $^{18}\text{O}/^{16}\text{O}$ Ratios of Meteoric Water and Surface Temperature: its Use in Investigating Terrestrial Climate Change over Geologic Time. *Earth Planet. Sci. Lett.* 170 , p. 181–196. 1999
- [Friedman and O'Neil 1977] Friedman, I. ; O'Neil, J. R.: Compilation of stable isotope fractionation factors of geochemical interest. Fleischer, M. (ed.): *Data of Geochemistry*. US Geological Survey, 1977
- [Friedrich 2007] Friedrich, R.: Aufbau eines Massenspektrometersystems und Untersuchung des Grundwassers in der Odenwald-Region, Ruprecht-Karls-Universität Heidelberg, PHD Thesis, 2007
- [Gat 1996] Gat, J. R.: Oxygen and Hydrogen Isotopes in the Hydrologic Cycle. *Annu. Rev. Earth Planet. Sci.* 24 , p. 225–262. 1996
- [Godwin 1962] Godwin, H.: Half-life of Radiocarbon. *Nature* 195 , p. 984. 1962
- [Gombos Jr. *et al.* 1995] Gombos Jr., A. M. ; Powell, W. G. ; Norton, I. O.: The Tectonic Evolution of Western India and its Impact on Hydrocarbon Occurrences: an Overview. *Sediment. Geol.* 96 , p. 119–129. 1995
- [Gonfiantini 1986] Gonfiantini, R.: Environmental isotopes in lake studies. Fritz, P. (ed.) ; Fontes, J.-Ch. (ed.): *Handbook of Environmental Isotope Geochemistry*, Elsevier, Amsterdam, 1986, p. 113–168
- [Gonfiantini and Zuppi 2003] Gonfiantini, R. ; Zuppi, G. M.: Carbon isotope exchange rate of DIC in karst groundwater. *Chem. Geol.* 197 , p. 319–336. 2003
- [Grothe 1992] Grothe, J.: Datenerfassung und Datenauswertung am Heidelberger Low-Level-Tritium-Messsystem, Ruprecht-Karls-Universität Heidelberg, diploma thesis, 1992
- [Gupta *et al.* 2003] Gupta, A. K. ; Anderson, D. M. ; Overpeck, J. T.: Abrupt changes in the Asian southwest monsoon during the Holocene and their links to the North Atlantic Ocean. *Nature* 421 , p. 354–357. 2003
- [Gupta *et al.* 2006] Gupta, A. K. ; Anderson, D. M. ; Pandey, D. N. ; Singhvi, A. K.: Adaptation and human migration, and evidence of agriculture coincident with changes in the Indian summer monsoon during the Holocene. *Current Science* 90(8) , p. 1082–1091. 2006
- [Gupta and Deshpande 2003] Gupta, S. K. ; Deshpande, R. D.: Origin of groundwater helium and temperature anomalies in the Cambay region of Gujarat, India. *Chem. Geol.* 198 , p. 33–46. 2003
- [Gupta *et al.* 2005] Gupta, S. K. ; Deshpande, R. D. ; Agarwal, M. ; Raval, B. R.: Origin of High Fluoride in Groundwater in the North Gujarat-Cambay Region, India. *Hydrogeol. J.* 13 , p. 596–605. 2005
- [Hall *et al.* 2005] Hall, C. M. ; Castro, M. C. ; Lohmann, K. C. ; Ma, L.: Noble gases and stable isotopes in a shallow aquifer in southern Michigan: Implications for noble gas paleotemperature reconstructions for cool climates. *Geophys. Res. Lett.* 32 , p. doi:10.1029/2005GL023582. 2005

- [Harnisch and Eisenhauer 1998] Harnisch, J. ; Eisenhauer, A.: Natural CF₄ and SF₆ on Earth. *Geophys. Res. Lett.* 25(13) , p. 2401–2404. 1998
- [Harnisch *et al.* 2000] Harnisch, J. ; Frische, M. ; Borchers, R. ; Eisenhauer, A. ; Jordan, A.: Natural fluorinated organics in fluorite and rocks. *Geophys. Res. Lett.* 27(13) , p. 1883–1886. 2000
- [Heaton *et al.* 1983] Heaton, T. H. E. ; Talma, A. S. ; Vogel, J. C.: Origin and history of nitrate in confined groundwater in the western Kalahari. *J. Hydrol.* 62 , p. 243–262. 1983
- [Heaton and Vogel 1981] Heaton, T. H. E. ; Vogel, J. C.: “Excess Air” in Groundwater. *J. Hydrol.* 50 , p. 201–216. 1981
- [Hendy 1970] Hendy, C. H.: The isotopic geochemistry of speleothems – I. The calculation of the effects of different modes of formation on the isotopic composition of speleothems and their applicability as palaeoclimatic indicators. *Geochim. Cosmochim. Acta* 35 , p. 801–824. 1970
- [Herzschuh 2006] Herzschuh, U.: Palaeo-moisture evolution in monsoonal Central Asia during the last 50,000 years. *Quat. Sci. Rev.* 25 , p. 163–178. 2006
- [Hoefs 2009] Hoefs, J.: Stable Isotope Geochemistry. Springer-Verlag Berlin Heidelberg, 2009
- [Hughen *et al.* 2004] Hughen, K. ; Lehman, S. ; Overpeck, J. ; Marchal, O. ; Herring, C. ; Turnbull, J.: ¹⁴C Activity and Global Carbon Cycle Changes over the Past 50,000 Years. *Science* 303 , p. 202–207. 2004
- [Hughen *et al.* 2006] Hughen, K. ; Southon, J. ; Lehman, S. ; Bertrand, C. ; Turnbull, J.: Marine-derived ¹⁴C calibration and activity record for the past 50,000 years updated from the Cariaco Basin. *Quatern. Sci. Rev.* 25 , p. 3216–3227. 2006
- [IAEA 2007] IAEA: GNIP database. 2007
- [Ingerson and Pearson Jr. 1964] Ingerson, E. ; Pearson Jr., F. J.: Estimation of age and rate of motion of groundwater by the ¹⁴C-method. *Recent Research in the Fields of Hydrosphere, Atmosphere and Nuclear Geochemistry*, Maruzen, Tokyo, 1964, p. 263–283
- [Ingram *et al.* 2007] Ingram, R. G. S. ; Hiscock, K. M. ; Dennis, P. F.: Noble gas excess air applied to distinguish groundwater recharge conditions. *Environ. Sci. Technol.* 41 , p. 1949–1955. 2007
- [IPCC 2007] IPCC ; Solomon, S. (ed.) ; Qin, D. (ed.) ; Manning, M. (ed.) ; Chen, Z. (ed.) ; Marquis, M. (ed.) ; Averyt, K. B. (ed.) ; Tignor, M. (ed.) ; Miller, H. L. (ed.): Climate Change 2007: The Physical Science Basis. Contribution of Working Group I to the Fourth Assessment Report of the Intergovernmental Panel on Climate Change. Cambridge University Press, Cambridge, United Kingdom and New York, NY, USA, 2007
- [Johnsen *et al.* 1995] Johnsen, S. J. ; Dahl-Jensen, D. ; Dansgaard, W. ; Gundestrup, N.: Greenland palaeotemperatures derived from GRIP bore hole temperature and ice core isotope profiles. *Tellus* 47B , p. 624–629. 1995
- [Jouzel *et al.* 1982] Jouzel, J. ; Merlivat, L. ; Lorius, C.: Deuterium excess in an East Antarctic ice core suggests higher relative humidity at the oceanic surface during the last glacial maximum. *Nature* 299 , p. 688–691. 1982
- [Juyal *et al.* 2006] Juyal, N. ; Chamyal, L. S. ; Bhandari, S. ; Bhushan, R. ; Singhvi, A. K.: Continental record of the southwest monsoon during the last 130 ka: evidence from the southern margin of the Thar Desert, India. *Quaternary Sci. Rev.* 25(19-20) , p. 2632–2650. 2006
- [Juyal *et al.* 2003] Juyal, N. ; Kar, A. ; Rajaguru, S. N. ; Singhvi, A. K.: Luminescence chronology of aeolian deposition during the Late Quaternary on the southern margin of Thar Desert, India. *Quatern. Int.* 104(1) , p. 87–98. 2003
- [Kalnay *et al.* 1996] Kalnay, E. ; Kanamitsu, M. ; Kistler, R. ; Collins, W. ; Deaven, D. ; Gandin, L. ; Iredell, M. ; Saha, S. ; White, G. ; Woollen, J. ; Zhu, Y. ; Leetmaa, A. ; Reynolds, R. ; Chelliah, M. ; Ebisuzaki, W. ; Higgins, W. ; Janowiak, J. ; Mo, K. C. ; Ropelewski, C. ; Wang, J. ; Jenne, R. ; Joseph, D.: The NCEP/NCAR reanalysis project. *Bull. Am. Meteorol. Soc.* 77 , p. 437–471. 1996
- [Kaneoka and Takaoka 1980] Kaneoka, I. ; Takaoka, N.: Rare Gas Isotopes in Hawaiian Ultramafic Nodules and Volcanic Rocks: Constraint on Genetic Relationships. *Science* 208 , p. 1366–1368. 1980
- [Keck 2001] Keck, L.: Climate significance of stable isotope records from Alpine ice cores, Ruprecht-Karls-Universität Heidelberg, PHD thesis, 2001

- [Kipfer *et al.* 2002] Kipfer, R. ; Aeschbach-Hertig, W. ; Peeters, F. ; Stute, M.: Noble gases in lakes and ground waters. Porcelli, D. (ed.) ; Ballentine, C. (ed.) ; Wieler, R. (ed.): *Noble gases in geochemistry and cosmochemistry* Vol. 47. Mineralogical Society of America, Geochemical Society, 2002, chap. 14, p. 615–700
- [Kluge *et al.* 2007] Kluge, T. ; Ilmberger, J. ; Rohden, C. von ; Aeschbach-Hertig, W.: Tracing and quantifying groundwater inflow into lakes using a simple method for radon-222 analysis. *Hydrol. Earth Syst. Sci.* 11 , p. 1621–1631. 2007
- [Kluge *et al.* 2010a] Kluge, T. ; Riechelmann, D. F. C. ; Wieser, M. ; Spötl, C. ; Sültenfuß, J. ; Schröder-Ritzrau, A. ; Niggemann, S. ; Aeschbach-Hertig, W.: Dating Cave Drip Water by Tritium. *J. Hydrol.* 394 , p. 396–406. 2010
- [Kluge *et al.* 2010b] Kluge, T. ; Wieser, M. ; Aeschbach-Hertig, W.: Assessing the use of ^3H - ^3He dating to determine the subsurface transit time of cave drip waters. *Isot. Environ. Health. S.* 10.1080 , p. 10256016.2010.503893. 2010
- [Kreuzer 2007] Kreuzer, A.: Paläotemperaturstudie mit Edelgasen im Grundwasser der Nordchinesischen Tiefebene, Ruprecht-Karls-Universität Heidelberg, Inaugural-Dissertation, 2007
- [Kreuzer *et al.* 2009] Kreuzer, A. M. ; Rohden, C. von ; Friedrich, R. ; Chen, Z. ; Shi, J. ; Hajdas, I. ; Kipfer, R. ; Aeschbach-Hertig, W.: A record of temperature and monsoon intensity over the past 40 kyr from groundwater in the North China Plain. *Chem. Geol.* 259 , p. 168–180. 2009
- [Kromer 2007] Kromer, B.: Radiokohlenstoffdatierung. Wagner, Günther A. (ed.): *Einführung in die Archäometrie*, Springer Verlag Berlin Heidelberg, 2007, p. 3–10
- [Kulongoski *et al.* 2004] Kulongoski, J. T. ; Hilton, D. R. ; Selaolo, E. T.: Climate variability in the Botswana Kalahari from the late Pleistocene to the present day. *Geophys. Res. Lett.* 31 , p. doi:10.1029/2003GL019238. 2004
- [Kutzbach 1981] Kutzbach, J. E.: Monsoon Climate of the Early Holocene: Climate Experiment with the Earth's Orbital Parameters for 9000 Years Ago. *Science* 214 , p. 59–61. 1981
- [Kyser and Rison 1982] Kyser, T. K. ; Rison, W.: Systematics of Rare Gas Isotopes in Basic Lavas and Ultramafic Xenoliths. *J. Geophys. Res.* 87(B7) , p. 5611–5630. 1982
- [Lachniet 2009] Lachniet, M. S.: Climatic and Environmental Controls on Speleothem Oxygen-Isotope Values. *Quat. Sci. Rev.* 28 , p. 412–432. 2009
- [Langmuir 1916] Langmuir, I.: The Constitution and Fundamental Properties of Solids and Liquids. *J. Am. Chem. Soc.* 38(11) , p. 2221–2295. 1916
- [Lee and Fung 2008] Lee, J. E. ; Fung, I.: “Amount effect” of water isotopes and quantitative analysis of post-condensation processes. *Hydrol. Process.* 22 , p. 1–8. 2008
- [Lee and Swann 2010] Lee, J.-E. ; Swann, A. L.: Evaluation of the “amount effect” at speleothem sites in the Asian monsoon region. *Earth Environ. Sci.* 9 , p. doi:10.1088/1755-1315/9/1/012023. 2010
- [LeGrande and Schmidt 2006] LeGrande, A. N. ; Schmidt, G. A.: Global gridded data set of the oxygen isotopic composition in seawater. *Geophys. Res. Lett.* 33 , p. doi:10.1029/2006GL026011. 2006
- [Lehmann *et al.* 2000] Lehmann, B. E. ; Lehmann, M. ; Neftel, A. ; Tarakanov, S. V.: Radon-222 Monitoring in Soil Diffusivity. *Geophys. Res. Lett.* 23 , p. 3917–3920. 2000
- [Lerman *et al.* 1970] Lerman, J. C. ; Mook, W. G. ; Vogel, J. C.: C14 in tree rings from different localities. Olsson, J. U. (ed.): *Radiocarbon variations and absolute chronology*, Wiley, New York, 1970, p. 275–301
- [Levin *et al.* 2010a] Levin, I. ; Naegler, T. ; Heinz, R. ; Osusko, D. ; Cuevas, E. ; Engel, A. ; Ilmberger, J. ; Langenfelds, R. L. ; Neininger, B. ; Rohden, C. v. ; Steele, L. P. ; Weller, R. ; Worthy, D. E. ; Zimov, S. A.: The global SF₆ source inferred from long-term high precision atmospheric measurements and its comparison with emission inventories. *Atmos. Chem. Phys.* 10 , p. 2655–2662. 2010
- [Levin *et al.* 2010b] Levin, I. ; Naegler, T. ; Kromer, B. ; Diehl, M. ; Francey, R. J. ; Gomez-Pelaez, A. J. ; Steele, L. P. ; Wagenbach, D. ; Weller, R. ; Worthy, D. E.: Observations and modelling of the global distribution and long-term trend of atmospheric $^{14}\text{CO}_2$. *Tellus* 62B , p. 26–46. 2010
- [Leya and Wieler 1999] Leya, I. ; Wieler, R.: Nucleogenic production of Ne isotopes in Earth's crust and upper mantle induced by alpha particles from the decay of U and Th. *J. Geophys. Res.* 104(B7) , p. 15439–15450. 1999

- [Libby 1946] Libby, W. F.: Atmospheric Helium Three and Radiocarbon from Cosmic Radiations. *Phys. Rev.* 69 , p. 11–12. 1946
- [Lippmann *et al.* 2003] Lippmann, J. ; Stute, M. ; Torgersen, T. ; Moser, D. P. ; Hall, J. A. ; Lin, L. ; Borcsik, M. ; Bellamy, R. E. S. ; Onstott, T. C.: Dating ultra-deep mine waters with noble gases and ^{36}Cl , Witwatersrand Basin, South Africa. *Geochim. Cosmochim. Acta* 67(23) , p. 4597–4619. 2003
- [Loosli *et al.* 2000] Loosli, H. H. ; Lehmann, B. E. ; Smethie Jr., W. M.: Noble Gas Radioisotopes. Cook, P. (ed.) ; Herczeg, A. L. (ed.): *Environmental Tracers in Subsurface Hydrology*. Kluwer Academic Publishers, 2000, p. 379–396
- [Lorius and Oeschger 1994] Lorius, C. ; Oeschger, H.: Palaeo-perspectives: Reducing Uncertainties in Global Change? *Ambio* 23(1) , p. 30–36. 1994
- [Lucas and Unterweger 2000] Lucas, L. L. ; Unterweger, M. P.: Comprehensive Review and Critical Evaluation of the Half-Life of Tritium. *J. Res. Natl. Inst. Stand. Technol.* 105 , p. 541–549. 2000
- [Lupton *et al.* 1989] Lupton, J. E. ; Baker, E. T. ; Massoth, G. J.: Variable $^3\text{He}/\text{heat}$ ratios in submarine hydrothermal systems: evidence from two plumes over the Juan de Fuca ridge. *Nature* 337 , p. 161–164. 1989
- [Mahrla 1978] Mahrla, P.: Die Messgenauigkeit des Heidelberger Low-Level-Tritiummessverfahrens für ozeanische Proben, Ruprecht-Karls-Universität Heidelberg, diploma thesis, 1978
- [Maiß and Brenninkmeijer 1998] Maiß, M. ; Brenninkmeijer, C. A. M.: Atmospheric SF_6 : Trends, Sources, and Prospects. *Environ. Sci. Technol.* 32 , p. 3077–3086. 1998
- [Mamyrin and Tolstikhin 1984] Mamyrin, B. A. ; Tolstikhin, I. N.: Helium isotopes in nature. Elsevier, Amsterdam, 1984
- [McCrea 1950] McCrea, J. M.: On the Isotopic Chemistry of Carbonates and a Paleotemperature Scale. *J. Chem. Phys.* 18(6) , p. 849–857. 1950
- [Merh 1995] Merh, S. S.: Geology of Gujarat. Geological Society of India, Bangalore, 1995
- [Merlivat and Jouzel 1979] Merlivat, L. ; Jouzel, J.: Global Climatic Interpretation of the Deuterium-Oxygen 18 Relationship for Precipitation. *J. Geophys. Res.* 84(C8) , p. 5029–5033. 1979
- [Meshik *et al.* 2004] Meshik, A. P. ; Hohenberg, C. M. ; Pravdivtseva, O. V.: Record of Cycling Operation of the Natural Nuclear Reactor in the Oklo/Okelobondo Area in Gabon. *Phys. Rev. Lett.* 93(18) , p. 182302.1–182302.4. 2004
- [Münnich 1958] Münnich, K. O.: Durch Atomexplosionen erzeugter Radiokohlenstoff in der Atmosphäre. *Naturwissenschaften* 45(7) , p. 327–329. 1958
- [Münnich 1968] Münnich, K. O.: Isotopen-Datierung von Grundwasser. *Naturwissenschaften* 55(4) , p. 158–163. 1968
- [Mook *et al.* 1974] Mook, W. G. ; Bommerson, J. C. ; Staverman, W. H.: Carbon isotope fractionation between dissolved bicarbonate and gaseous carbon dioxide. *Earth Planet Sci. Lett.* 22 , p. 169–176. 1974
- [Mook and van der Plicht 1999] Mook, W. G. ; Plicht, J. van der: Reporting ^{14}C activities and concentrations. *Radiocarbon* 41(3) , p. 227–239. 1999
- [Mook and Vogel 1968] Mook, W. G. ; Vogel, J. C.: Isotopic Equilibrium between Shells and Their Environment. *Science* 159 , p. 874–875. 1968
- [Mook and de Vries 2001] Mook, W. G. ; Vries, J. J. de: Environmental Isotopes in the Hydrological Cycle, Principles and Applications. International Atomic Energy Agency, 2001
- [Muscheler *et al.* 2008] Muscheler, R. ; Kromer, B. ; Björck, S. ; Svensson, A. ; Friedrich, M. ; Kaiser, K. F. ; Southon, J.: Tree rings and ice cores reveal ^{14}C calibration uncertainties during the Younger Dryas. *Nature Geoscience* 1 , p. 263–267. 2008
- [Neff *et al.* 2001] Neff, U. ; Burns, S. J. ; Mangini, A. ; Mudelsee, M. ; Fleitmann, D. ; Matter, A.: Strong coherence between solar variability and the monsoon in Oman between 9 and 6 kyr ago. *Nature* 411 , p. 290–293. 2001

- [Neubert 1992] Neubert, R.: Messung der stabilen Isotopomere des atmosphärischen Kohlendioxids, Ruprecht-Karls-Universität Heidelberg, PHD thesis, 1992
- [NOAA 2010a] NOAA: Global Historical Climatology Network. 2010
- [NOAA 2010b] NOAA: HISPLIT model, GDAT data. 2010
- [von Oehsen 2008] Oehsen, A. von: Parameter Estimation and Model Validation for Models of dissolved Noble Gas Concentrations in Groundwater, Ruprecht-Karls-Universität Heidelberg, diploma thesis, 2008
- [O'Leary 1981] O'Leary, M. H.: Carbon Isotope Fractionation in Plants. *Phytochemistry* 20(4) , p. 553–567. 1981
- [Overpeck *et al.* 1996] Overpeck, J. ; Anderson, D. ; Trumbore, S. ; Prell, W.: The southwest Indian Monsoon over the last 18 000 years. *Climate Dynamics* 12(3) , p. 213–225. 1996
- [Panichi and Gonfiantini 1978] Panichi, C. ; Gonfiantini, R.: Environmental isotopes in geothermal studies. *Geothermics* 6 , p. 143–161. 1978
- [Patra *et al.* 1997] Patra, P. K. ; Lal, S. ; Subbaraya, B. H.: Observed vertical profile of sulphur hexafluoride (SF6) and its atmospheric applications. *J. Geophys. Res.* 102(D7) , p. 8855–8859. 1997
- [Pearson Jr. 1965] Pearson Jr., F. J.: Use of C-13/C-12 ratios to correct radiocarbon ages of material initially diluted by limestone. *Radiocarbon and Tritium Dating, Proceedings of Sixth International Conference on Radiocarbon*, Pullman, Washington, 1965, p. 357–366
- [Peeters *et al.* 2003] Peeters, F. ; Beyerle, U. ; Aeschbach-Hertig, W. ; Holocher, J. ; Brennwald, M. S. ; Kipfer, R.: Improving noble gas based paleoclimate reconstruction and groundwater dating using 20Ne/22Ne ratios. *Geochim. Cosmochim. Acta* 67(4) , p. 587–600. 2003
- [Peisker 1984] Peisker, M.: Modellvorstellungen zur Kohlenstoff-Isotopendiskriminierung bei der Photosynthese von C3- und C4-Pflanzen. *Genet. Resour. Crop. Ev.* 32 , p. 35–65. 1984
- [Plummer and Busenberg 1982] Plummer, L. N. ; Busenberg, E.: The solubilities of calcite, aragonite and vaterite in CO₂-H₂O solutions between 0 and 90°C, and an evaluation of the aqueous model for the system CaCO₃-CO₂-H₂O. *Geochim. Cosmochim. Acta* 46 , p. 1011–1040. 1982
- [Plummer *et al.* 1994] Plummer, L. N. ; Prestemon, E. C. ; Parkhurst, D. L.: An Interactive Code (NETPATH) for Modeling Net Geochemical Reactions along a Flow Path Version 2.0. 1994
- [Porcelli *et al.* 2002] Porcelli, D. ; Ballentine, C. J. ; Wieler, R.: An Overview of Noble Gas Geochemistry and Cosmochemistry. Porcelli, D. (ed.) ; Ballentine, C. (ed.) ; Wieler, R. (ed.): *Noble gases in geochemistry and cosmochemistry* Vol. 47. Mineralogical Society of America, Geochemical Society, 2002, p. 1–18
- [Poreda and Craig 1989] Poreda, R. ; Craig, H.: Helium isotope ratios in circum-Pacific volcanic arcs. *Nature* 338 , p. 473–478. 1989
- [Prasad *et al.* 1997] Prasad, S. ; Kusumgar, S. ; Gupta, S. K.: A mid to late Holocene record of palaeoclimatic changes from Nal Sarovar: a palaeodesert margin lake in western India. *J. Quatern. Sci.* 12(2) , p. 153–159. 1997
- [von Rad *et al.* 1999] Rad, U. von ; Schaaf, M. ; Michels, K. H. ; Schulz, H. ; Berger, W. H. ; Sirocko, F.: A 5000-yr Record of Climate Change in Varved Sediments from the Oxygen Minimum Zone off Pakistan, Northeastern Arabian Sea. *Quatern. Res.* 51 , p. 39–53. 1999
- [Rafter and Fergusson 1957] Rafter, T. A. ; Fergusson, G. J.: “Atom Bomb Effect” – Recent Increase of Carbon-14 Content of the Atmosphere and Biosphere. *Science* 126 , p. 557–558. 1957
- [Ramesh 2001] Ramesh, R.: High resolution Holocene monsoon records from different proxies: An assessment of their consistency. *Current Science* 81(11) , p. 1432–1436. 2001
- [Raven and Edwards 2001] Raven, J. A. ; Edwards, D.: Roots: evolutionary origins and biogeochemical significance. *J. Experim. Botany* 52 , p. 381–401. 2001
- [Rödel 1996] Rödel, W.: Physik unserer Umwelt: Die Atmosphäre. Springer Verlag, Heidelberg, 1996

- [Reichel 2009] Reichel, T.: Optimierung eines Verfahrens zur Radonmessung in Wasser, Ruprecht-Karls-Universität Heidelberg, diploma thesis, 2009
- [Reimer *et al.* 2009] Reimer, P. J. ; Baillie, M. G. L. ; Bard, E. ; Baylis, A. ; Beck, J. W. ; Blackwell, P. G. ; Bronk Ramsey, C. ; Buck, C. E. ; Burr, G. S. ; Edwards, R. L. ; Friedrich, M. ; Grootes, P. M. ; Kromer, B. ; McCormac, F. G. ; Manning, S. W. ; Reimer, R. W. ; Richards, D. A. ; Southon, J. R. ; Talamo, S. ; Turney, C. S. M. ; Plicht, J. van der ; Weyhenmeyer, C. E.: Intcal09 and Marine09 Radiocarbon Age Calibration Curves 0-50,000 Years Cal BP. *Radiocarbon* 51(4) , p. 1111–1150. 2009
- [Rison and Craig 1983] Rison, W. ; Craig, H.: Helium isotopes and mantle volatiles in Loihi Seamount and Hawaiian Island basalts and xenoliths. *Earth Planet. Sci. Lett.* 66 , p. 407–426. 1983
- [Roether 1967] Roether, W.: Estimating the Tritium Input to Groundwater from Wine Samples: Groundwater and Direct Run-Off Contribution to Central European Surface Waters. *Isotopes in Hydrology*. International Atomic Energy Agency, Vienna, 1967, p. 73–89
- [Roether *et al.* 1970] Roether, W. ; Münnich, K. O. ; Östlund, H. G.: Tritium Profile at the North Pacific (1969) Geosecs Intercalibration Station. *J. Geophys. Res.* 75(36) , p. 7672–7675. 1970
- [von Rohden 2002] Rohden, C. von: Tracerstudie zur Quantifizierung des Vertikaltransports in meromiktischen Seen, Ruprecht-Karls-Universität Heidelberg, PhD thesis, 2002
- [von Rohden and Ilmberger 2001] Rohden, C. von ; Ilmberger, J.: Tracer experiment with sulfur hexafluoride to quantify the vertical transport in a meromictic pit lake. *Aquat. Sci.* 63 , p. 417–431. 2001
- [von Rohden *et al.* 2010] Rohden, C. von ; Kreuzer, A. ; Chen, Z. ; Aeschbach-Hertig, W.: Accumulation of natural SF₆ in the sedimentary aquifers of the North China Plain as a restriction on groundwater dating. *Isotopes Environ. Healt. S.* 46 , p. 279–290. 2010
- [Rozanski *et al.* 1993] Rozanski, K. ; Araguas-Araguas, L. ; Gonfiantini, R.: Isotopic Patterns in Modern Global Precipitation. *Climate Change in Continental Isotopic Records* Vol. 78. American Geophysical Union, 1993, p. 1–36
- [Rozanski *et al.* 1991] Rozanski, K. ; Gonfiantini, R. ; Araguas-Araguas, L.: Tritium in the global atmosphere: Distribution patterns and recent trends. *J. Phys. G. Nucl. Part. Phys.* 17 , p. 523–536. 1991
- [Rushton 1986] Rushton, K. R.: Vertical Flow in Heavily Exploited Hard Rock and Alluvial Aquifers. *Ground Water* 24(5) , p. 601–608. 1986
- [Scheffer and Schachtschabel 1960] Scheffer, F. ; Schachtschabel, P.: Lehrbuch der Agrikulturchemie und Bodenkunde: 1. Teil Bodenkunde. Ferdinand Enke Verlag, Stuttgart, 1960
- [Schlosser *et al.* 1988] Schlosser, P. ; Stute, M. ; Dörr, H. ; Sonntag, C. ; Münnich, K. O.: Tritium/³He dating of shallow groundwater. *Earth Planet. Sci. Lett.* 89 , p. 353–362. 1988
- [Schneider 2009] Schneider, T. C.: Einfluss von Sauerstoffzehrung auf Edelgaspartialdrücke in Bodenluft, Ruprecht-Karls-Universität Heidelberg, diploma thesis, 2009
- [Schulz *et al.* 1998] Schulz, H. ; Rad, U. von ; Erlenkeuser, H.: Correlation between Arabian Sea and Greenland climate oscillations of the past 110,000 years. *Nature* 393 , p. 54–57. 1998
- [Schuster *et al.* 2002] Schuster, P. ; Krabbenhoft, D. P. ; Naftz, D. L. ; Cecil, L. D. ; Olson, M. L. ; Dewild, J. F. ; Suson, D. D. ; Green, J. R. ; Abbott, M. L.: Atmospheric Mercury Deposition during the Last 270 Years: A Glacial Ice Core Record of Natural and Anthropogenic Sources. *Environ. Sci. Technol.* 36 , p. 2303–2310. 2002
- [Sengupta and Sarkar 2006] Sengupta, S. ; Sarkar, A.: Stable isotope evidence of dual (Arabian Sea and Bay of Bengal) vapour sources in monsoonal precipitation over north India. *Earth Planet. Sci. Lett.* 250 , p. 511–521. 2006
- [Shackleton 2000] Shackleton, N. J.: The 100,000-Year Ice-Age Cycle Identified and Found to Lag Temperature, Carbon Dioxide, and Orbital Eccentricity. *Science* 289(5486) , p. 1897–1902. 2000
- [Shi *et al.* 2001] Shi, Y. ; Yu, G. ; Liu, X. ; Li, B. ; Yao, T.: Reconstruction of the 30-40 ka BP enhanced Indian monsoon climate based on geological records from the Tibetan Plateau. *Palaeogeogr. Palaeoclim. Palaeoecol.* 169 , p. 69–83. 2001

- [Singh *et al.* 1990] Singh, G. ; Wasson, R. J. ; Agrawal, D. P.: Vegetational and seasonal climatic changes since the last full glacial in the Thar Desert, northwestern India. *Rev. Palaeobot. Palynol.* 64 , p. 351–358. 1990
- [Smith and Kennedy 1983] Smith, S. P. ; Kennedy, B. M.: The solubility of noble gases in water and in NaCl brine. *Geochim. Cosmochim. Acta* 47 , p. 503–515. 1983
- [Solomon *et al.* 1996] Solomon, D. K. ; Hunt, A. ; Poreda, R. J.: Source of radiogenic helium 4 in shallow aquifers: Implications for dating young groundwater. *Water Resour. Res.* 32(6) , p. 1805–1813. 1996
- [Sonntag *et al.* 1979] Sonntag, C. ; Klitzoch, E. ; Löhnert, E. P. ; Münnich, K. O. ; Junghaus, C. ; Thorweihe, O. ; Weistroffer, K. ; Swailen, F. M.: Palaeoclimatic Information from Deuterium and Oxygen-18 in Carbon-14-dated North Saharian Groundwaters. *Isotope Hydrology Vol. II 1978*, International Atomic Energy Agency, Vienna, 1979, p. 569–581
- [Sorger 2010] Sorger, S.: Bestimmung der SF-6-Konzentration von Wasserproben mit Kupferzylindern als Probenahmegefäßen, Ruprecht-Karls-Universität Heidelberg, diploma thesis, 2010
- [Stanley *et al.* 2009] Stanley, R. H. R. ; Baschek, B. ; Lott III, D. E. ; Jenkins, W. J.: A new automated method for measuring noble gases and their isotopic ratios in water samples. *Geochem. Geophys. Geosys.* 10(5) , p. doi:10.1029/2009GC002429. 2009
- [Staubwasser *et al.* 2002] Staubwasser, M. ; Sirocko, F. ; Grootes, P. M. ; Erlenkeuser, H.: South Asian monsoon climate change and radiocarbon in the Arabian Sea during early and middle Holocene. *Paleoceanography* 17(4) , p. doi:10.1029/2000PA000608. 2002
- [Staubwasser *et al.* 2003] Staubwasser, M. ; Sirocko, F. ; Grootes, P. M. ; Segl, M.: Climate change at the 4.2 ka BP termination of the Indus valley civilization and Holocene south Asian monsoon variability. *Geophys. Res. Lett.* 30(8) , p. doi:10.1029/2002GL016822. 2003
- [Stern *et al.* 1968] Stern, M. J. ; Spindel, W. ; Monse, E. U.: Temperature Dependences of Isotope Effects. *J. Chem. Phys.* 48(7) , p. 2908–2919. 1968
- [Stuiver and Polach 1977] Stuiver, M. ; Polach, H. A.: Discussion: Reporting of 14C data. *Radiocarbon* 19(3) , p. 355–363. 1977
- [Stumm and Morgan 1996] Stumm, W. ; Morgan, J. J.: Aquatic Chemistry. John Wiley & Sons, New York, 1996
- [Stute *et al.* 1995] Stute, M. ; Forster, M. ; Frischkorn, H. ; Serejo, A. ; Clark, J. F. ; Schlosser, P. ; Broecker, W. S. ; Bonani, G.: Cooling of Tropical Brazil (5°C) during the Last Glacial Maximum. *Science* 269 , p. 379–383. 1995
- [Stute and Schlosser 1993] Stute, M. ; Schlosser, P.: Principles and applications of the noble gas paleothermometer. Swart, P. K. (ed.) ; Lohmann, K. C. (ed.) ; McKenzie, J. (ed.) ; Savin, S. (ed.): *Climate Change in Continental Isotopic Records*. American Geophysical Union, Washington, DC, 1993, p. 89–100
- [Tamers 1975] Tamers, M. A.: Validity of Radiocarbon Dates on Ground Water. *Geophys. Surv.* 2 , p. 217–239. 1975
- [Tans *et al.* 1979] Tans, P. P. ; Jong, A. F. M. de ; Mook, W. G.: Natural atmospheric 14C variation and the Suess effect. *Nature* 280 , p. 826–828. 1979
- [Todd 1980] Todd, D. K.: Ground Water Hydrology. John Wiley & Sons, New York, 1980
- [Tolstikhin and Kamenskiy 1969] Tolstikhin, I. N. ; Kamenskiy, I. L.: On the Possibility of Groundwater Age Determination Using Tritium-Helium-3 Method. *Geokhimiya* 8 , p. 1027–1029. 1969
- [Torgersen 1980] Torgersen, T.: Controls on Pore-Fluid Concentration of 4He and 222Rn and the Calculation of 4He/222Rn Ages. *J. Geochem. Explor.* 13 , p. 57–75. 1980
- [Torgersen 2010] Torgersen, T.: Terrestrial helium degassing fluxes and the atmospheric helium budget: Implications with respect to the degassing processes of continental crust. *Chem. Geol.* 79(1) , p. 1–14. 2010
- [Troughton 1979] Troughton, J. H.: $\delta^{13}\text{C}$ as an indicator of carboxylation reactions. M. Gibbs, M. (ed.) ; Latzko, E. (ed.) ; Pirson, André (ed.) ; Zimmermann, Martin H. (ed.): *Encyclopedia of Plant Physiology*, Springer Verlag Berlin Heidelberg, 1979, p. 140–149

- [Träumner 2005] Träumner, K.: Inbetriebnahme, Tests und erste Anwendung einer neuen Aufbereitungslinie zur massenspektrometrischen Messung von Edelgasen aus Grundwasser- und Stalagmitproben, Ruprecht-Karls-Universität Heidelberg, diploma thesis, 2005
- [Unkel 2006] Unkel, I.: AMS-14C-Analysen zur Rekonstruktion der Landschafts- und Kulturgeschichte in der Region Palpa (S-Peru), Ruprecht-Karls-Universität Heidelberg, Inaugural-Dissertation, 2006
- [Urey 1947] Urey, H. C.: The Thermodynamic Properties of Isotopic Substances. *J. Chem. Soc.* 1947 , p. 562–581. 1947
- [Vimeux *et al.* 2001] Vimeux, F. ; Masson, V. ; Jouzel, J. ; Petit, J. R. ; Steig, E. J. ; Stievenard, M. ; Vaikmai, R. ; White, J. W. C.: holocene hydrological cycle changes in the Southern Hemisphere documented in East Antarctic deuterium excess records. *Clim. Dynam.* 17 , p. 503–513. 2001
- [Vogel 1967] Vogel, J. C.: Investigation of groundwater with Radiocarbon. *Isotopes in Hydrology*, International Atomic Energy Agency, Vienna, 1967, p. 355–368
- [Vogel 1970] Vogel, J. C.: Carbon-14 dating of groundwater. *Isotope Hydrology*, International Atomic Energy Agency, Vienna, 1970, p. 225–240
- [Vogel *et al.* 1970] Vogel, J. C. ; Grootes, P. M. ; Mook, W. G.: Isotopic Fractionation between Gaseous and Dissolved Carbon Dioxide. *Z. Physik* 230 , p. 225–238. 1970
- [Wang *et al.* 2005] Wang, Y. ; Cheng, H. ; Edwards, L. ; He, Y. ; Kong, X. ; An, Z. ; Wu, J. ; Kelly, M. J. ; Dykoski, C. A. ; Li, X.: The Holocene Asian Monsoon: Links to Solar Changes and North Atlantic Climate. *Science* 308(5723) , p. 854–857. 2005
- [Wang *et al.* 2008] Wang, Y. ; Cheng, H. ; Edwards, L. ; Kong, X. ; Shao, X. ; Chen, S. ; Wu, J. ; Jiang, X. ; Wang, X. ; An, Z.: Millennial- and orbital-scale changes in the East Asian monsoon over the past 224,000 years. *Nature* 451 , p. 1090–1093. 2008
- [Wang *et al.* 2001] Wang, Y. J. ; Cheng, H. ; Edwards, R. L. ; An, Z. S. ; Wu, J. Y. ; C.-C., Shen ; Dorale, J. A.: A High-Resolution Absolute-Dated Late Pleistocene Monsoon Record from Hulu Cave, China. *Science* 294(5550) , p. 2345–2348. 2001
- [Wanninkhof and Ledwell 1996] Wanninkhof, R. ; Ledwell, J. R.: Analysis of Sulfur Hexafluoride in Seawater. *J. Geophys. Res.* 96(C5) , p. 8733–8740. 1996
- [Weiss 1970] Weiss, R. F.: The solubility of nitrogen, oxygen and argon in water and seawater. *Deep-Sea Res.* 17 , p. 721–735. 1970
- [Weiss 1971] Weiss, R. F.: Solubility of helium and neon in water and seawater. *J. Chem. Eng. Data* 16(2) , p. 235–241. 1971
- [Weiss and Kyser 1978] Weiss, R. F. ; Kyser, T. K.: Solubility of krypton in water and seawater. *J. Chem. Eng. Data* 23(1) , p. 69–72. 1978
- [Weiss *et al.* 1979] Weiss, W. ; Bullacher, J. ; Roether, W.: Evidence of pulsed discharges of tritium from nuclear energy installations in Central European precipitation. *Behaviour of tritium in the environment*. International Atomic Energy Agency, San Francisco 1978, 1979, p. 17–30
- [Welte *et al.* 2010] Welte, J. ; Ritterbusch, F. ; Steinke, I. ; Henrich, M. ; Aeschbach-Hertig, W. ; Oberthaler, M. K.: On the Possibility of Groundwater Age Determination Using Tritium-Helium-3 Method. *New J. Physics* 12 , p. 1367–2630/10/065031. 2010
- [Weyhenmeyer *et al.* 2000] Weyhenmeyer, C. E. ; Burns, S. J. ; Waber, H. N. ; Aeschbach-Hertig, W. ; Kipfer, R. ; Loosli, H. H. ; Matter, A.: Cool Glacial Temperatures and Changes in Moisture Source Recorded in Oman Groundwaters. *Science* 287(5454) , p. 842–845. 2000
- [Wieser 2006] Wieser, M.: Entwicklung und Anwendung von Diffusionssamplern zur Beprobung gelöster Edelgase in Wasser, Ruprecht-Karls-Universität Heidelberg, diploma thesis, 2006
- [Wölfli 1987] Wölfli, W.: Advances in Accelerator Mass Spectrometry. *Nucl. Instr. Meth. Phys. Res.* B29 , p. 1–13. 1987

- [Wölfli *et al.* 1983] Wölfli, W. ; Bonani, G. ; Suter, M. ; Balzer, R. ; Nessi, M. ; Stoller, C.: Radioisotope Dating with the ETHZ-EN-Tandem Accelerator. *Radiocarbon* 25(2) , p. 745–753. 1983
- [Wonneberger 2008] Wonneberger, A.: Novel Methods of Water Sample Preparation for ^{39}Ar Analysis, Ruprecht-Karls-Universität Heidelberg, diploma thesis, 2008
- [Wutz 2010] Wutz, M. ; Jousten, K. (ed.): Handbuch Vakuumtechnik. Vieweg und Teubner, Wiesbaden, 2010
- [www.gwrdc.gujarat.gov.in 2010] www.gwrdc.gujarat.gov.in: visited 2010-11-22. 2010
- [www.worldclimate.com 2010] www.worldclimate.com: visited 2010-11-22. 2010
- [Yadava and Ramesh 2005] Yadava, M. G. ; Ramesh, R.: Monsoon reconstruction from radiocarbon dated tropical Indian speleothems. *Holocene* 15(1) , p. 48–59. 2005
- [Yatsevich and Honda 1997] Yatsevich, I. ; Honda, M.: Production of nucleogenic neon in the Earth from natural radioactive decay. *J. Geophys. Res.* 102(B5) , p. 10291–10298. 1997
- [Yurtsever 1975] Yurtsever, Y.: Worldwide survey of isotopes in precipitation. 1975
- [Yurtsever and Gat 1981] Yurtsever, Y. ; Gat, J. R.: Atmospheric Waters. Gat, J. R. (ed.) ; Gonfiantini, R. (ed.): *Stable Isotope Hydrology – Deuterium and Oxygen-18 in the Water Cycle*. International Atomic Energy Agency, Vienna, 1981, p. 103–142
- [Zhu and Kipfer 2010] Zhu, C. ; Kipfer, R.: Noble gas signatures of high recharge pulses and migrating jet stream in the late Pleistocene over Black Mesa, Arizona, United States. *Geology* 38(1) , p. 83–86. 2010
- [Ziegler *et al.* 1981] Ziegler, H. ; Batanouny, K. H. ; Sankhla, N. ; Vyas, O. P. ; Stichler, W.: The Photosynthetic Pathway Types of some Desert Plants from India, Saudi Arabia, Egypt, and Iraq. *Oecologia* 48 , p. 93–99. 1981

Aknowledgements – Danksagung

I want to express my gratitude to many people who supported me during the last years.

Above all I thank my PhD advisor Prof. Werner Aeschbach-Hertig, who gave me the possibility to take part in this interesting research project. His extensive assistance was not only helpful in scientific and technical ways, but he also paid attention to all kinds of topics and problems. Especially his huge patience concerning developments in the laboratory provided a pleasant working atmosphere which let me enjoy my work and get the most out of the mass spectrometrical setup and my results.

Furthermore, I want to thank my second referee Prof. Augusto Mangini, who could provide additional information concerning stable isotope effects and palaeoclimate in general, and accepted the job in spite of further obligations for his own PhDs.

Many thanks go to my Indian colleagues from the Physical Research Laboratory and their families, Dr. Maurya, Prof. Gupta, and above all Dr. Deshpande. Deshpande pulled double shifts during our stay in India to organise our accomodation, guide us on field trips, wrest our cargo from the omnipresent, omnipotent and enigmatic customs service, and simultaneously assembled and organised his laboratory. In addition, we could enjoy his hospitality on numerous occasions. Not for nothing, we are of the opinion that every project should have a Deshpande!

The rural population of Gujarat deserves my highest gratitude. It is moving, and thought-provoking, that poorest folks of the Indian countryside show plenty hospitality and helpfulness in an extent that baffles us westerners.

Weiterhin möchte ich allen Mitgliedern meiner Arbeitsgruppe danken, auf deren Unterstützung und Unterhaltung ich jetzt schon seit 2004 bauen kann. Neben den Doktoranden und Technikern möchte ich besonders Christian für die Unterstützung auf der Zielgeraden danken. Ganz besonders möchte ich Tim für seine Unterstützung in Indien danken. Ohne ihn hätte das erstens eh nicht geklappt und zweitens verdammt viel weniger Spaß gemacht. Nicht zuletzt möchte ich meinen Altvorderen Andi, Ronny und Tobi danken, die mir zum Einen die beste Basis für eine erfolgreiche Doktorarbeit hinterlassen haben und zum Anderen in der Endphase

mit Rat und Tat zur Seite standen.

Im Zuge meiner Labor-Analysen konnte ich im Besonderen auf die Hilfe von einigen Personen bauen. Dazu gehören Sabine Sorger und Christoph von Rohden, die mich maßgeblich bei der SF₆-Analyse und Auswertung unterstützt haben, sowie Michael Sabasch, der mir stets in Rekordzeit meine stabilen Isotope gemessen hat und dabei jederzeit bei Fragen für mich da war. Jens Fohlmeister, mein Leidgenosse an der Kohlenstoffextraktions-Anlage, half mir sowohl bei der Instandhaltung der Anlage, als auch, meinen Proben ein ordentliches Alter zu verpassen. An dieser Stelle möchte ich einen Dank in die Schweiz schicken, wo Irka Hajdas meinen Brunnen sehr schöne ¹⁴C-Verhältnisse entlocken konnte.

Frau Clos, Frau Thomas, Frau Weirich und Herrn Bayer als das Rückgrad unseres Instituts möchte ich für ihre Unterstützung in den letzten Jahren bei allen Verwaltungsangelegenheiten danken. Weiterhin danke ich Ralph Pfeifer und unserer gesamten Werkstattcrew für ihr permanentes Engagement, uns immer wieder Reparaturen, Teile oder ganze Apparaturen zu zaubern, und daneben auch noch mit Sommerfesten und Weihnachtsfeiern diesem Institut Leben einzuhauchen.

Den 420ern Passo, Anne, Hannes und ganz besonders Babs danke ich hier für eine echt geile Zeit, und schließe hier gleich noch Felix, Sam, Lena, Daniela, Claudi, Alex, meinem Lieblings-WG-Genossen Werner und und und... ein. Danke für Aprichokenkuchen und Brownie-Flatrates, für TT-Sessions, für Korrekturlesen, für Matlab-Codes, für Wider-die-Mensa, Instituts-Videoabende, Grillen hinterm Haus, und auch sonst einfach alles was das Leben eines Doktoranden lebens- und (manchmal sogar) beneidenswert macht.

Meiner Freundin Bettina möchte ich von ganzem Herzen danken, dass sie die Sache mit mir zusammen durchgestanden hat, und manchmal sehr wenig von ihrem Freund hatte, um mir dadurch die Gelegenheit zu geben, dieses Projekt erfolgreich durchzubringen. Zusätzlich hat sie mit Engelsgeduld versucht, das Englisch dieser Arbeit zu verbessern.

Zuletzt gilt mein Dank meiner Familie, die mich über all die Jahre in meinem Studium unterstützt, bestärkt und aufgemuntert hat. Besonders meiner Oma möchte ich danken, die in den letzten Jahren mehr von meinen Physik- und Spektrum-Journalen gelesen hat als ich selbst und deren reges Interesse an der Wissenschaft und der Musik mir immer ein Beispiel sein wird.